



U.S. Department
of Transportation

**Federal Highway
Administration**

Publication No. FHWA/RD-87/026

October 1987

Improved Fracture Toughness and Fatigue Characteristics of Electroslag Welds

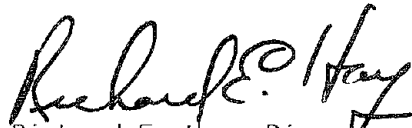
Research, Development, and Technology
Turner-Fairbank Highway Research Center
6300 Georgetown Pike
McLean, Virginia 22101-2296

FOREWORD

This report, "Improved Fracture Toughness and Fatigue Characteristics of Electroslag Welds," presents the results of research conducted by the Oregon Graduate Center for the Federal Highway Administration (FHWA), Office of Engineering and Highway Operations Research and Development, under contract Number DTFH61-83-C-00112.

This work was conducted as part of Program Area D1, Bridge Design, and is intended for engineers and fabricators contemplating the use of Electroslag Welding process for joining the structural materials in fabrication of structural members, and concerned with resistance of weld metal and heat-affected zone (HAZ) of weldments to crack formation and unstable crack propagation.

Copies of this report are being given widespread distribution by FHWA Transmittal Memorandum. Sufficient copies are being distributed to provide a minimum of one copy to each regional office, division office, and State highway agency. Direct distribution is being made to the division offices. Additional copies may be obtained from the National Technical Information Service (NTIS), 5285 Port Royal Road, Springfield, Virginia 22161.



Richard E. Hay, Director
Office of Engineering and Highway
Operations Research and Development

NOTICE

This document is disseminated under the sponsorship of the Department of Transportation in the interest of information exchange. The United States Government assumes no liability for its contents or use thereof. The contents of this report reflect the views of the author, who is responsible for the accuracy of the data presented herein. The contents do not necessarily reflect the official policy of the Department of Transportation. This report does not constitute a standard, specification, or regulation.

The United States Government does not endorse products or manufacturers. Trade or manufacturers' names appear herein only because they are considered essential to the object of this document.

1. Report No. FHWA/RD-87/026		2. Government Accession No. PB89 - 211056/AS		3. Recipient's Catalog No.	
4. Title and Subtitle IMPROVED FRACTURE TOUGHNESS AND FATIGUE CHARACTERISTICS OF ELECTROSLAG WELDS				5. Report Date October 1987	
				6. Performing Organization Code	
				8. Performing Organization Report No.	
7. Author(s) W. E. Wood and J. H. Devletian				10. Work Unit No. (TRAIS) NCP 3D1b2022	
9. Performing Organization Name and Address Dept. of Materials Science and Engineering Oregon Graduate Center 19600 N.W. Von Neumann Drive Beaverton, OR 97006-1999				11. Contract or Grant No. DTFH61-83-C-00112	
				13. Type of Report and Period Covered Final Report Oct. 1983 - May 1987	
12. Sponsoring Agency Name and Address Offices of Research and Development Federal Highway Administration U.S. Department of Transportation Washington, DC 20590				14. Sponsoring Agency Code	
15. Supplementary Notes FHWA contract manager: Jerar Nishanian					
16. Abstract <p>This project was designed to increase the reliability, integrity and mechanical behavior of electroslag welds in type A36 and A588 steel alloys. The parameters developed in this program utilized a narrow gap and a consumable plate guide tube in combination with reduced voltages and higher welding currents. This reduced heat input, increased welding speed, and also reduced weld imperfection tendency. Alloy additions, nickel and molybdenum, develop an acicular weld metal tough microstructure. To minimize heat input, alloy additions were made through a tubular alloyed powder-containing wire.</p> <p>Charpy impact toughness data exhibited uniformly high weld metal toughness. Heat affected zone impact toughness exhibited wide variations and was sensitive to test location. The lowest impact toughness were within approximately 1 mm of the fusion boundary and were approximately equivalent to the zone 2 impact toughness requirements. Full-thickness fracture toughness data were comparable to base metal when the optimized procedures and alloying conditions were utilized. Full thickness toughness data did not show wide variations in the heat affected zone. Hence, Charpy impact toughness assessment without standardized test locations and relative to full thickness data may not be the best method to assess toughness. None of the 12 electroslag welds evaluated under fatigue conditions developed cracks within the test conditions studied. These data suggest that sound electroslag welds in the absence of weld imperfections more than meet AASHTO fatigue requirements for category B weldments.</p>					
17. Key Words Electroslag, Weld, Toughness, Microstructure, Fatigue, A36, A588, Flux, Alloying			18. Distribution Statement No restrictions. This document is available to the public through the National Technical Information Service, Springfield, Virginia 22161.		
19. Security Classif. (of this report) Unclassified		20. Security Classif. (of this page) Unclassified		21. No. of Pages 257	22. Price A10

METRIC (SI*) CONVERSION FACTORS

APPROXIMATE CONVERSIONS TO SI UNITS

Symbol	When You Know	Multiply By	To Find	Symbol
--------	---------------	-------------	---------	--------

LENGTH

in	inches	2.54	millimetres	mm
ft	feet	0.3048	metres	m
yd	yards	0.914	metres	m
mi	miles	1.61	kilometres	km

AREA

in ²	square inches	645.2	millimetres squared	mm ²
ft ²	square feet	0.0929	metres squared	m ²
yd ²	square yards	0.836	metres squared	m ²
mi ²	square miles	2.59	kilometres squared	km ²
ac	acres	0.395	hectares	ha

MASS (weight)

oz	ounces	28.35	grams	g
lb	pounds	0.454	kilograms	kg
T	short tons (2000 lb)	0.907	megagrams	Mg

VOLUME

fl oz	fluid ounces	29.57	millilitres	mL
gal	gallons	3.785	litres	L
ft ³	cubic feet	0.0328	metres cubed	m ³
yd ³	cubic yards	0.0765	metres cubed	m ³

NOTE: Volumes greater than 1000 L shall be shown in m³.

TEMPERATURE (exact)

°F	Fahrenheit temperature	5/9 (after subtracting 32)	Celsius temperature	°C
----	------------------------	----------------------------	---------------------	----

APPROXIMATE CONVERSIONS TO SI UNITS

Symbol	When You Know	Multiply By	To Find	Symbol
--------	---------------	-------------	---------	--------

LENGTH

mm	millimetres	0.039	inches	in
m	metres	3.28	feet	ft
m	metres	1.09	yards	yd
km	kilometres	0.621	miles	mi

AREA

mm ²	millimetres squared	0.0016	square inches	in ²
m ²	metres squared	10.764	square feet	ft ²
km ²	kilometres squared	0.39	square miles	mi ²
ha	hectares (10 000 m ²)	2.53	acres	ac

MASS (weight)

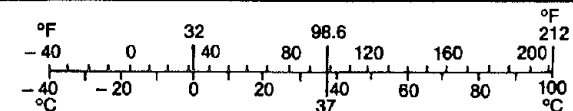
g	grams	0.0353	ounces	oz
kg	kilograms	2.205	pounds	lb
Mg	megagrams (1 000 kg)	1.103	short tons	T

VOLUME

mL	millilitres	0.034	fluid ounces	fl oz
L	litres	0.264	gallons	gal
m ³	metres cubed	35.315	cubic feet	ft ³
m ³	metres cubed	1.308	cubic yards	yd ³

TEMPERATURE (exact)

°C	Celsius temperature	9/5 (then add 32)	Fahrenheit temperature	°F
----	---------------------	-------------------	------------------------	----



These factors conform to the requirement of FHWA Order 5190.1A.

* SI is the symbol for the International System of Measurements

TABLE OF CONTENTS

	<u>Page</u>
I. INTRODUCTION	1
1. Electroslog Welding Process	1
a. Advantages	2
b. Problems	2
2. Project Objective	6
II. BACKGROUND	9
1. Literature Review	9
a. Heat-Affected Zone Microstructure	10
b. Fusion Zone Microstructure	10
c. Process Variables	13
(1) Current, Voltage, and Resistance	13
(2) Electrode	16
(3) Slag Depth	18
(4) Guide Tube Geometry	19
(5) Welding Speed	20
(6) Weld Pool Agitation	21
d. Alloy Additions	22
e. Mechanical Properties	23
f. Postweld Heat Treatment	24
2. Overview of Previous PNL/OGC Results	25
a. Process Variables Results and Discussion	25
b. Fusion Zone Microstructure Control	34
c. Charpy V-Notch Impact Toughness	35
III. MATERIALS	40
1. Alloy	40
2. Flux	40
3. Electrode Filler Wire	40
4. Identification System	45
IV. EXPERIMENTAL PROCEDURES	48
1. Welding Related	48
a. Conventional and Consumable Guide ESW	48
b. Narrow Gap	49
c. Flux Addition	49
d. Alloying	51
e. Grain Refinement	51
2. Metallographic Practices	51
3. Impact Testing	54
4. Plane Strain Fracture Toughness Testing	57
5. I-Beam Design and Fabrication	61

TABLE OF CONTENTS (cont.)

	<u>Page</u>
6. Chemical Analyses	61
7. Nondestructive Examination	63
8. Hardness Evaluation	63
 V. RESULTS	 64
1. Welding Parameter Study	64
2. Filler Metal Alloy Development	88
3. Characteristic Grain Structures	98
a. Type I	98
b. Type II	101
c. Type III	103
d. Type IV	103
e. Type V	104
f. Charpy V-Notch Toughness	106
4. Optimized Weld Parameters and Alloy Composition	109
5. Weld Metal Grain Refinement	109
6. Charpy V-Notch Toughness of Optimized Electroslag	120
7. ASTM E399 Fracture Toughness Tests	160
a. A36 Material	160
b. A588 Material	160
8. Full Scale I-Beam Fatigue Tests	167
9. Weld Defect Formation and Detection.....	169
10. Solidification Study	178
 VI. DISCUSSION	 185
1. Control of Weld Microstructure	185
2. Toughness Optimization through Microstructure Control	190
3. Toughness Assessment	191
a. Charpy V-Notch Impact Toughness	192
b. K_{IC} Behavior	193
4. Fatigue Performance	194
5. Weld Metal Imperfection Formation/Detection.....	195
 VII. CONCLUSIONS	 196
 VIII. RECOMMENDED PROCEDURE FOR ESW USING OPTIMIZED ALLOY FILLER METAL AND WELDING PARAMETERS	 198
1. ESW Equipment	198
2. Consumables	200
3. Operating Guidelines	200

TABLE OF CONTENTS (cont.)

	<u>Page</u>
APPENDIX A: CVN Impact Test Data	204
APPENDIX B: Full Copy of NDE Report	229
REFERENCES	240

LIST OF TABLES

	<u>Page</u>
1. Composition of base metal, weld filler wire and guide plate materials	41
2. Flux chemistries used in this program	42
3. Hobart PF201 running flux chemistry	43
4. OGC-defined weld metal structure types	98
5. Optimum welding conditions	109
6. ESW practices for mechanical property evaluation	121
7. CVN transition curve analysis as a function of ESW weld condition	122
8. Weld metal and heat affected zone CVN impact toughness summary .	157
9. Test temperatures (°C) at which key levels of CVN toughness were obtained	158
10. Full thickness ASTM E399 fracture toughness of 76-mm thick A36 and A588 base metal alloys	161
11. Full thickness ASTM E399 fracture toughness of 76-mm thick A36 electroslag weld metal	162
12. Full thickness ASTM E399 fracture toughness of 76-mm thick A36 electroslag weld coarse heat affected zone	163
13. Full thickness ASTM E399 fracture toughness of 76-mm thick A588 electroslag weld metal	164
14. Full thickness ASTM E399 fracture toughness of 76-mm thick A588 electroslag weld coarse heat affected zone	165
15. Full-scale category B I-beam fatigue tests of A588 at room temperature	166
16. Electroslag weld defect summary	173
17. Welding parameters for 2- and 3-in square butt joints in A588 and A36 plates	202
18. Welding parameters for 1.5- to 4-in square butt joints in A588 and A36 plates	203

LIST OF FIGURES

	<u>Page</u>
1. Schematic representation of conventional electroslag welding in process by the non-consumable guide technique	3
2. Schematic illustration of consumable guide electroslag welding process	4
3. Schematic illustration of consumable guide electroslag process .	5
4. Retrofitting an electroslag weld by bolting a cover plate onto the bridge structure	7
5. Standard ES weld macrostructure indicating various structural zones present	11
6. Schematic representation of ES process boundaries for successful joining	17
7. Schematic representation of various consumable guide tube designs used in the investigation	26
8. Summary of effects of ground location and electrode positioning on ES weld penetration	28
9. Oscillographs illustrating the sequence of slag depletion during the welding process	29
10. Effect of welding voltage on base metal dilution for various guide tube geometries and joint spacings in ESW	31
11. Relationship between welding current and wire feed rate for various guide tube geometries and joint spacings in ESW	32
12. Trace of macroscopic current fluctuations on the electroslag macrostructure	33
13. ES weld centerline 0°F Charpy impact energy for 25-P weld wire weldments	36
14. ES weld centerline 0°F Charpy impact energy as a function of weld wire alloy	37
15. Heat affected zone 0°F Charpy impact energy of ES weldments	39
16. Microstructures of as-received alloys	44
17. Weldments for macro/microstructural analysis identification system	45
18. CVN specimen identification system	46
19. K_{Ic} fracture toughness specimen identification system	46
20. I-beam for fatigue test identification system	46
21. Defect formation weld identification system	47
22. Guide tube plate designs	50
23. Schematic illustration of the continuous metered flux feed system	52
24. Schematic illustration of quartz shrouded guide tube design	53
25. Standard CVN test specimen geometry	55
26. CVN specimen location configuration for ES welds	56
27. Compact tension fracture toughness specimen geometry	58
28. Location of K_{Ic} specimens with respect to ES weld location	59
29. Location of compact tension fracture toughness samples with respect to ES heat affected zone locations	60
30. Schematic illustration of the full-scale I-beam containing electroslag weldments for fatigue testing	62

LIST OF FIGURES (cont.)

	<u>Page</u>
31. Heat input vs. sidewall penetration	65
32. Relationship between heat input and base metal penetration showing decrease of heat input compared to standard ESW	66
33. Influence of current on base metal dilution	68
34. Influence of voltage on base metal dilution	69
35. Influence of voltage on form factor	70
36. Influence of current on form factor	71
37. Percent coarse columnar grains vs. voltage	72
38. Percent coarse columnar grains vs. voltage for narrow gap welds	73
39. Percent coarse columnar grains vs. current for narrow gap welds	74
40. Heat input vs. heat affected zone size, 50mm	75
41. Heat input vs. heat affected zone size, 76mm	76
42. Empirically determined relation between the welding current, electrode velocity and welding voltage	78
43. Macrograph of hot cracks in ES welds	79
44. Minimum current to produce hot cracking as a function of weld gap configuration	80
45. Dilution vs. welding voltage for solid vs. tubular fillers	81
46. Hardness traverse across electroslog welds	83
47. Typical weld metal macrostructures in standard and narrow gap welds	84
48. Typical coarse columnar grain microstructure	85
49. Typical thin columnar grain zone microstructure	86
50. Characteristic descriptions of grain structure in narrow gap electroslog welds	87
51. Effect of alloy addition on the constituent volume fractions in A36 and A588 weld metal	89
52. Density of acicular ferrite plates as a function of nickel and molybdenum content	90
53. Typical microstructural feature of standard electroslog weld- ments	91
54. Typical microstructural feature of Ni-Mo alloyed electroslog weldments	92
55. Typical microstructural feature of Cr and Mo alloyed electroslog weldments	93
56. Acicular ferrite size distributions as a function of alloy con- tent in 50 mm thick A36 plate	94
57. Comparison of microstructure of 50 mm thick A588 plate between bainitic ferrite and acicular ferrite produced by Cr and Mo additions vs. Ni and Mo additions	96
58. Summary figure showing the effects of alloy elements on hardness and impact toughness	97
59. Classification of electroslog weld metal type by microstructure, macrostructure, and solidification structure	99
60. Percentage thin columnar grains vs. weld metal oxygen content ..	100
61. Relationship between weld metal solidification structure and subsequent solid state structure	102

LIST OF FIGURES (cont.)

	<u>Page</u>
62. Relationships among percentage of coarse columnar, thin columnar, and equiaxed zones as a function of alloy content and oxygen content in electroslag welds	105
63. Distribution of ferrite content types as a function of weld metal oxygen content	107
64. Summary of CVN impact energies as a function of electroslag weld metal type and oxygen content	108
65. Hot cracking resistance influenced by the addition of a quartz shroud during electroslag welding	110
66. Fragmented dendrites due to intense molten pool stirring during quartz grain-refined electroslag welding	111
67. Base metal dilution vs. quartz additions during quartz grain-refined welding	113
68. Influence of electrode misalignment and asymmetrical heat generation during quartz welding	114
69. Base metal dilution vs. voltage during quartz electroslag welding	115
70. Form factor vs. voltage during quartz electroslag welding	116
71. Oxygen content vs. amount of quartz addition during quartz grain refinement welding	117
72. Percent acicular ferrite formation vs. weld metal oxygen content	118
73. Inclusion distribution as a function of oxygen potential and oxygen content	119
74. CVN transition curve for A36 and 588 base material.....	125
75. CVN transition curves for 50 mm A588, notch location: WM 1/2T ϵ	126
76. CVN transition curves for 50 mm A588, notch location: HAZ 1.....	127
77. CVN transition curves for 50 mm A588, notch location: WM 1/4T ϵ	128
78. CVN transition curves for 50 mm A36, notch location: 1/2T.....	129
79. CVN transition curves for 50 mm A36, notch location: 1/4T.....	130
80. CVN transition curves for 50 mm A36, notch location: HAZ 1.....	131
81. CVN transition curves for 76 mm A36, notch location: 1/2T.....	132
82. CVN transition curves for 76 mm A36, notch location: 1/4T.....	133
83. CVN transition curves for 76 mm A36, notch location: HAZ 1.....	134
84. CVN transition curves for 76 mm A588, notch location: 1/2T.....	135
85. CVN transition curves for 76 mm A588, notch location: 1/4T.....	136
86. CVN transition curves for 76 mm A588, notch location: HAZ 1	137
87. CVN transition curves for A36 at the 1/2T position, weld condition: NG 25P.....	138
88. CVN transition curves for A36 at the 1/2T position, weld condition: NG, ST.....	139
89. CVN transition curves for A36 at the 1/4T position.....	140
90. CVN transition curves for A588 at the 1/2T position.....	141
91. CVN transition curves for A588 at the 1/4T position.....	142
92. CVN transition curves for A588 in the heat affected zone	143
93. CVN transition curves for 50 mm A36, notch location: HAZ 1.....	144
94. CVN transition curves for 76 mm A36, notch location: HAZ 1.....	145
95. CVN transition curves for 50 mm A588, notch location: HAZ 1.....	146
96. CVN transition curves for 76 mm A588, notch location: HAZ 1.....	147
97. CVN transition curves for 50 mm A36, weld condition: NG, ST.....	148

LIST OF FIGURES (cont.)

	<u>Page</u>
98. CVN transition curves for 76 mm A36, weld location: NG, ST2.....	149
99. CVN transition curves for 50 mm A588, weld location: NG, ST.....	150
100. CVN transition curves for 76 mm A588, weld condition: NG, ST2...	151
101. CVN transition curves for 50 mm A36, weld condition: SG, 25P....	152
102. CVN transition curves for 50 mm A36	153
103. CVN toughness as a function of distance from the fusion line in 450 mm thick A588	154
104. Impact energy summary for standard and quartz shrouded welds ...	155
105. Impact energy summary for quartz grain refined plus the influ- ence of alloy additions	156
106. Typical ferrite vein cracking along prior austenite grain boundaries	170
107. Schematic illustration of defects produced in OGC's defect- controlled electroslog welds	172
108. Ultrasonic and radiograph schematic results for controlled defect electroslog weld, plate 4.....	174
109. Ultrasonic and radiograph schematic results for controlled defect electroslog weld, plate 1.....	175
110. Ultrasonic and radiograph schematic results for controlled defect electroslog weld, plate 3.....	176
111. Ultrasonic and radiograph schematic results for controlled defect electroslog weld, plate 2.....	177
112. Variation of dendrite inclination angle for various weld cases .	179
113. Renucleation events in primary solidification structure	181
114. Primary dendrite arm spacing as a function of distance from the fusion line	182
115. Correlation between form factor and amount of coarse columnar grains	183

I. INTRODUCTION

The electroslag welding (ESW) process was originally developed at the Paton Electric Welding Institute in the Union of Soviet Socialist Republics (U.S.S.R.) in the early 1950's. ⁽¹⁾ The process was further developed in Czechoslovakia (Bratislava Institute of Welding) and Belgium (Arcos Corporation). ⁽²⁾ The technique eventually was introduced into the United States in 1959 by the Arcos Corporation. ⁽³⁾ Since then, it has been used in the U.S. for heavy structure fabrications, which include highway bridges.

1. Electroslag Welding Process

Electroslag welding is a joining method in which a molten slag simultaneously melts the filler metal and the surfaces of the work to be welded. Both the molten weld pool, which is shielded by the molten slag, and the molten slag extend along the full cross section of the joint as the weld progresses. Copper shoes are used on both sides of the plates being welded to contain the molten pool during welding and provide the final weld contour.

The process is initiated by an electric arc between the electrode and the bottom of the joint. Powdered flux is then added and subsequently melted by the heat of the arc. The arc stops and the welding current (500 to 700A) passes from the electrode through the slag by electrical conduction once a layer of molten slag is established (1.5 to 2 in). The passage of the current provides the necessary heat for fusion.

The process requires a larger heat input accompanied by slower cooling than other welding processes. Water-cooled copper shoes are generally used to contain the molten metal and slag, but solid copper shoes and even steel plates are also sometimes used. Electroslag welds are usually prepared in the vertical or the near-vertical direction and utilize a starting sump and runoff block to eliminate defects associated with the initiation and the termination of the process.

The two types of electroslog welding are: a) conventional, and b) consumable guide. The conventional system utilizes a nonconsumable contact tube to direct the electrode into the molten slag pool (figure 1). The contact tube is maintained about 50 mm above the slag pool surface. The entire welding head, along with the containment shoes, is moved upward at a predetermined rate consistent with the welding speed.

The consumable guide electroslog welding system uses a stationary consumable tube to guide the welding electrode into the slag pool (figures 2 and 3). The guide tube runs from the top of the weld to the bottom of the weld and is positioned with its tip about 37 mm above the bottom of the joint for weld initiation. As the name implies, the guide tube is consumed into the weld pool as the weld progresses. This method requires no moving parts except the welding electrode.

a. Advantages

Electroslog welding provides great savings in manpower, time, and welding consumables, especially for welding thicker sections. Sections several inches in thickness can be welded in a single pass by selecting a suitable number of electrodes and/or electrode oscillation. The sections being welded do not require machined edge preparation, and a combination of the weld pool size, high heat input, and welding speed eliminates the necessity for preheating. Postweld distortion is minimal when compared with other processes. The slag/metal reaction involved in the process provides sound, "defect-free" welds, if properly controlled.

b. Problems

Despite the many advantages, there are certain problems associated with the process. Once initiated, the process has to be completed without interruption, as intermittent stopping produces serious defects at re-start locations. The large heat input and resultant slow cooling rate results in

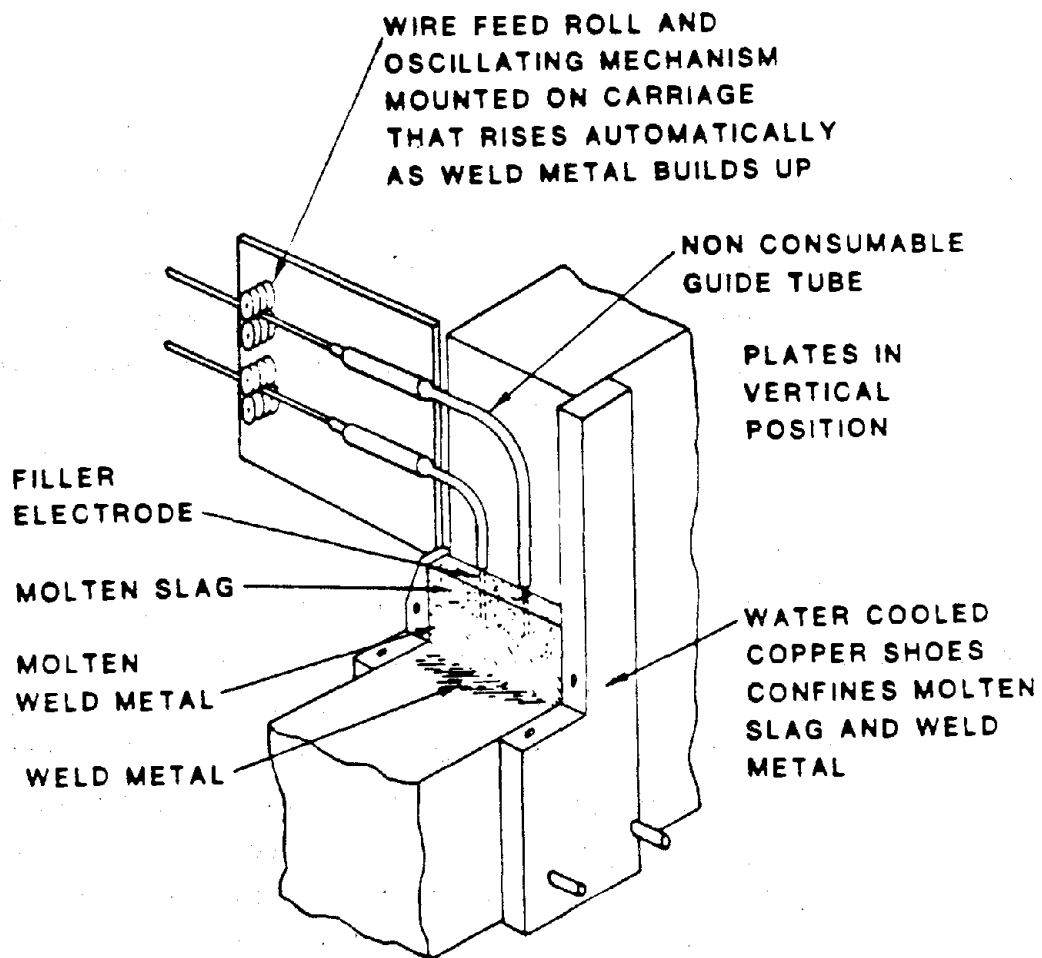


Figure 1. Schematic representation of conventional electroslag welding in process by the non-consumable guide technique. (Schematic.)

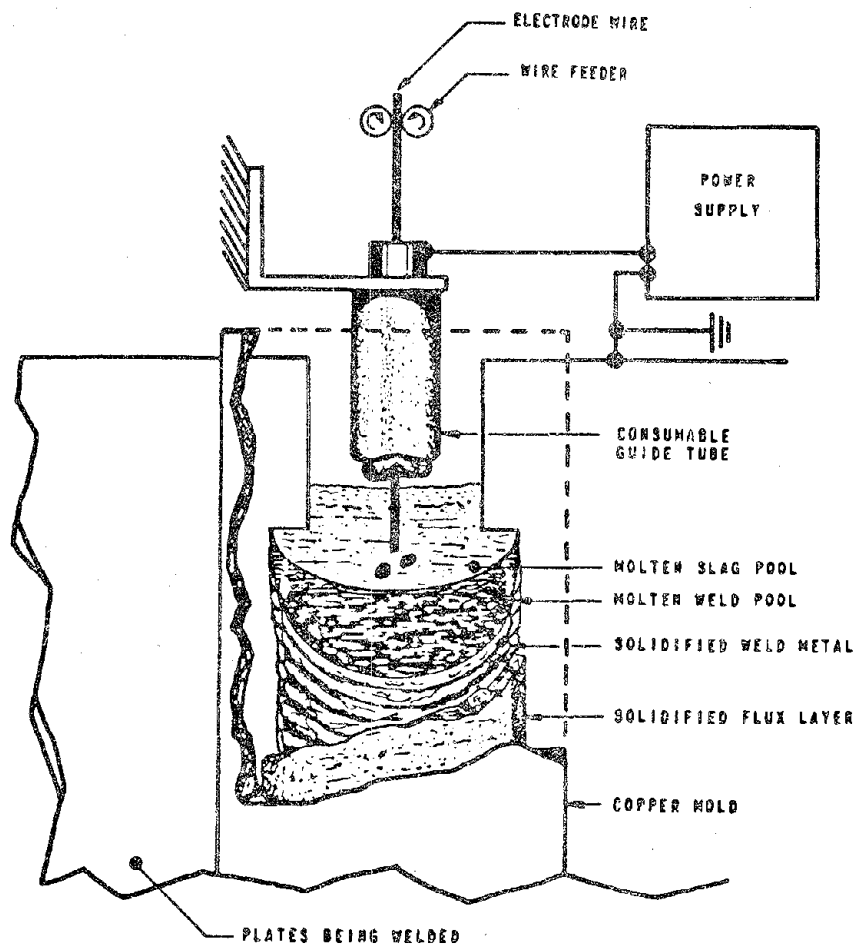


Figure 2. Schematic illustration of consumable guide electroslag welding process. (Schematic.)

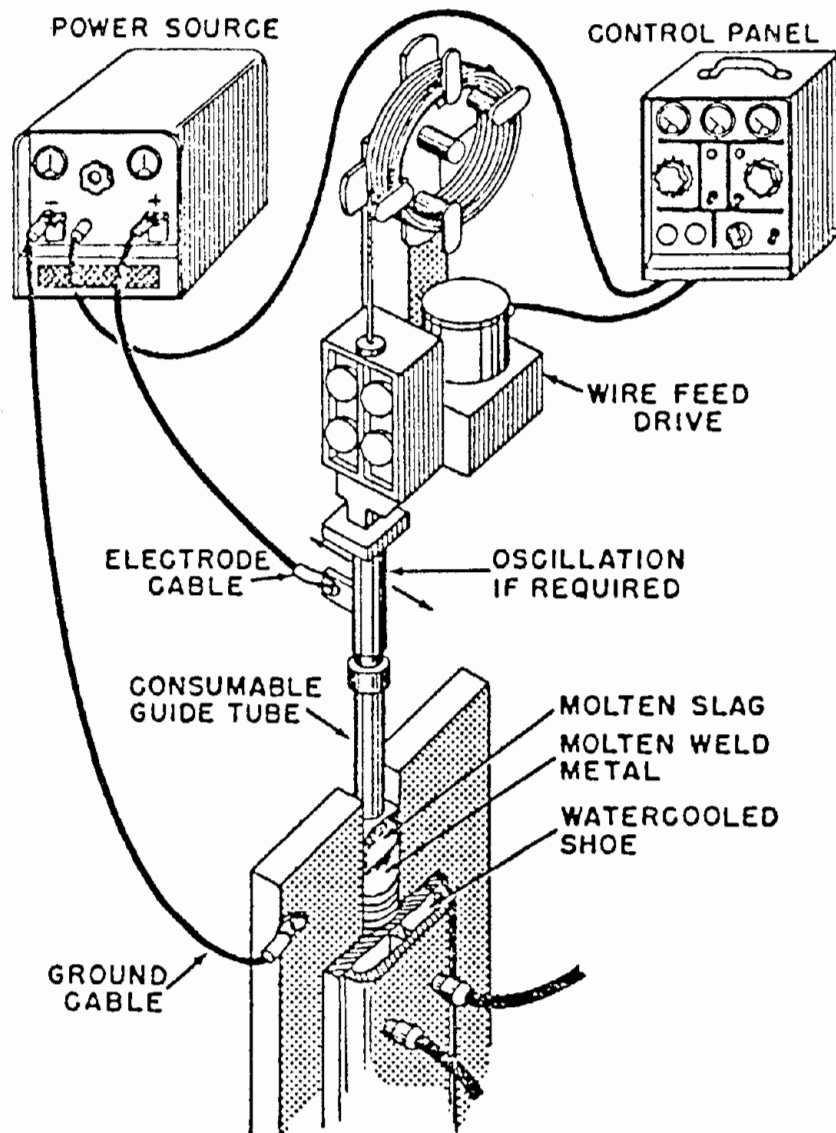


Figure 3. Schematic illustration of consumable guide electroslag process. (Schematic.)

a coarse cast structure in the weld metal with anisotropic mechanical properties. The solidification-induced, highly-textured grain orientation and tramp element segregation lead to hot cracking near the center of the weldment. The prolonged thermal cycles in the base metal adjacent to the fusion line produces a coarse-grained heat-affected zone (HAZ) which is more susceptible to brittle fracture than the parent material. In addition, the coarse structure of the weld metal and the HAZ makes reliable nondestructive testing of the weldments more difficult.

Recent research indicates that tight control over welding parameters is considerably more critical in achieving sound electroslag welds than originally anticipated. This is particularly true for consumable guide welding where slag depth control is much more difficult than in nonconsumable welding. Reinspection of electroslag welds in highway bridges has revealed that a high percentage of these welds contain unacceptable weld imperfections and/or low impact properties. Some of these weldments were judged to be structurally unsafe and unreasonable, and were retrofitted through the use of splice plates to cover the electroslag weld (figure 4).⁽⁴⁾ Thus, the Federal Highway Administration has prohibited the use of electroslag weldments on main structural tension members on any federally-aided projects.⁽⁵⁾

2. Project Objective

This research project addressed the fundamental relationships between process variables, microstructure, and properties of electroslag welds. The investigation optimized procedures for increasing the reliability, integrity, and inspectability of ESW, and was oriented toward eventual reinstatement of ESW as an acceptable bridge steel joining technique.

The primary objectives of this research program were to improve the fracture toughness and fatigue characteristics of electroslag weldments in A36 and A588 steel alloys. The program's first objective was to establish the limits under which sound reliable electroslag welds can be consistently

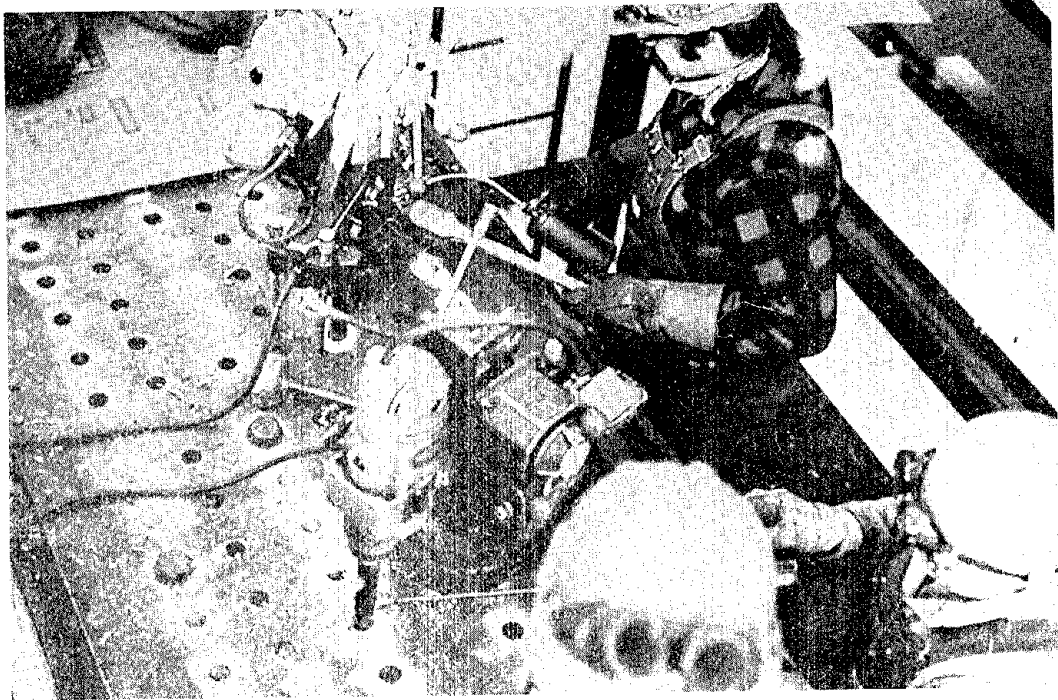


Figure 4. Retrofitting an electroslog weld by bolting a cover plate onto the bridge structure. (Micrograph.)



produced, then to develop the electroslag welding conditions to optimize toughness, fatigue, and weld imperfection control.

The major fracture toughness objective was to improve weldment microstructure and Charpy V-notch (CVN) impact levels above minimum requirements for zone 2 temperatures. A secondary fracture objective was to assess the plane-strain fracture toughness behavior. An additional objective was to evaluate the fatigue behavior of the electroslag welds fabricated under normal conventional practice versus the optimized practices developed under this program. This was done using full-scale fatigue electroslag-welded I-beams.

A final objective was to assess the inspectability of electroslag weldments. Thus, lastly, imperfections and their detection have been a concern with respect to electroslag welds. Thus, methodologies to reproducibly induce controlled imperfections in electroslag welds were developed, the conditions that result in these imperfections were defined, and the degree to which they could be detected with standard ultrasonic and radiographic analysis was established.

II. BACKGROUND

The Federal Highway Administration initiated a research contract at the Oregon Graduate Center (OGC) in CY1983 entitled "Improved Fracture Toughness and Fatigue Characteristics of Electroslag Welds." This work was completed in CY1986 and is reported herein.

This section presents: a) a literature review of the state of the art in electroslag welding, and b) a summary of the major research findings from the previous research program that influenced this present study.

The research thrust areas for this work were based upon the results of a previously-funded FHWA electroslag welding research project entitled "Improving the Reliability and Integrity of Consumable Guide Electroslag Weldments in Bridge Structures" conducted jointly at OGC and Battelle Pacific Northwest Laboratory (PNL). The work was completed in CY1982 and reported in the DOT Report No. DOT-FH-11-9612.

1. Literature Review

This literature review begins with a general discussion of the characteristics of ESW, then assesses these various characteristics under separate headings below. The discussion in each section presents the rationale for the experimental avenues investigated in the study reported herein.

Electroslag welding of thick section materials requires a larger heat input than other welding processes, which yields both low heating and cooling rates and results in a long dwell time at high temperatures. The large heat input accounts for the complex HAZ and weld metal microstructures present in electroslag weldments.

a. Heat-Affected Zone Microstructure

The HAZ in mild steel weldments can be divided into two regions: 1) the coarse-grained zone formed in the base metal immediately adjacent to the fusion line, and 2) the fine-grained zone found at a distance from the fusion line (figure 5). The coarse-grained HAZ consists of large equiaxed grains bounded by a proeutectoid ferrite network outlining the prior austenitic grain boundaries. The grain interior is normally made up of Widmanstätten structure;^(2,6) however, a bainitic structure has been reported in this region for A588 materials.⁽⁷⁾ The coarse-grained HAZ region is subjected to long dwell times well above the AC_3 temperature, which results in complete transformation to austenite and extensive growth of the austenite grains. Ferrite is nucleated at the austenitic grain boundaries during postweld cooling and results in a thick, continuous ferrite layer outlining the prior austenite grain boundaries. Ferrite also is nucleated upon cooling in the interior of the large austenite grains. This matrix ferrite grows in an acicular morphology (Widmanstätten structure) prior to the initiation of the pearlite transformation. The resulting microstructure is coarser than the starting structure of the base metal⁽²⁾ and may vary according to the base metal chemistry.

The fine-grained HAZ is a result of the region only being raised enough above the AC_3 temperature to result in transformation to austenite but not to result in grain growth. Subsequent transformation to ferrite and pearlite upon cooling results in a fine-grained structure similar to that achieved in a normalization heat treatment. The resulting microstructure is usually finer than the original base metal structure.

b. Fusion Zone Microstructure

The weld metal of a mild steel electroslag weld consists of a coarse columnar grain (CCG) zone located on the weld periphery. In this zone, the grains grow mainly in the direction of the heat flow. The heat removal becomes increasingly retarded and alloy segregation increases as

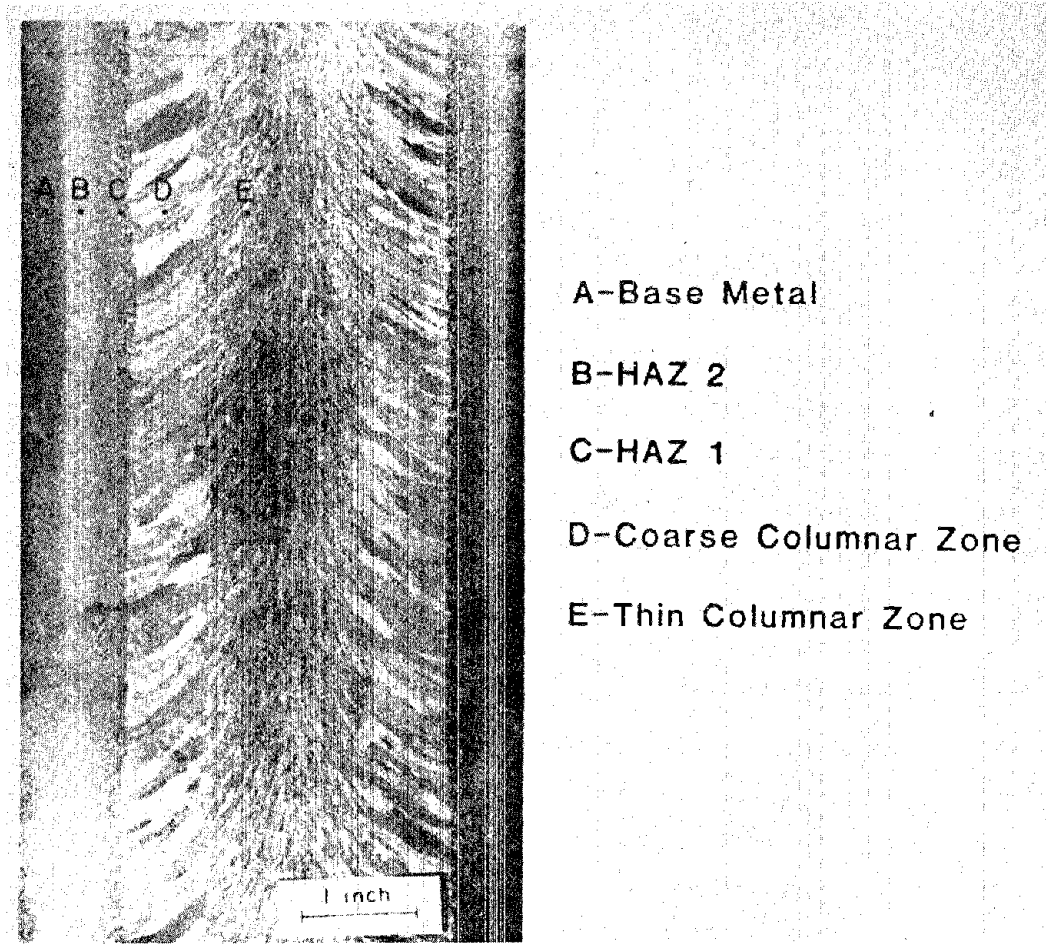


Figure 5. Standard ES weld macrostructure indicating various structural zones present. (Micrograph.)

the CCG zone develops, and, at a certain distance from the fusion boundary, a more refined thin columnar grain (TCG) structure is achieved. Both coarse and thin columnar grains are bordered by proeutectoid ferrite films, and the grain interior consists of a Widmanstätten structure. Transverse solute bands are observed in most electroslog weldments and are caused by temperature perturbations during the solidification process.⁽⁸⁾ The columnar grains do not change either their orientation or their shape while growing across these bands of chemical inhomogeneity.

Coarse columnar grains and thin columnar grains are the major structural zones usually observed in electroslog welds made using water-cooled copper shoes (figure 5). An additional equiaxed grain structure may be present at the weld center in welds made using shoes with no supplemental cooling provisions. Only CCG may exist in welds made with low current and voltage and with a high thickness of base metal per electrode. On the other hand, welds with minimum penetration may consist solely of thin columnar grains.⁽⁴⁾

The structure of the weld is determined by the chemical composition of the melt and the process variable conditions governing the solidification of the weld pool. For instance, the temperature, the holding time of the melt at this temperature, the volume of the weld pool, the direction and the intensity of the heat removal, and the intensity of the agitation of the liquid metal control the weld metal grain size.⁽⁴⁾ A radial-axial grain growth phenomenon occurs during solidification since grain growth is perpendicular to the liquid/solid metal solidus surface at the bottom of the weld pool and, therefore, parallel to the direction of heat flow. The weld center consists of thin columnar grains oriented parallel to the welding direction.

The complex, directional microstructure of the fusion zone of electroslog welds also results in anisotropic weld metal mechanical properties. The influence of various process variables and weld metal chemistry on both

the weld structure and properties, as reported by previous investigators, is reviewed in the following sections.

c. Process Variables

Although the large heat input associated with the ESW process is a major concern, the total weld heat input is not of primary significance in determining the weld characteristics. The interaction of the electrical variables, namely, current, voltage, and slag resistance, as well as the influence of factors such as joint geometry, electrode types and positioning, slag depth, guide tube geometry, welding speed, weld pool agitation, and material being welded determine final characteristics of the weld. Variations in one or more of these conditions may result in significant spatial variations in weld properties. Hence, complete understanding of the influences of these variables on the weld characteristics is necessary to produce welds with consistent structure and properties.

(1) Current, Voltage, and Resistance. A constant voltage dc power supply is standard for ESW. Current and electrode feed rates are interdependent in this system, and increasing the electrode feed rate increases the welding current. Some investigators⁽⁹⁻¹¹⁾ have found a linear relationship between the current and electrode feed rate at a fixed voltage, while Frost et al.⁽¹²⁾ have reported that the current is proportional to the square root of the electrode feed rate at a constant voltage. Irrespective of the exact current-electrode feed rate relationship, the current rise is slower than the rise in the electrode feed rate and leads to a decrease in unit power input with increasing electrode feed rate. (See references 2, 6, 12, 13.) Thus, the current/wire feed rate at a given voltage should be selected carefully to provide the proper unit input power. For example, a higher voltage is required when using low wire feed rates.⁽⁶⁾

Jones et al.⁽¹⁴⁾ have suggested that the weld morphology is controlled by the current and voltage for a particular slag composition since the heat

for the welding process is obtained from resistance heating of the slag ($I^2R;IV$), assuming an ohmic slag heating model. They propose two possible modes of current transfer in ESW based on their "most direct current path" assumption. Current is either transferred from the electrode sides to the plate edges or from the tip of the electrode to the bottom of the pool. It is assumed that both transfer methods occur simultaneously, but one usually predominates over the other. A discussion of resultant heat distribution profiles predicted by this model, assuming a fixed current and varying voltage, is presented below.

The ohmic model predicts that the effective slag resistance is relatively high at high voltages. This high resistance results in a short electrode extension into the slag with most of the heat being generated near the top of the slag pool and causing an increased base metal penetration, although a significant portion of this heat may be lost by radiation. The dominant current transfer mechanism is from the electrode sides to the plate edges, and further voltage increases will eventually result in arcing at the slag surface. On the other hand, ohmic behavior requires a much lower effective resistance at relatively low voltages. This lower resistance leads to electrode extension nearly to the bottom of the slag pool where most of the current then flows from the tip of the electrode to the bottom of the slag pool and provides the maximum heat generation at the bottom of the slag pool. As a result, less heat is available for base metal penetration.

Finally, the electrode will extend a moderate distance into the slag pool with the voltage midway between the extremes, and the heat will be generated primarily in the central region of the slag pool. The portion of the current flowing from the side of the electrode to the side of the slag pool will provide the heat for base metal penetration. Hence, both voltage and current influence the heat distribution.

Two major characteristics influenced by the heat distribution profiles are the shape and the size of the molten weld pool. The shape is expressed

by the term "form factor," while a base metal dilution (BMD) factor indicates weld penetration. The combination of these two factors defines the size of the weld pool. The form factor of an electroslag weld is defined as the ratio between the width and the depth of the weld pool, while the BMD is determined from the relation:

$$\text{Percent BMD} = \frac{b_w - b_g}{b_w} (100) \quad (1)$$

where b_w is the width of the weld, which is taken as the mean value of the measurements at the edges and at the center of the weld, and b_g is the initial spacing between the plates being welded.⁽⁶⁾

The weld grain orientation is determined by the shape of the weld pool as the heat flow and, therefore, the direction of grain growth is perpendicular to the molten pool surface at the solidus interface. Welds possessing a low form factor in which grains meet butt-end to butt-end at the weld center are less resistant to hot cracking. Welds with medium and high form factors have a grain structure meeting at an acute angle at the weld center and are more resistant to hot cracking.⁽⁶⁾ Welds made at higher voltages and lower currents possess high form factors, while those made at low voltages and high currents possess low form factors. As a result, welds made using high current (high-speed welds) are prone to centerline cracking.⁽¹⁵⁾

Voltage influence on BMD is pronounced at medium voltages with the BMD increasing as voltage increases. The heat transfer efficiency is reduced at higher voltages and, as a result, the BMD decreases. The BMD also decreases at lower voltages where decreasing heat input leads to a lack of penetration.^(2,6) Intentional voltage variations have been made in certain investigations to produce diffused fusion boundaries.^(15,16) The current influence on BMD is negligible at medium currents.

It is clear that the current and voltage parameters require very critical selection. Even though theoretical calculations suggest possibilities for welding at low power levels, it is not possible in practice because of the rapid conduction of the heat into the base plates. Frost et al⁽¹²⁾ have considered these current and voltage effects and have suggested an operable range to produce successful welds, as shown in figure 6.

The lowest possible voltage is governed by a threshold level for achieving complete penetration (boundary A). The second boundary (B) is established by a critical energy input below which hot cracking may occur at the weld center. The third boundary (C) is set by the power supply limitation. The final limit (D) is established by the minimum electrode velocity capable of producing defect-free welds.

The final electrical variable, the resistance, is a slag property. The slag must be sufficiently conductive to carry the welding current from the electrode to the weld pool and the edges of the plates without arcing.⁽¹⁷⁾ The electrical resistance of the molten slag controls the current distribution in the slag pool and governs the weld pool shape. A high slag resistance will draw too little current and allow the slag to cool. On the other hand, a low resistance slag will draw excessive current and raise the slag temperature. In turn, this temperature increase may increase the slag resistance. For a stable process operation, the slag resistance should not change appreciably with temperature, and slag viscosity must be in the range between a "sluggishness," which would prevent settling of small metal droplets, and a fluidity, which would leak through small crevices between the shoes and the work.⁽¹⁷⁾ Calcium fluoride additions have been shown to increase the fluidity of the slag and allow lower voltages and increased welding speed, thus reducing HAZ size.^(18,19)

(2) Electrode. The electrode geometry and size play an important role in controlling the heat distribution in the slag and the weld pool. Dilawari et al.⁽²⁰⁾ have suggested two forces which cause fluid motion: 1) buoyancy forces caused by density differences, and 2) Lorentz forces

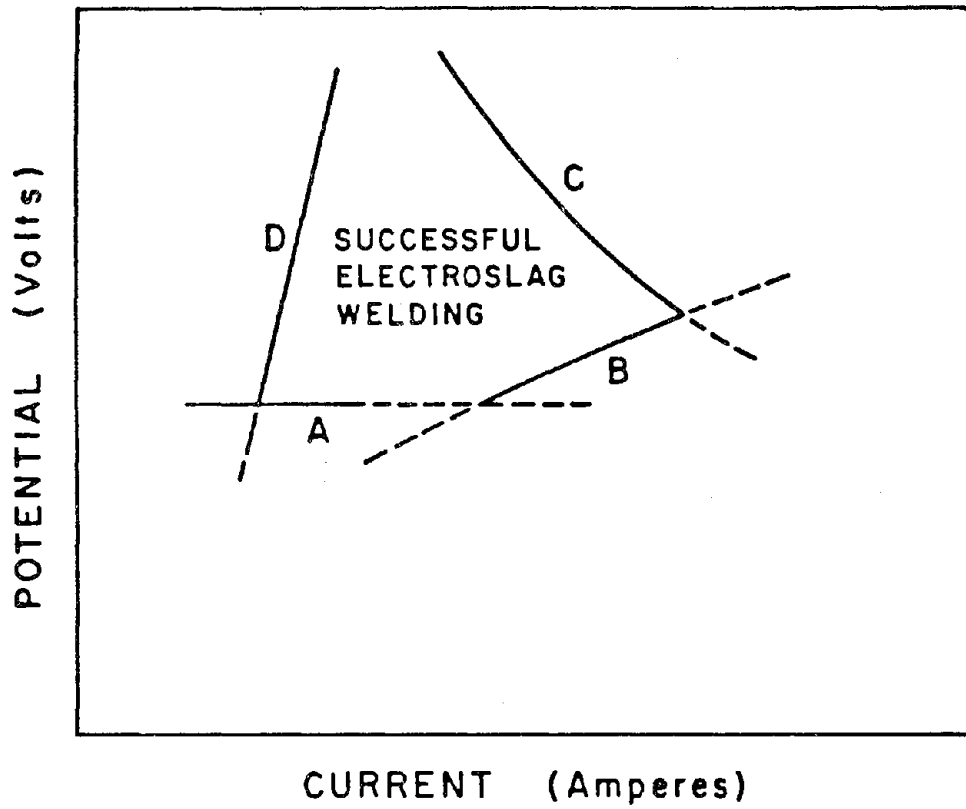


Figure 6. Schematic representation of ES process boundaries for successful joining. (Schematic.)

caused by the interaction between a spatially nonuniform current distribution and the magnetic field. A bend or a "cast" in the electrode affects the Lorentz forces and changes the heat distribution in the weld pool.⁽²⁰⁻²²⁾ Thus, electrode straightening is essential to maintaining symmetrical weld penetration about the weld axis. Jones et al.⁽¹⁴⁾ have shown a drastic anisotropy of HAZ width and penetration occurring in misaligned vertical electroslag welds in which the weld axis is inclined only slightly from vertical. The intensity of heat generation near the electrode can be up to an order of magnitude greater than the heat generated near the slag/plate interface and the variation is significantly larger in the direction of the cooling shoe. By displacing the electrode by about 10 percent from the central planes of symmetry, DebRoy et al.⁽²¹⁾ have shown through theoretical calculations that significant asymmetry occurs in the heat generation irrespective of the heat transport in the slag through conduction and convection. This asymmetry causes an excessive dilution in one plate while producing lack of fusion in the second plate.

Both cylindrical as well as strip (rectangular) electrodes have been used in the past.⁽²³⁾ Dilawari et al.⁽²⁰⁾ have indicated a more efficient electrode melting with the use of strip electrodes.

(3) Slag Depth. Slag pool temperatures in ESW are nonuniform and are several hundred degrees higher than the molten metal pool temperatures.⁽²⁰⁾ These differences lead to a higher heat flux occurring from the slag to the base metal than from slag to the molten weld metal. Thus, a majority of the heat generated in the slag is transferred to the base metal and is used to heat and melt the base metal. The actual heat flux going from the slag to the base metal is governed by the slag pool depth.⁽⁶⁾ Hence, knowing the proper slag depth, and monitoring and controlling it during welding, is mandatory.

Variations in slag depth affect the shape and the size of the weld pool because the heat input is redistributed in the slag pool. The proportion of the heat dissipated from the slag into the base metal increases as

the slag depth increases, while the weld pool becomes deeper and narrower under constant energy input conditions. This action adversely affects the weld metal grain orientation and causes weld center hot cracking.⁽⁵⁾ The decrease in weld width is accentuated by the increased slag volume to be heated.⁽²⁾ A shallow slag pool results in large fluctuations in current and voltage due to periodic electrode arcing to the molten metal pool and enhances the probability of microcrack formation along the proeutectoid ferrite boundaries in the weld center.⁽²⁴⁾ In addition, hydrogen reportedly diffuses easily across the shallow slag pool into the weld metal and causes microcracking.⁽²⁵⁾ Hence, the weld pool shape can be controlled and microcracking eliminated by using a medium slag depth (1-1/2 to 2 in).

A thin layer of slag freezes between the cooling shoe and the weld metal and leads to continuous slag loss during welding. Continuous slag level monitoring and replenishment is, thus, necessary. Probing the molten pool with a wire has been practiced to measure the slag depth intermittently.⁽³⁾ Schwenk et al.⁽²⁶⁾ and Mitchell et al.⁽²⁷⁾ indicate that there is a potential for using acoustic emission monitoring during welding as a method for detecting slag depletion.

(4) Guide Tube Geometry. The standard consumable guide electroslag weld utilizes a cylindrical guide tube to direct the welding electrode into the slag pool. In such cases, the guide tube and the welding gap cross sections are circular and rectangular, respectively. This combination leads to lack of penetration near plate edges when welding at low voltages and/or narrow gaps. Welding at high currents can lead to excessive resistance heating and warping of the guide tube. Evstratov⁽²⁸⁾ has proposed using a larger guide tube cross-sectional area to solve the warping problem, but a large guide tube cross section can also lead to loss in current control because of the large currents required.⁽²⁹⁾

A wing guide tube design in which rectangular fins are welded onto a cylindrical tube meets most of the requirements for a guide tube with optimal cross-sectional area and geometry.^(3,16,30-32) A higher ratio of the

guide-to-gap cross-sectional area also helps to increase the welding speed.^(29,33,34) The wing guide tube can be used for welding plates with varying thickness^(31,35) and eliminates the necessity for electrode oscillation when welding thicker section materials.⁽³⁾ Narrow-gap welds can be made using the wing guide tube without edge penetration difficulties.⁽³²⁾ The guide tube chemistry can be manipulated to alter weld properties since the guide tube constitutes a finite fraction of the weld metal.

(5) Welding Speed. The specific energy used in the welding process and the thermal and physical properties of the metal welded determine the temperature field, heat input, and, consequently, the depth to which plate edges are penetrated and the HAZ is overheated.^(29,34,36) The specific energy, in turn, depends mainly on the voltage, welding current, and welding speed. Two methods of reducing the specific energy are: 1) lowering the welding voltage, which leads to lack of penetration, and 2) increasing the welding rate, which can result in centerline cracking. The latter requires increasing the electrode feed rate and/or reducing the gap to a minimum such that arcing between the guide tube and plate edges does not occur.

The wire feed rates of higher welding currents will reduce the specific energy input and decrease the weld penetration since the rise in the current is slower than the rise in the electrode feed rate.⁽³⁷⁾ Decreasing the specific heat input in standard welds through welding at higher currents/wire feed rates leads to the formation of hot cracks at the weld center since the weld surface in an electroslag weld is in compression, while the weld center experiences triaxial tension as it solidifies last.⁽³⁸⁾ Narrow-gap procedures can reduce these tension stresses and lower hot-cracking susceptibility.⁽¹⁵⁾ Thus, a combination of narrow gap, high welding current, and optimum guide tube geometries can be expected to yield full-penetration, sound welds with no centerline cracking. The reduced specific heat associated with narrow-gap welding can also be expected to improve the mechanical properties and refine the weld microstructure.^(15,23)

A reduced specific heat input will help to control the size and properties of the HAZ. The HAZ characteristics are essentially controlled by the peak temperature experienced and the dwell time above the AC_3 transformation temperature.^(39,40) Eichhorn et al.^(41,42) have suggested that by decreasing the specific heat input, the beginning of coarse grain formation in the HAZ can be shifted to a higher peak temperature because the dwell time in the critical temperature range is shortened. Effectively, the size of the coarse-grained HAZ is decreased.

An increase in welding speed also has been achieved by several investigators through external metal powder additions to the slag pool.⁽⁴²⁻⁴⁴⁾ The metal powder additions increase the metal deposition rate, thereby increasing the welding speed. The powder additions also quench the slag pool as it melts. Both of these effects lower the specific energy input for the weld.

(6) Weld Pool Agitation. Vibration has been reported in the literature to produce grain refinement in solidifying castings.⁽⁴⁵⁻⁵³⁾ Various types of vibrations, including electromagnetic, mechanical, ultrasonic, and impact, have been used. Campbell⁽⁵⁴⁾ has extensively reviewed the effects of vibration during solidification and reported a technique that induces vibration within the solidifying liquid by using a probe inserted into the liquid metal.

Sytrin⁽⁵¹⁾ and Garlic et al.⁽⁴⁵⁾ have suggested that vibration during solidification causes favorable nucleation at higher temperatures and increases the number of crystallite nuclei to provide a fine grain size. Coward⁽⁴⁷⁾ has shown that the effects of vibration depend on process conditions and the material being welded.

There are two generally-accepted hypotheses available to explain the grain refinement achieved in castings through vibration. Garlic et al.⁽⁴⁷⁾ have proposed the "pressure wave theory" in which the pressure wave of vibration decreases the size of the critical nucleus during solidification.

As a result, the rate of nucleation increases to provide grain refinement. The other hypothesis, proposed by Brown et al.,⁽⁵⁷⁾ has attributed the grain refinement to the shear forces originating from the relative flow motion between the solid/liquid metal interface. The shear-dependent mechanism postulates the fragmentation of dendrites to increase the number of nuclei, the viscous shear growth of embryos, and the mixing of the higher melting composition into the lower temperature layers enhancing the nucleation and growth potential at a given melt temperature.

d. Alloy Additions

Culp⁽⁵⁾ has suggested that the proeutectoid ferrite phase bordering the columnar grains provides the least resistance to propagating cracks in low alloy electroslog welds. Other investigators have found imperfections (microcracks, grain boundary separations, and hydrogen-induced cracking) in the proeutectoid ferrite phase.^(7,24,56) Apps et al.⁽⁵⁵⁾ have found an improvement in the Charpy impact toughness of the weld metal with a reduction in the amount of the proeutectoid ferrite phase.

Several investigators have controlled the amount of proeutectoid ferrite by adding alloying elements, such as molybdenum, manganese, chromium, etc., to the weld metal.^(41,57,58) Alloy additions also result in refined microstructures and improved mechanical properties.^(33,55,58,59) Kawaguchi et al.⁽⁶⁰⁾ have shown that reducing the silicon content promotes polygonal ferrite formation in certain welds and improves weld toughness. Meanwhile, Medovar et al.⁽⁶¹⁾ reported that silicon, phosphorus, and sulfur reductions improved the hot-cracking resistance. These microstructure and mechanical property improvements can be achieved in low-alloy structural steel weldments through selective weld-metal additions which can be made through flux, guide tube, and electrode modifications. The level of additions must be chosen carefully to accommodate the base metal dilution in the weld metal and the slag/metal reaction.

Alloy additions cannot be made through fused fluxes as they react during the fusion processing of the flux.⁽⁶²⁾ Unfused fluxes must be used for such additions. Suzuki⁽⁶³⁾ has used an insulated consumable guide tube containing Ferro-Molybdenum as an alloying agent to strengthen the weld. Alloy additions through the welding electrode is the most effective method as more volume of wire is melted during welding than either the flux or the guide tube. Both solid and flux-cored type wires have been used in the past for this purpose.^(20,64)

e. Mechanical Properties

Mechanical properties criteria for nonconventional welding techniques, such as ESW, are usually taken from recommendations valid for conventional welding processes. Thus, Charpy impact toughness evaluation serves as an initial qualification test for electrosag welds. Charpy impact toughness evaluations of electrosag welds have, in general, revealed low toughness values in both the weld centerline (WCL) and the coarse-grained HAZ.^(5,19,20) This has led to considerable controversy over whether Charpy specimen results are valid for the large-grained microstructures found in electrosag weldments where the total Charpy volume may be enveloped in two or three grains.⁽⁶⁵⁾

In general, a coarse grain structure indicates a higher susceptibility to brittle fracture, particularly in going from a wrought to a cast structure. However, Charpy impact results for specimens tested with the resultant crack running in the direction of welding indicate that the CCG zone is tougher than the WCL zone made up of thin columnar grains.⁽²⁾ A complicating factor in this comparison is the large variations in Charpy toughness evident at the WCL.⁽⁶⁶⁻⁷⁰⁾

Several investigators believe that Charpy toughness evaluations do not rate welds in their true order of practical resistance to fracture failure.^(15,38,66,67,71) They argue that the failure of electrosag welds to reach the Charpy impact energy values of weld joint toughness analogous to

those of manual or submerged arc weld joints, or to achieve the weld joint toughness equivalent to that of the base metal, may not express the true resistance of the whole welded joint toward brittle failure under real loading conditions. Thus, the suggestion has been made that other testing methods, such as the Pellini drop weight test or full thickness CTOD test, be used to evaluate electroslag welds that fail to meet Charpy toughness requirements before requiring heat-treatment procedures.^(15,67)

f. Postweld Heat Treatment

Postweld heat treatments of electroslag welds are employed when the electroslag welded joint toughness properties in the as-welded condition are considered inadequate. A postweld heat treatment, if properly selected, will increase the weld toughness and reduce mechanical property variations across the joint.⁽⁷²⁾ There are, basically, three types of postweld heat treatments applied to electroslag weld joints. First, a normalizing treatment is performed above the AC_3 transformation temperature (approximately 900°C).^(29,73) However, distortion problems frequently have been encountered when this treatment is used. Secondly, an inner critical anneal made below the AC_3 temperature at 780°C to partially recrystallize the welded joint has been reported by Patchett⁽²⁹⁾ to reduce distortion. Finally, a stress relief treatment has been carried out at about 650°C .^(38,57,59) Additionally, localized normalizing of electroslag welds has been studied by Soroka.⁽⁷⁴⁾

The response to these different heat-treatment techniques varies widely from alloy to alloy, and depends mainly on the base and weld metal chemistry. Resultant fusion zone and HAZ properties for a given alloy may increase, decrease, or be unaffected by various heat treatments, while another relatively comparable alloy may react to similar treatments in an entirely different manner. Thus, the decision to use a postweld heat treatment and to use a specific type of treatment must be made with care.

2. Overview of Previous PNL/OGC Results

This section presents an overview of the prior PNL/OGC study experimental procedures and the results that impacted phase two research directions. Comprehensive presentation of the results and conclusions reached in the PNL/OGC study are presented in DOT Report No. DOT-FH-11-9612.

The experimental work consisted of fabricating and, subsequently, evaluating electroslog welds in typical highway bridge steels. Both A588 and A36 steels in 25-mm, 55-mm, and 76-mm thicknesses were procured, but the majority of ESW experiments involved 50-mm thick A588 steel. All ESW was performed with the consumable guide method. Various innovative welding techniques were assessed, including varying the initial plate gap, increasing the welding current, and using winged and shrouded guide tubes. A standard 12.5-mm diameter mild steel guide tube (Hobart Type 48), with three standard ceramic consumable insulators placed at regular intervals, was used for the majority of the welds fabricated in this program. Various innovative guide tube configurations were also used to achieve complete edge fusion during the fabrication of narrow-gap, controlled base-metal dilution, and grain refinement electroslog welds (figure 7).

a. Process Variables Results and Discussion

Several process variables exert a strong influence on the resulting electroslog weld and on weld consistency and quality. It was found that the proper selection and control of these variables are necessary to reproducibly produce optimum welds. The first process variable studied was guide tube centering. Welds with off-centered and centered electrode positions with both single and double ground connections were fabricated. When a single ground was used, weld penetration into the grounded plate was enhanced with either a centered or off-centered electrode. Similarly, more penetration into the plate occurred closer to the electrode in welds made with an off-centered electrode for either single or double grounding. Grounding both plates, positioning the guide tube (electrode) within 1.5 mm

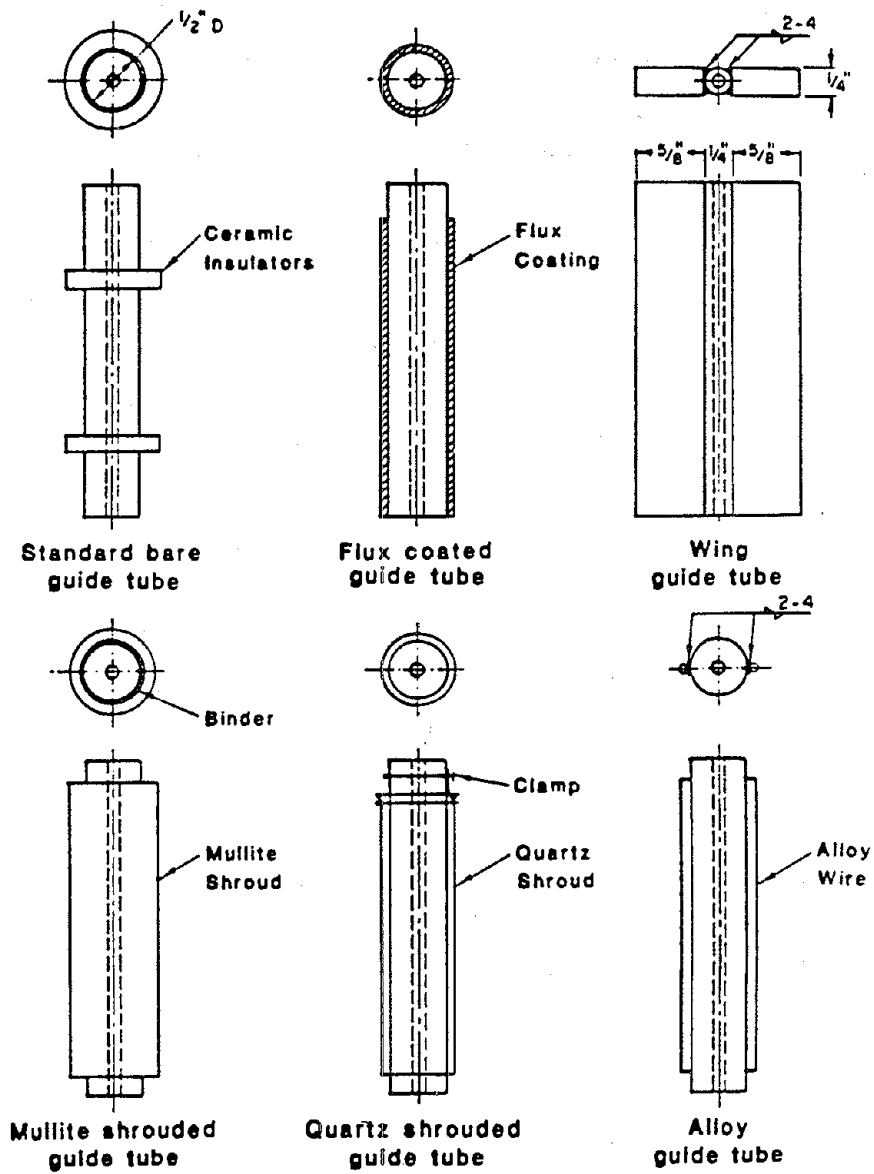


Figure 7. Schematic representation of various consumable guide tube designs used in the investigation. (Schematic.)

from the geometric center of the joint gap, and eliminating electrode cast provided a symmetrical weld with equal penetration into both of the plates, figure 8.

A second process control variable is the slag level. Heat generation during the ESW process occurs mainly in the slag pool. Hence, the slag level used during welding and the constant maintenance of this level are critical in establishing and maintaining steady-state welding conditions.

The continuous loss of the slag freezing between the cooling shoes and the solidifying metal necessitated flux additions during welding to maintain a proper slag level. The quantity and the frequency of these additions were found to be critical since they affect the thermal equilibrium established during the process and, thus, influence weld characteristics.

Fluctuations in the current and the voltage are affected by slag depletion during ESW. Photographs of the voltage-current display taken at three different slag levels are shown in figure 9. Optimum slag level was maintained and/or reestablished by adding flux until the current level reaches the stage shown in the top photo in figure 9.

Intermittent flux additions can be avoided by using a continuous flux feeding device. A continuous flux addition maintains a constant slag level throughout the process without affecting its dynamic thermal equilibrium. Current and voltage fluctuations associated with continuous flux additions were found to be minimal.

Operating characteristics of the standard ESW consumable guide technique were compared with those for narrow gap welding with a cylindrical guide tube, and with those for winged guide tube welding in a standard and a narrow gap configuration. A detailed study was undertaken to determine the effects of changing voltage and current (electrode feed rate) and changing the joint gap. The use of the winged guide tube was also studied; this guide tube design has the potential for reducing the susceptibility of

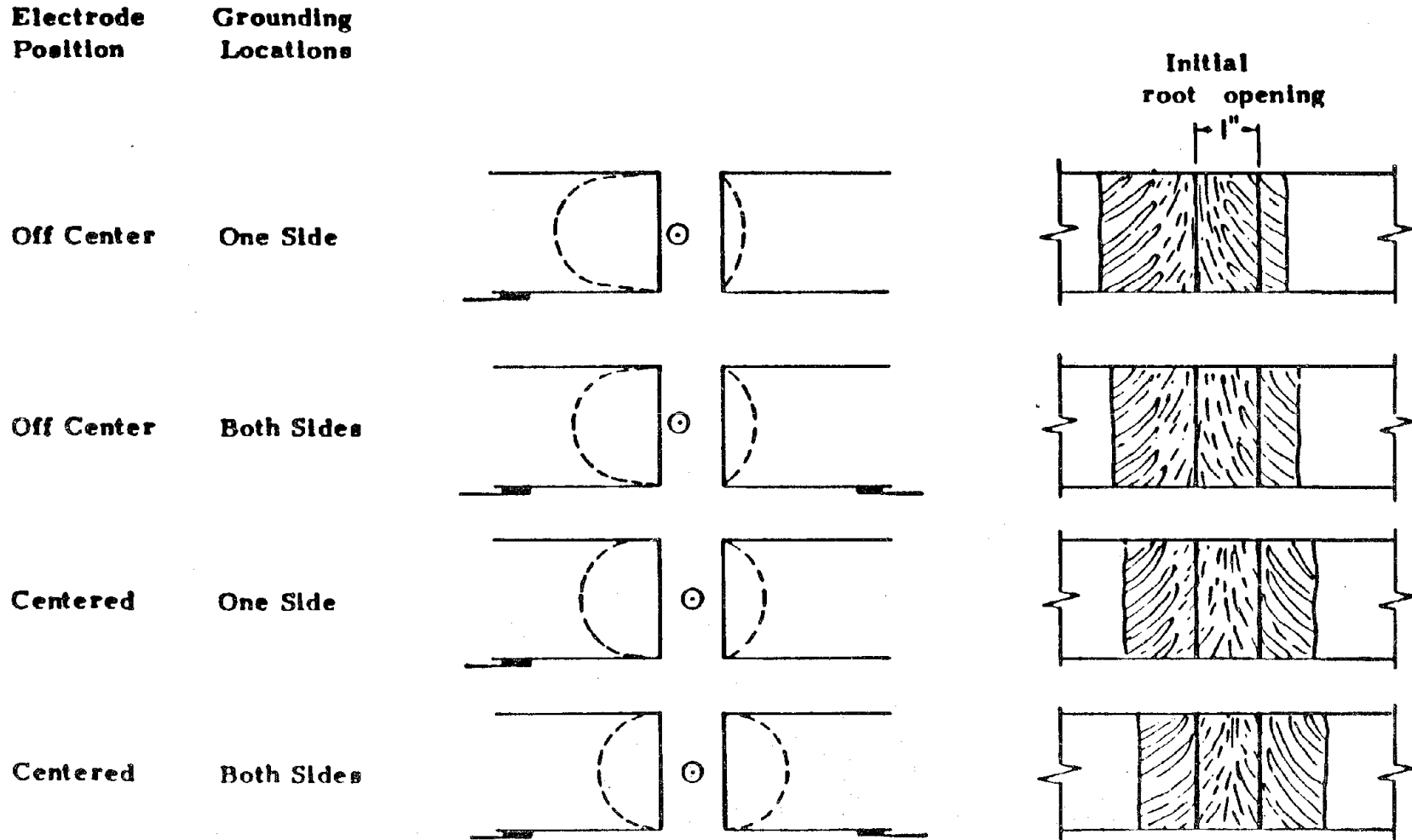


Figure 8. Summary of effects of ground location and electrode positioning on ES weld penetration. (Schematic.)

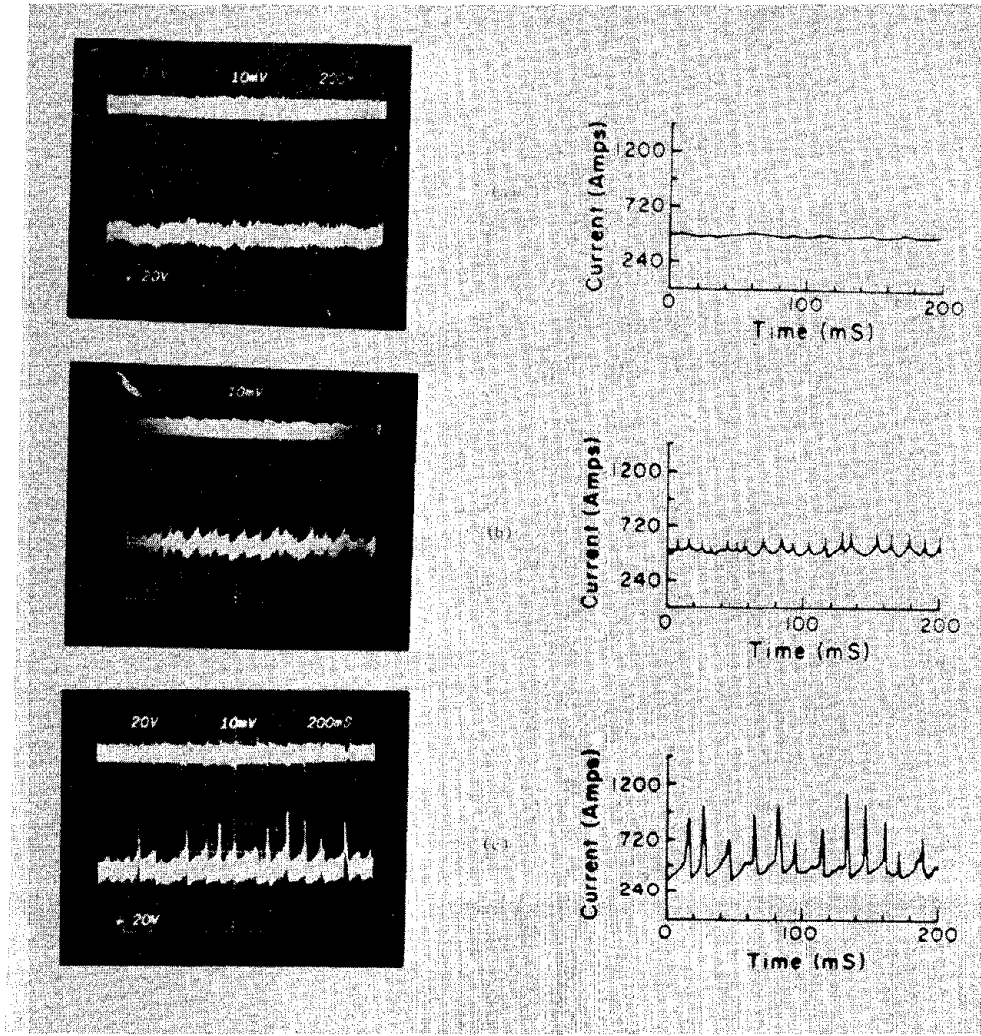


Figure 9. Oscilloscopes illustrating the sequence of slag depletion during the welding process. (Schematic.)

electroslag welds to lack-of-edge penetration defects--a major and persistent shop fabrication defect--due to its shape symmetry with the joint gap.

The welding voltage was found to essentially control weld penetration (figure 10), and, therefore, has a direct effect on the propensity for lack-of-edge penetration defects. The welding current had a minimal influence on the base metal dilution.

At any given voltage and current, narrow-gap winged guide tube electroslag welds possess maximum base metal dilution while standard-gap cylindrical guide tube electroslag welds have the minimum. At any given voltage and current, narrow gap welds possess a higher percent base metal dilution in comparison to standard gap welds, irrespective of the guide tube design used (figure 10).

The current versus wire feed rate relationships for various guide tube designs and joint spacings are shown in figure 11. For any given current value, narrow-gap electroslag welds exhibited lower wire feed rates in comparison to standard gap electroslag welds, irrespective of the guide tube design. The winged guide tube design used lower wire feed rates than the cylindrical guide tube design in welds made with identical joint spacing at any given current. The current versus electrode feed rate relationships showed a decrease in the electrode feed rate with the use of narrow joint spacings as well as winged guide tubes for any given current setting.

Current and voltage fluctuations occur when the guide tube interacts with the slag pool and during electrode arcing to the molten metal pool. Periodic current fluctuations due to guide tube melt off were observed in standard welds made with the cylindrical base metal consumable guide tube. Macrostructural analysis of these welds revealed a relationship between such fluctuations and solute banding in welds. This relationship is illustrated in figure 12.

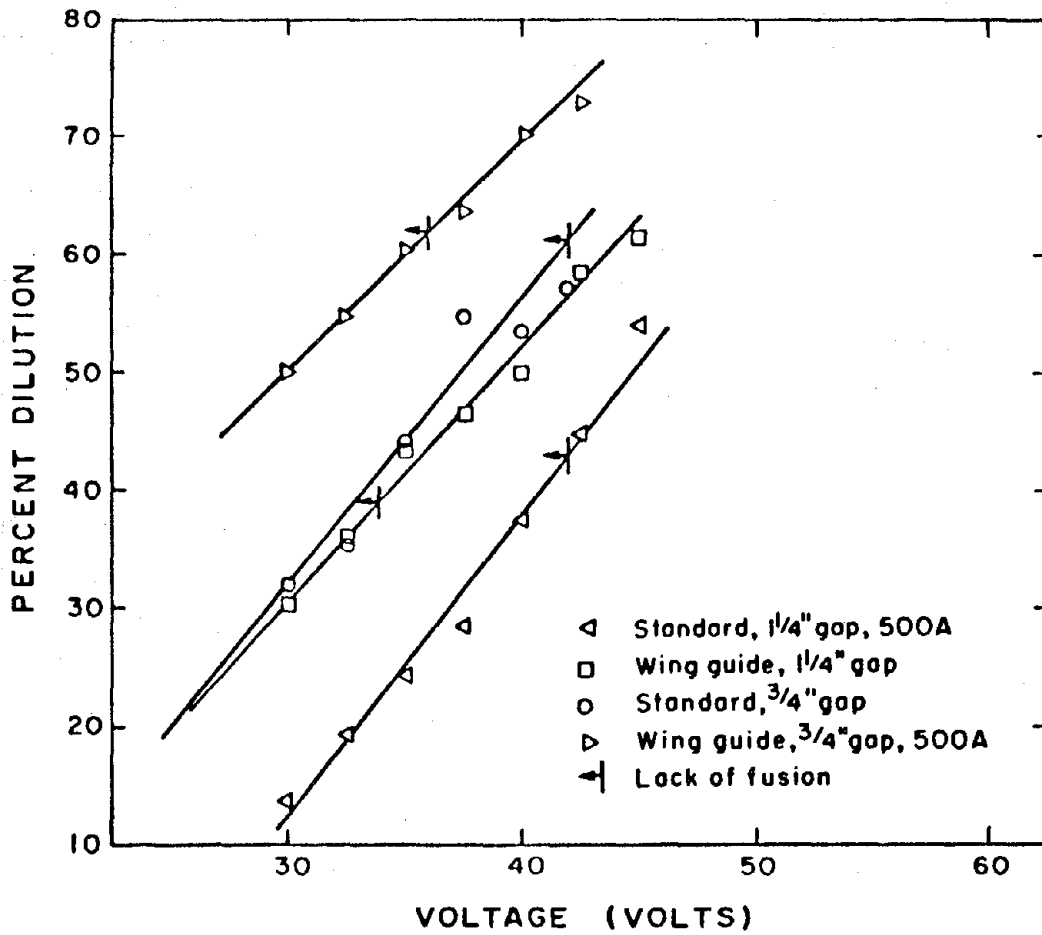


Figure 10. Effect of welding voltage on base metal dilution for various guide tube geometries and joint spacings in ESW. (Schematic.)

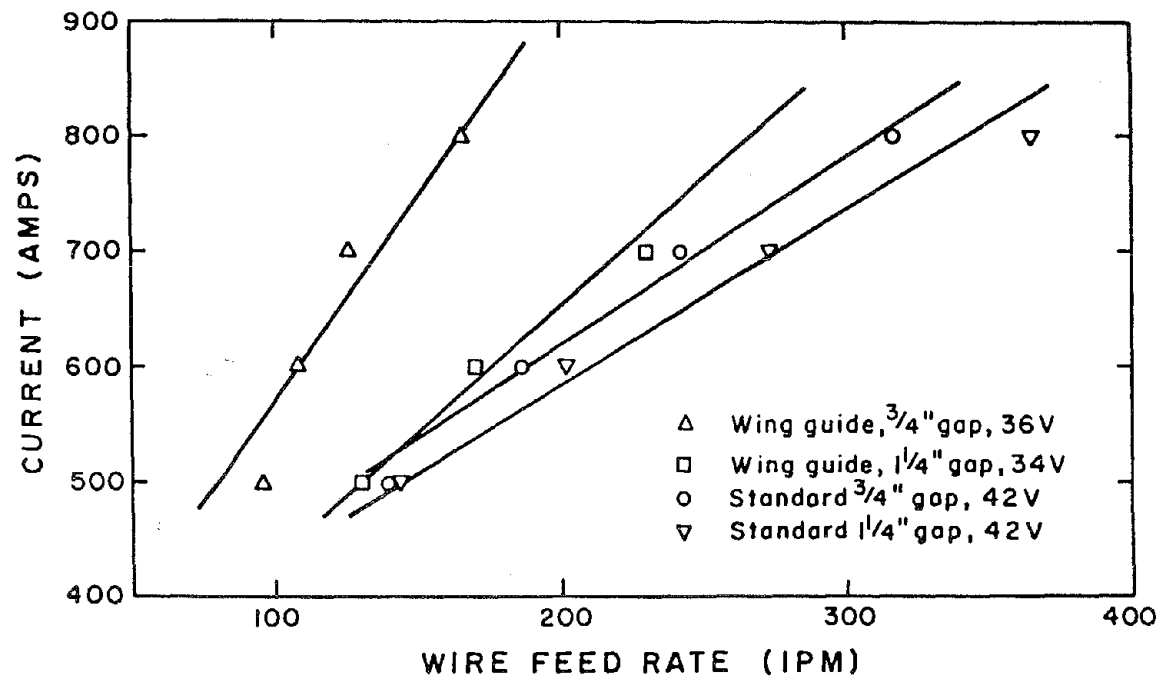


Figure 11. Relationship between welding current and wire feed rate for various guide tube geometries and joint spacings in ESW. (Schematic.)

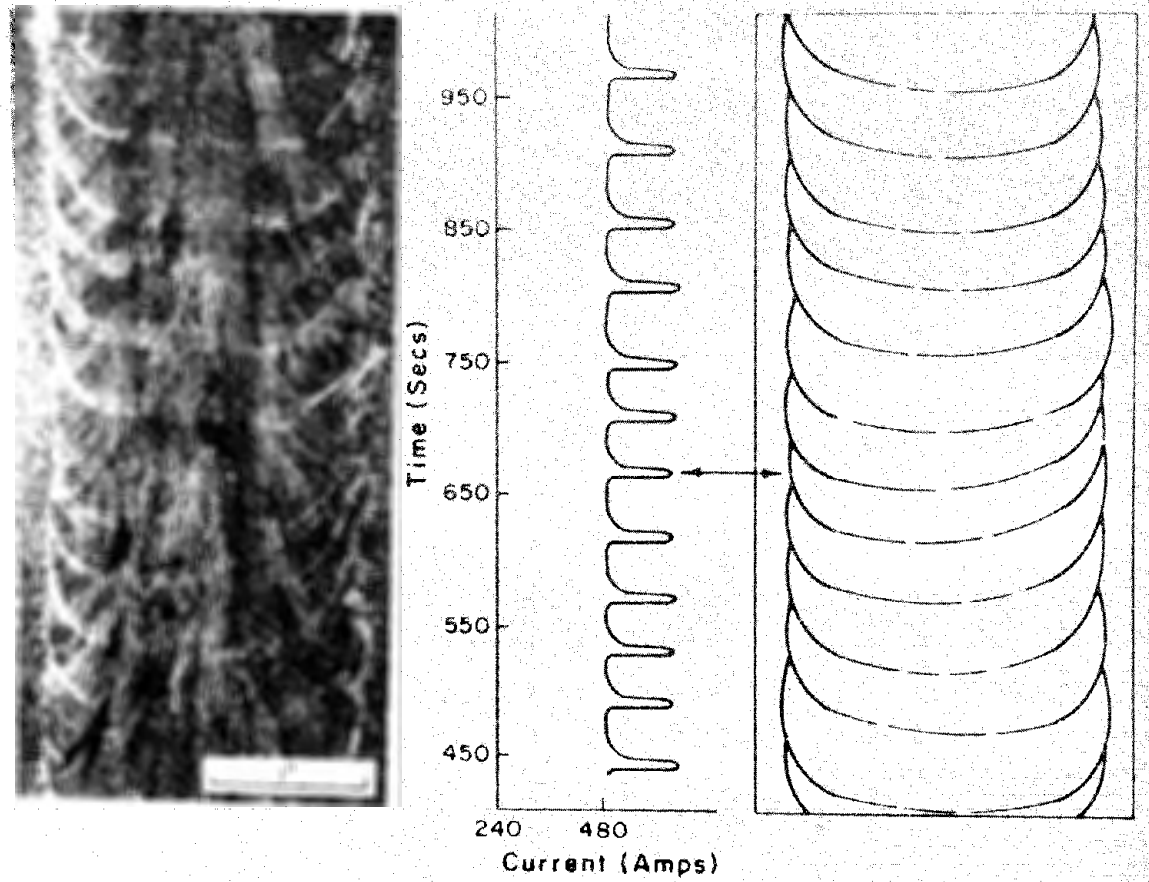


Figure 12. Trace of macroscopic current fluctuations on the electroslag macrostructure. (Micrograph and Schematic.)

The high current, narrow-gap, winged guide tube welds were produced exhibiting about 50 percent of the heat input of that required for standard welds. The welding time was also reduced to 1/3 of that required for the standard procedure, while the fusion zone width of the high current, narrow-gap, winged guide electroslog weld was much smaller than that of the standard weld.

Weld center microstructures indicated significant refinement for high current, narrow-gap, winged guide welds, and the proeutectoid ferrite films bordering the grain boundaries were well dispersed as opposed to continuous films present in standard welds. The solidification structures for both welds were of cellular morphology with the average cell spacing in the narrow gap weld 50 percent smaller than in the standard weld.

A marked reduction in the coarse-grained HAZ width was achieved in high current, narrow-gap, winged guide electroslog welds. The HAZ width was about half of that in standard welds. However, the first few grains of the HAZ adjacent to the fusion line were comparable in size for both welds and were surrounded by proeutectoid ferrite. Thus, the peak temperature/times experienced in that region were high enough for both welds to cause undesirable grain growth and solid-state transformations in the HAZ.

b. Fusion Zone Microstructure Control

Structural steel electroslog welds are known to exhibit a high degree of undesirable solidification segregation and grain growth. The resultant grain growth is accompanied by undesirable microstructural constituents. Two basic approaches to modifying fusion zone microstructure were successful. One was the use of quartz-shielded guide tubes. The use of quartz-shielded cylindrical guide tubes essentially eliminated fusion zone columnar structure and resulted in an equiaxed grain across the complete fusion zone. The second approach was to add alloying elements to the filler material to suppress proeutectoid ferrite formation.

Several different alloying element combinations were added as weld wire filler metal in an effort to reduce the amount of proeutectoid ferrite present in the standard A36 welds.

The macro and microstructures of the electroslag weld made with chromium-molybdenum (Cr-Mo) wire consisted of a bainitic microstructure. Complete absence of proeutectoid films in the alloyed weld metal was found. A high current, narrow-gap, winged guide tube weld was made with Cr-Mo wire, and the bainitic-ferrite structure was again present without the proeutectoid ferrite present in A36 wire welds.

c. Charpy V-Notch Impact Toughness

Mechanical property assessment of electroslag welds is complicated by two major factors: 1) the extreme anisotropy of the weld structure, and 2) the very large grain size commonly associated with electroslag welds. Great care was taken during this program to achieve constant form factor and percent dilution over the complete weldment length so that a given specimen would be representative of the average microstructure of a given weld zone.

CVN impact energy values were determined at 0°F for A588 base metal and for the various structural zones of several A588 electroslag weldments. The weld centerline data from these tests are plotted in figures 13 and 14.

None of the various welding techniques tried using 25-P wire was capable of raising the average impact energy above 15 ft-lb (figure 13). Figure 14 presents Charpy impact data for the various alloy wires used in this task. The only alloy that substantially improved the standard gap impact properties was the high Si:2-1/4 Cr:1 Mo.

The use of the narrow gap, winged guide tube technique increased the impact properties for both of the weld wires used (figure 14). It increased the average impact values as well as increased the minimum impact

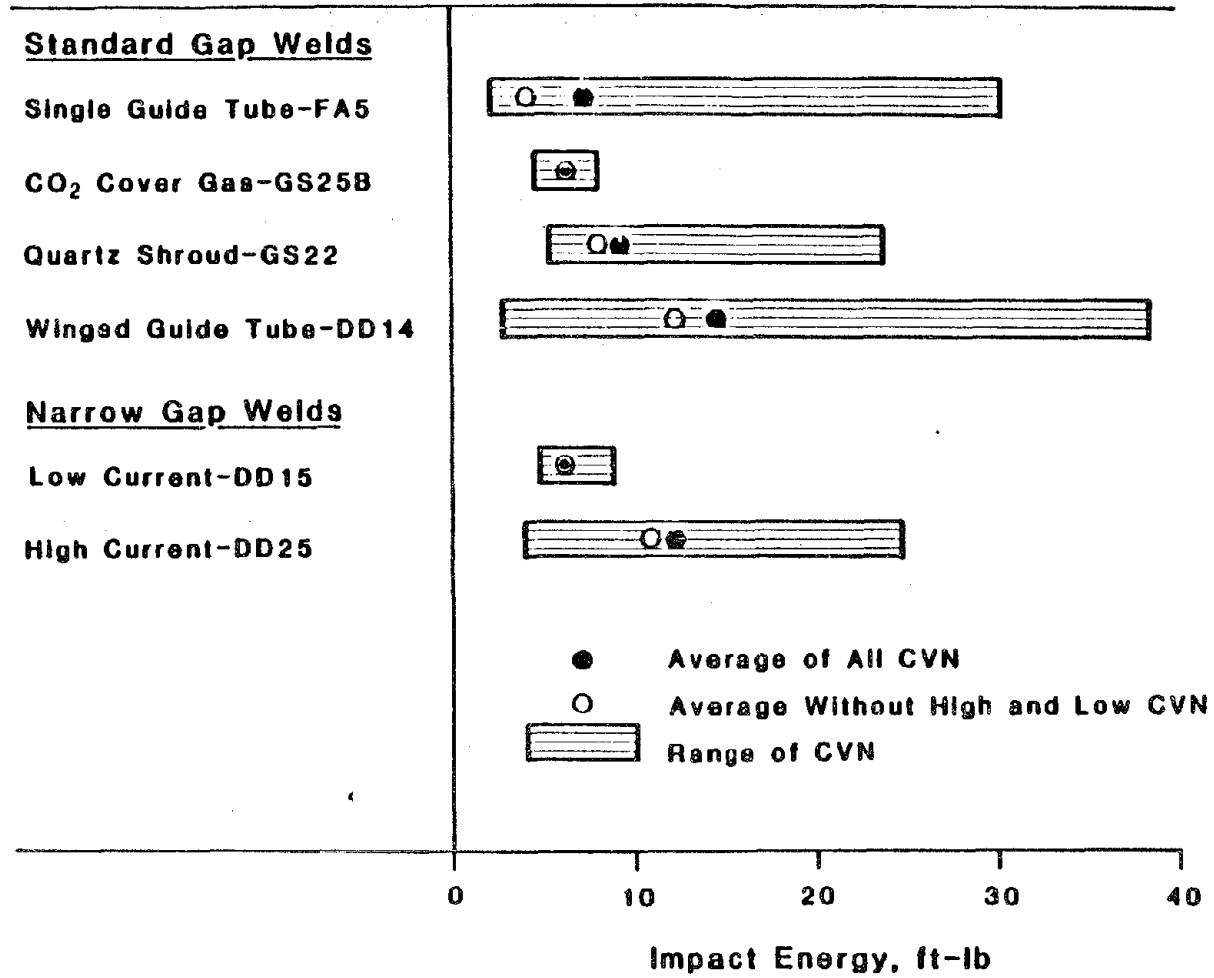


Figure 13. ES weld centerline 0°F Charpy impact energy for 25-P weld wire weldments. (Schematic.)

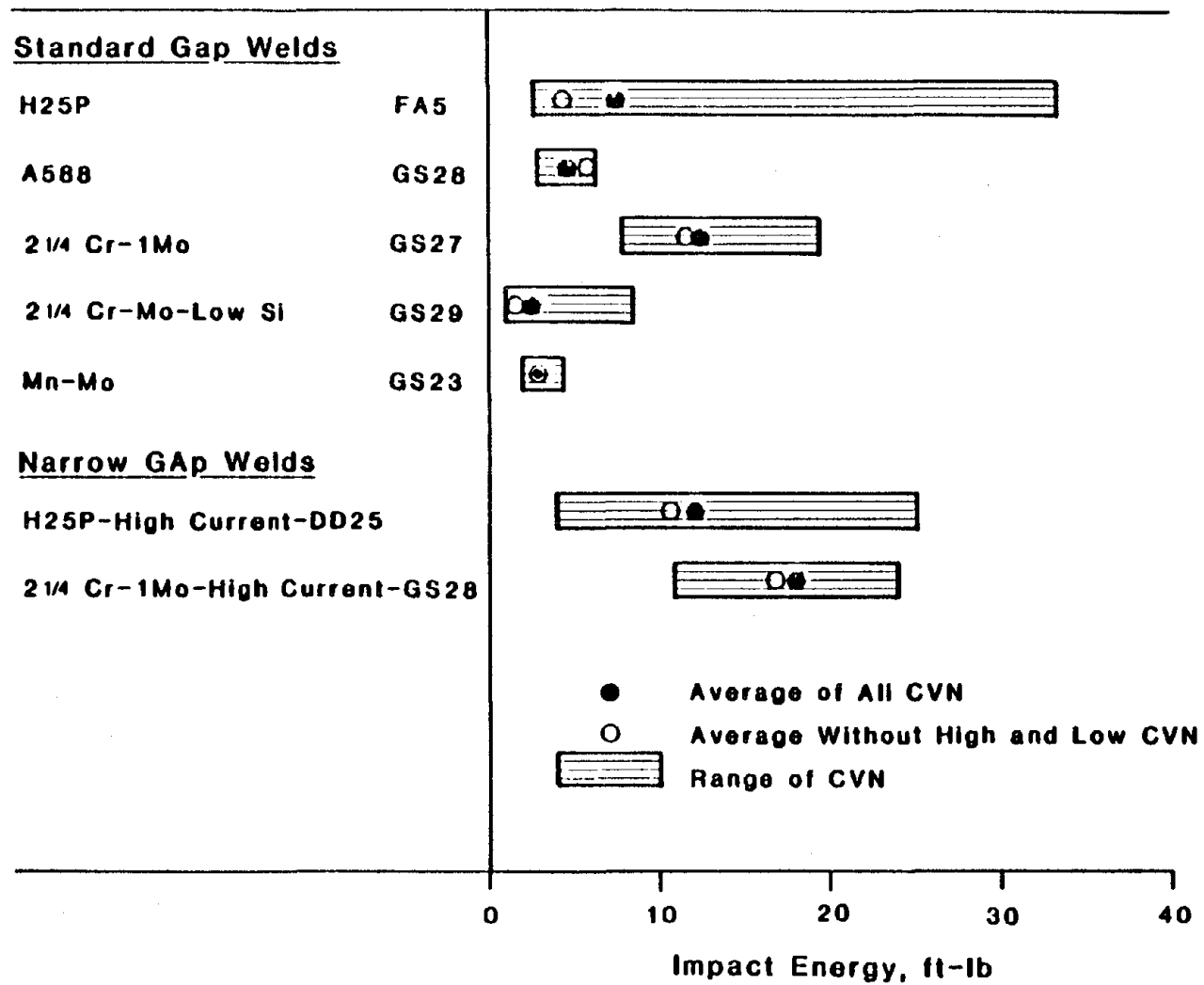


Figure 14. ES weld centerline 0°F Charpy impact energy as a function of weld wire alloy. (Schematic.)

values. The average impact value of the 2-1/4 Cr:1 Mo weld wire weldment was over 15 ft-lb at 0°F, while the minimum value was over 10 ft-lb.

A composite plot of all the HAZ impact energies is shown by the welding technique in figure 15. The data show that there is a considerable scatter in expected HAZ impact values, but that the minimum and average values are relatively independent of welding technique. The average HAZ value is below 15 ft-lb.

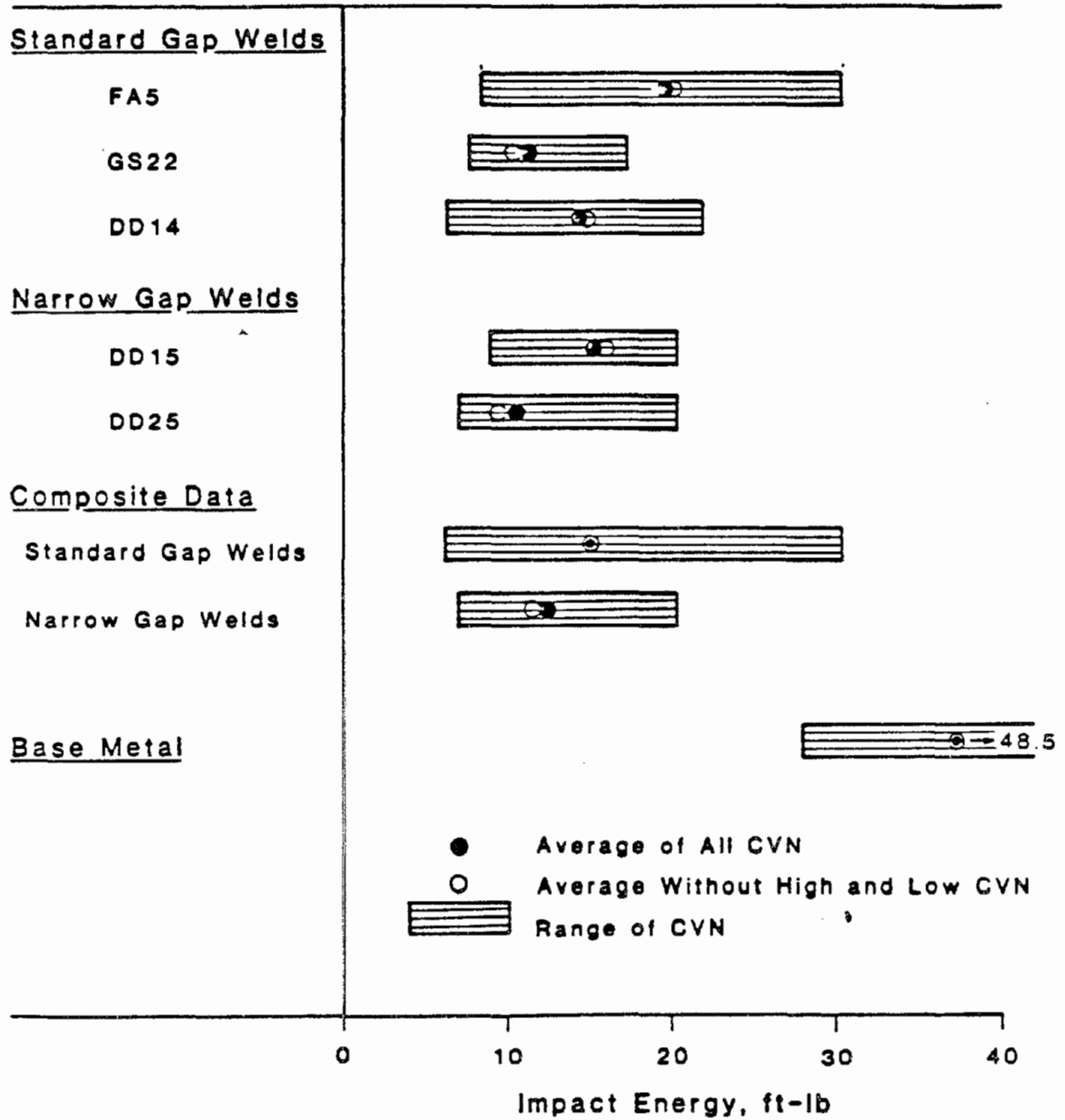


Figure 15. Heat affected zone 0°F Charpy impact energy of ES weldments. (Schematic.)

III. MATERIALS

1. Alloy

The base metals used for this investigation included ASTM A36 and A588 structural steel plates in 50-mm (2-in) and 76-mm (3-in) thick sections. The winged and webbed guide plates were made of type 1010 mild steel. The chemical compositions are given in table 1. The microstructures of as-received plate materials are shown in figure 16.

2. Flux

The commercial Hobart 201 flux was used for starting and running in most welds, except for the modification of quartz shroud welding. In order to improve the welding quality of quartz-added welds, high conductivity and low oxygen potential fluxes were introduced. The main constituents of those special fluxes were CaF_2 , CaO and Al_2O_3 , which were designed as different fractions of combination. These low-oxygen-potential fluxes were also applied on selected regular welds. Tables 2 and 3 provide this information in detail.

3. Electrode Filler Wire

Several electrode filler wires were used in this investigation. Low-carbon steel wire, Hobart 25P and Linde WS, respectively, matched the compositions of A36 and A588 base metals. To develop suitable alloy additions, Page AS521, Airco AX90, and Stody TW8544 wires were deposited. All chemical analysis data are included in table 1. All weld wire had a diameter of 2.38 mm (3/32 in).

Table 1. Composition of base metal, weld filler wire and guide plate materials.

Material	C	Mn	Si	Cr	Ni	Mo	Cu	S	P	V
<u>Base Alloy</u>										
A-36	0.17	0.92	0.20	0.02	0.10	--	0.20	0.02	0.01	0.06
A-588	0.18	1.20	0.37	0.56	0.16	--	0.32	0.02	0.01	0.08
<u>Filler Wire</u>										
Hobart-25P	0.11	1.12	0.50	--	--	--	0.32	0.02	0.02	--
Linde-WS	0.09	0.50	0.30	0.55	0.50	--	0.30	0.03	0.02	--
Hobart PS-588	0.07	1.10	0.50	0.50	0.80	1.00	0.45	0.01	0.01	--
Page-AS521	0.10	0.80	0.50	2.25	--	1.00	--	0.03	0.02	--
Airco-AX90	0.08	1.40	0.46	0.06	2.10	0.40	--	0.02	0.02	0.007
Stoody-TW8544*	0.03	1.20	0.45	--	2.30	0.45	--	0.02	0.02	0.05
<u>Guide Plate</u>										
1010	0.10	0.45	--	--	--	--	--	0.05 (max)	0.04 (max)	--

* Stoody powder-cored tubular wire.
Balance: Fe

Table 2. Flux chemistries used in this program.

1. Hobart PF201

2. 100% CaF₂

3. Mixtures of CaF₂-Al₂O₃-CaO

(1) 50% CaF₂ - 25% CaO - 25% Al₂O₃

(2) 33% CaF₂ - 33% CaO - 33% Al₂O₃

(3) 80% CaF₂ - 10% CaO - 10% Al₂O₃

4. Hobart PF201 + CaF₂-CaO-Al₂O₃ Flux

(1) 1/2 (Hobart PF201) + 1/2 (50% CaF₂ - 25% CaO - 25% Al₂O₃)

(2) 2/3 (Hobart PF201) + 1/3 (50% CaF₂ - 25% CaO - 25% Al₂O₃)

Table 3. Hobart PF201 running flux chemistry.

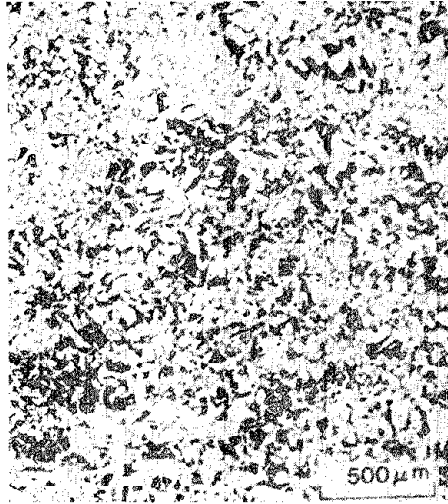
Compound	Amount (wt.%)
CaO	12.20
MgO	2.34
MnO	22.46
SiO ₂	32.95
CaF ₂	8.62
Al ₂ O ₃	8.32
TiO ₂	8.02
K ₂ O	0.88
Na ₂ O	0.57
FeO	1.81
P ₂ O ₅	0.05

Basicity* - 0.9 (neutral)

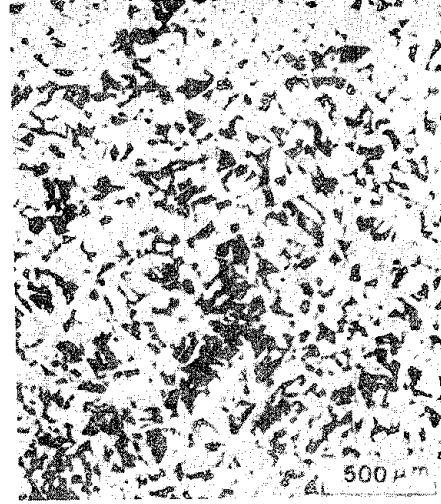
*Basicity index (B.I.) is determined using the relation

$$\text{B.I.} = \frac{\text{CaO} + \text{MgO} + \text{CaF}_2 + \text{Na}_2\text{O} + \text{K}_2\text{O} + 1/2(\text{MnO} + \text{FeO})}{\text{SiO}_2 + 1/2 (\text{Al}_2\text{O}_3 + \text{TiO}_2)}$$

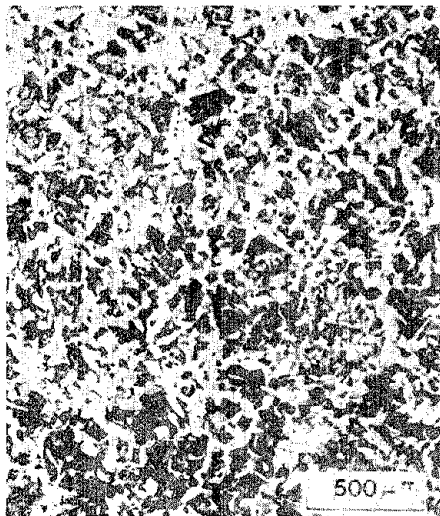
(Each component: mole fraction)



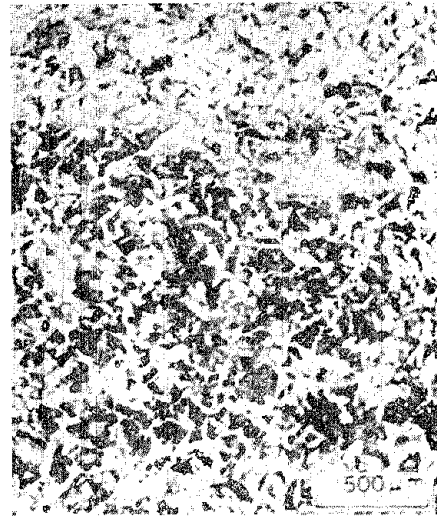
A36, 50 mm thick



A36, 76 mm thick



A588, 50 mm thick



A588, 76 mm thick

Figure 16. Microstructures of as-received alloys. (Micrographs.)

4. Identification System

Each weldment for macrostructural and microstructural analysis, CVN specimen, K_{IC} fracture toughness specimen, I-beam fatigue test specimen, and defect formation weld was coded with a special identification number. The details of the numbering systems are shown in figures 17-21.

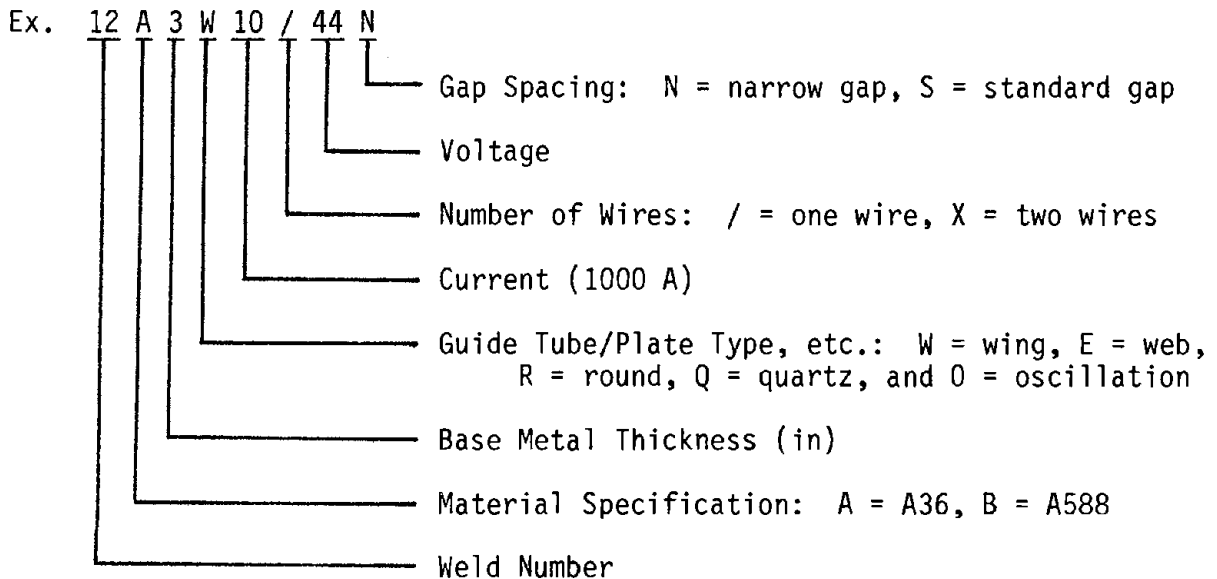


Figure 17. Weldments for macro/microstructural analysis identification system.

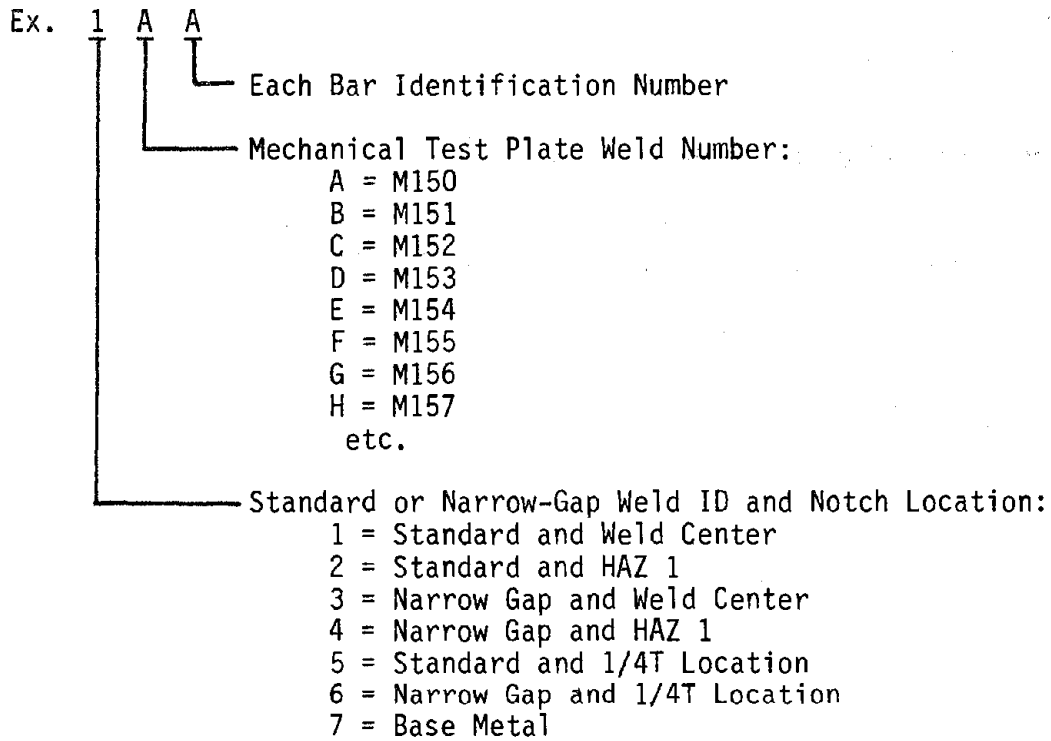


Figure 18. CVN specimen identification system.

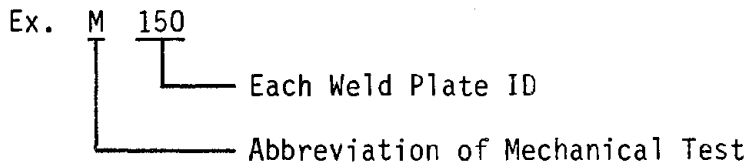


Figure 19. K_{IC} fracture toughness specimen identification system.

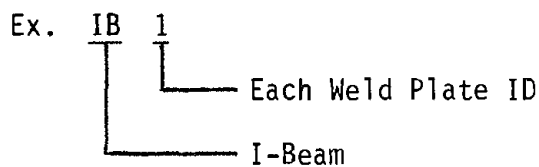


Figure 20. I-beam for fatigue test identification.

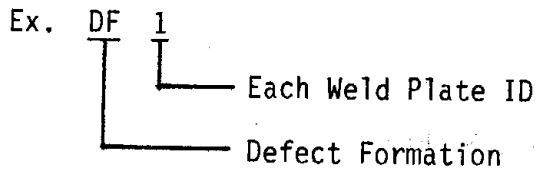


Figure 21. Defect formation weld identification system.

IV. EXPERIMENTAL PROCEDURES

1. Welding Related

a. Conventional and Consumable Guide ESW

There are two major types of ESW processes: 1) conventional, and 2) consumable guide. In the conventional method, a non-consumable contact tube is used to direct the filler electrode into the molten weld pool (figure 1). The contact tube is moving to maintain a position about 50 mm above the slag pool surface, which requires the entire welding head along with the cooling shoes to move up together at a predetermined rate consistent with the welding speed.

The consumable guide method uses a guide tube to direct the filler electrode into the molten weld pool. The guide tube also carries the current until the electrode passes from it. As the name implies, the guide tube, along with the filler electrode wires, is consumed into the weld pool as the weld progresses. This method involves no moving parts except the welding electrode wires (figure 1). The principle of this method is illustrated in figures 2 and 3. All welds were made by the consumable guide method for this investigation.

The guide tube (or plate) is a key part in successful electroslag welding. Standard 12-mm round or 16-mm round guide tubes have limited the current-carrying capacities and tend to generate excess heat in the middle at the expense of the edges, thus contributing to lack of fusion and undercut condition. A far more efficient way to distribute the heat across the slag bath, reduce the amount of filler metal and greatly increase the current-carrying capacity employs the plate consumable guide configuration. Based on the understanding of previous OGC studies under FHWA Contract No. FH-11-9612, the winged and webbed guide plates were designed for this purpose. Only a few welds were made with a standard guide tube for comparison. The configuration and dimension of the standard guide tube and the

winged and webbed guide plates are shown in figure 22. The winged guide plate was designed for joining 50-mm base metals while the two types of webbed guide plates were designed for joining 50-mm and 76-mm base metals, respectively. The guide plate design is very useful in making thicker joints, since it avoids the complexity of guide tube oscillation and produces an even weld metal penetration.

Water-cooled copper shoes were used to dam the weld and slag pools and extract the heat. The permanent shoe assembly consisted of an aluminum box for water circulation that was sandwiched between a copper and aluminum backing plate. The copper plate confined the weld, and a weld reinforcement depression was machined into its face. The shoe was wedged in place between the joining plates and the strongback during welding.

b. Narrow Gap

The plates were positioned with a 19-mm gap between the vertical faying edges. In comparison with the conventional 32-mm joint gap, the narrow gap technique significantly reduced the weld-related cost and time. To evaluate the improvement of narrow-gap welds, standard-gap welds were made for comparison.

c. Flux Addition

Because slag freezes between the cooling shoe and the weld metal during the ESW process, slag depletion occurs as the weld progresses. This slag loss was compensated for by a continuous flux addition using a precision metal-powder feeder system manufactured by TAPCO International. In this system, flux stored in a hopper flows through a tube into a cylindrical reservoir. A paddle wheel rotated by an electrically-driven variable speed dc motor scoops the flux from the reservoir and transfers it down a tube into the slag pool. The rate of flux addition can be controlled by both motor speed and paddle wheel size.

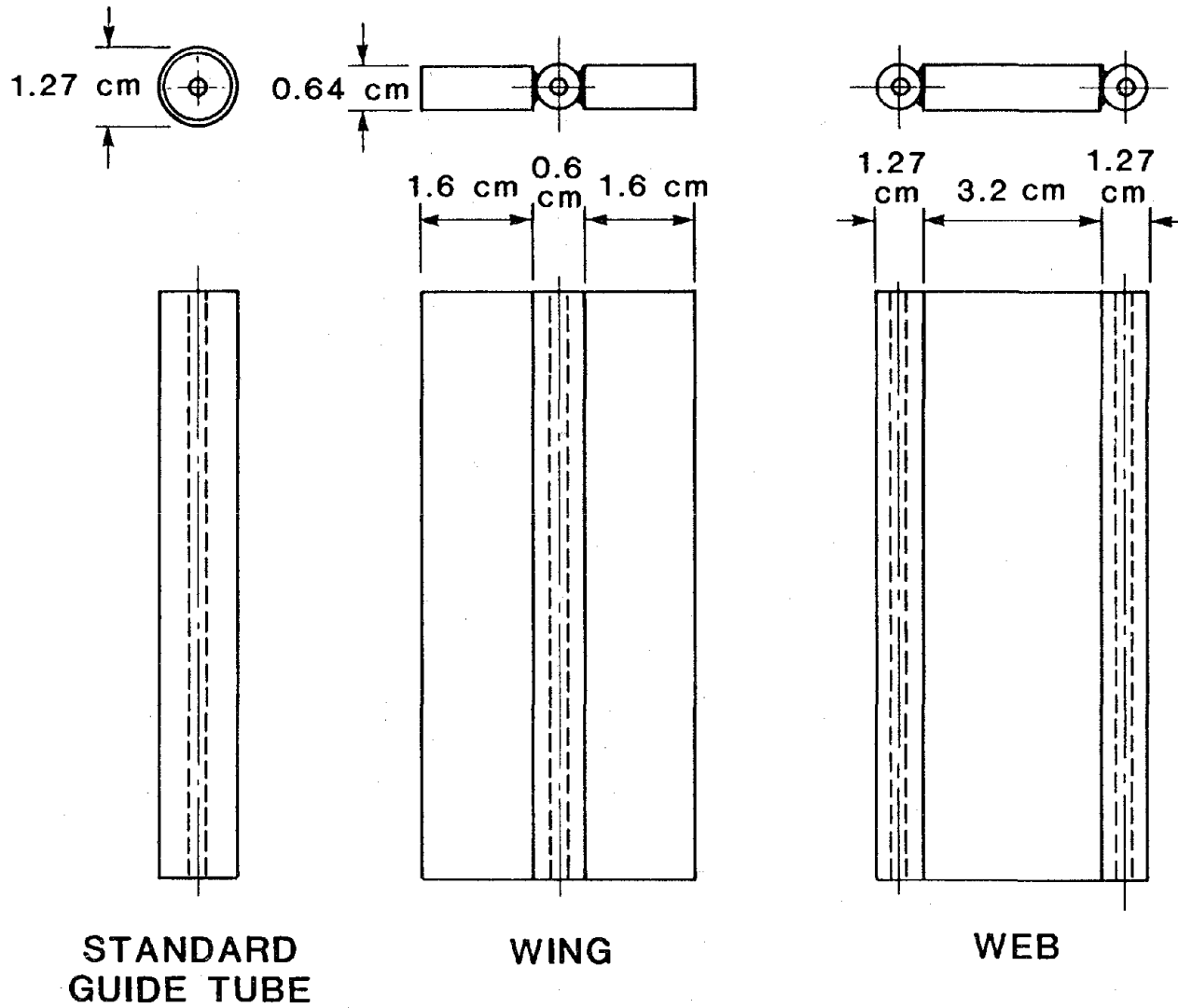


Figure 22. Guide tube plate designs. (Schematic.)

For this work, the flux hopper was mounted above the welding head, with the powder metering device located just above the guide tube mount (figure 23). The flux was added at a rate of approximately 4 g/min in order to balance the slag losses.

d. Alloying

Alloys were added to the electroslag weld metal by solid and tubular alloyed weld wires. This method made weld alloying easy, and no special devices or complex procedures were required.

e. Grain Refinement

The methodology used to produce fine, uniform grain structures utilized a thin-walled quartz shroud placed around: a) the 12.5-mm (1/2-in) diameter standard consumable guide, and b) the rectangular-shaped consumable guide plate (wing or web guide plates). This shroud provides a means for deep immersion and enhanced molten pool mixing by the electrode. The methodology also included standard gap (32 mm) and narrow gaps (25 mm and 19 mm) with different welding conditions to ensure the proper heat input and base metal dilution using different electrodes for alloy variables. Both the thickness and diameter of the quartz were varied to induce different degrees of molten pool stirring for 12.5-mm diameter standard consumable guide. Oscillation of the electrode was also applied in some cases. A flare that was formed on the top edge of the quartz shroud facilitated securing the quartz to the guide tube (figure 24) so the binder was not needed with a quartz shroud. In addition, different flux compositions were also applied to control: a) oxygen transfer into the molten metal, b) molten pool stirring, and c) heat input.

2. Metallographic Practices

The macrostructure of each electroslag weld was evaluated after being surface ground. The longitudinal and transverse section specimens were

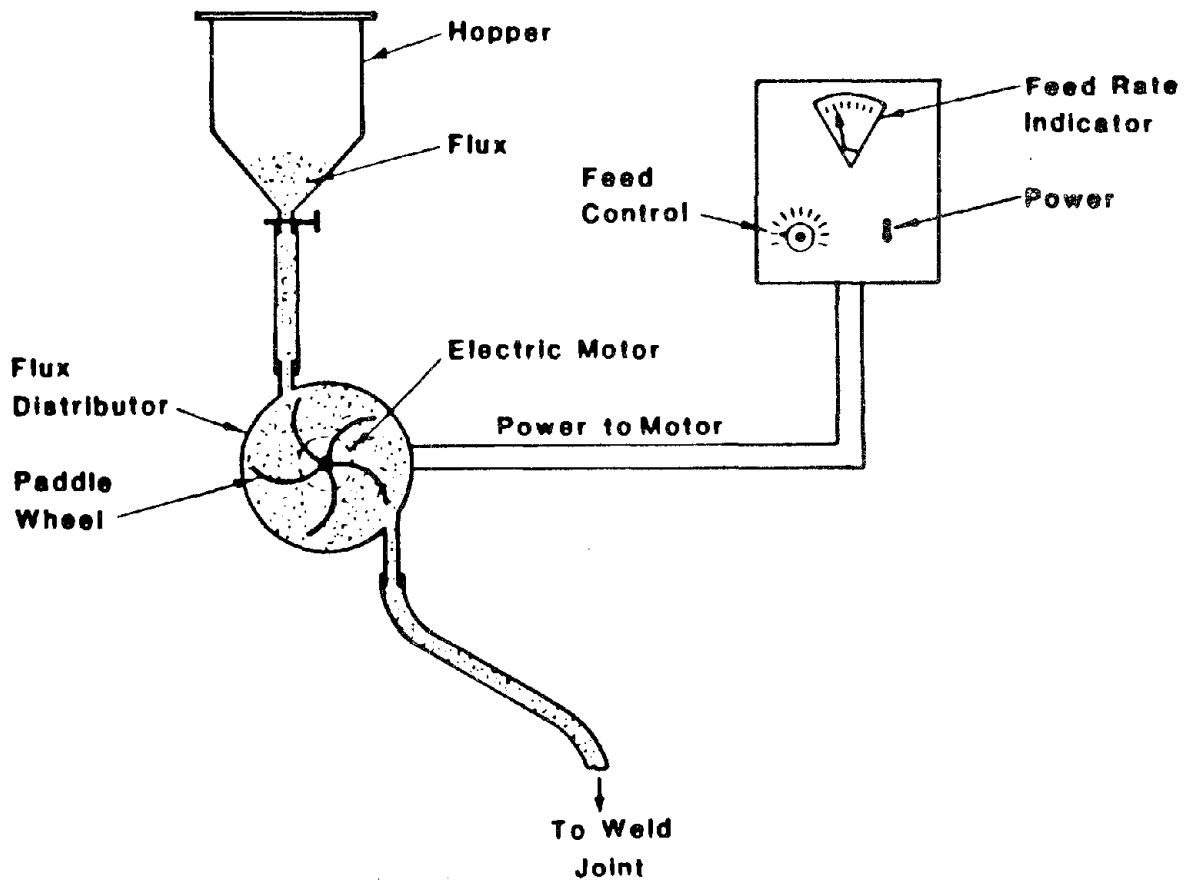
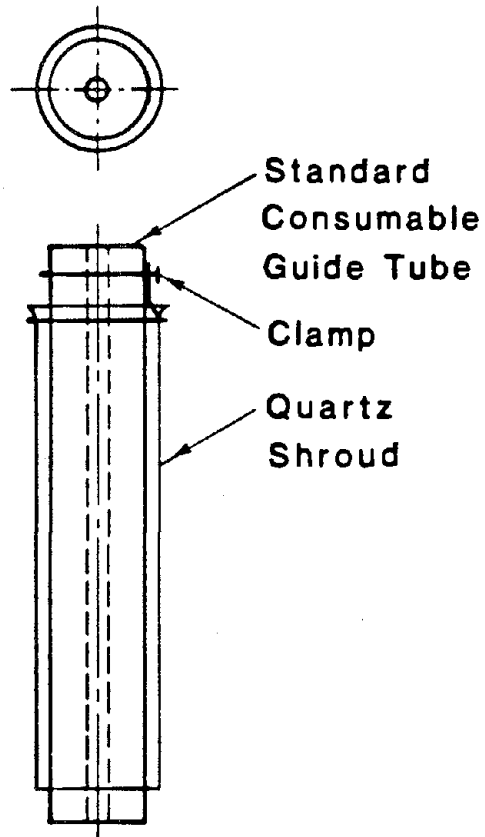


Figure 23. Schematic illustration of the continuous metered flux feed system. (Schematic.)



**Quartz shrouded
guide tube**

Figure 24. Schematic illustration of quartz shrouded guide tube design. (Schematic.)

etched with a 10 percent nital solution to expose the macrocharacteristic of weld metal and HAZ. The microstructure of each weldment was evaluated using longitudinal section specimens. Solidification structures were revealed by a reagent with the following composition: 5 g CuCl_2 , 20 g MgCl_2 , 10 ml HCl and 500 ml methanol. Solid-state transformation products were examined by etching in a 2 percent nital solution at room temperature. A subsequent light repolishing with alumina reveals the solidification substructure.

3. Impact Testing

Standard ASTM E23 Charpy impact specimens (figure 25) were machined in both weld and HAZ locations. The V-notch was ground perpendicular to the welding direction. Notches were located in the mid-thickness and quarter-thickness for the weld zone and at around 1 mm to 1.5 mm away from the fusion line for HAZ. The notch was precisely located by etching of the weld prior to sectioning.

Impact tests on selected welds were conducted over a temperature range of -73°C to $+65^\circ\text{C}$ (-100°F to $+150^\circ\text{F}$) to determine the temperature transition characteristics. Two or three samples were machined for each test, except the 0°F (-18°C) test for which six samples were machined.

Selected welds were also machined, and notches were located in four regions, namely weld centerline, thin columnar grain, coarse columnar grain and HAZ1 (figure 26). A total of six samples were used for this test and were performed at 0°F (-18°C).

A separate series of experiments were performed to examine the effect of HAZ location. Notches were ground at different locations, from the exact estimated fusion line to approximately 4 mm from the fusion line, to look at the toughness variations on A588 50-mm and 76-mm thickness welds made using the tubular alloyed electrode practice.

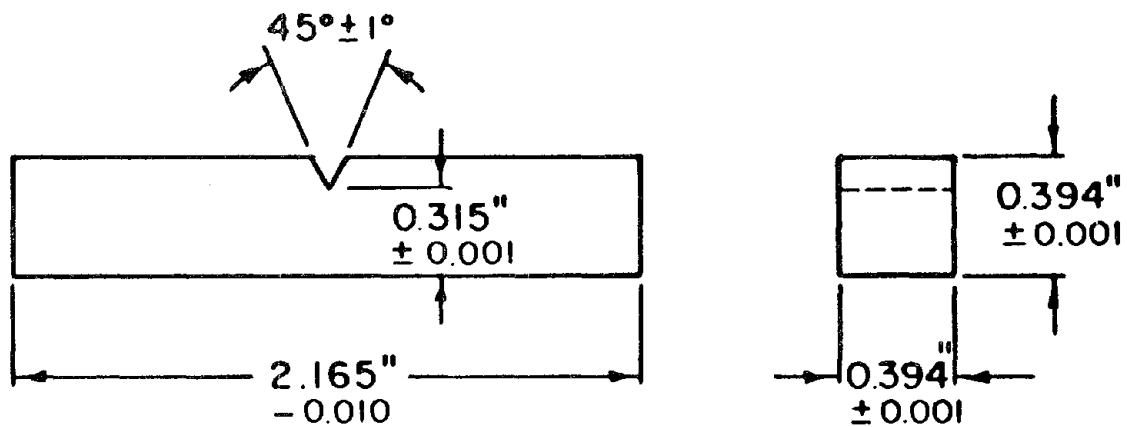


Figure 25. Standard CVN test specimen geometry. (Schematic.)

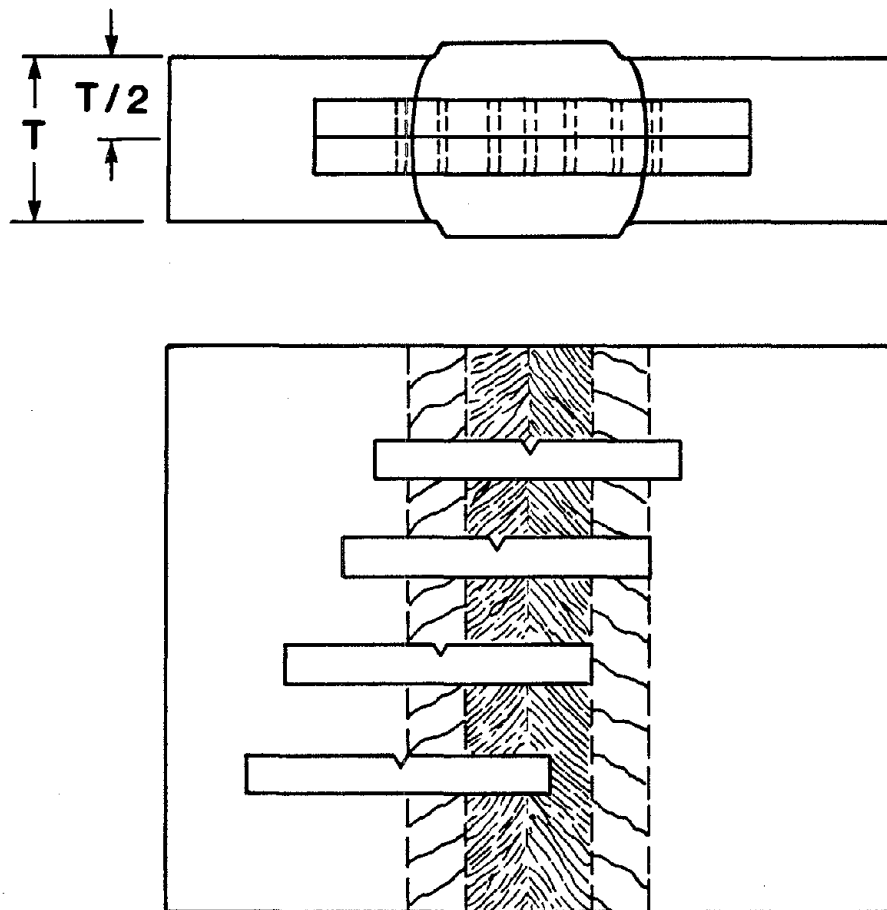


Figure 26. CVN specimen location configuration for ES welds. (Schematic.)

Specimens were coded with respect to their notch location, weld number, materials, etc., and were tested individually in a 264 ft-lb Tinius Olsen pendulum-type instrumented impact testing machine.

The fracture surface was sectioned perpendicular to the notch line to study the relationship between the microstructure and the fracture path on selected CVN specimens.

4. Plane Strain Fracture Toughness Testing

The compact tensile K_{IC} specimens were prepared and tested in accordance with the ASTM test for plane strain fracture toughness of metallic materials (E399-83). They were full thickness (76 mm) fatigue-precracked specimens and cut from as-deposited 76-mm A36 and A588 welds. Each specimen contained a chevron-shaped notch parallel to the welding direction, which was also extended by fatigue precracking as required by E399. The configuration and dimensions are shown in figure 27. Two weld locations, the weld centerline and HAZ1, were chosen to perform the K_{IC} test. The location of specimens and their notches is shown in figures 28 and 29.

Due to the geometrical consideration of the weld and HAZ microstructure, it was impossible to produce a full section sample that tests the entire zone. For example, the weld centerline sample included both thin columnar as well as coarse columnar zones, and the coarse HAZ sample involved the fine HAZ as well as a portion of the fusion line due to the curvature of the boundaries between regions.

Four K_{IC} test specimens were machined in the weld metal and four in the HAZ for each optimized welding condition. Both precracking and K_{IC} tests were performed in a MTS 810 testing machine.

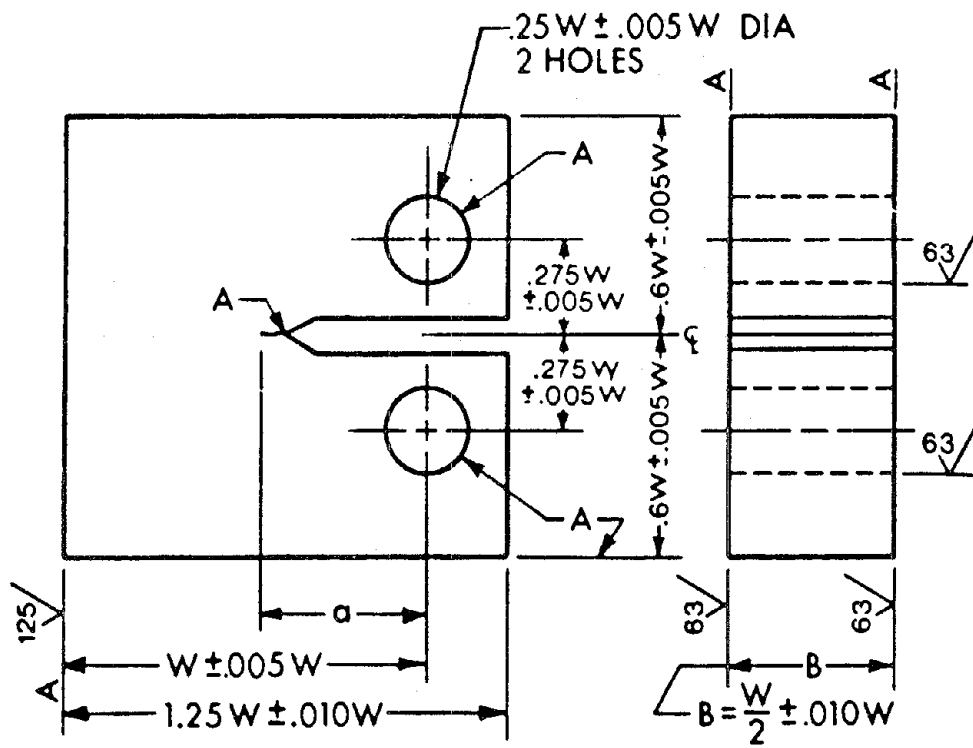


Figure 27. Compact tension fracture toughness specimen geometry. (Schematic.)

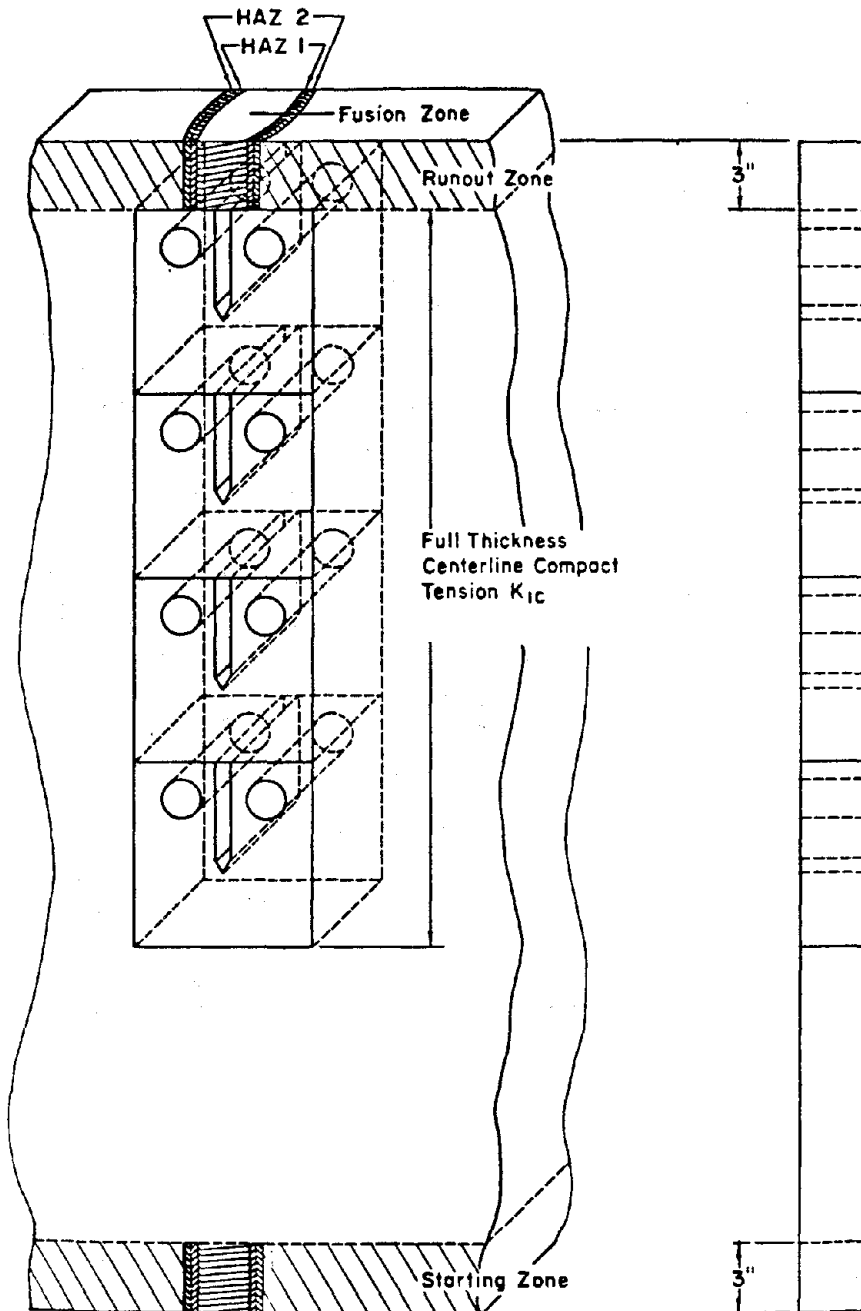


Figure 28. Location of K_{IC} specimens with respect to ES weld location. (Schematic.)

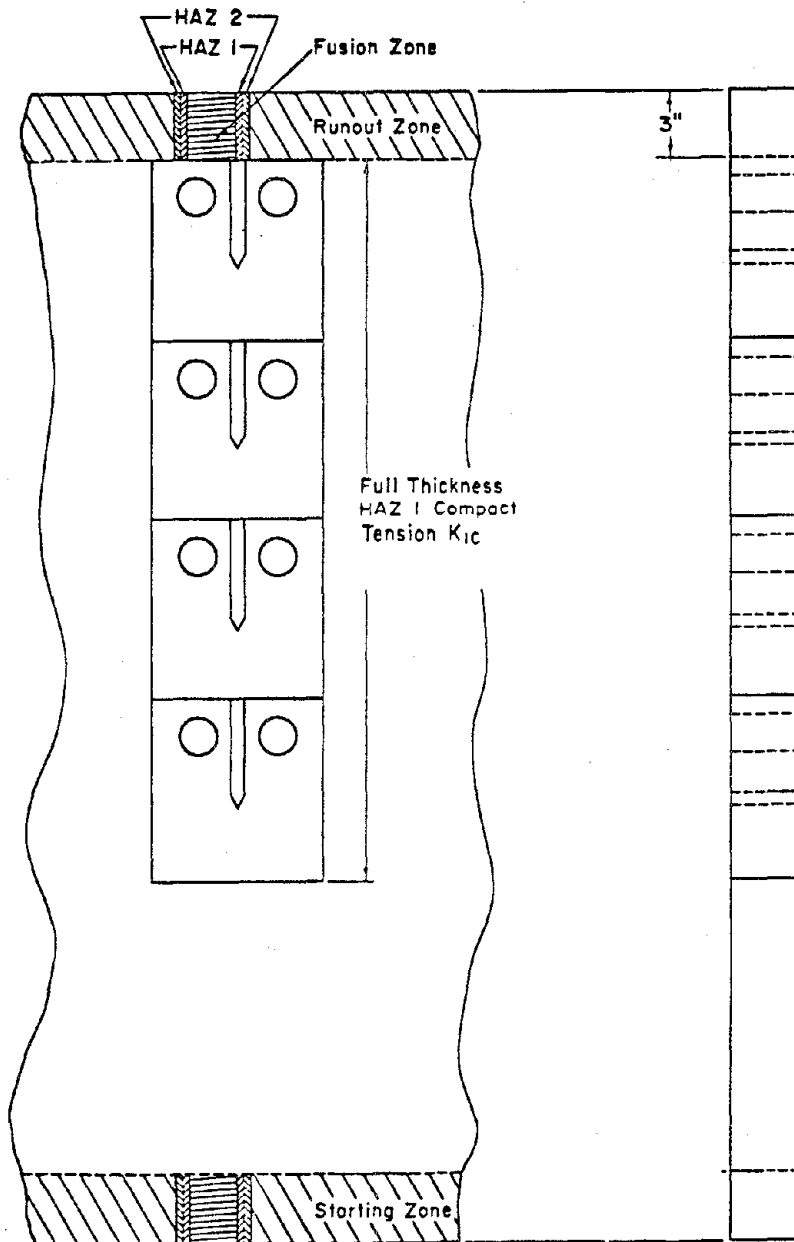


Figure 29. Location of compact tension fracture toughness samples with respect to ES heat affected zone locations. (Schematic.)

5. I-Beam Design and Fabrication

The I-beam design shown in figure 30 was developed at Lehigh University under the guidance of Professors John Fisher and Roger Slutter. This design produces the required stress range within the load and deflection capacity of their test system. The test system has been used for many beam fatigue tests, and the beam design and test conditions in this program were designed in accordance with the established practices at Lehigh University.

An evaluation of the basic fatigue behavior of electroslag weldments was required without any conflicting factors of weld imperfections that might induce early fatigue cracks or accelerated rates in these weldments. In order to minimize these imperfections, weldments were fabricated at OGC under carefully-controlled conditions. After fabrication, the electroslag reinforcements were ground flush and ultrasonically inspected prior to being incorporated into the I-beam itself. Since large I-beam fabrication is not readily possible at OGC, a commercial structural steel fabrication shop in Portland completed fabrication of the I-beams. The lower flange containing the electroslag weld was submerged arc welded to the rest of the flange and then the web was welded to the flange sections. The central portion of the I-beam was then inspected ultrasonically to ensure no submerged arc-related weld imperfections were developed during fabrication.

Electroslag welding conditions utilized a 12.5-mm consumable guide tube with a 32-mm gap, 600 A and 42 V for standard practice, and modified consumable guide plate (wing type) with narrow gap (19 mm), 1000 A and 38 V for recommended high quality weld practice. In addition, Linde WS (2.38 mm diameter) electrode and Hobart PF201 flux were used for both practices. Fatigue tests were performed at Lehigh University.

6. Chemical Analyses

Chemical analyses of the base metal and selected welds were carried out using a spectrographic analyzer located at ESCO Corporation. Oxygen

and nitrogen potential of the base metal and selected welds were also determined at ESCO Corporation.

7. Nondestructive Examination

Prior to ESW, all steel plates were ultrasonically tested to record the location of any imperfections. Both ultrasonic and radiographic examinations were conducted on mechanical property welds and I-beams. All tests were performed by Pittsburgh Testing Laboratory. Both ultrasonic (0°, 45° and 70°) and radiographic examinations were also applied to the artificially-induced imperfection formation welds to check size, shape, orientation and inspectability.

8. Hardness Evaluation

A 25-mm wide strip was removed from the macroetched specimen for hardness analysis. The side opposite to the etched surface was ground flat and parallel. The hardness was measured across the weld fusion zone, HAZ and base metal using a Rockwell hardness tester. A B-scale (1.6-mm diameter) spherical steel indenter under a 100-kg major load was employed. A C-scale (Brale indenter under a 150-kg major load) measurement was made whenever the hardness value exceeded R_B 100. Three or four measurements were made at each region of interest and an average was determined.

V. RESULTS

1. Welding Parameter Study

A total of seven welding variables were evaluated to determine their effects on fusion zone width, penetration, HAZ width, hardness, grain size, microstructure and production of imperfections such as inclusions, lack of fusion and cracking. These variables included: joint gap, guide tube design (standard, wing and web), current, voltage, heat input, oxygen potential and slag basicity.

The joint gap was found to directly control the heat input of the weld since the travel speed is a function of the volume of filler metal that is required to "fill" the weld joint cavity in ESW. Since the total heat input (H) is given by:

$$H = EI/v \quad (2)$$

where E is voltage, I is current, and v is velocity, increasing travel speed directly reduced heat input. For example, relative measures of heat input in ESW are the width of the fusion zone and the sidewall penetration into the base metal. The heat input and width of the weld deposited were shown in figure 31 to be linearly related. The sidewall penetration values of standard 32-mm gap welds were compared with those of 19-mm (narrow) gap welds, as shown in figure 32. Clearly, the narrow-gap weld achieved the same penetration as the standard-gap weld, but with a substantially lower heat input. Narrow-gap conditions were utilized to facilitate reduced heat input ESW. However, narrow-gap ESW required a means to better distribute the heat from the electrode to the outer perimeter of the pool near the cooling shoes in order to prevent lack of fusion. This requirement led to the development of the "wing" and "web" guide systems.

Although both web and wing guides accomplished the primary task of distributing welding heat more uniformly throughout the molten slag pool,

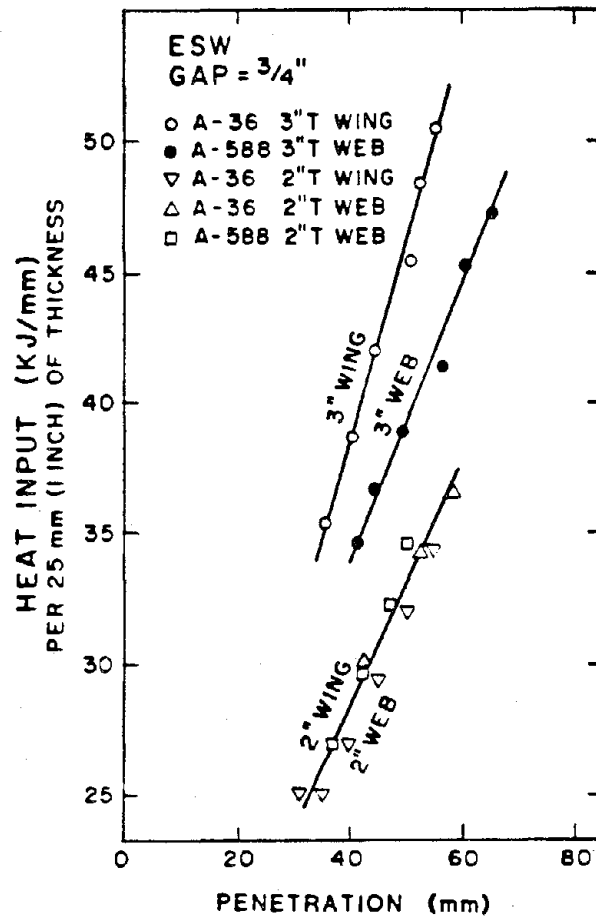


Figure 31. Heat input vs. sidewall penetration. (Line Drawing.)

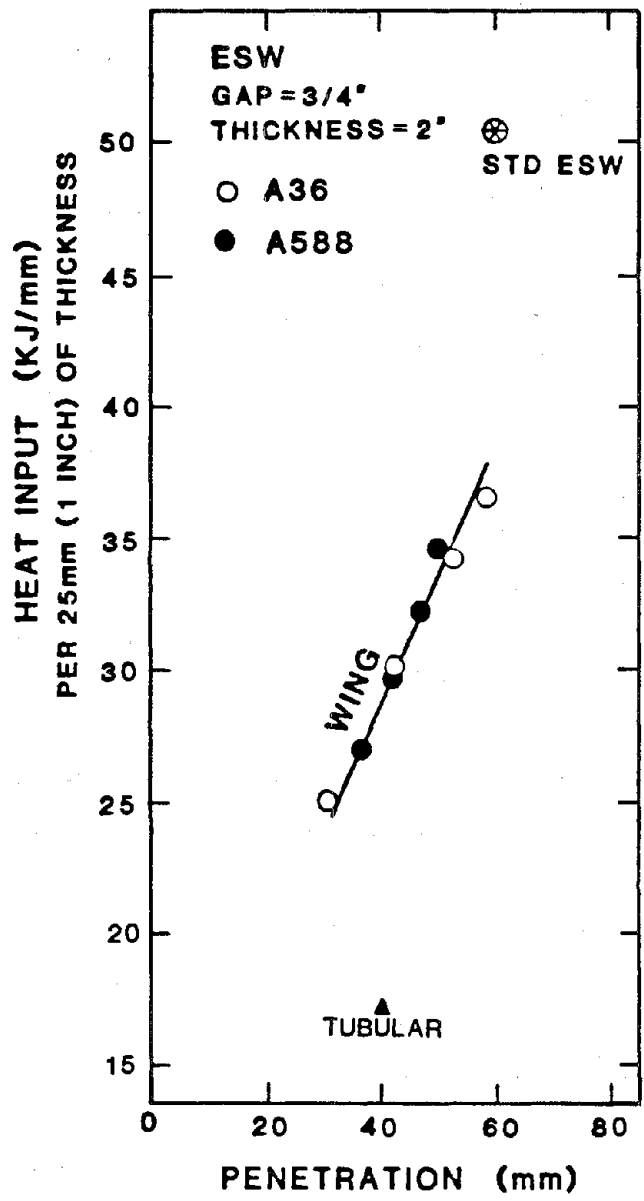


Figure 32. Relationship between heat input and base metal penetration showing decrease of heat input compared to standard ESW. (Line Drawing.)

notable differences in performance resulted from the fact that the wing utilized a single filler wire while the web required a dual filler wire feeding system, as illustrated in figure 22. Base metal dilution, form factor and the size of the coarse columnar zone were most affected by the geometry of the guide system. Although the web guide provided the best quality assurance against lack of fusion imperfections in narrow-gap ESW by virtue of its uniform penetration, it consistently produced greater base metal dilution than the wing guide, as shown in figures 33 and 34. The form factor, which is an indicator of hot cracking susceptibility, was superior in welds made with the web guide system, as shown on figures 35 and 36. The size of the coarse columnar zone was the greatest when using the web guide and the narrow gap, as seen in figures 37 to 39.

Unlike other fusion welding processes, the power input, which is the product of the current and the voltage, was not an indicator of heat input because of the dependence of travel speed on welding current. However, taken separately, the current and voltage settings were vitally important in achieving the desired weld characteristics. Increasing voltage, for example, was shown to generally increase not only the width of the weld and HAZ, but also the overall size of the molten weld pool. This is because heat input increases linearly with voltage. Although HAZ width generally increased with increasing voltage, a great deal of scatter was encountered in making such measurements, as shown in figures 40 and 41. Most notably, the tubular filler metal always produced the smallest HAZ widths.

Since current was a non-linear function of wire feed rate and affected welding speed, an increase in current setting for a given weld could either increase or decrease heat input. For example, the weld metal dilution (which is a sensitive indicator of heat input) was shown to increase with increasing current up to a maximum value and then decrease with further increases in current, as shown in figure 33. The maxima in the curves in figure 33 were shifted to higher current values with increasing plate thickness. Because of the proximity of the electrode/guide to the side-wall, the base metal dilution in narrow-gap welds exceeded that for the

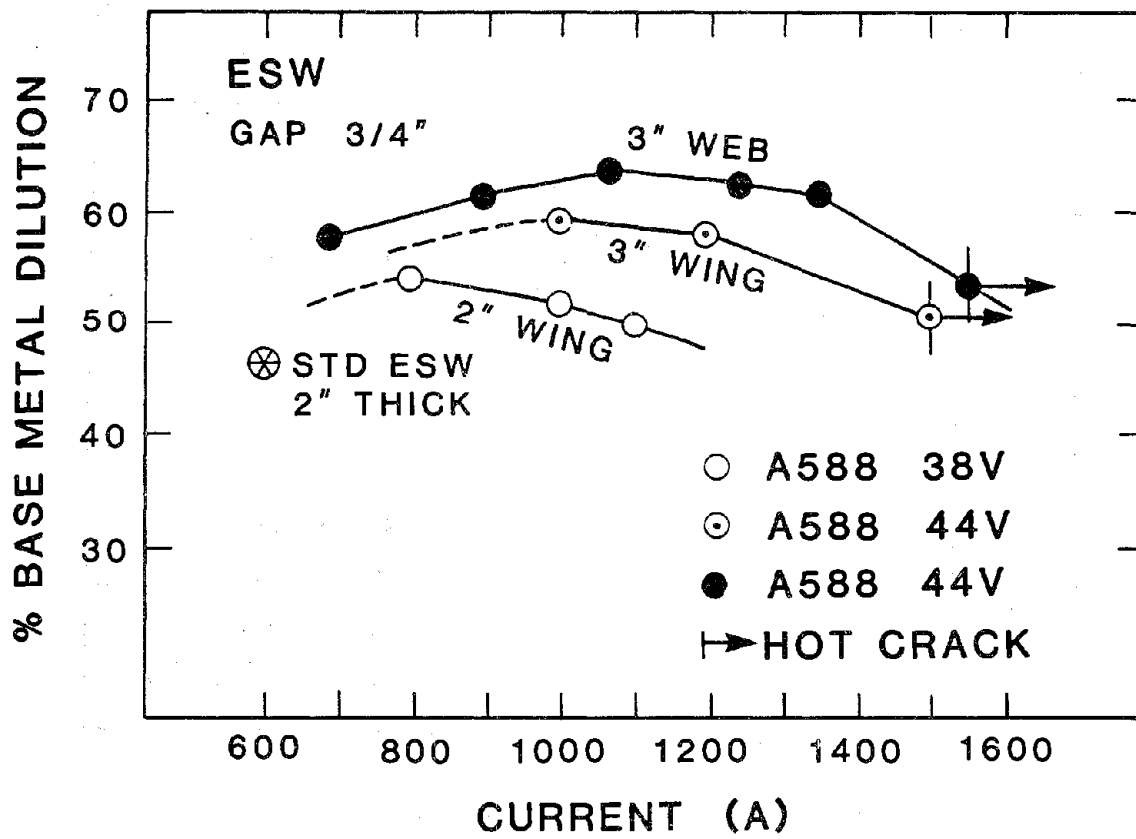


Figure 33. Influence of current on base metal dilution. (Line Drawing.)

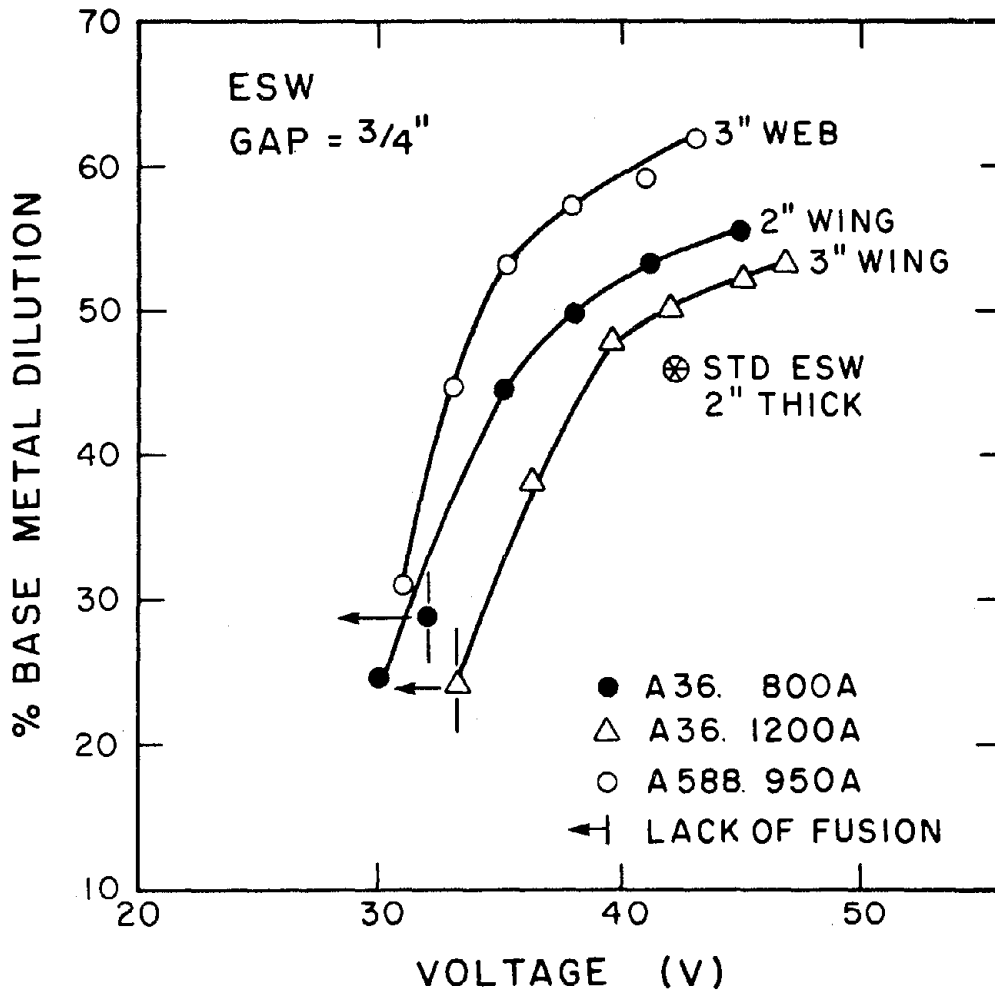


Figure 34. Influence of voltage on base metal dilution. (Line Drawing.)

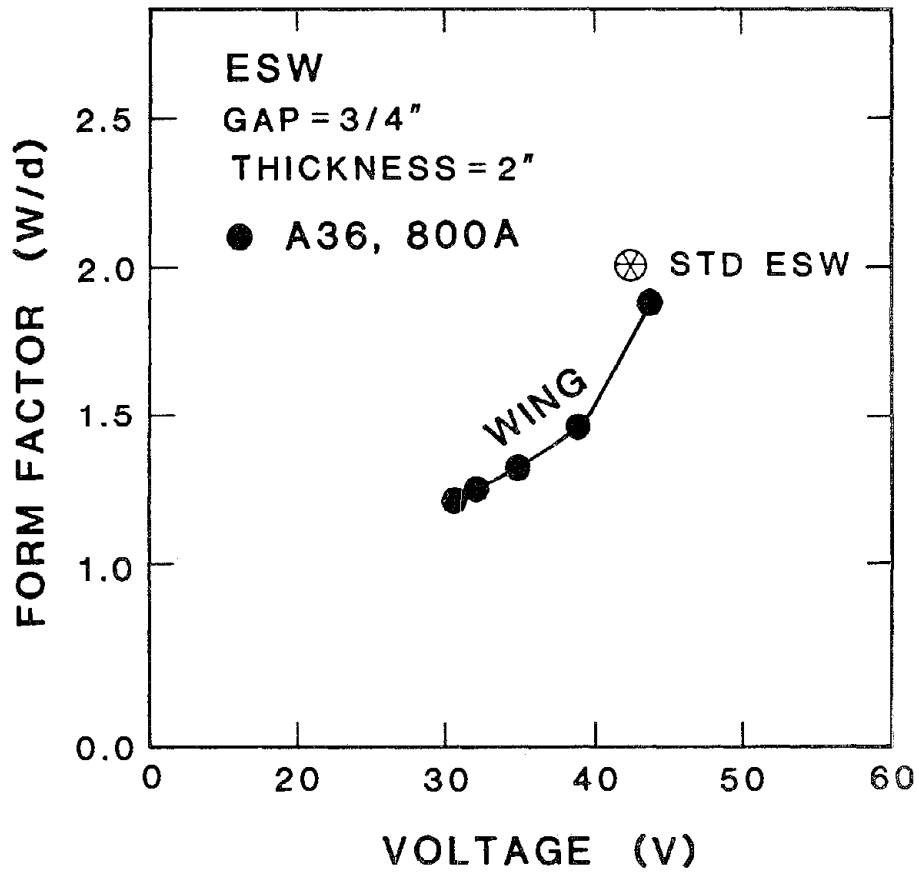


Figure 35. Influence of voltage on form factor. (Line Drawing.)

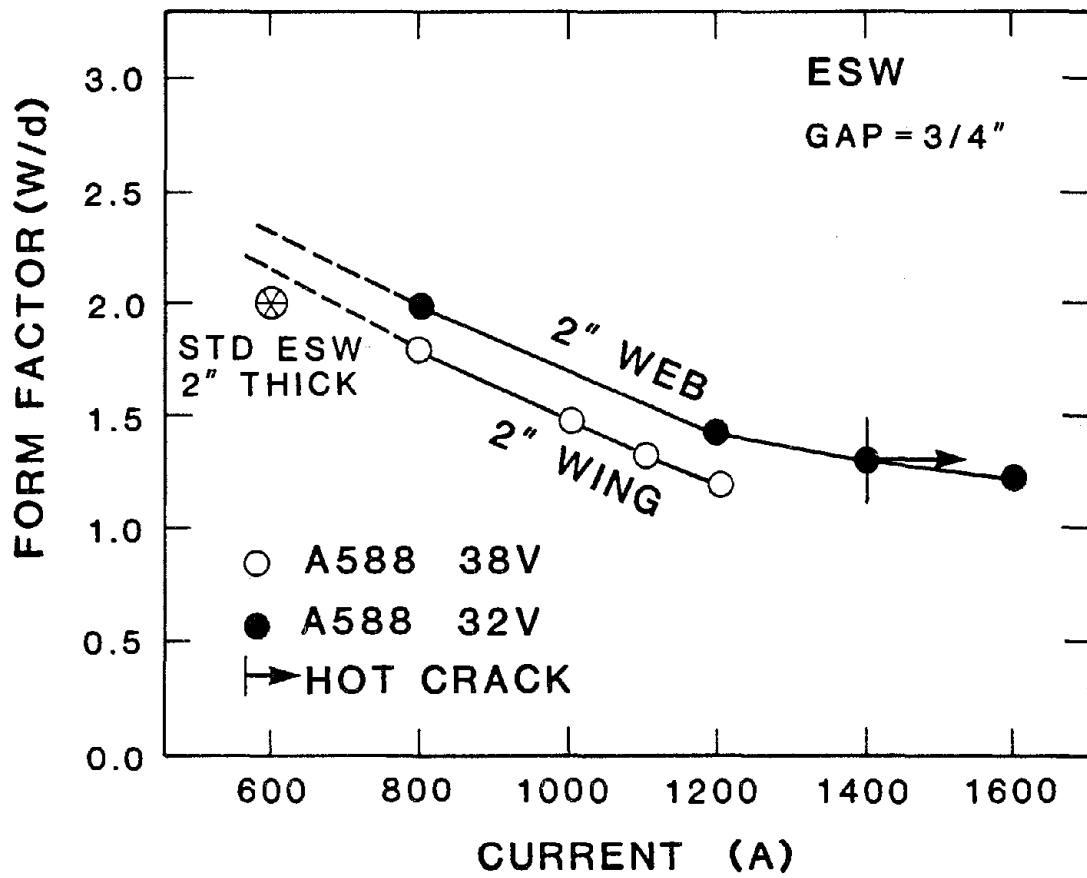


Figure 36. Influence of current on form factor. (Line Drawing.)

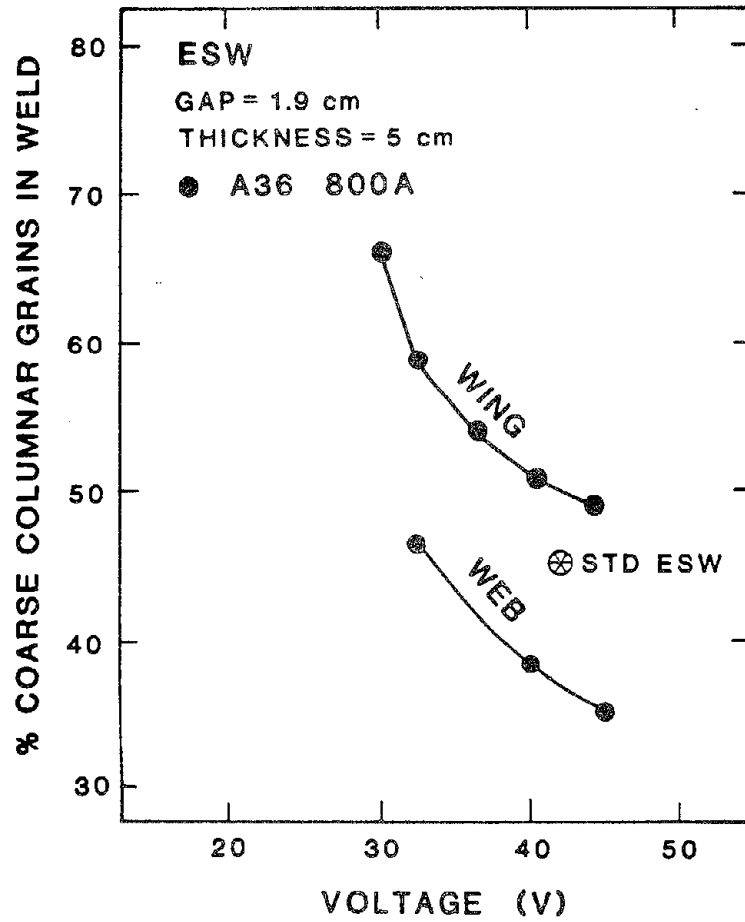


Figure 37. Percent coarse columnar grains vs. voltage. (Line Drawing.)

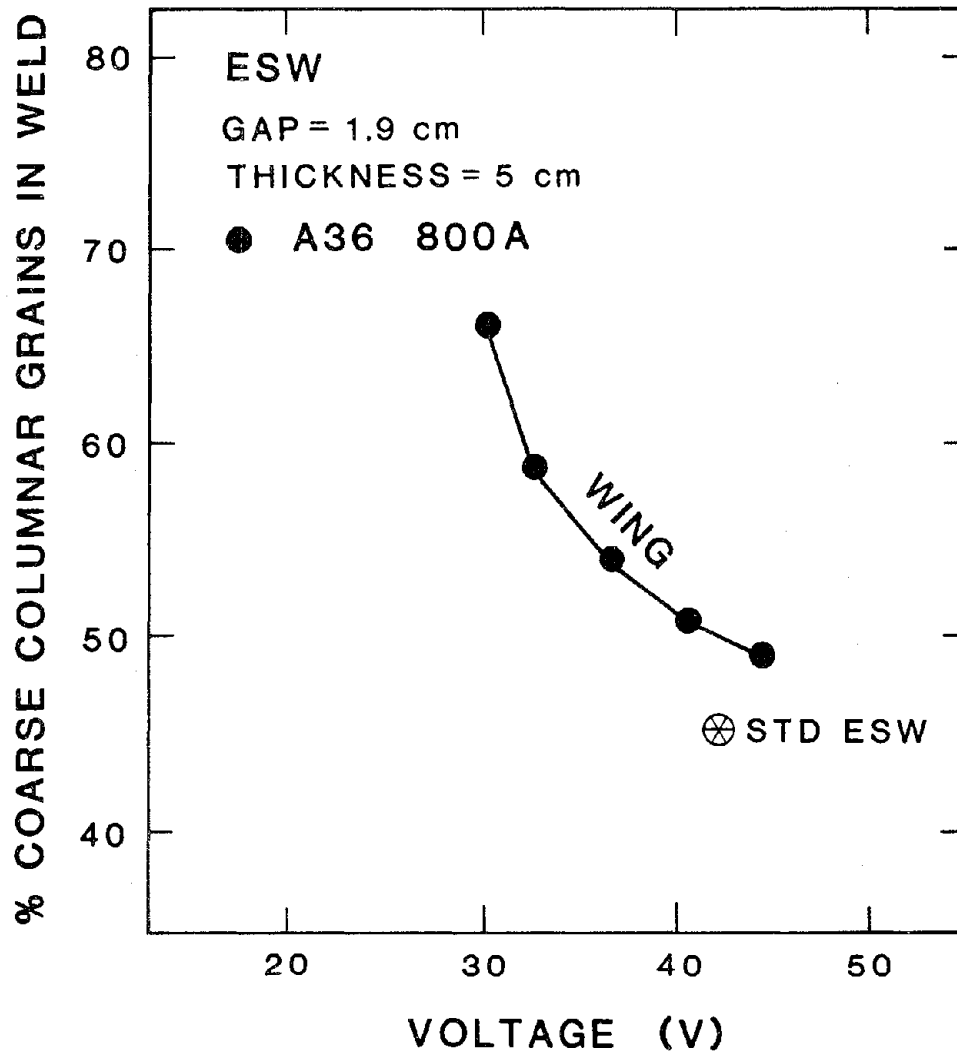


Figure 38. Percent coarse columnar grains vs. voltage for narrow gap welds. (Line Drawing.)

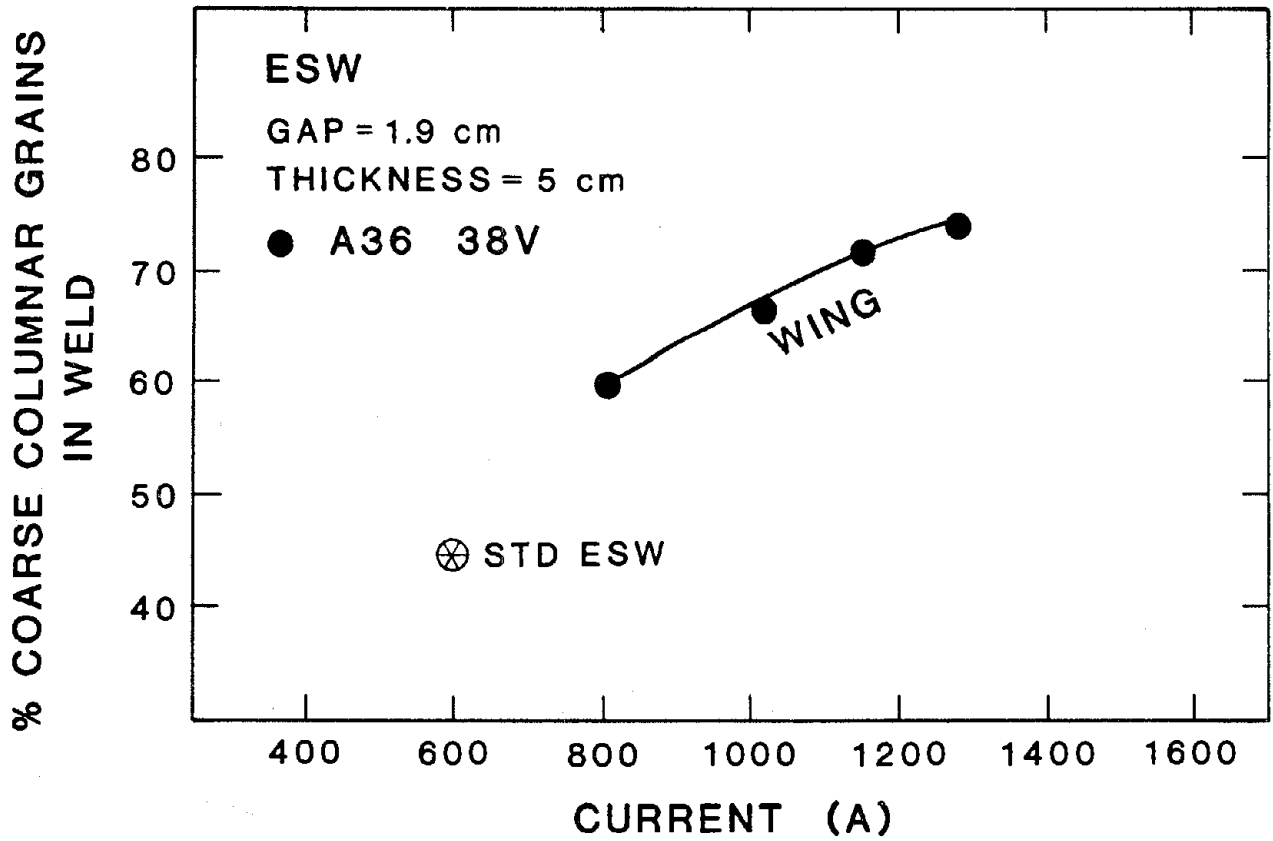


Figure 39. Percent coarse columnar grains vs. current for narrow gap welds. (Line Drawing.)

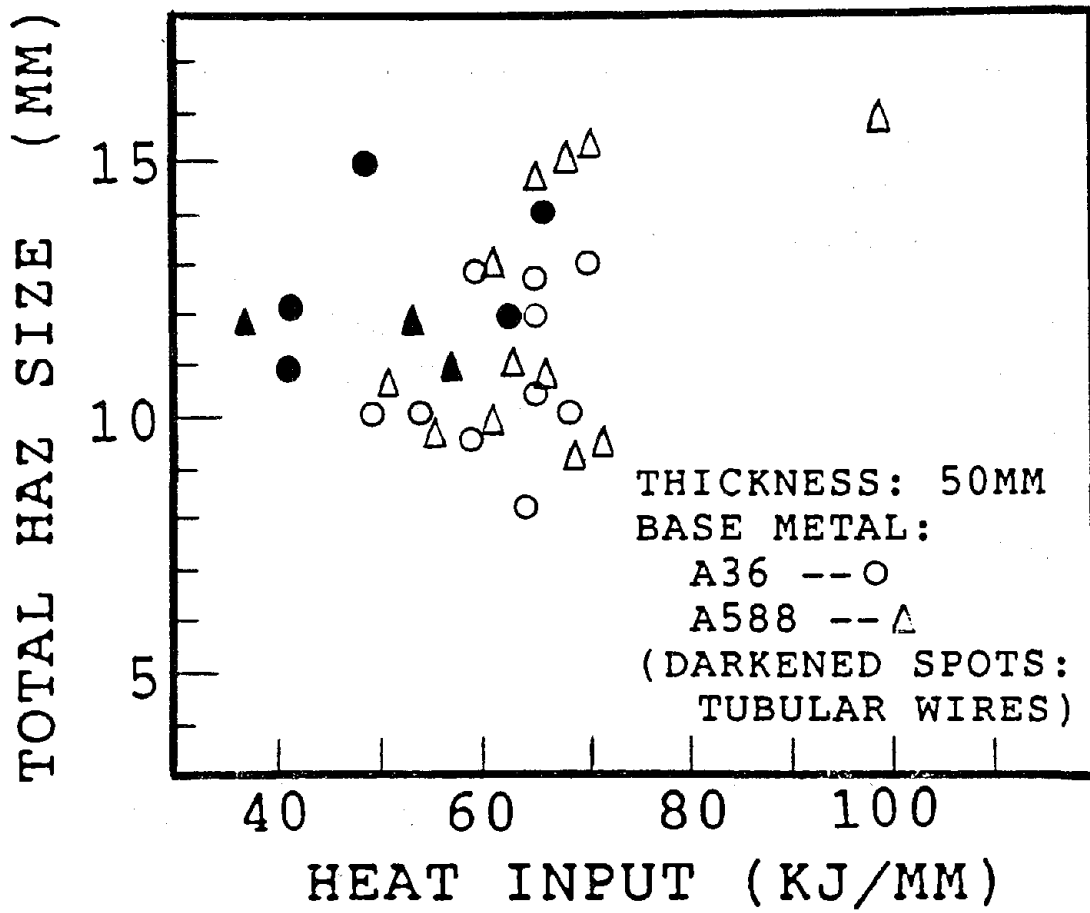


Figure 40. Heat input vs. heat affected zone size, 50mm.

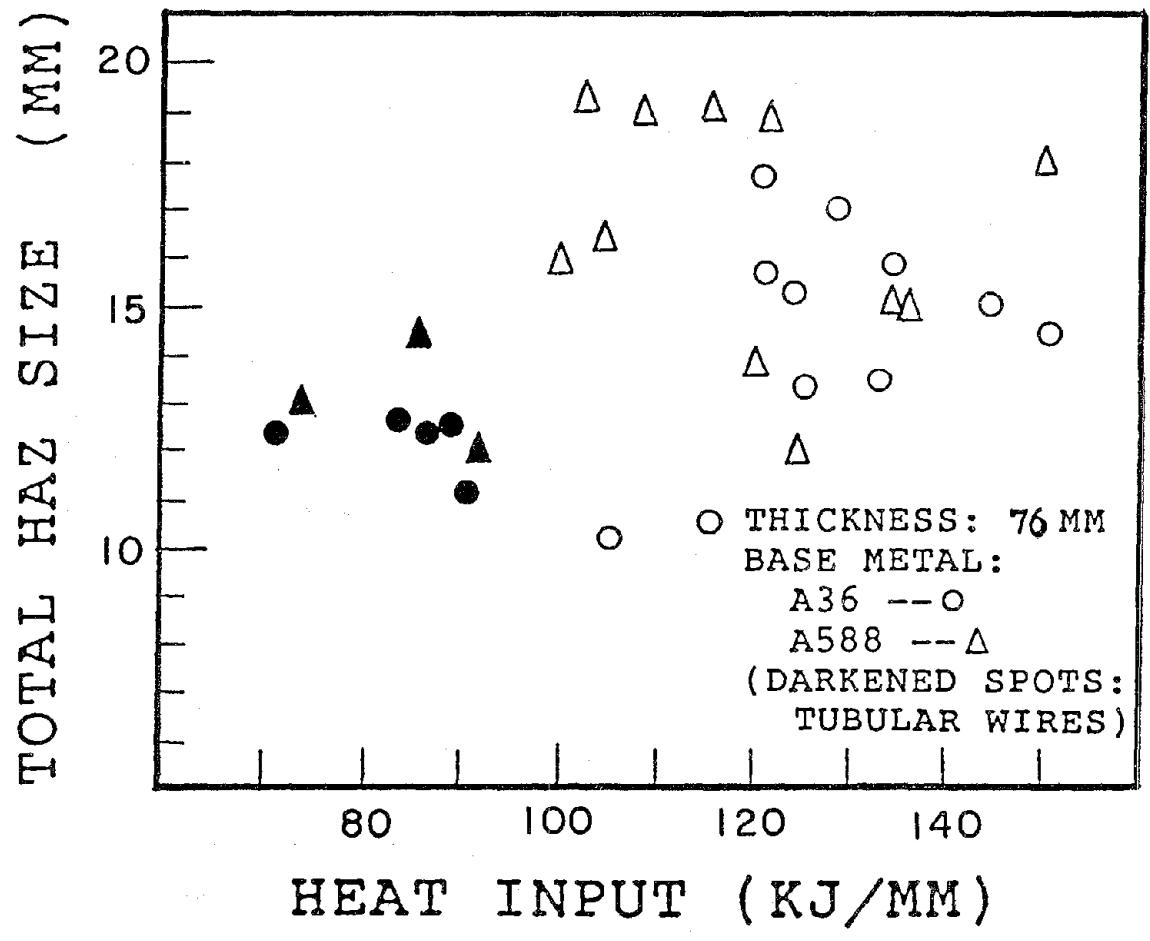


Figure 41. Heat input vs. heat affected zone size, 76mm.

standard gap (1.25 in) welds (figure 33) despite the higher heat input used in the standard weld (figure 31). An empirically-derived relationship for narrow-gap ESW was found between the current, voltage and electrode velocity as given in figure 42. The current was found to be function of (voltage)^{1/3} and (electrode velocity)^{1/2}. Thus, the elements comprising the heat input equation, namely current, voltage, and electrode velocity, were not independently-controllable variables.

Resistance to weld metal hot cracking, developed through alloying and innovative guide tube design, was essential to the success of narrow-gap ESW because hot cracking is promoted by the high currents and travel speeds required to minimize narrow-gap ESW heat input. Typical hot cracks, which can occur as a result of excessive current, are illustrated in figure 43.

The threshold current required to cause hot cracking in A588 and A36 welds was lowest for the standard guide ESW process, substantially improved using the wing guide, and improved further with the web guide system (figure 44). Best resistance to weld metal hot cracking was achieved by combining the beneficial effects of the web guide and tubular filler metal.

The use of a tubular filler metal compared to solid filler metal provided not only excellent resistance to hot cracking, but also provided additional benefits including: 1) highest deposition rate, 2) lowest heat input for given current and voltage settings, 3) smallest HAZ width, 4) highest value of form factor, and 5) reduced base metal dilution (figure 45). Since the filler metal was tubular containing metal powder, resistance heating of the tubular filler metal was greater than that of the solid filler. Increased resistance of the hot tubular filler above the slag increased the deposition rate for a given power setting compared to the solid filler. This is because the power supply must maintain an Ohm's law relationship. An increased filler metal feed rate was needed for tubular filler to attain the specified current, thus, accounting for the observed characteristics of ESW with tubular filler metal.

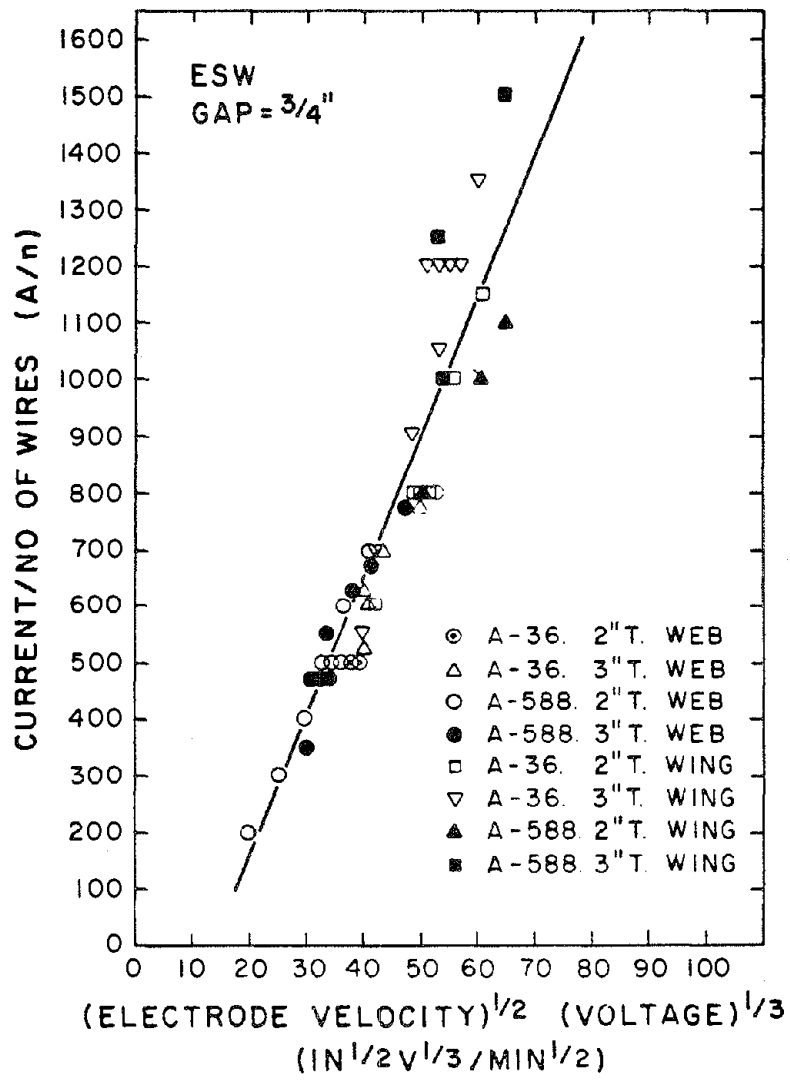


Figure 42. Empirically determined relation between the welding current, electrode velocity and welding voltage. (Line Drawing.)

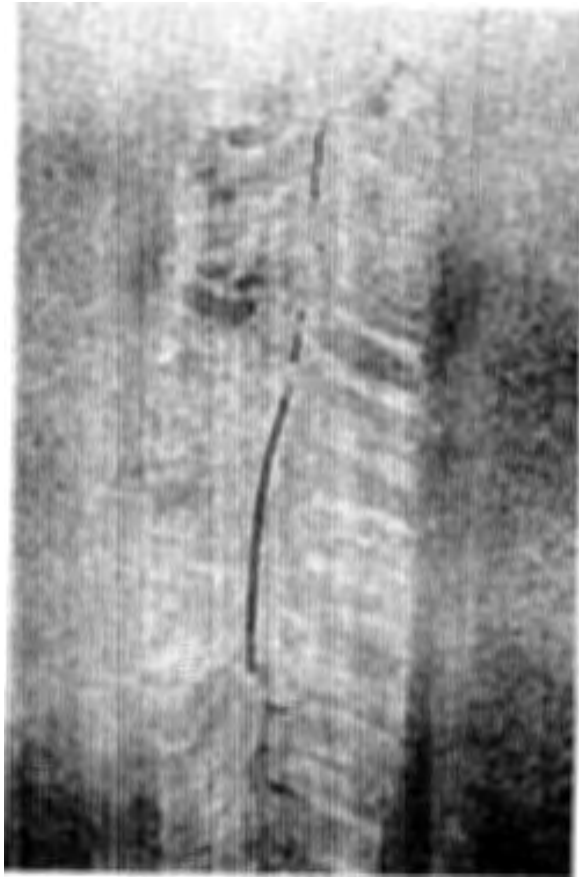


Figure 43. Macrograph of hot cracks in ES welds. (Micrograph.)

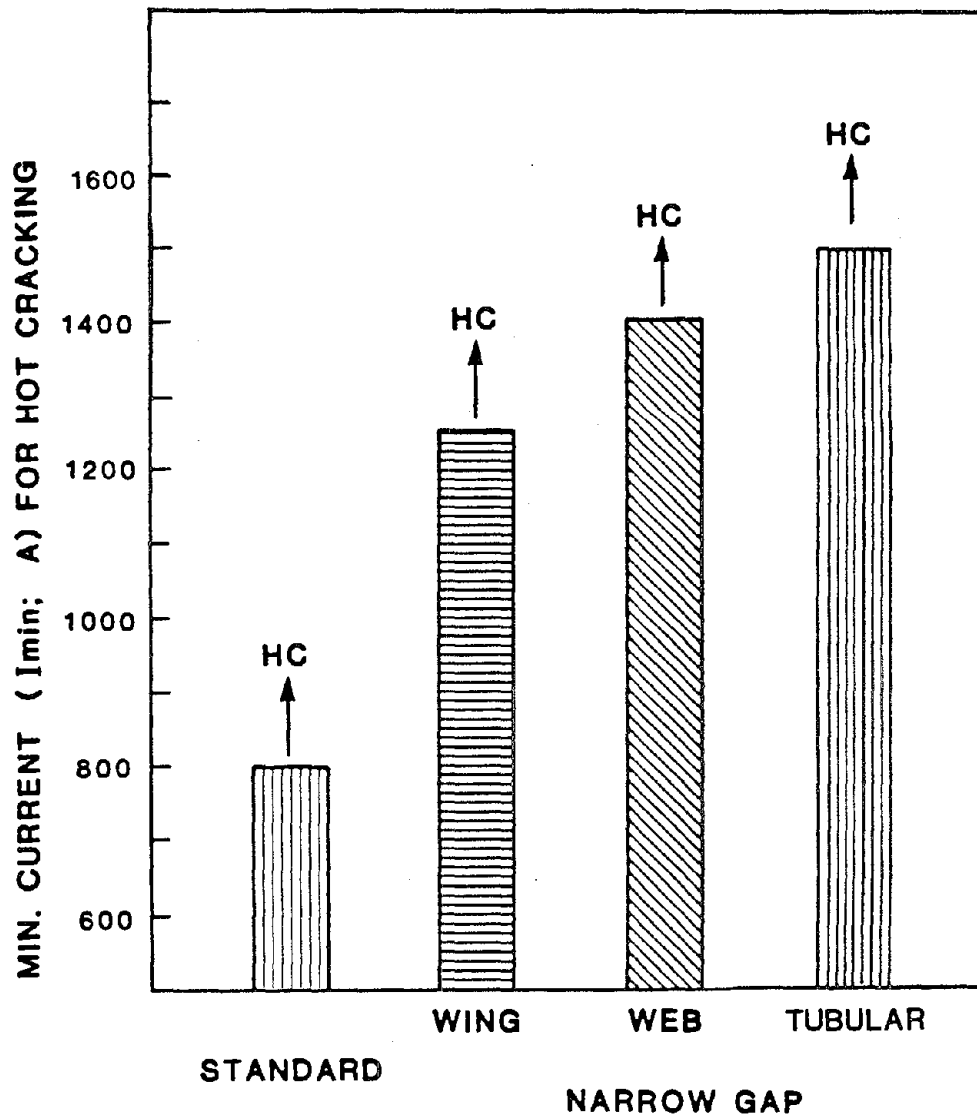


Figure 44. Minimum current to produce hot cracking as a function of weld gap configuration. (Line Drawing.)

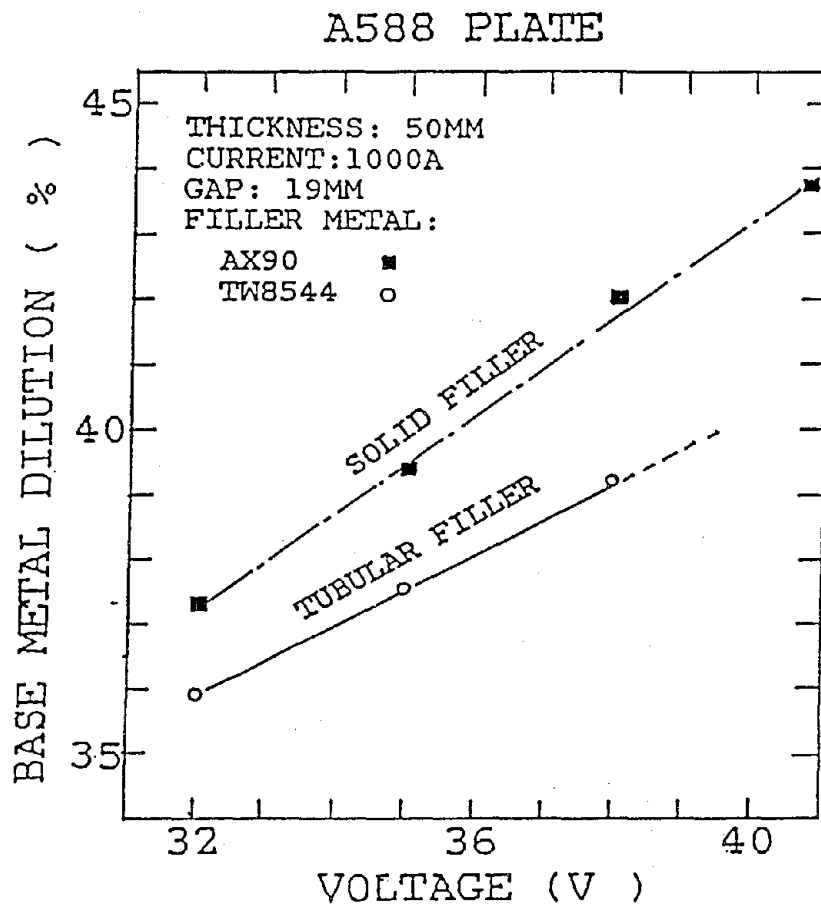


Figure 45. Dilution vs. welding voltage for solid vs. tubular fillers. (Line Drawing.)

Hardness profiles across the weld, HAZ and base metal were not significantly affected by variations in welding parameters. The primary reason for this was that the cooling rates for both the narrow-gap and standard-gap welds were too slow to substantially affect hardness. The typical hardness profiles for electroslag welds deposited on A36 and A588 steels in 50-mm and 76-mm thicknesses are shown in figure 46. The hardness profile of the A588 weldment exhibits higher hardness values than a similar A36 weldment by virtue of its greater alloy content in both the plate and filler metal.

The microstructures of the weld and HAZ were substantially affected by the welding parameters despite the fact that hardness values were essentially unchanged. The key microstructural changes involved: 1) the amount and coarseness of acicular ferrite in the weld, and 2) the amount and coarseness of grain boundary ferrite, Widmanstatten ferrite and upper bainite in both the weld and the HAZ. The typical weld metal grain structures in standard- and narrow-gap welds, shown in figure 47, consists of coarse columnar grains (CCG), fine columnar grains (FCG) and, under conditions of extremely-fast welding speeds, equiaxed (E) grains at the weld center. The CCG structure was desirable because its substructure consisted almost entirely of acicular ferrite (figure 48). The FCG structure (figure 49) was not considered desirable due to the abundant presence of grain boundary (proeutectoid) ferrite. The occurrence of the CCG structure containing the acicular ferrite substructure was strongly promoted by: 1) increasing the current or travel speed, 2) decreasing the voltage, and 3) utilizing the wing guide narrow-gap ESW method, as shown in figures 37 to 39. A summary of the effects of current, voltage and travel speed on the resulting microstructure is shown in figure 50. Clearly, increasing current or travel speed increases the amount of acicular ferrite in A36 or A588 weld metal, but results in hot cracking. At the fastest welding speeds, a small equiaxed zone developed at the weld centerline which prevented hot cracking at the centerline (figure 50, right-hand photographs). However, hot cracking occurred in the CCG zone instead.

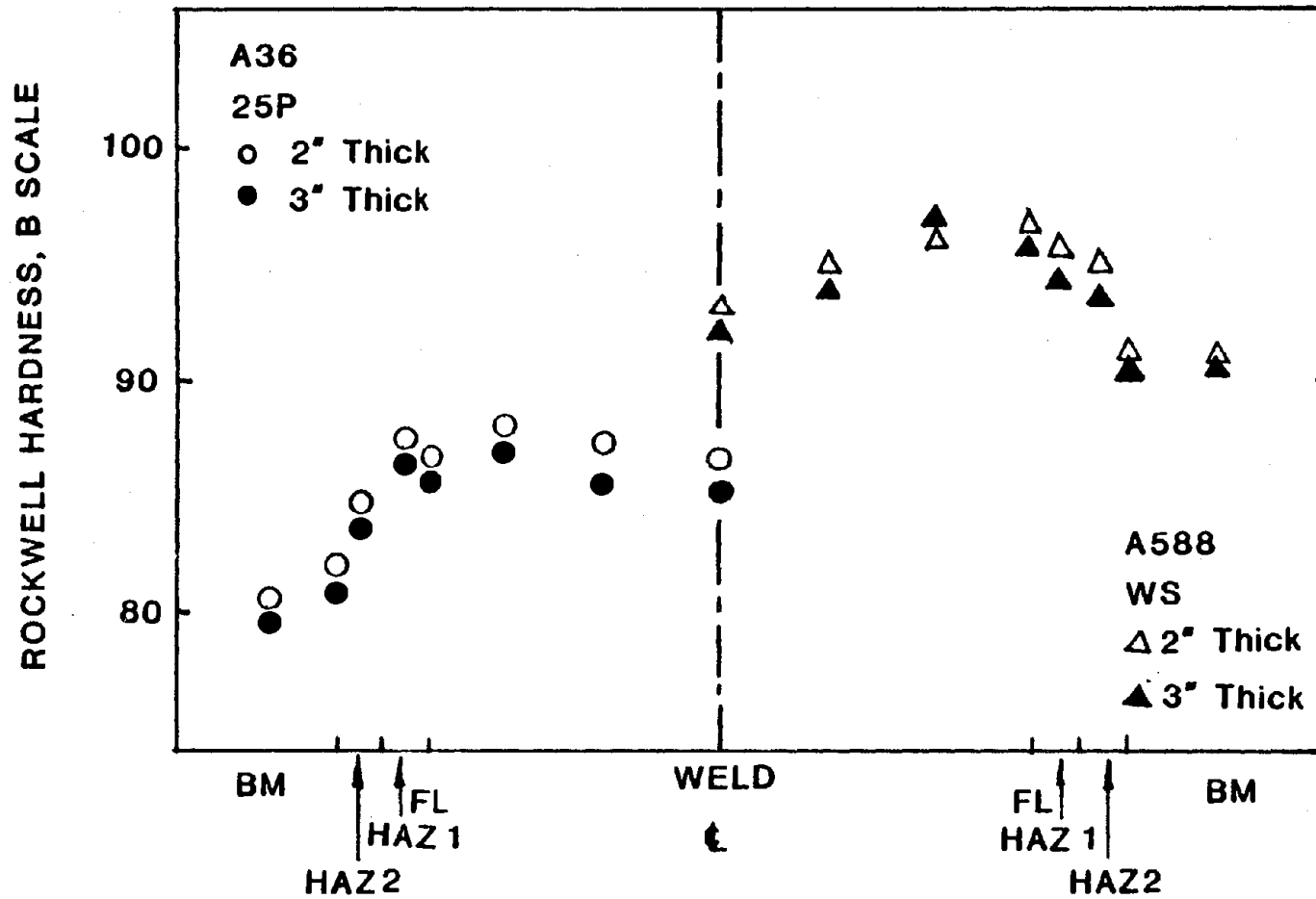


Figure 46. Hardness traverse across electroslag welds. (Line Drawing.)

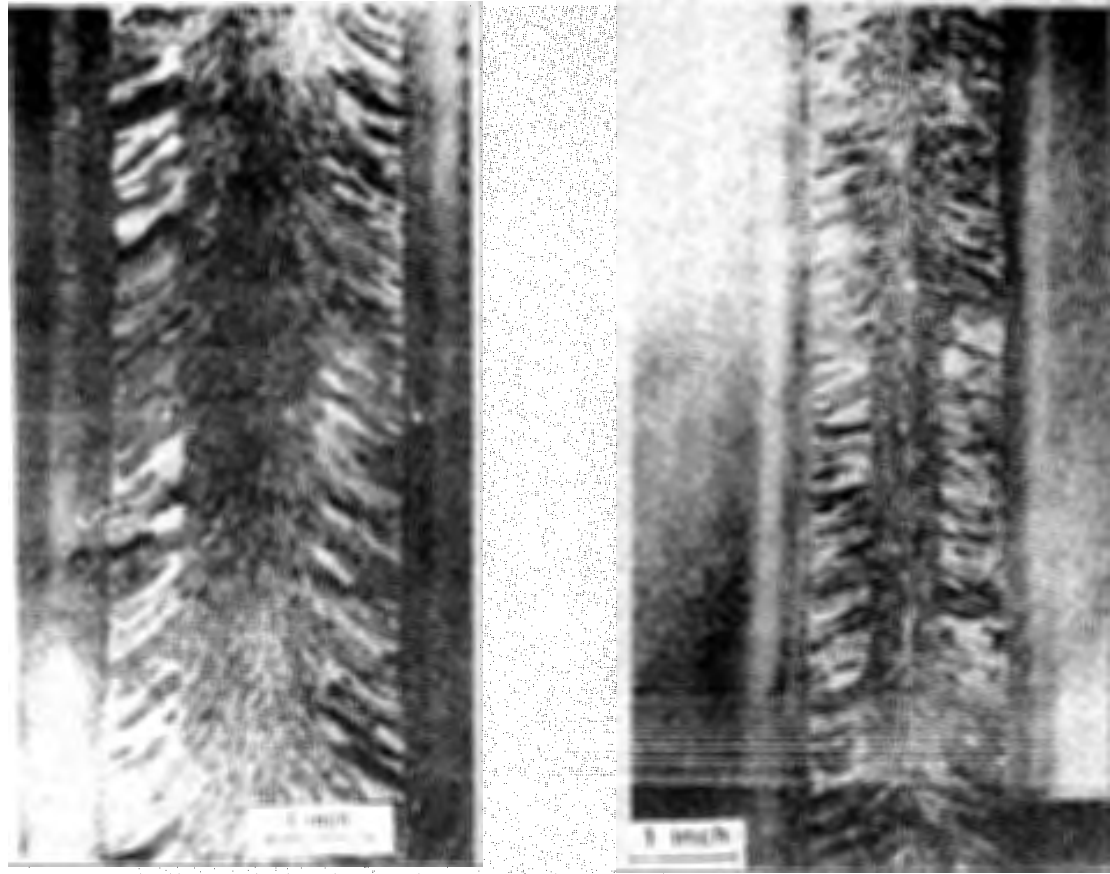


Figure 47. Typical weld metal macrostructures in standard and narrow gap welds. (Micrograph.)

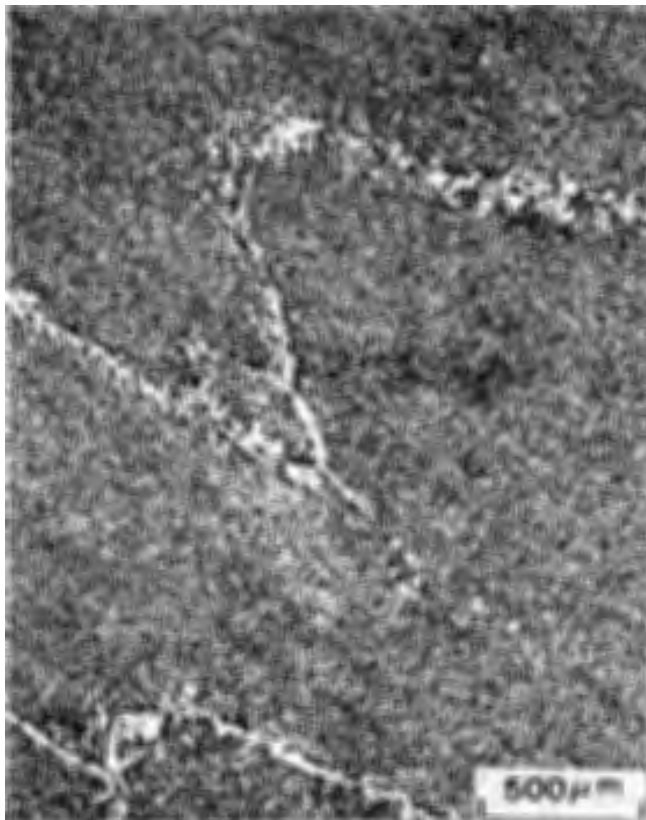


Figure 48. Typical coarse columnar grain microstructure. (Micrograph.)



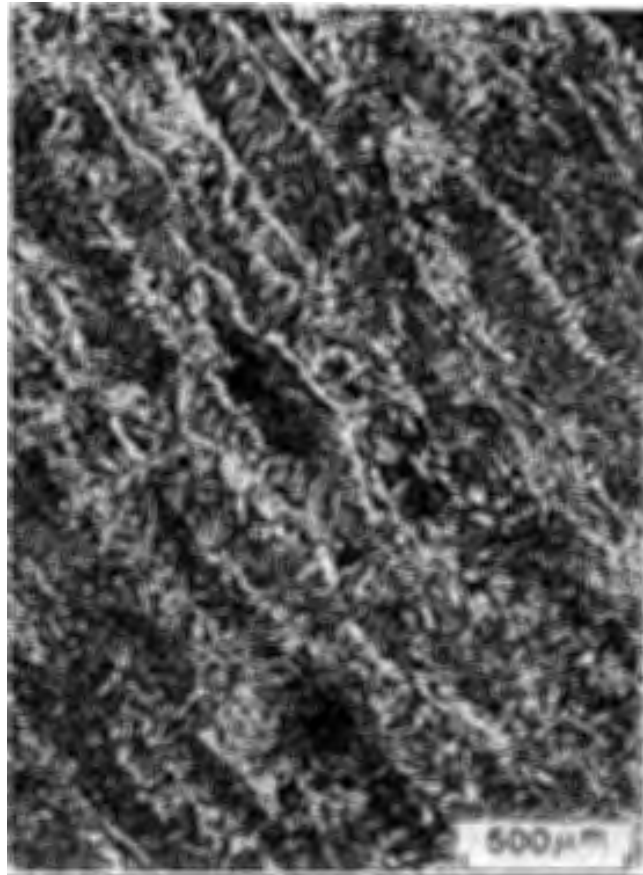


Figure 49. Typical thin columnar grain zone microstructure.
(Micrograph.)



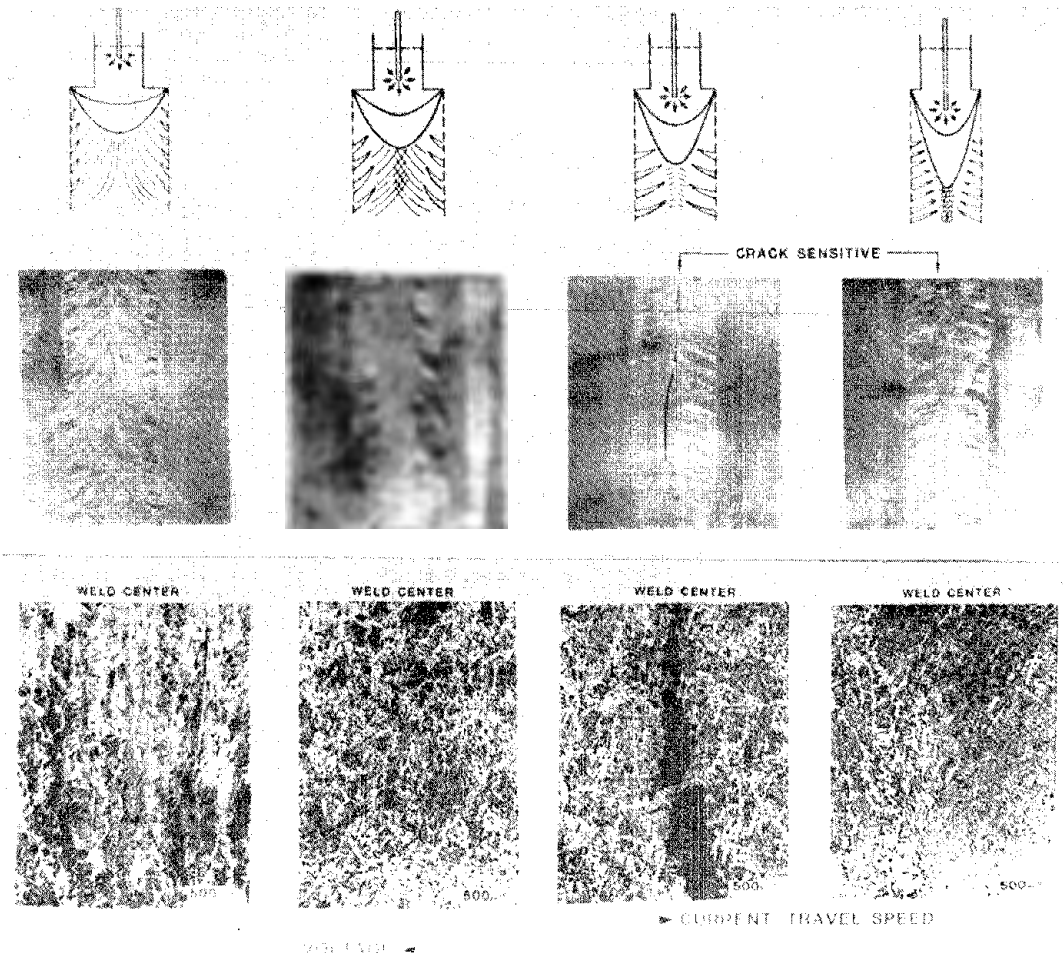


Figure 50. Characteristic descriptions of grain structure in narrow gap electroslag welds. (Micrograph.)



2. Filler Metal Alloy Development

Filler metal alloy development was necessary to insure adequate amounts of fine acicular ferrite in the weld fusion zone. To provide a cost-effective and reliable filler metal, only manganese (Mn), nickel (Ni), molybdenum (Mo) and chromium (Cr) additions were evaluated, and the total alloy content of the alloy did not exceed 3.0 percent by weight. The microalloying elements were not utilized since their effects on microstructure were extremely dependent upon the amount present in the weld metal which was, in turn, dependent upon both dilution from the base metal and the transfer of these elements across the arc. Because of its use in all steel filler metals and its well-known beneficial effects in promoting acicular ferrite in steel weld metal, Mn content was intentionally maintained at a constant level in each weld between 1.0 and 1.3 percent.

The effects of Ni, Mo and Cr were, thus, evaluated in A588 and A36 (narrow-gap) electroslag weld metal. Typically, electroslag welds deposited with the Hobart 201 (neutral) running flux contain approximately 200 ppm oxygen. Increasing Ni and Mo concentrations up to 1.5 percent and 0.3 percent, respectively, substantially increased the amount of acicular ferrite from less than 50 percent to well above 90 percent, as shown in figure 51. Since both Ni and Mo additions lowered the acicular ferrite transformation temperature, the acicular ferrite became finer with increased alloying (figure 52). Cr additions, however, were beneficial in promoting acicular ferrite only up to approximately 0.5 percent, beyond which Cr additions promoted the formation of bainite.

The effectiveness of Ni, Mo and Cr in reducing grain boundary (proeutectoid) ferrite at prior austenite grain boundaries in A588 and A36 weld metal is evident upon comparing the microstructures of unalloyed weldments (figure 53) with weldments alloyed with Ni-Mo (figure 54) and Cr-Mo (figure 55). In comparing welds having approximately the same total alloy content, the Ni-Mo alloyed weld metal produced a finer structure of acicular ferrite than did the Cr-Mo addition (figure 56) primarily because Ni and Mo reduced

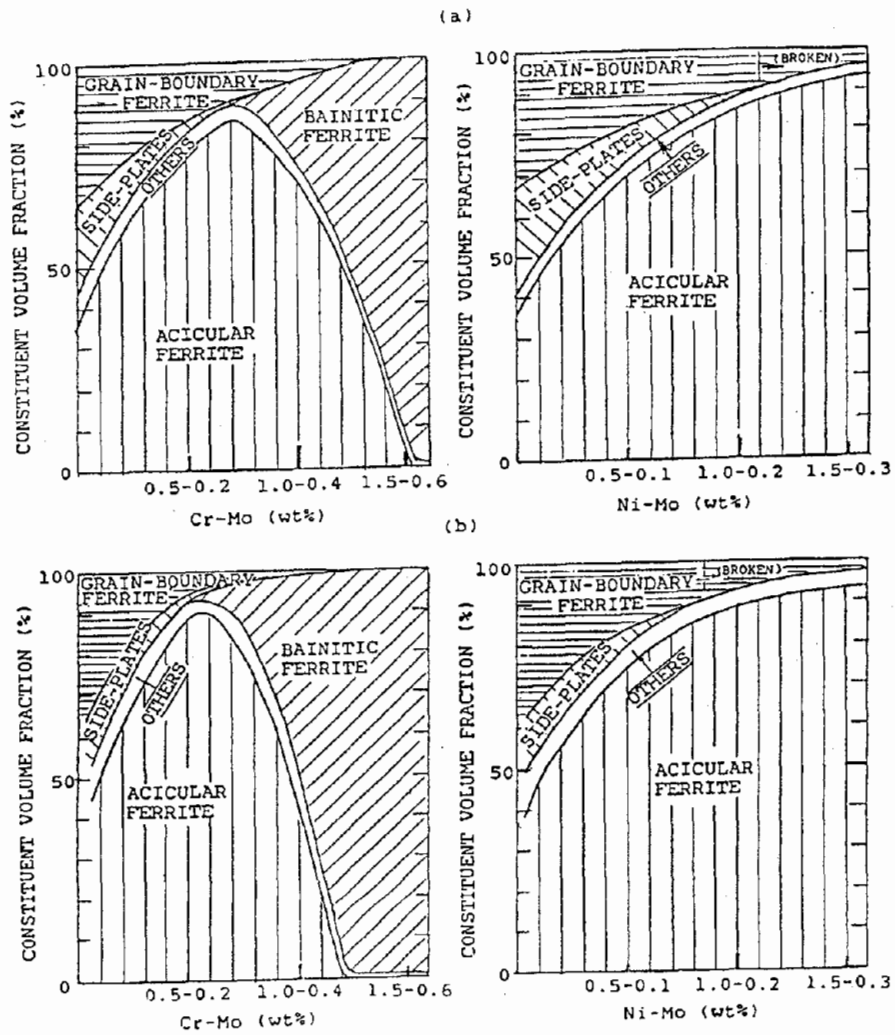


Figure 51. Effect of alloy addition on the constituent volume fractions in A36 and A588 weld metal. (Line Drawing.)

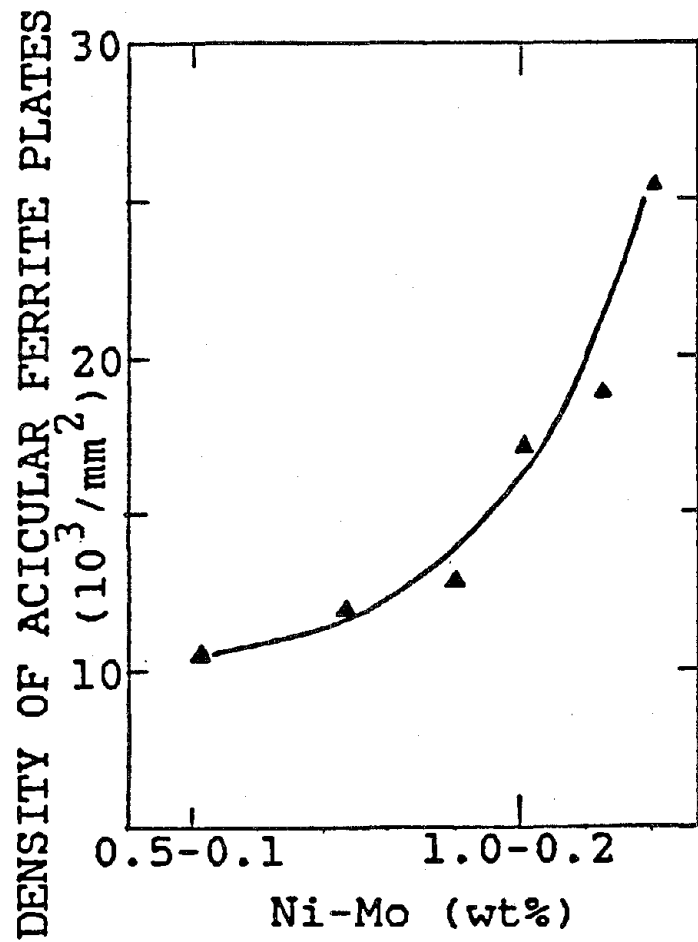


Figure 52. Density of acicular ferrite plates as a function of nickel and molybdenum content. (Line Drawing.)

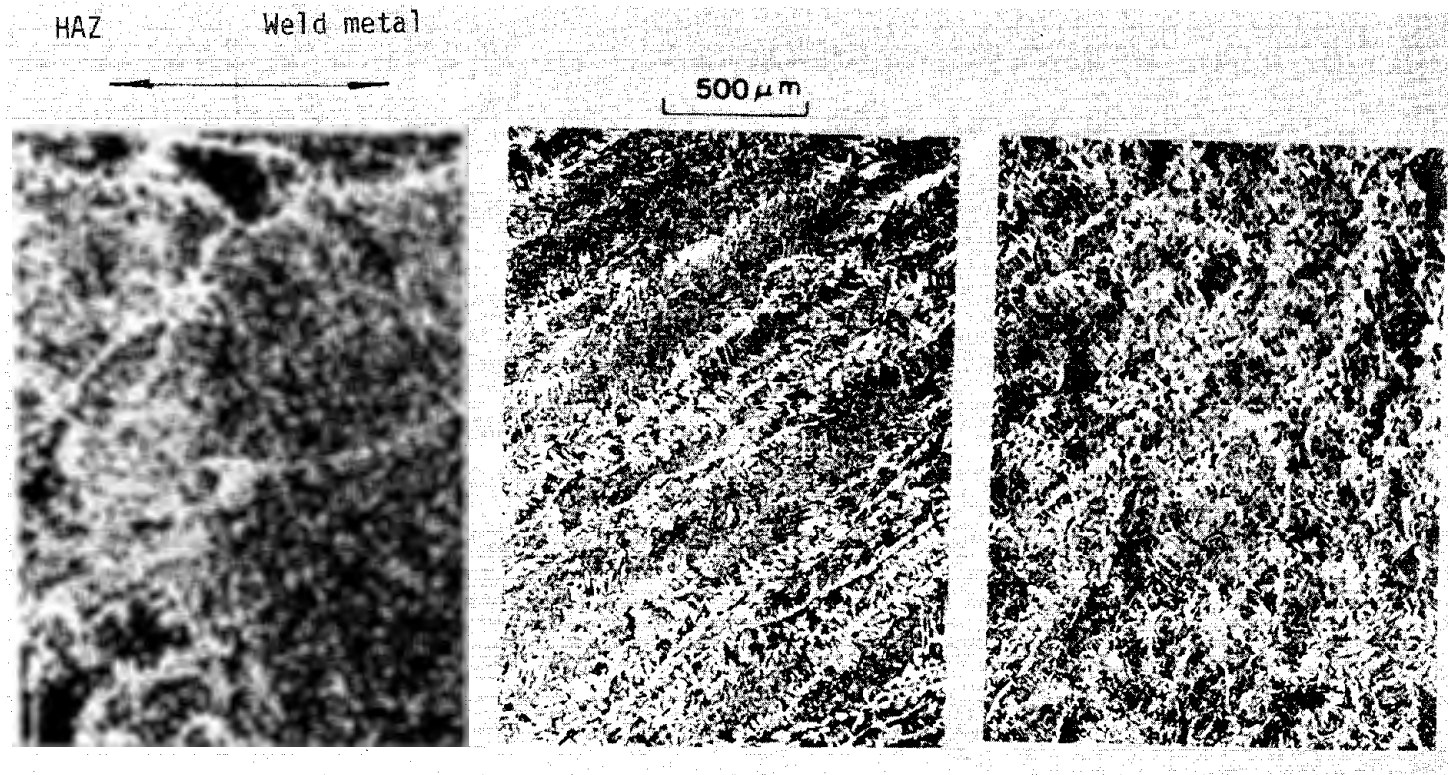


Figure 53. Typical microstructural feature of standard electroslag weldments. (Micrograph.)

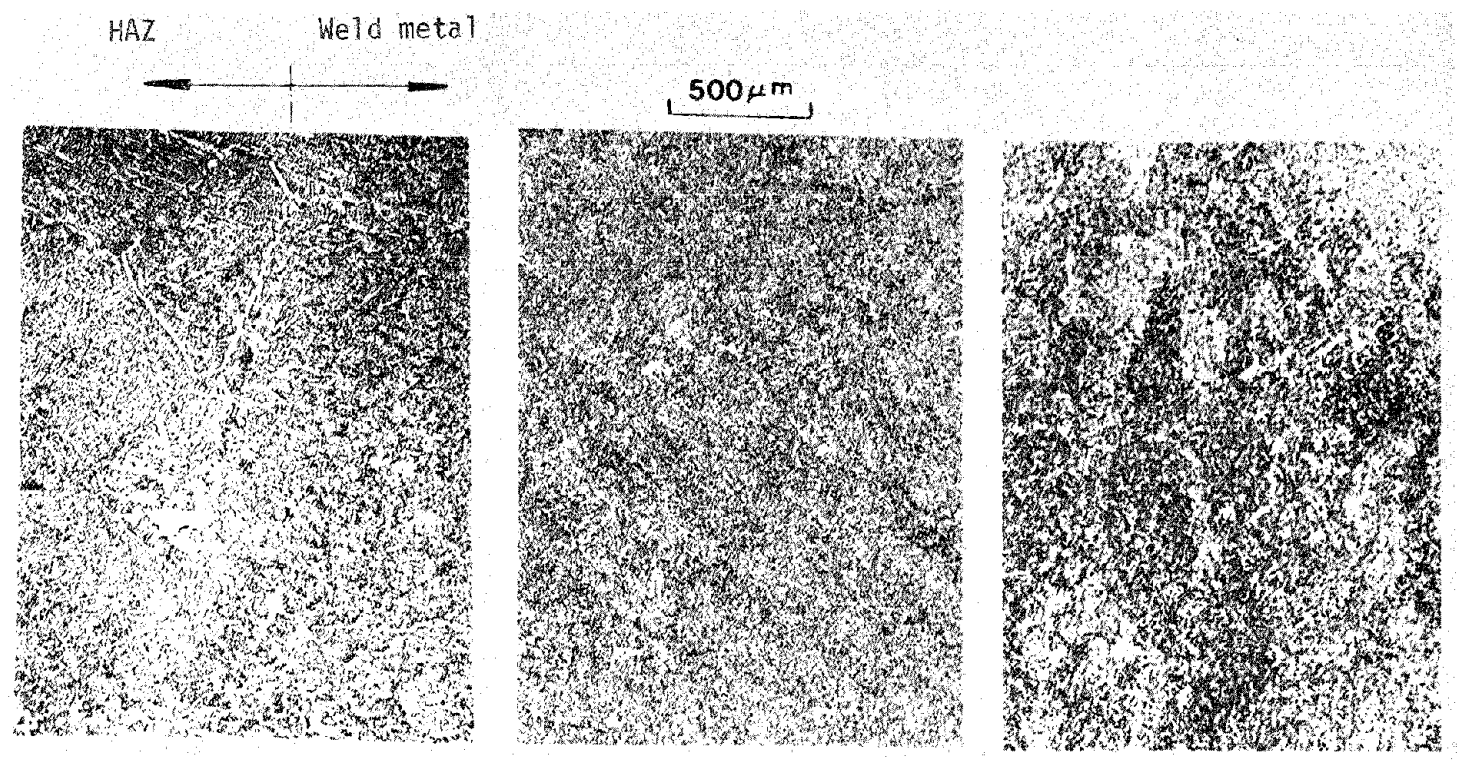


Figure 54. Typical microstructural feature of Ni-Mo alloyed electroslag weldments.
(Micrograph.)

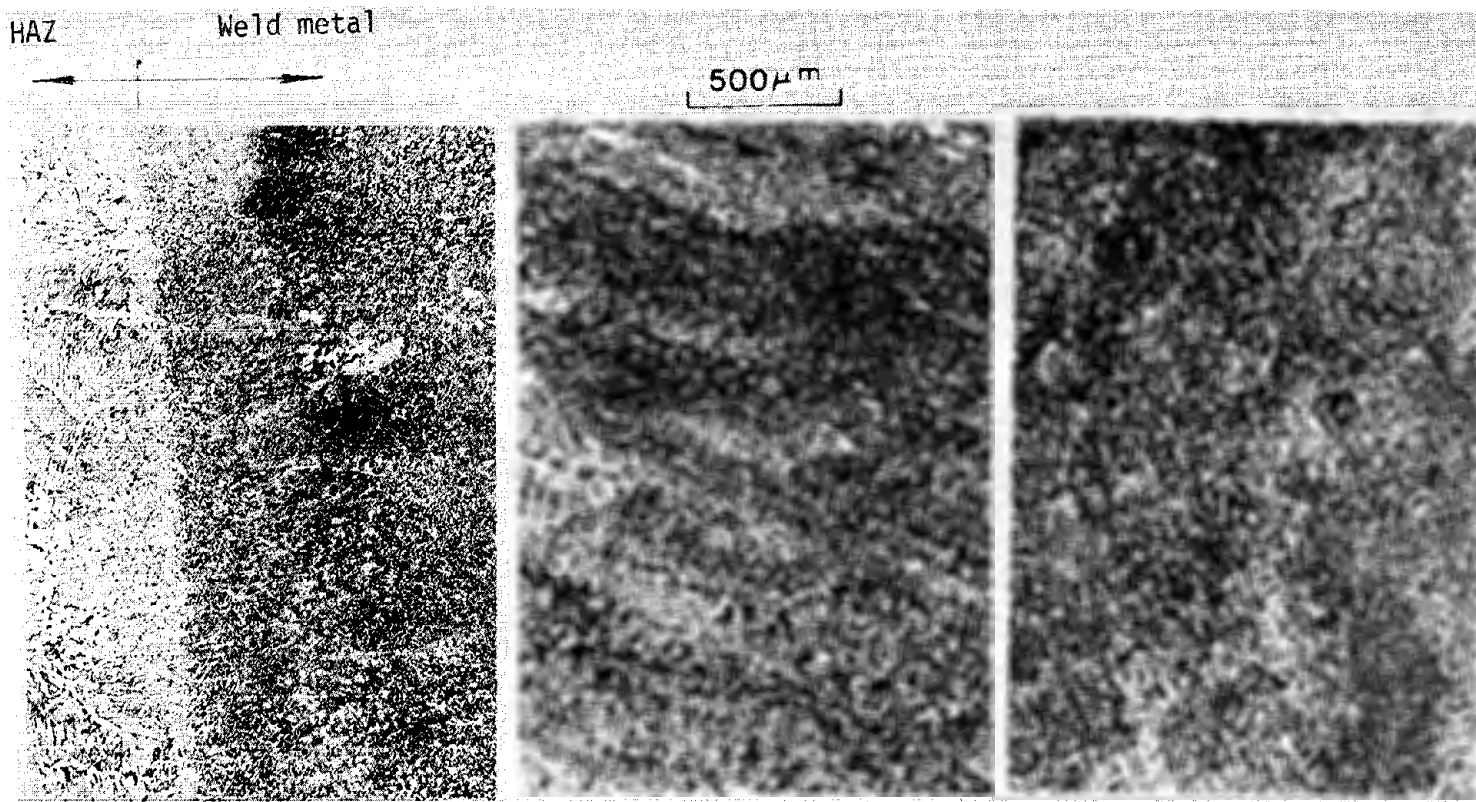
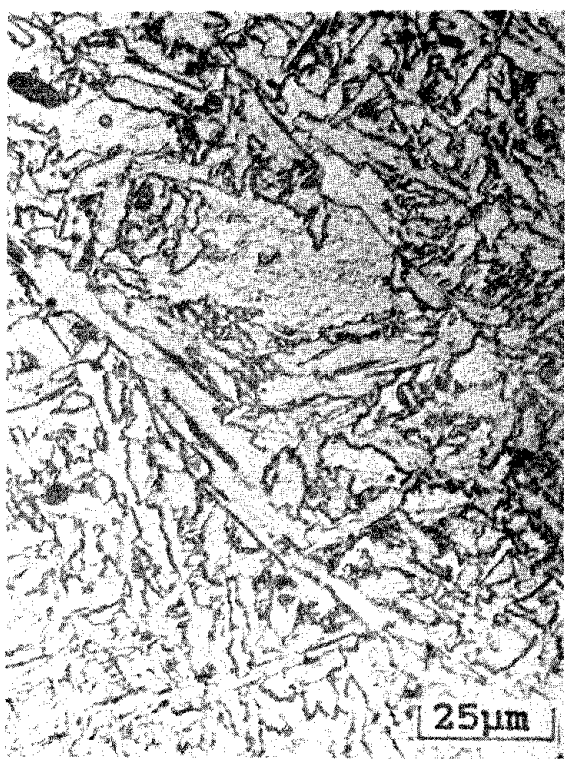


Figure 55. Typical microstructural feature of Cr and Mo alloyed electroslag weldments. (Micrograph.)



0.79%Cr-0.30%Mo



0.94%Ni-0.16%Mo

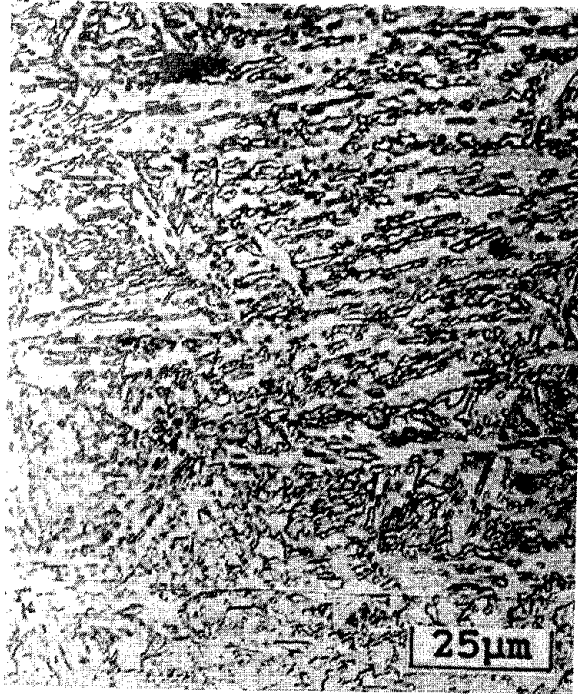
Figure 56. Acicular ferrite size distributions as a function of alloy content in 50 mm thick A36 plate. (Micrograph.)

the austenite transformation temperature while Cr raised it. Thus, nucleation of acicular ferrite at a lower temperature resulted in a finer ferrite plate size. As the Cr concentration increased, the weld metal microstructure consisted of bainite instead of acicular ferrite (figure 57).

The hardness of the Ni-Mo alloyed weld metal was compatible with both the A588 and A36 base metal hardness values, as shown in figure 58. The addition of Cr-Mo raised the hardness of the weld metal by about 20 percent over that of the base metal. Ideally, it is best to provide matching filler metal as much as possible. Therefore, the Ni-Mo addition is preferred over the Cr-Mo addition.

The optimum alloy content for filler metal to ensure satisfactory microstructure and toughness for all practical values of base metal dilution was formulated by OGC and fabricated by Stoodly Company. The composition of the 3/32-in diameter tubular electrode was identified as TW8544 (Stoodly's heat number) and is given in table 1. TW8544 typically contains 0.11 percent carbon, 1.21 percent manganese, 1.30 percent nickel and 0.20 percent molybdenum, and resembles, to some extent, Airco's AX-90 formulation. The major differences between the TW8544 and the conventional AX-90 include: 1) reduced carbon (C), 2) increased Ni, Mn and Mo, 3) slightly increased aluminum (Al) as a killing agent, and 4) the use of tubular filler metal for the TW8544. The TW8544 filler metal was used for all subsequent narrow-gap ESW to be used in mechanical testing.

Paton originally defined possible electroslog grain structure. The need to explain ESW microstructures observed during this study has resulted in the need for OGC to redefine possible ESW-induced solidified weld metal microstructures.



1.20%Cr-0.40%Mo
Bainitic Ferrite



0.91%Ni-0.20%Mo
Acicular Ferrite

Figure 57. Comparison of microstructure of 50 mm thick A588 plate between bainitic ferrite and acicular ferrite produced by Cr and Mo additions vs. Ni and Mo additions. (Micrograph.)

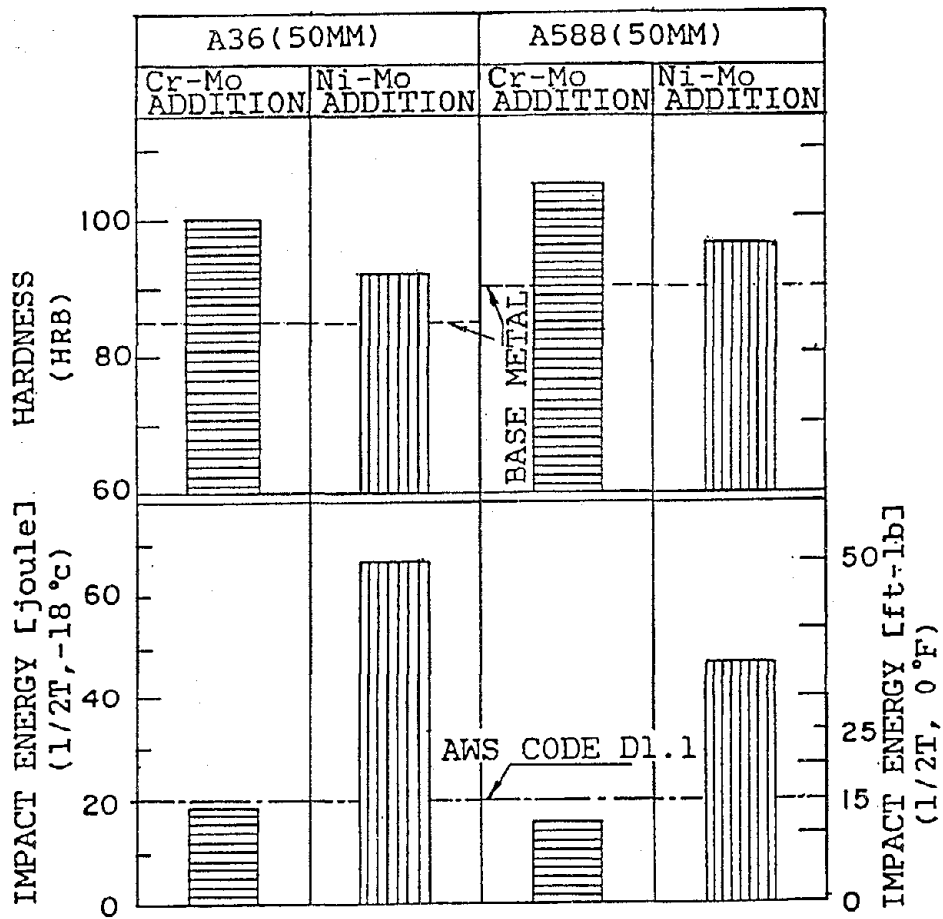


Figure 58. Summary figure showing the effects of alloy elements on hardness and impact toughness. (Line Drawing.)

3. Characteristic Grain Structures

OGC has defined five characteristic grain structures which have been found to occur in welds deposited by ESW as a result of the various conditions and parameters imposed during welding. These OGC-defined weld metal structure types are illustrated in figure 59 and described in table 4.

Table 4. OGC-defined weld metal structure types.

Type	Characteristics	Cause
I	100% FCG	High O potential flux
II	FCG + CCG	Commercial practice
III	100% CCG	Low O, highly basic flux
IV	FCG + CCG + E	High travel speed
V	FCG + E	Alloy

Note: FCG--fine columnar grain zone
CCG--coarse columnar grain zone
E--equiaxed zone

Factors affecting weld metal structures included voltage, current, gap size, welding speed, flux variables (oxygen potential, basicity, and conductivity), and minor alloying additions (up to 2 percent Ni and 0.4 percent Mo in the filler metal). A new classification system, representing five different types of grain structures, was produced in A36 and A588 electroslag weldments as a result of varying process factors.

a. Type I

This weld structure was obtained by applying high oxygen potential fluxes resulting in weld metal oxygen concentrations exceeding about 600 ppm, as illustrated in figure 60. The increased oxygen potential made with a 40 weight percent SiO_2 (manganese silicate) flux produced abundant weld metal inclusions which tended to inhibit austenite grain growth. These

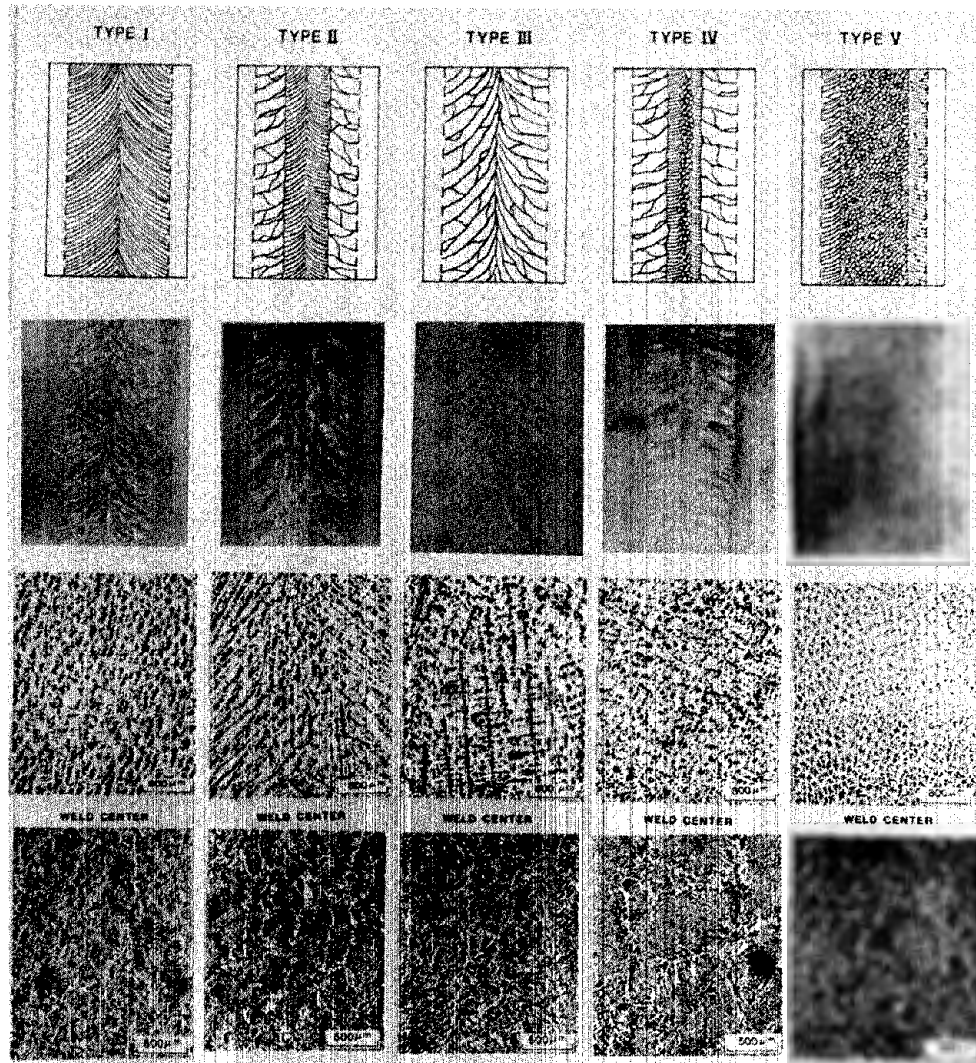


Figure 59. Classification of electroslag weld metal type by microstructure, macrostructure, and solidification structure. (Micrograph and Schematic.)



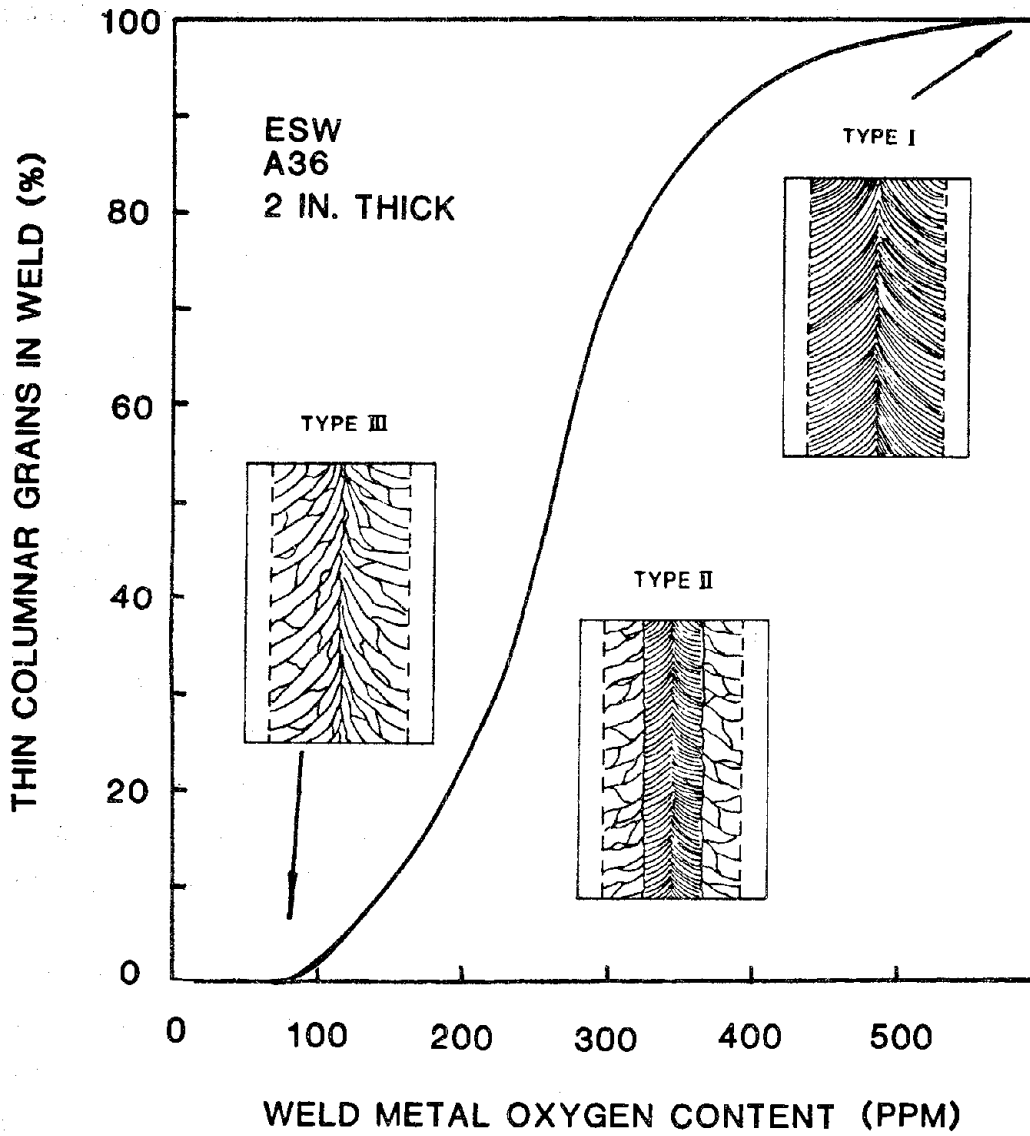


Figure 60. Percentage thin columnar grains vs. weld metal oxygen content. (Line Drawing.)

results show that oxide segregation at dendritic boundaries hinders the migration (or grain growth) of austenite grain boundaries, thus inhibiting grain growth. Thin columnar austenite grains dominated the entire weld. These oxides, in turn, nucleated copious amounts of blocky, Widmanstätten and grain boundary ferrite.

b. Type II

This weld structure was generated under normal welding conditions (including commercial welding practice) using a mild steel electrode, neutral flux and either standard or narrow gaps (table 1). The sizes of the coarse and fine columnar grain zones varied with changes in welding parameters. For example, the form factor exceeded 2.0 for low current, low welding speed and high voltage settings, and the weld metal macrostructure consisted of a small outer zone of coarse columnar grains and a large interior zone of thin elongated columnar grains. With increasing welding current and travel speed, the form factor decreased and the proportion of coarse columnar grains increased at the expense of the fine columnar grains near the weld center. For high current and welding speeds, the lowest form factor for type II (about 0.9) was accompanied with centerline hot cracking. The weld metal macrostructure consisted of a large outer zone of coarse columnar grains and a small interior zone of thin columnar grains.

The solidification of type II welds was characterized by cellular dendrites dominating near the weld edges and columnar dendrites near the weld center (figure 61). The cellular dendritic structure was associated with coarse columnar austenite grains, which transformed to large amounts of acicular ferrite. The columnar dendritic morphology prevented lateral grain growth of austenite resulting in the thick columnar structure (figure 59) which transformed predominantly into blocky and grain boundary ferrite. Increasing the welding speed increased the size of the cellular dendritic zone, which resulted in a high acicular ferrite content. Similarly, the amount and fineness of acicular ferrite increased with increasing welding

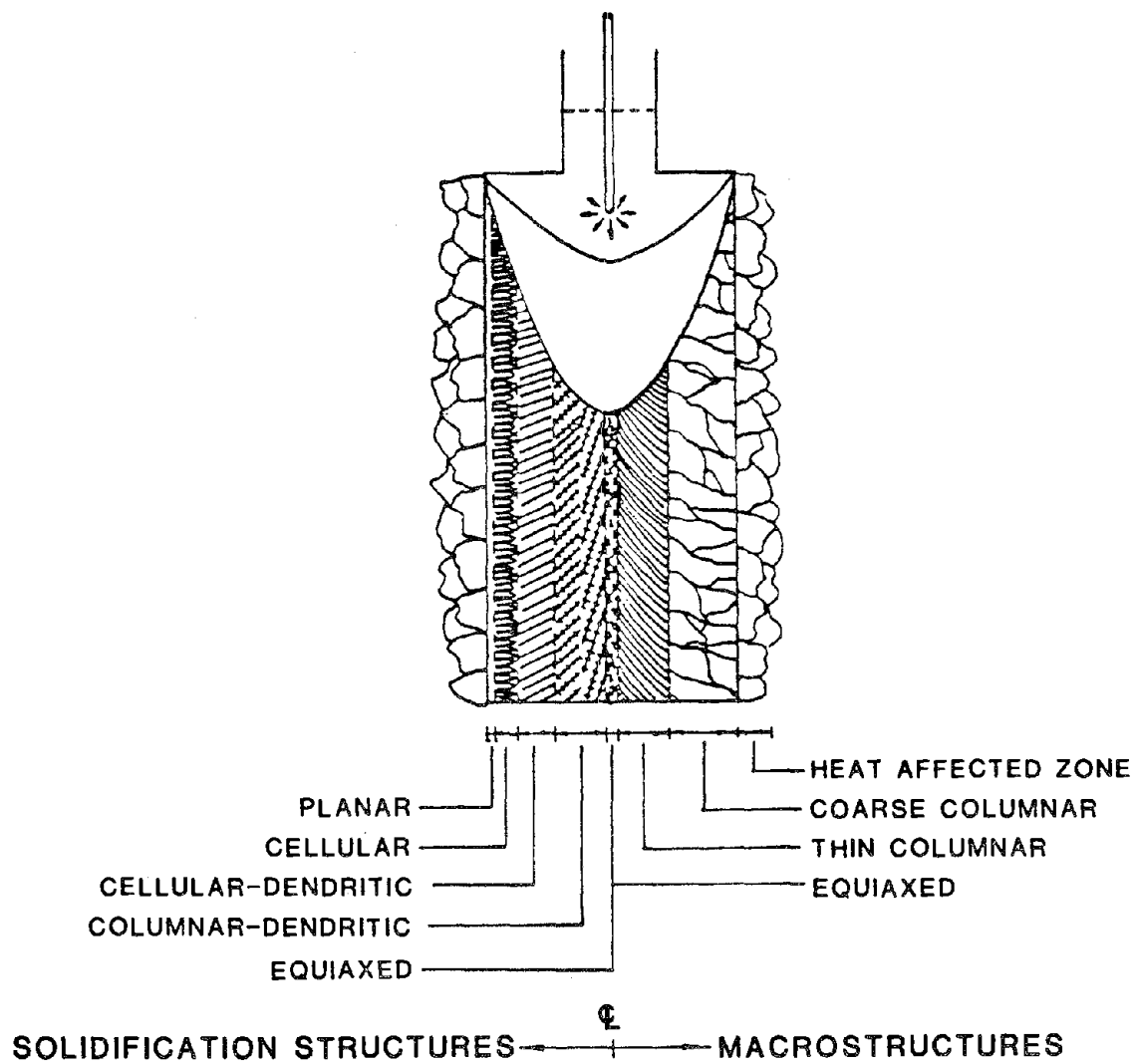


Figure 61. Relationship between weld metal solidification structure and subsequent solid state structure. (Schematic.)

speed. In addition, pearlitic structures along with the proeutectoid ferrite were observed in these steel weldments.

c. Type III

This fully coarse-grained weld structure was produced by ESW with low oxygen potential and high basicity fluxes containing $\text{CaF}_2\text{-CaO-Al}_2\text{O}_3$. The weld metal oxygen and sulfur content was typically only 80 ppm and 0.012 weight percent, respectively (a standard weld using a neutral flux would contain 2.250 ppm and 0.025 weight percent). Improved welding efficiency was also observed because of the increased conductivity of the basic slag (compared to commercial PF-201 flux). All of these effects provided a larger dendrite arm spacing due to the improved ohmic slag heating and development of coarse columnar grains. The low oxygen and impurity levels in the interdendritic regions were insufficient to retard the grain boundary migration of austenite. Thus, virtually unrestricted lateral austenite growth during weld cooling produced a fully coarse grain structure, as shown in figures 59 and 60. The reduced oxygen content decreased the amount of acicular ferrite nucleation while increasing blocky and grain boundary ferrite.

d. Type IV

This weld was developed using a mild steel electrode, neutral flux and the highest values of current and welding speeds to produce an extremely deep weld pool with a form factor of <0.9 . This solidification structure was characterized by a small zone of equiaxed dendrites at the weld center. The transition from columnar to equiaxed dendrites was believed to be associated with a fast growth rate, high amount of solute segregation and low thermal gradient at the weld center. The high degree of constitutional supercooling provided the driving force for dendrite arm remelting for nucleation of equiaxed dendrites at the weld center. Subsequent solid state transformations produced equiaxed grains containing large amounts of acicular ferrite and proeutectoid ferrite at prior austenite grain

boundaries (figure 59). The equiaxed grain structure of the weld center was so resistant to hot cracking that the high solidification-induced tensile stresses were relieved by small radial-type hot cracks (usually less than 6.4 mm [1/4 in] in length) developed intergranularly in the thin columnar grain zone.

e. Type V

When the low alloyed filler metal (AX90 and TW8544) containing Ni and Mo was added to the medium and high oxygen welds, equiaxed dendrites resulted without the aid of rapid welding speeds. This was due to the extensive degree of constitutional supercooling provided by additional alloying. It is believed that the fragile tips of growing dendrites are broken away from the main dendrites and carried into the supercooled region to provide nuclei to form equiaxed dendrites. Unlike type IV, the equiaxed dendritic structure in type V welds can occur at much lower growth rates and high temperature gradients. The solid state microstructure also showed equiaxed grains at the weld center with a high volume fraction of acicular ferrite.

The role of Ni-Mo alloy addition to the weld metal appears to promote the following: a) equiaxed dendritic and grain structures around the weld center, b) grain boundary and blocky ferrite reductions, c) acicular ferrite increases up to about 90 percent, and d) elimination of the coarse columnar austenite grain structure near the fusion line. The Ni-Mo alloying additions tended to reduce the nucleation rate of high temperature transformation products (blocky, grain boundary and Widmanstätten ferrite.) The retardation of austenite grain growth due to solute interdendritic segregation made the development of TCG structures across much of the weld possible with a high volume fraction of acicular ferrite.

The proportions of the coarse columnar, thin columnar and equiaxed zones varied with alloy content and oxygen concentration in the weld (figure 62). Generally, as these variables increased, the size of the thin

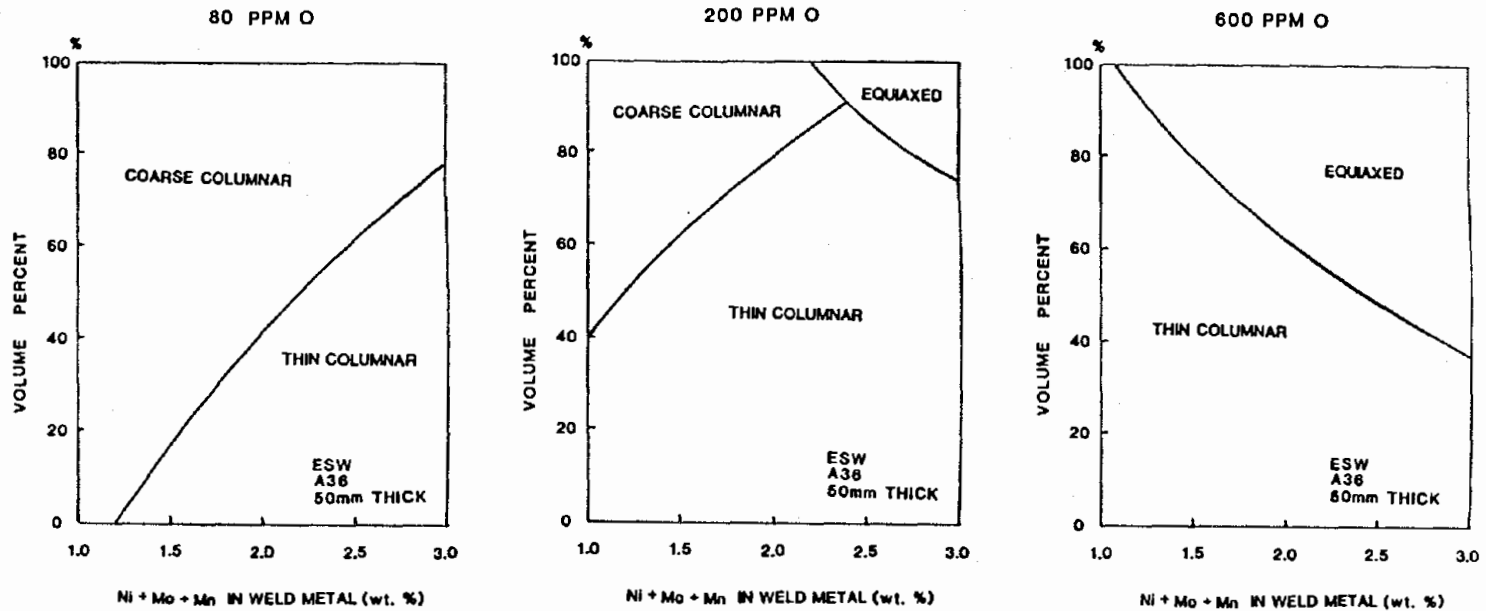


Figure 62. Relationships among percentage of coarse columnar, thin columnar, and equiaxed zones as a function of alloy content and oxygen content in electrosag welds. (Line Drawing.)

columnar zones increased. Further increases of alloy and oxygen concentration in the weld increased the size of the equiaxed zone at the expense of the thin columnar zone.

Increasing the oxygen content promoted the nucleation of the higher temperature ferrite transformation products. The effect of oxygen concentration on the ferrite content in electroslag welds is shown in figure 63. Welds made with CaF_2 -rich basic fluxes showed the lowest weld metal oxygen contents. With increasing silica content in the flux, the weld metal oxygen and silicon contents were found to increase. The best microstructures for maximum acicular ferrite and good toughness were obtained with fluxes having a basicity index of about 1.2, which corresponds to around 180 ppm of oxygen and 50 percent acicular ferrite at the weld center of A36 welds using mild steel electrodes. Up to 90 percent acicular ferrite and the best toughness values obtained in this study resulted with neutral flux and minor additions of Ni and Mo (AX90 or TW8544) to the weld.

f. Charpy V-Notch Toughness

The CVN impact energies at -18°C (0°F) for each structure type are compared in figure 64. Type I structures exhibited low impact energy due to the large amount of oxygen inclusions. A588 welds with the type II structures developed slightly lower toughness than similar A36 welds, despite the high amount of acicular ferrite. In both A36 and A588 welds, the minor additions of Ni-Mo (AX-90 or TW8544) filler substantially increased fracture toughness and lowered the ductile/brittle transition temperature of the weld metal. The Ni-Mo alloying additions provided the further benefits of substantially increased resistance to hot cracking because of the development of equiaxed grains to the weld center zone. An important achievement in types I, III, and V structures was the uniformity of CVN impact toughness and grain structure across the entire weld.

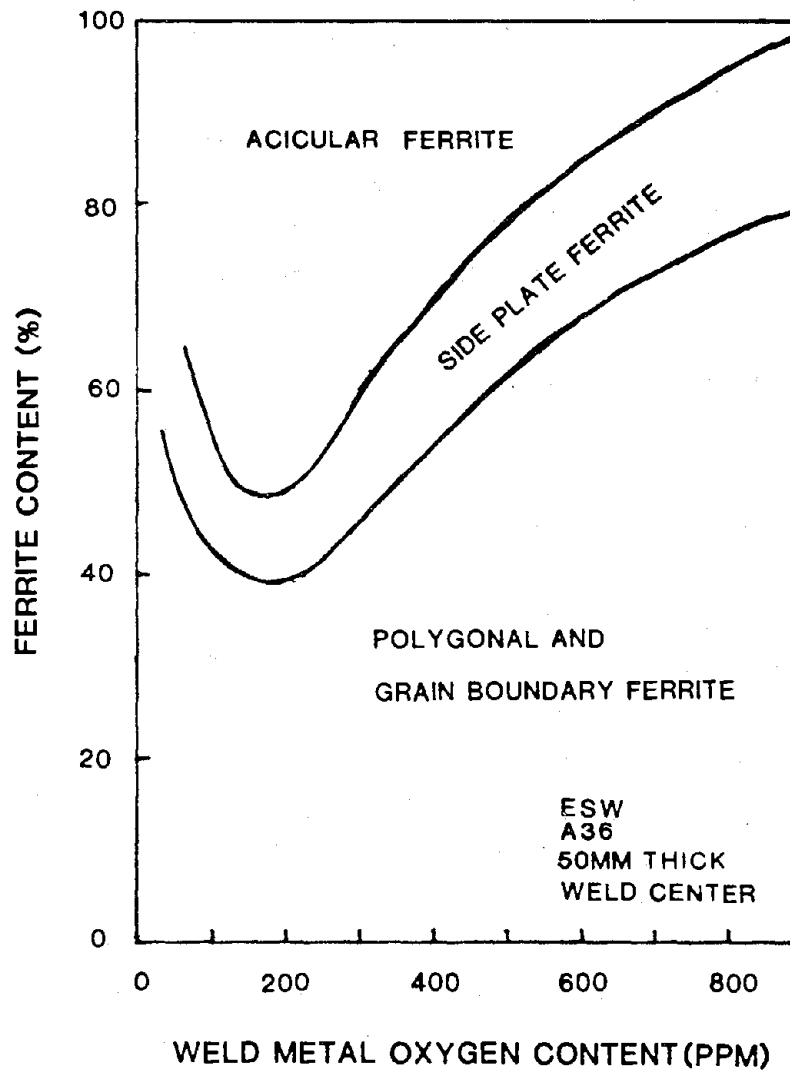


Figure 63. Distribution of ferrite content types as a function of weld metal oxygen content. (Line Drawing.)

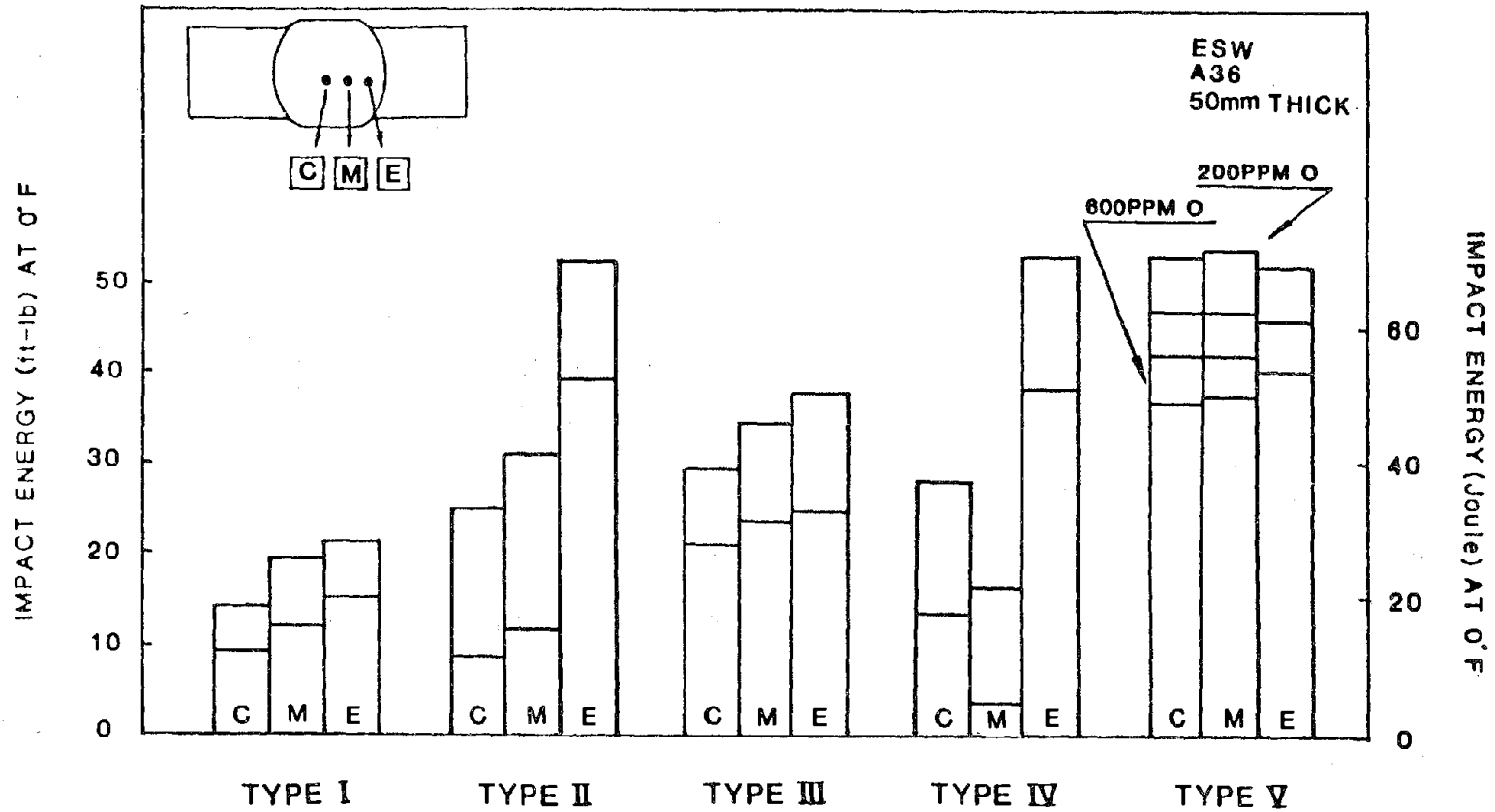


Figure 64. Summary of CVN impact energies as a function of electroslag weld metal type and oxygen content. (Line Drawing.)

4. Optimized Weld Parameters and Alloy Composition

By combining high-speed narrow-gap ESW parameters with the TW8544 tubular filler metal, weld deposits were both structurally sound and substantially tougher than the zone 2 requirement. The optimum conditions required to produce the toughest welds while maintaining reliable welding procedures are listed below in table 5:

Table 5. Optimum welding conditions.

Plate	Thickness	Guide	Gap	Current	Voltage
A36 & A588	50 mm	Wing	19 mm	1100 A	35 V
A36 & A588	76 mm	Web	19 mm	1300 A	35 V

5. Weld Metal Grain Refinement

The outstanding capability of the quartz shroud to resist hot cracking (illustrated in figure 65) and its uniform (type I) grain structure are the primary reasons for development of this method of ESW. The quartz shroud resulted in substantial grain refinement (figure 66), because the guide tube provided a narrow jet stream of superheated/gaseous slag and a sharp thermal gradient between weld center and the unmelted base metal. This condition extended the guide and electrode filler metal deep into the slag pool. Consequently, the intense forced-convective field, in addition to the electromagnetic Lorentz force, permitted an extensive crystal multiplication by fragmentation or remelting of previously solidified dendrites protruding ahead of the advancing solid-liquid interface.

The ESW process using the quartz shielded guide tube assembly involved heat transfer which is markedly influenced by the fluid flow phenomena in

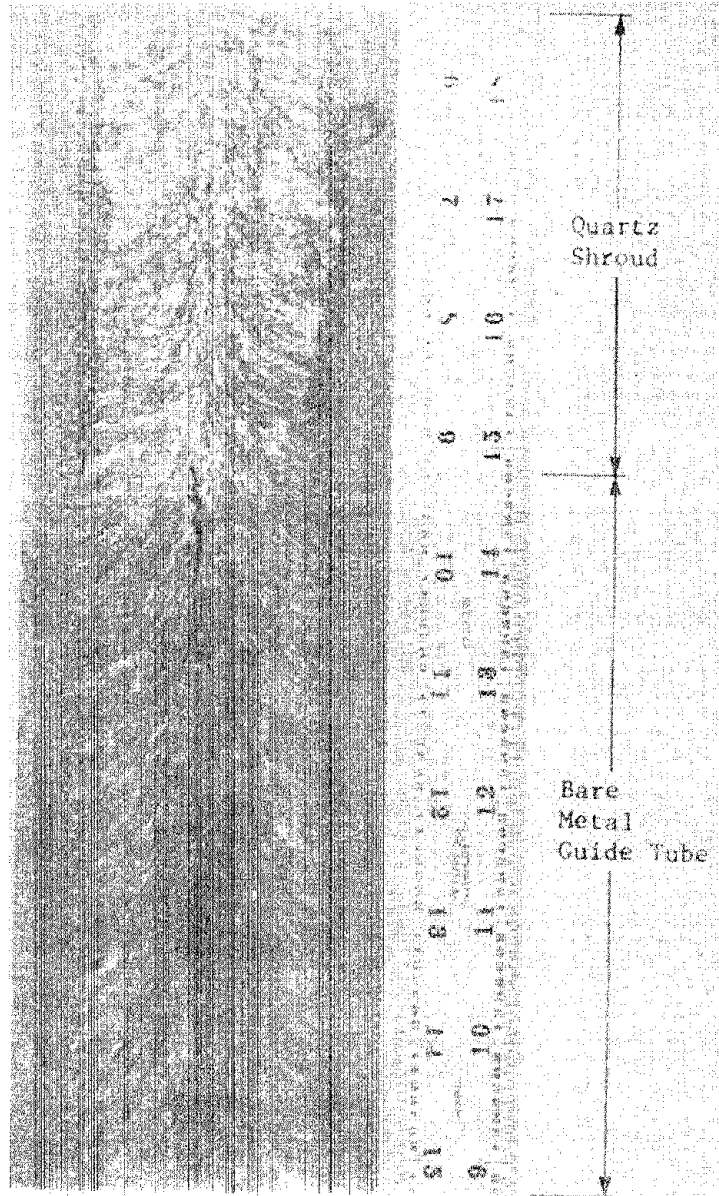


Figure 65. Hot cracking resistance influenced by the addition of a quartz shroud during electroslog welding. (Micrograph.)



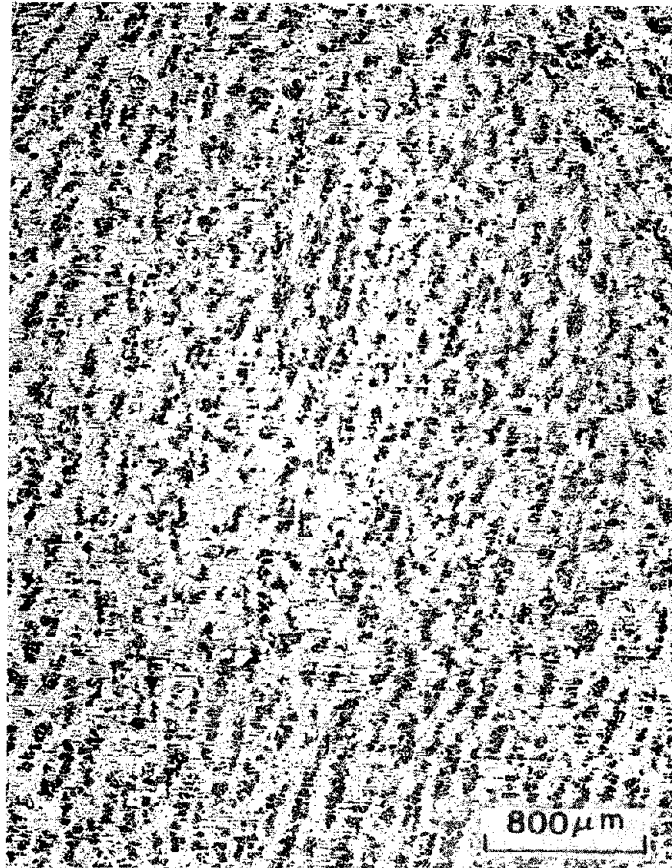


Figure 66. Fragmented dendrites due to intense molten pool stirring during quartz grain-refined electroslag welding. (Micrograph.)



the weld pool. A decrease in the effective conductivity (and increasing viscosity) of the slag by quartz dissolution decreased both the generation and local transport of the ohmic heat (figure 67). Since this decreased the proportion of the total heat transported to the base metal side, local heat generation patterns were extremely sensitive of the electrode location and wire straightening. Even minor misalignment of the electrode resulted in a markedly asymmetrical heat generation pattern and lack of fusion (see figure 68). The use of electrode oscillation provided more uniform heat-generation patterns.

A non-linear relationship between base metal dilution and voltage (figure 69) was observed at a given current. In order to generate sufficient heat to melt the base metal, it was necessary to apply a higher voltage (around 48 V) than that used in welds without quartz shielding. Any overpotential led to severe arcing. Apparently, a jet stream of superheated/vaporized slag generated by joule heating at the electrode tip area was sufficient to blow the slag out and locally boil the slag, introducing a gas envelope which caused persistent submerged and exposed arcing. Form factor was not greatly influenced by either the welding voltage or current (figure 70). Ironically, the conditions necessary to produce sound, tough welds in the standard ESW process were the worst conditions for the quartz-shielded guide grain-refined ESW process.

The sequence of solidification and the slag-metal reactions played a key role in determining the weld properties. Excessive oxygen potential in the manganese silicate fluxes with quartz shielding (figure 71) significantly increased the nucleation of polygonal, grain-boundary and Widmanstatten ferrite (figure 72). The high oxygen potential also led to many large inclusions (figure 73) which help to nucleate ferrite early in the austenite-ferrite transformation. By increasing the oxygen in the weld metal through quartz dissolution, the amount of acicular ferrite was decreased. With the further increase of weld metal oxygen up to 800 ppm, the amount of acicular ferrite approached zero as shown in figure 72. Composition control through the introduction of low alloy filler metal was

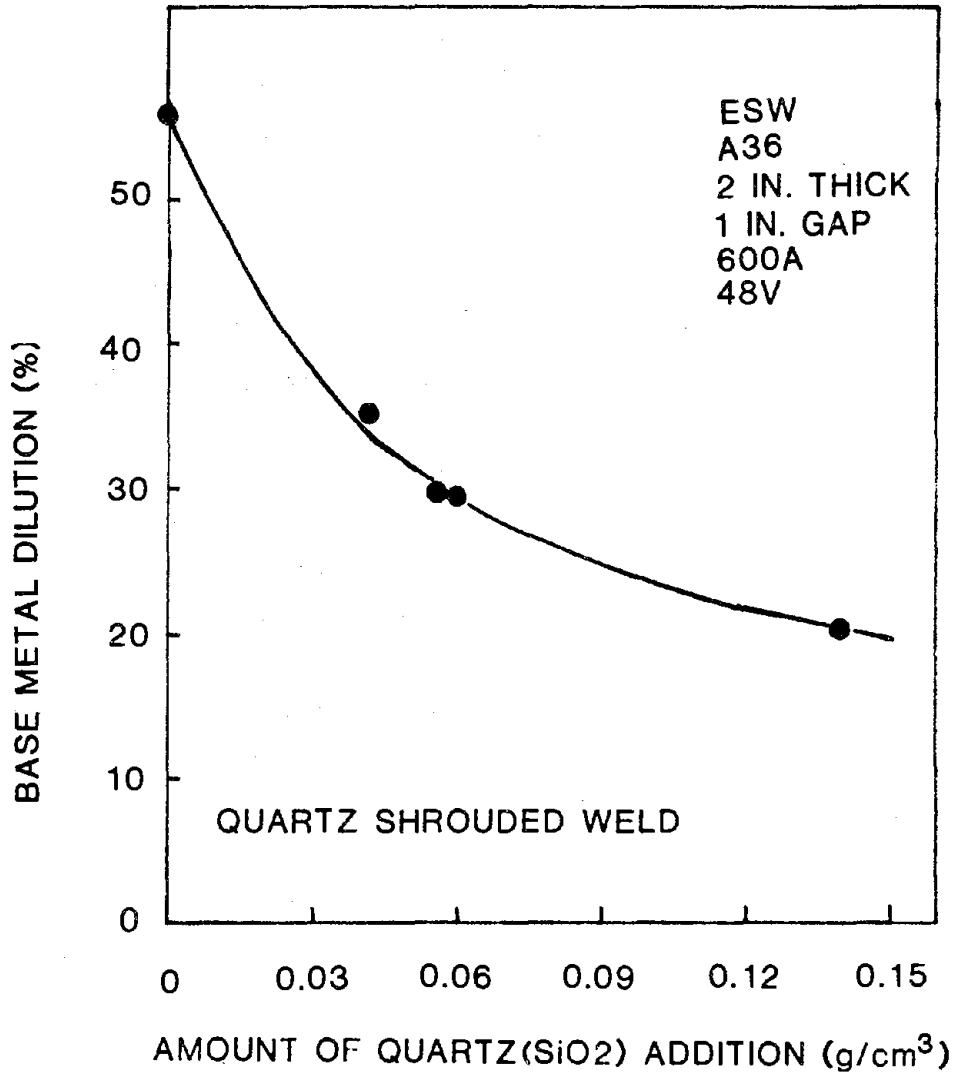


Figure 67. Base metal dilution vs. quartz additions during quartz grain-refined welding. (Line Drawing.)

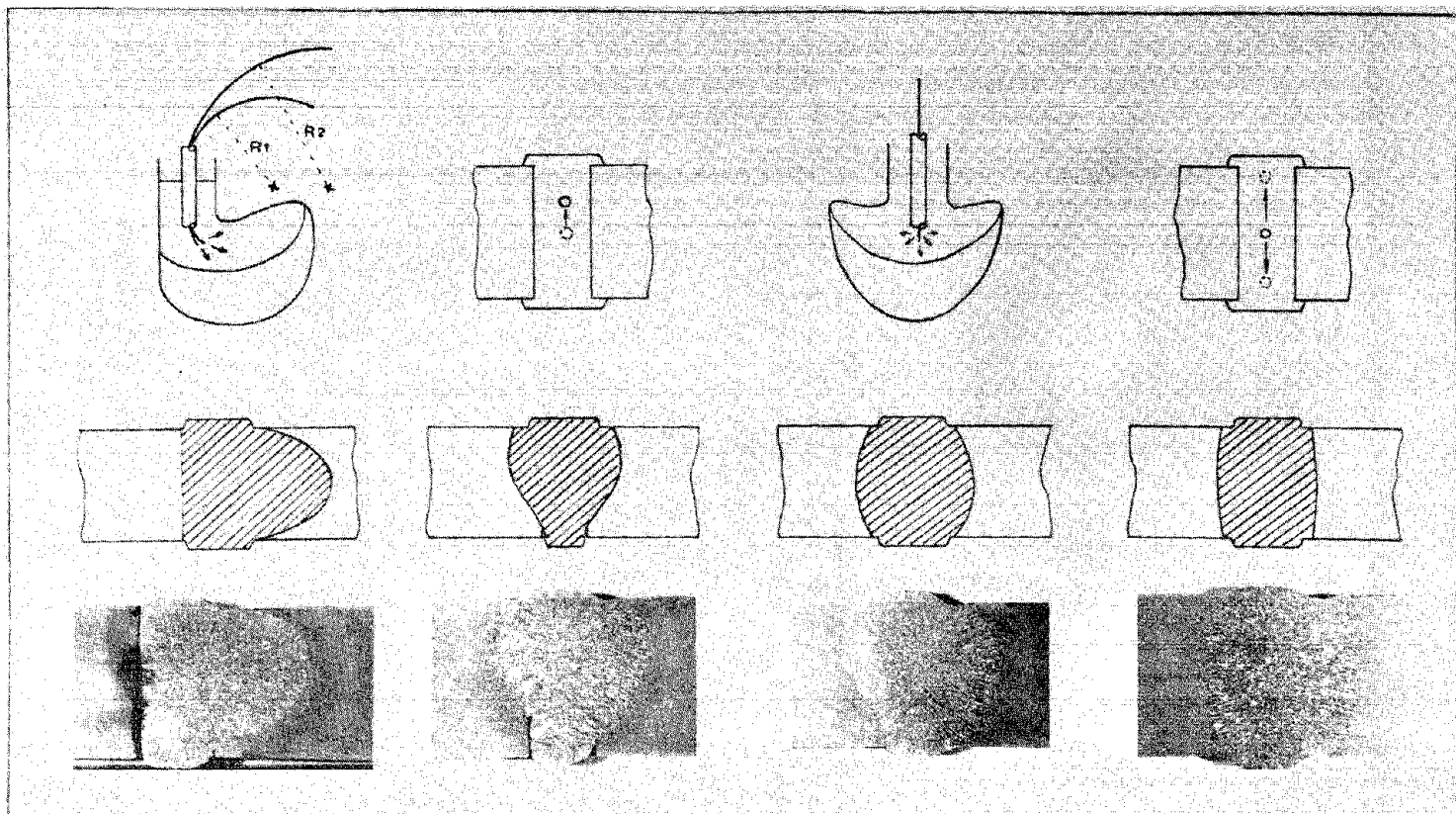


Figure 68. Influence of electrode misalignment and asymmetrical heat generation during quartz welding. (Micrograph and Schematic.)

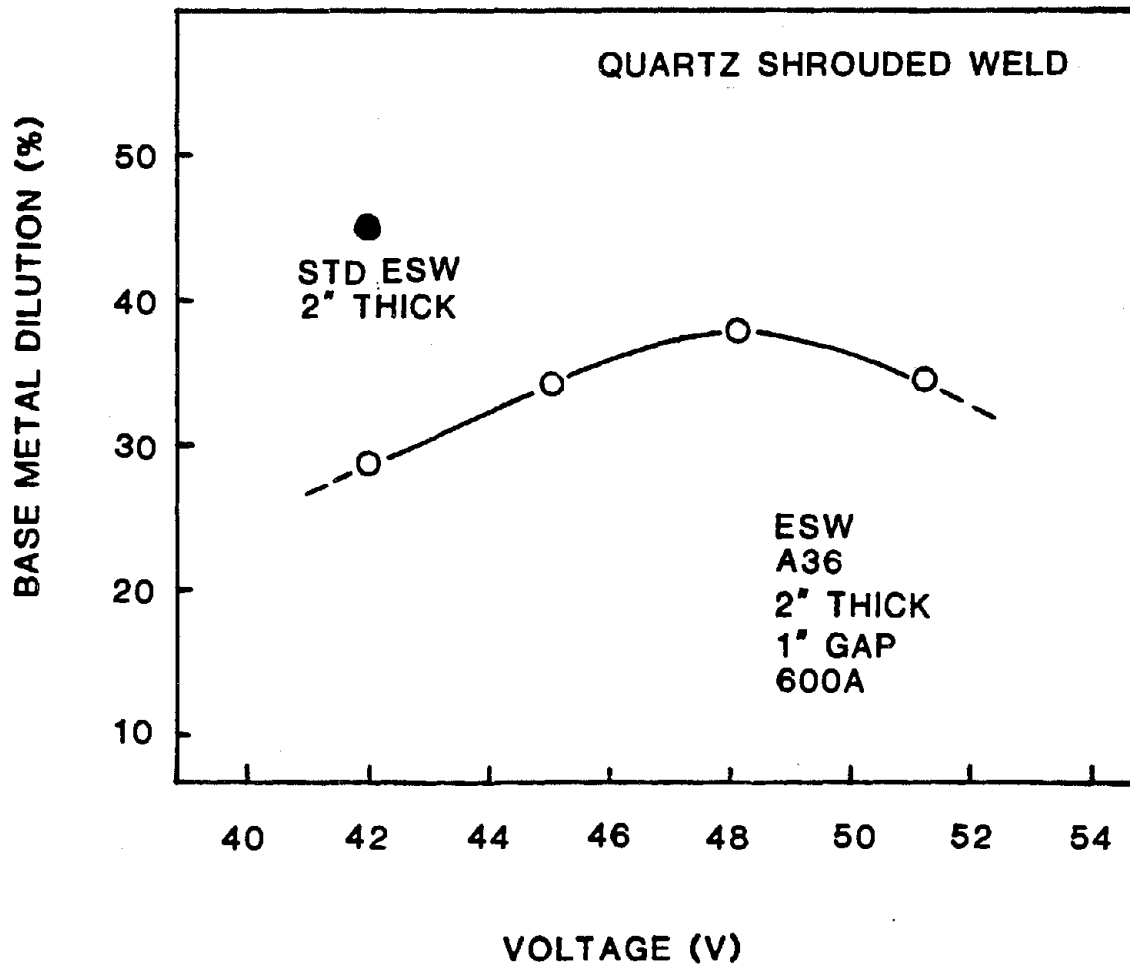


Figure 69. Base metal dilution vs. voltage during quartz electroslag welding. (Line Drawing.)

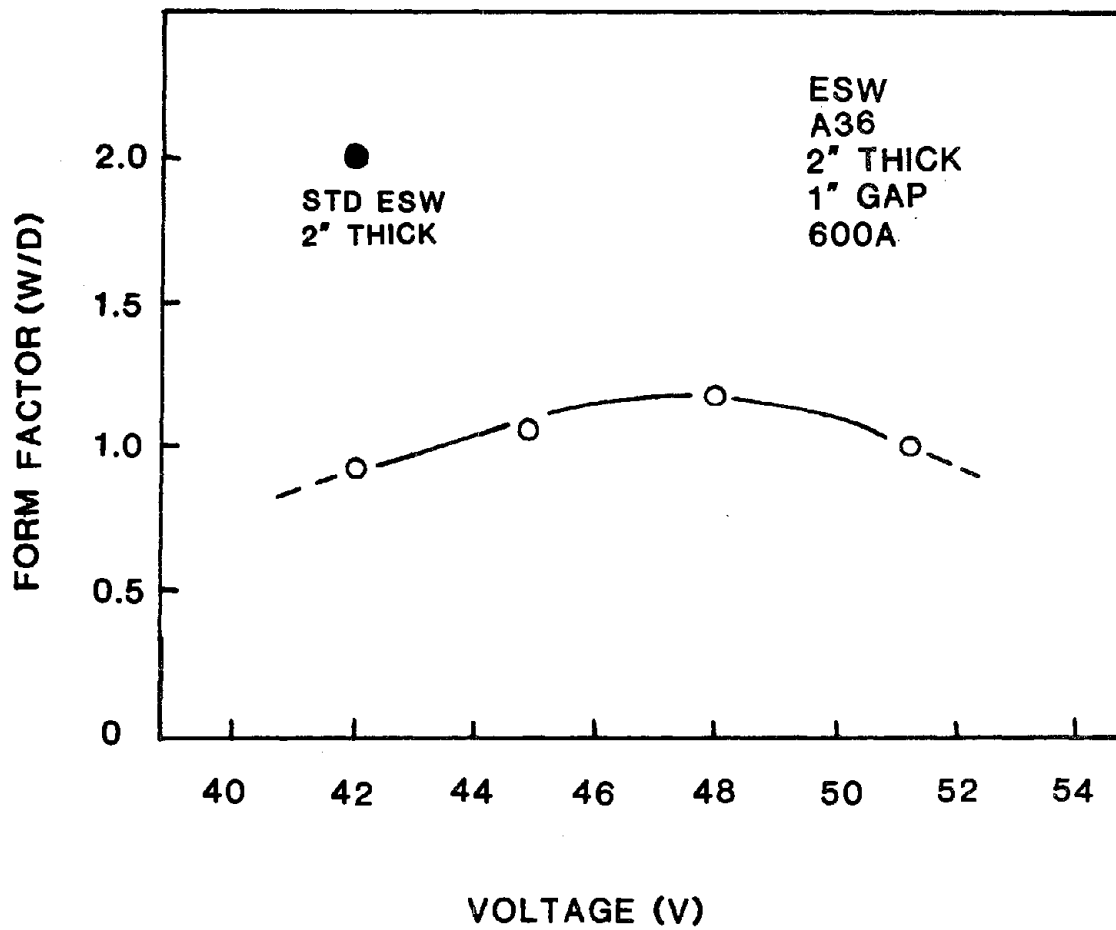


Figure 70. Form factor vs. voltage during quartz electroslag welding. (Line Drawing.)

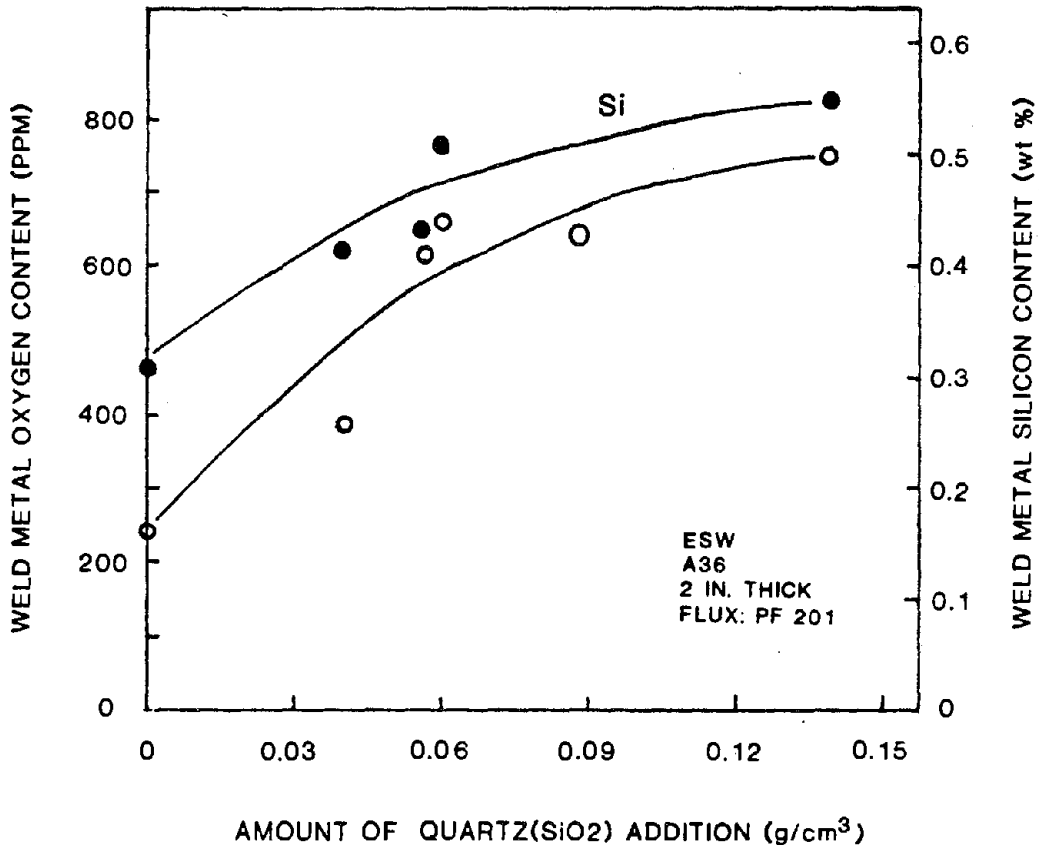


Figure 71. Oxygen content vs. amount of quartz addition during quartz grain refinement welding. (Line Drawing.)

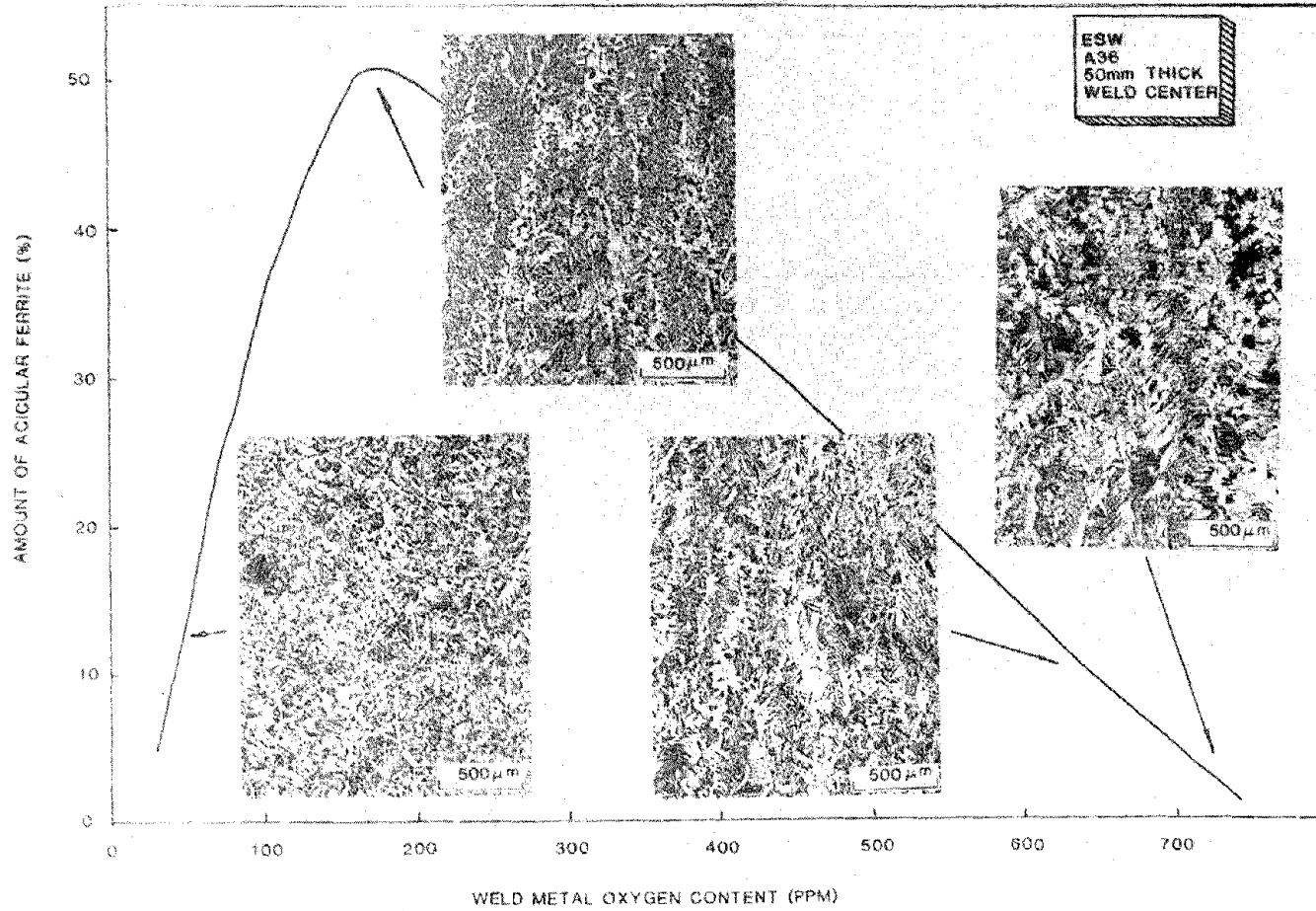


Figure 72. Percent acicular ferrite formation vs. weld metal oxygen content. (Micrograph.)

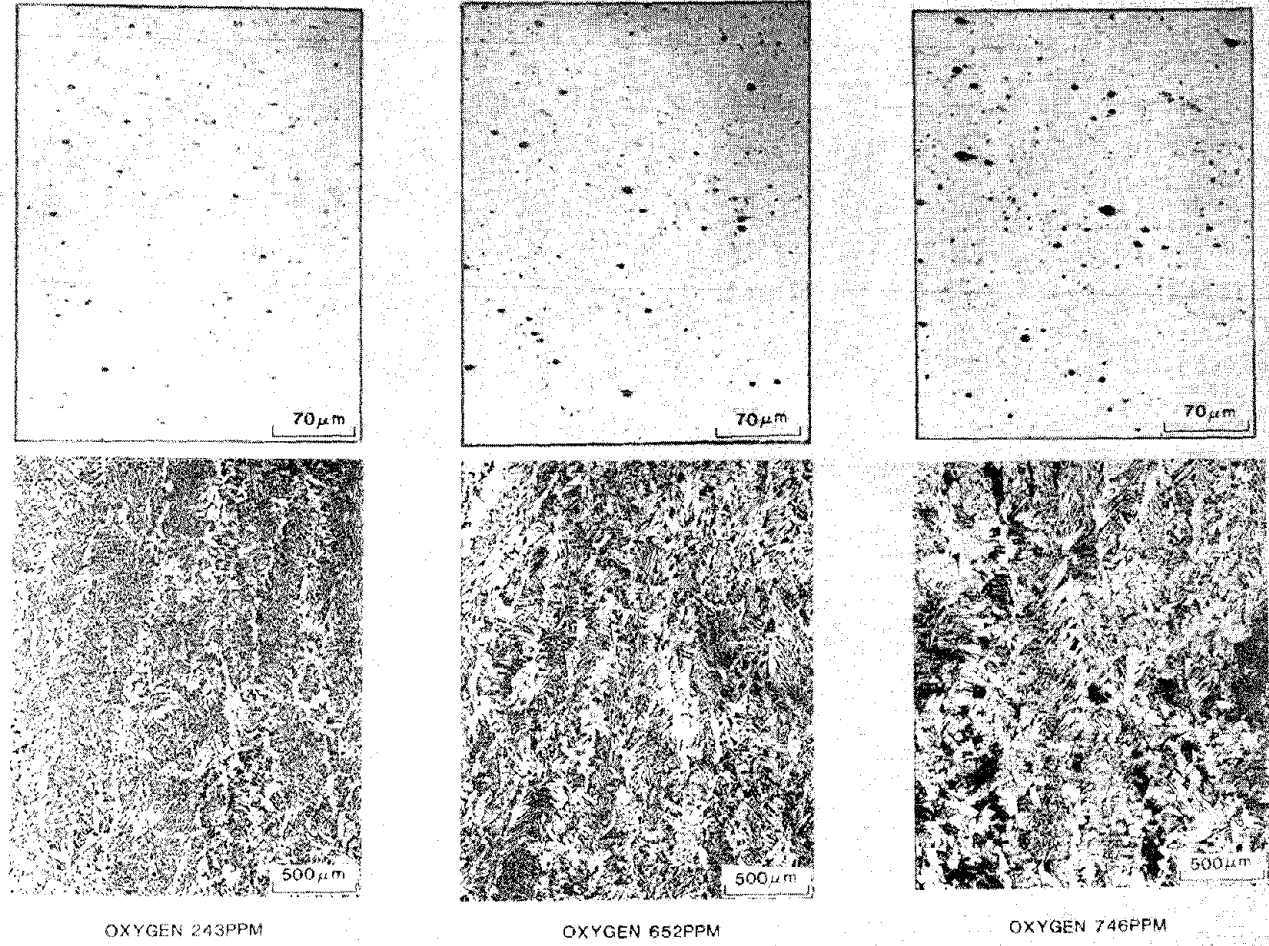


Figure 73. Inclusion distribution as a function of oxygen potential and oxygen content. (Micrograph.)

necessary in order to increase the volume fraction of acicular ferrite. The amount of acicular ferrite was significantly increased (75 percent) by alloy modifications (AX90, high Ni electrode) with refined grain boundary ferrite. In addition, weld metal carbon content was found to be substantially decreased with increasing weld metal oxygen content because of the degassing by carbon monoxide formation during vigorous agitation.

Despite the fact that the quartz shroud method of ESW achieved refined grain structures, the reliability in producing weld deposits free of imperfections was seriously in doubt. In more than 50 percent of the quartz shrouded welds made in the laboratory, severe lack of fusion imperfections resulted. At this time, no solution to the lack of fusion problem was found for quartz-shrouded ESW.

6. Charpy V-Notch Toughness of Optimized Electroslag

For all ESW-optimized welds analyzed in this study, standard CVN transition curves were conducted in three locations. These were: 1) midthickness weld centerline, 2) quarter-thickness weld centerline, and 3) midthickness in the coarse heat affected zone (HAZ1). The HAZ specimens were taken within approximately 1.5 mm from the fusion line, unless noted otherwise. A schematic illustration of the specimen locations is given in figure 26. In all cases, CVN specimen blanks were subjected to surface grinding and etching prior to identification of the proper notch location.

CVN tests were conducted on many process development welds prior to fabrication of the optimized welds. The results from approximately 500 CVN tests were used in determining optimum process parameters and alloy additions. These initial results formed the basis for the choice of parameters used for ESW 120 cm long mechanical property test weldments fabricated at OGC using the three basic practices explained below. Overall, considering both alloys and thicknesses, and all the various weld practices and

alloying additions, together with the grain refining tests, over 200 conditions were evaluated prior to fabricating the final mechanical property weldments.

The results presented in this section were obtained from the 120 cm long mechanical property weldments. These weldments also contained material for the full thickness K_{IC} tests. A total of 46 CVN transition curves are reported, and data include both A36 and A588 in both 50-mm and 76-mm thicknesses. For each alloy and thickness, three conditions were studied. These include: 1) a standard gap (SG) practice, 2) an OGC-modified narrow gap (NG) practice, and 3) an OGC narrow-gap weld and metal alloy addition practice. The third condition, (NG, ST), was varied to allow further reduction of heat input, which effectively increased the weld metal alloy content. This condition is noted by the addition of a "2" to the notation, i.e., NG, ST2. The last procedure, a pseudo fourth condition, resulted in the lowest heat input, the fastest welding condition, and the best toughness level in all regions.

Table 6. ESW practices for mechanical property evaluation.

Conditions	Alloy	Nomenclature	Heat Input
Standard gap practice	A36	SG, 25P	highest
Standard gap practice	A588	SG, WS	
Narrow gap	A36	NG, 25P	low
Narrow gap	A588	NG, WS	
Narrow gap/alloyed	A36	NG, ST	lower
Narrow gap/alloyed	A588	NG, ST	
Narrow gap/alloyed	A36	NG, ST2	lowest
Narrow gap/alloyed	A588	NG, ST2	

Note: 25P is standard A36 wire, WS is standard A588 wire, and ST is Stoodly tubular wire.

The welding conditions and nomenclature in table 6 are referenced in the remaining figures and tables.

One special non-optimized condition was also evaluated in this program. This consisted of two "quartz" grain-refined welds, one welded using standard filler wire while the other used alloyed wire. Development of optimum welding parameters was precluded due to consistent lack of fusion difficulties. This last data does confirm the potential to achieve a significant reduction in ESW grain size together with enhanced impact toughness using quartz-shrouded guide tubes. Transition curves for the various optimized welds conducted in this program are listed in table 7.

Table 7. CVN transition curve analysis as a function of ESW weld condition.

Alloy	Thickness (mm)	Weld Designation	Location	Report Figures
A36	50	SG, 25P	1/2 T 1/4 T HAZ 1	78, 101 79, 101 80, 93, 101
A36	50	NG, 25P	1/2 T 1/4 T HAZ 1	78, 87 79, 89, 80
A36	50	NG, ST	1/2 T 1/4 T HAZ 1	78, 88, 97 79, 97 80, 93, 97
A36	76	SG, 25P	1/2 T 1/4 T HAZ 1	81 82 83
A36	76	NG, 25P	1/2 T 1/4 T HAZ 1	81, 87 82, 89 83, 94
A36	76	NG, ST	1/2 T 1/4 T HAZ 1	81, 88 82 83, 94

Table 7. CVN transition curve analysis as a function of ESW weld condition. (cont.)

Alloy	Thickness (mm)	Weld Designation	Location	Report Figures
A36	76	NG, ST2	1/2 T 1/4 T HAZ 1	81, 88, 98 82, 98 83, 94, 98
A588	50	SG, WS	1/2 T 1/4 T HAZ 1	75, 90 77 76, 92, 95
A588	50	NG, WS	1/2 T 1/4 T	75 77, 91
A588	50	NG, ST	1/2 T 1/4 T HAZ 1	75, 90, 99 77, 91, 99 76, 92, 95, 99
A588	76	SG, WS	1/2 T 1/4 T HAZ 1	84, 90 85 86, 92, 96
A588	76	NG, WS	1/2 T 1/4 T HAZ 1	84 85, 91 86
A588	76	NG, ST	1/2 T 1/4 T HAZ 1	84 85 86
A588	76	NG, ST2	1/2 T 1/4 T HAZ 1	84, 90, 100 85, 91, 100 86, 92, 96, 100
A588	76	Quartz, 25P	1/2 T 1/4 T	-- --
A36	50	Quartz, ST	1/2 T 1/4 T	102 --
A36	50	Base Metal	1/4 T	74, 97
A36	76	Base Metal	1/4 T	74, 98
A588	50	Base Metal	1/4 T	74, 99
A588	76	Base Metal	1/4 T	74, 100

Unless otherwise noted, each data point in the transition curve is the average of two or more points. Six tests were conducted at -18°C . The curves representing these data are shown in figures 74 through 102. See appendix A for complete Charpy data. Selected data are shown in tabular form in table 8. Also, the temperatures at which selected CVN energies were obtained are shown in table 9 in order to facilitate comparison for three impact test requirements (20, 27 or 33 Joules).

There are many ways to group these data, and the figures and tables in this report are meant to facilitate key comparisons. Based on these data the following results can be summarized:

- o The base metal CVN properties for both alloys and both thicknesses met the required impact properties.
- o Assessment of the CVN properties at the 1/4 T position is not conservative and can produce widely-varying results depending on the specific weld metal microstructure at that location.
- o While the narrow gap process improves the CVN data, it is insufficient by itself to sufficiently increase the toughness. Further changes in the form of alloy additions are required, especially in thickness section sizes.
- o Alloy additions, together with narrow gap practices and the related OGC process changes designed to reduce heat input, produce significant increases in the weld metal CVN properties in all cases where the alloy additions were sufficient to induce a predominately acicular ferrite.
- o The use of tubular electrode wire to further reduce weld heat input further increased the toughness of the weld and heat affected zones.
- o The improvement in the weld metal CVN properties between the OGC-recommended and the standard practice is dramatically demonstrated in figures 90 and 91 for the 1/2 T and 1/4 T test locations in A588 alloy.
- o The HAZ1 shows similar results for A588, and at the 76-mm thickness, a greater than 50°C decrease in the transition temperature was observed.
- o Figure 97 summarizes the optimized 50-mm A36 data as acceptable for all CVN locations, including the base metal.

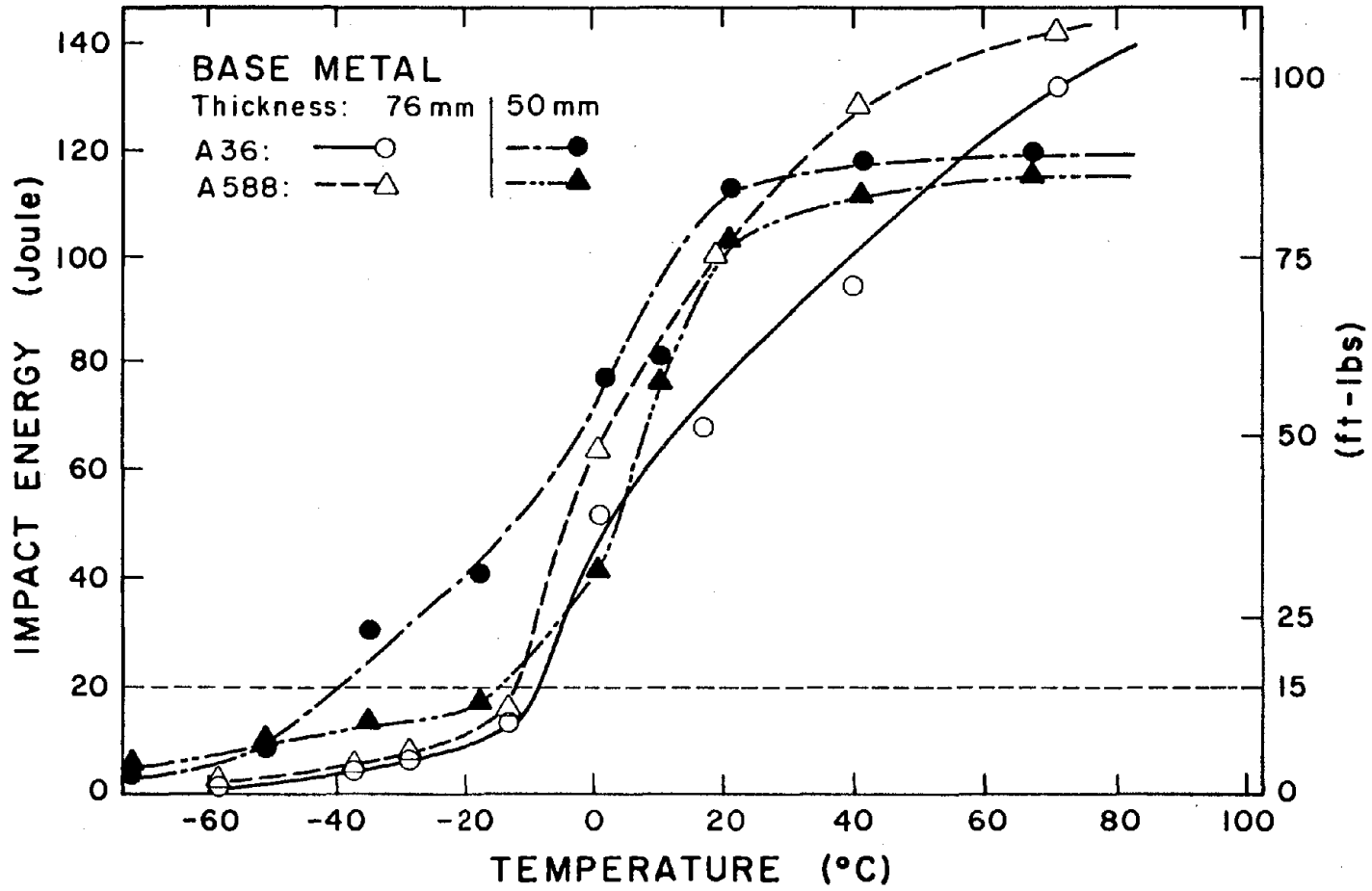


Figure 74. CVN transition curve for A36 and A588 base material.

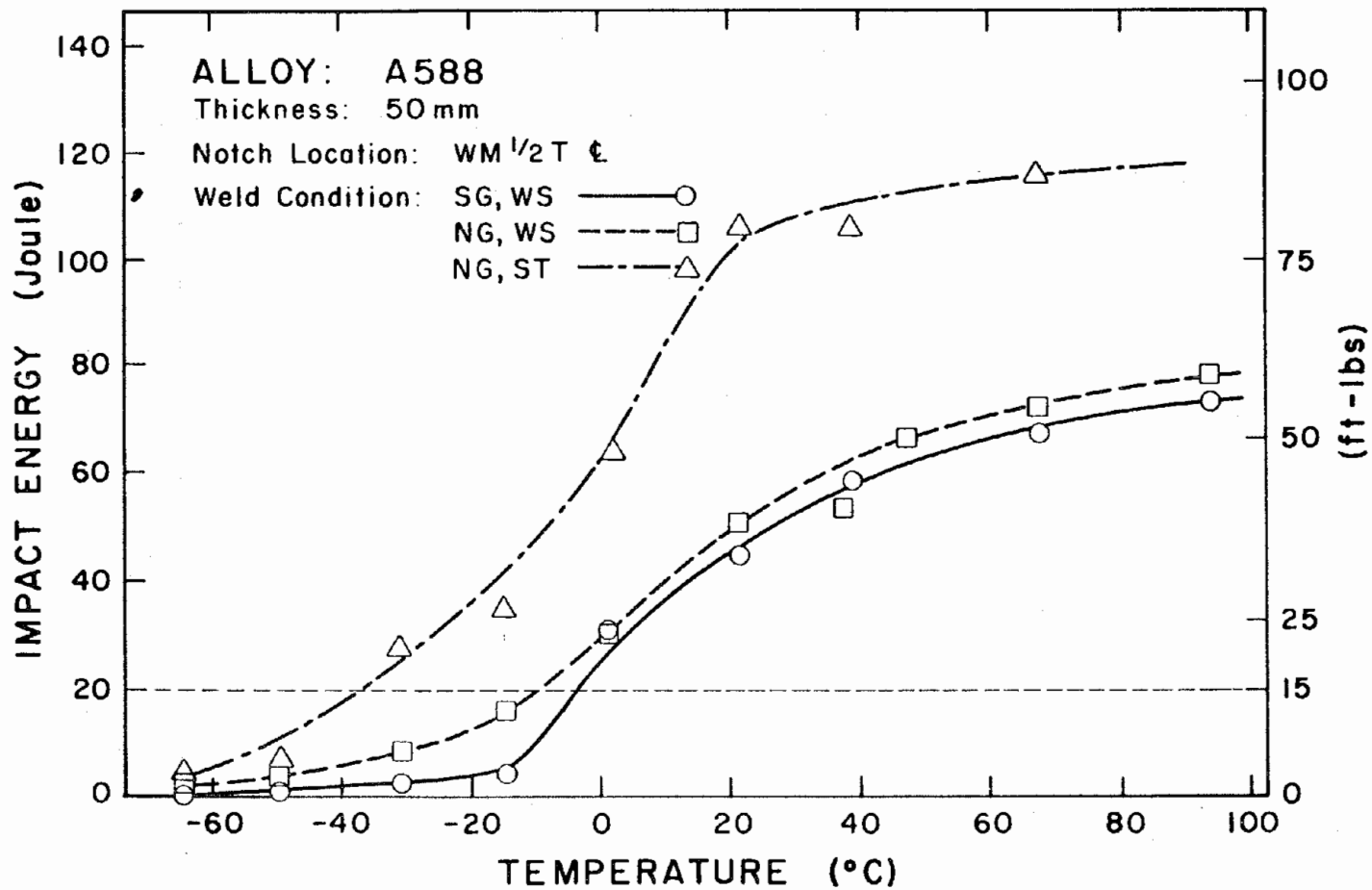


Figure 75. CVN transition curves for 50 mm A588, notch location WM $\frac{1}{2}$ T \perp .

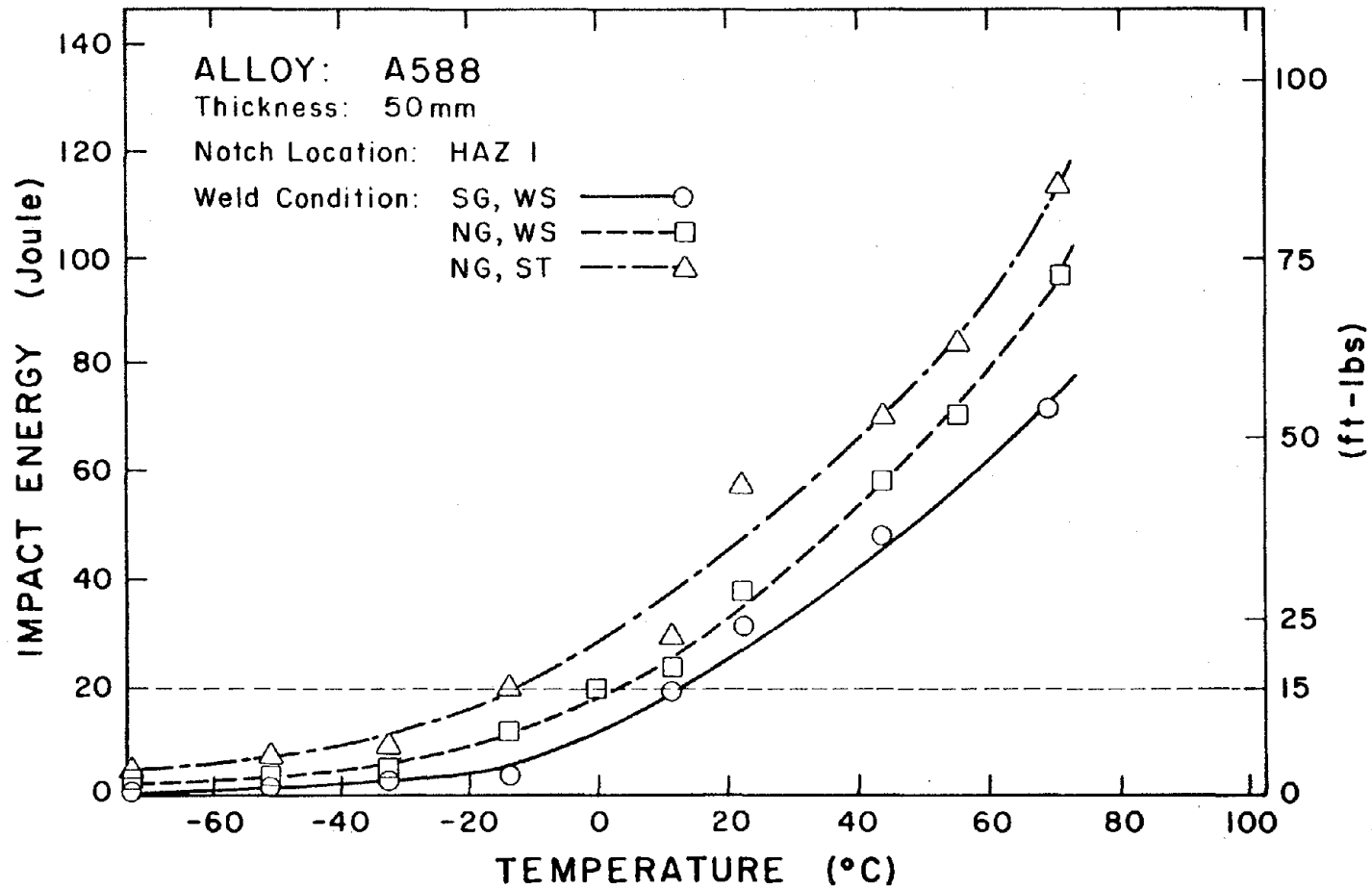


Figure 76. CVN transition curves for 50 mm A588, notch location: HAZ 1.

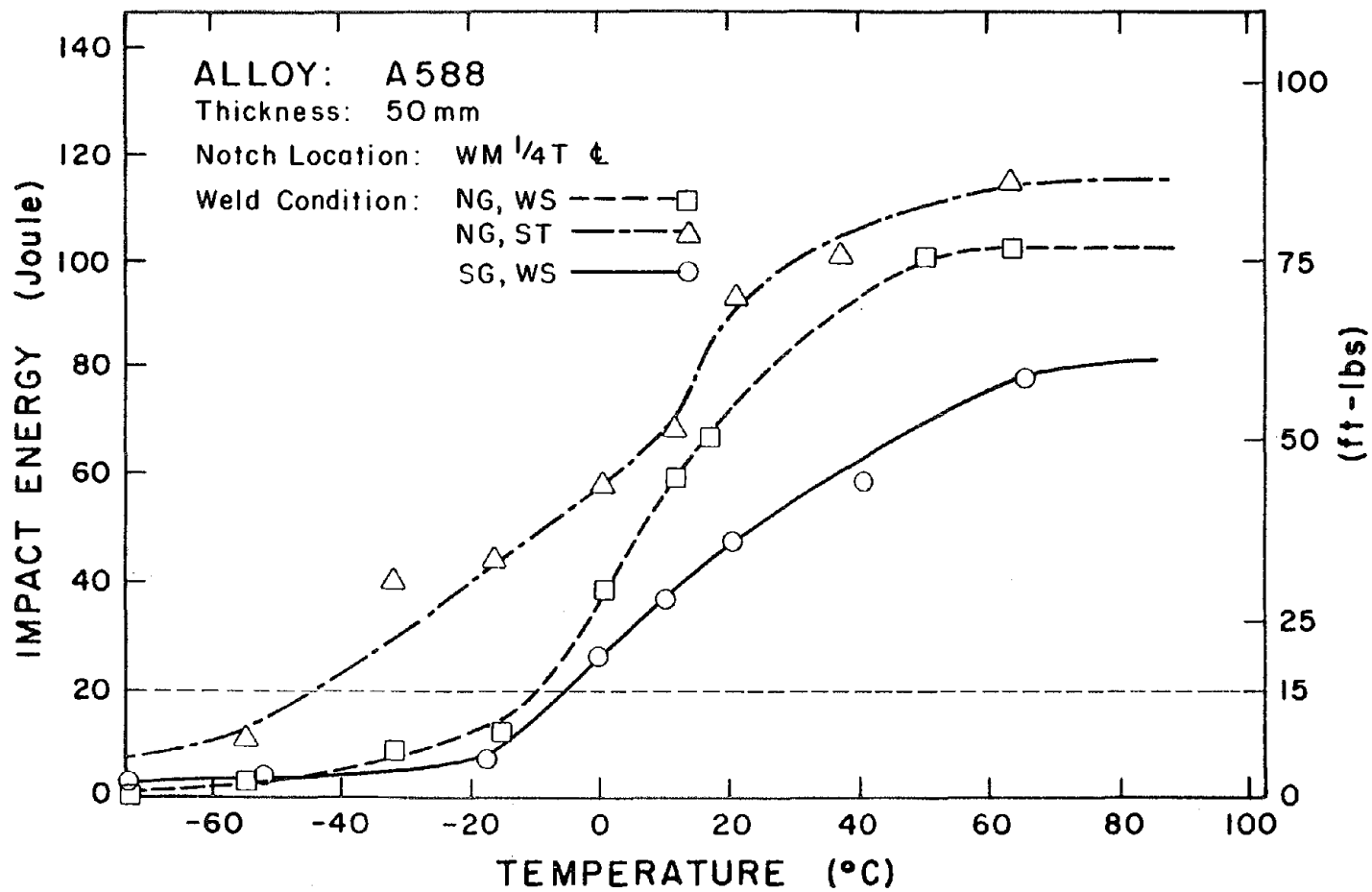


Figure 77. CVN transition curves for 50 mm A588, notch location: WM 1/4T ϵ .

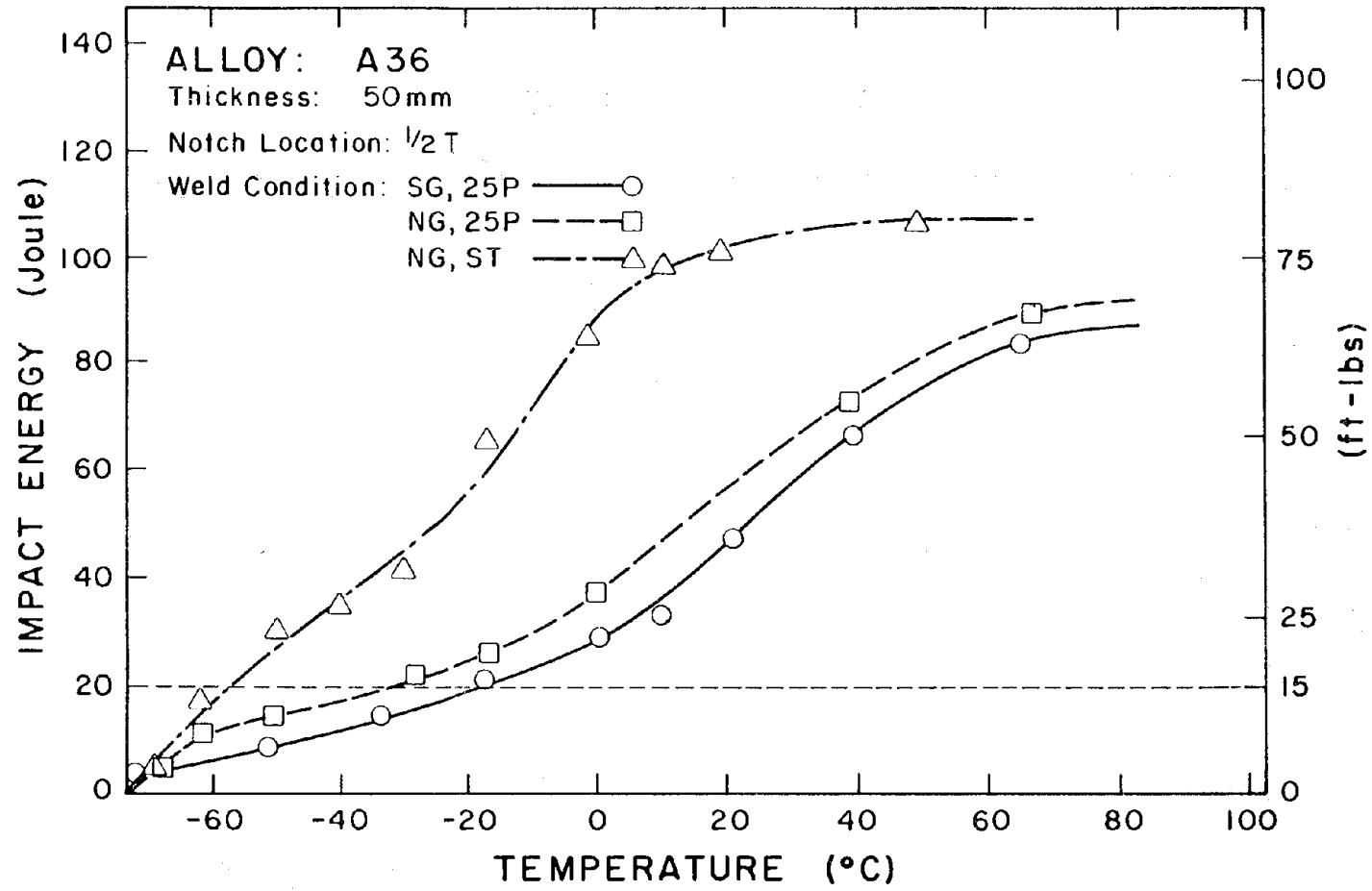


Figure 78. CVN transition curves for 50 mm A36, notch location: 1/2T.

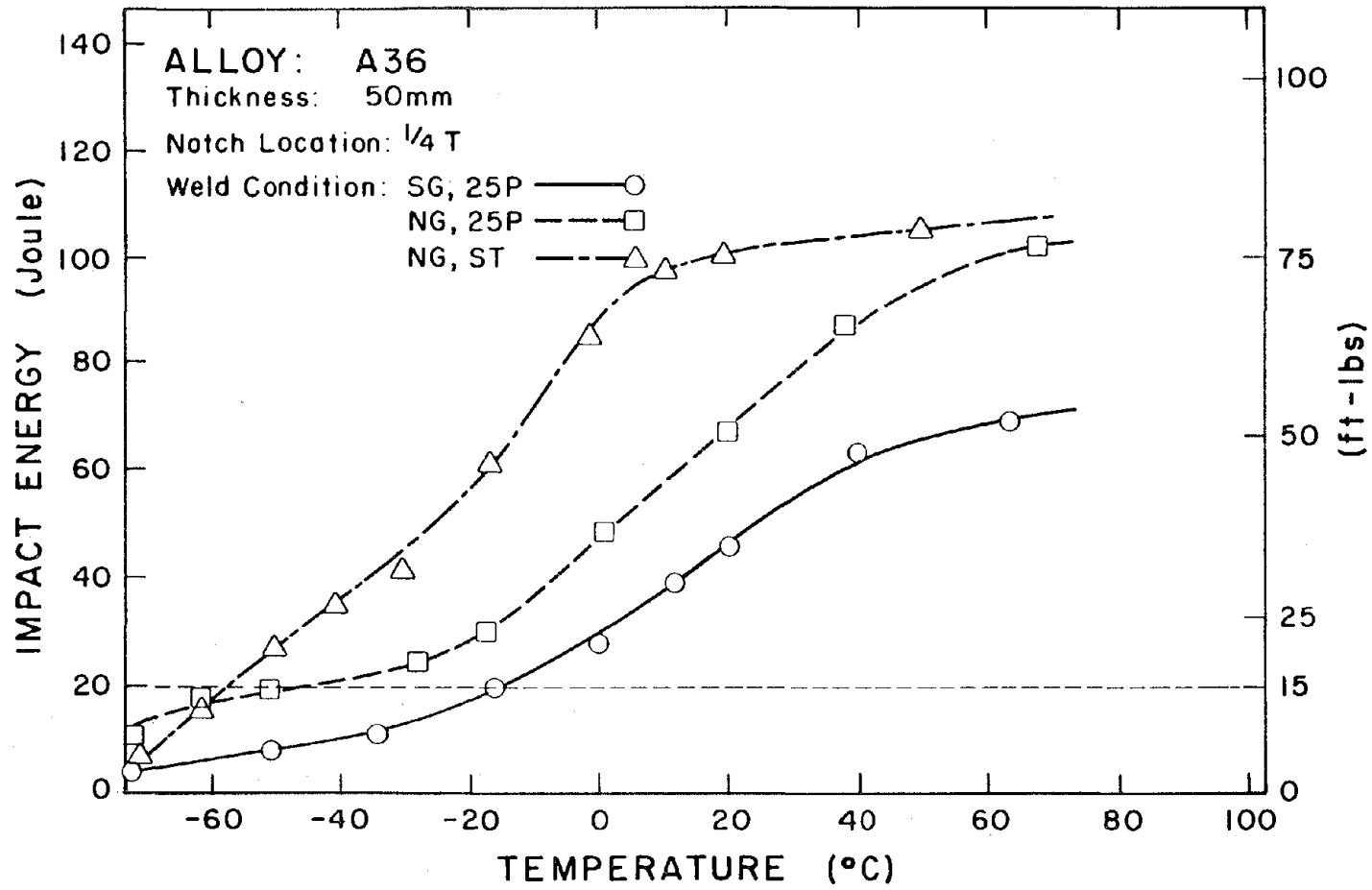


Figure 79. CVN transition curves for 50 mm A36, notch location: 1/4T.

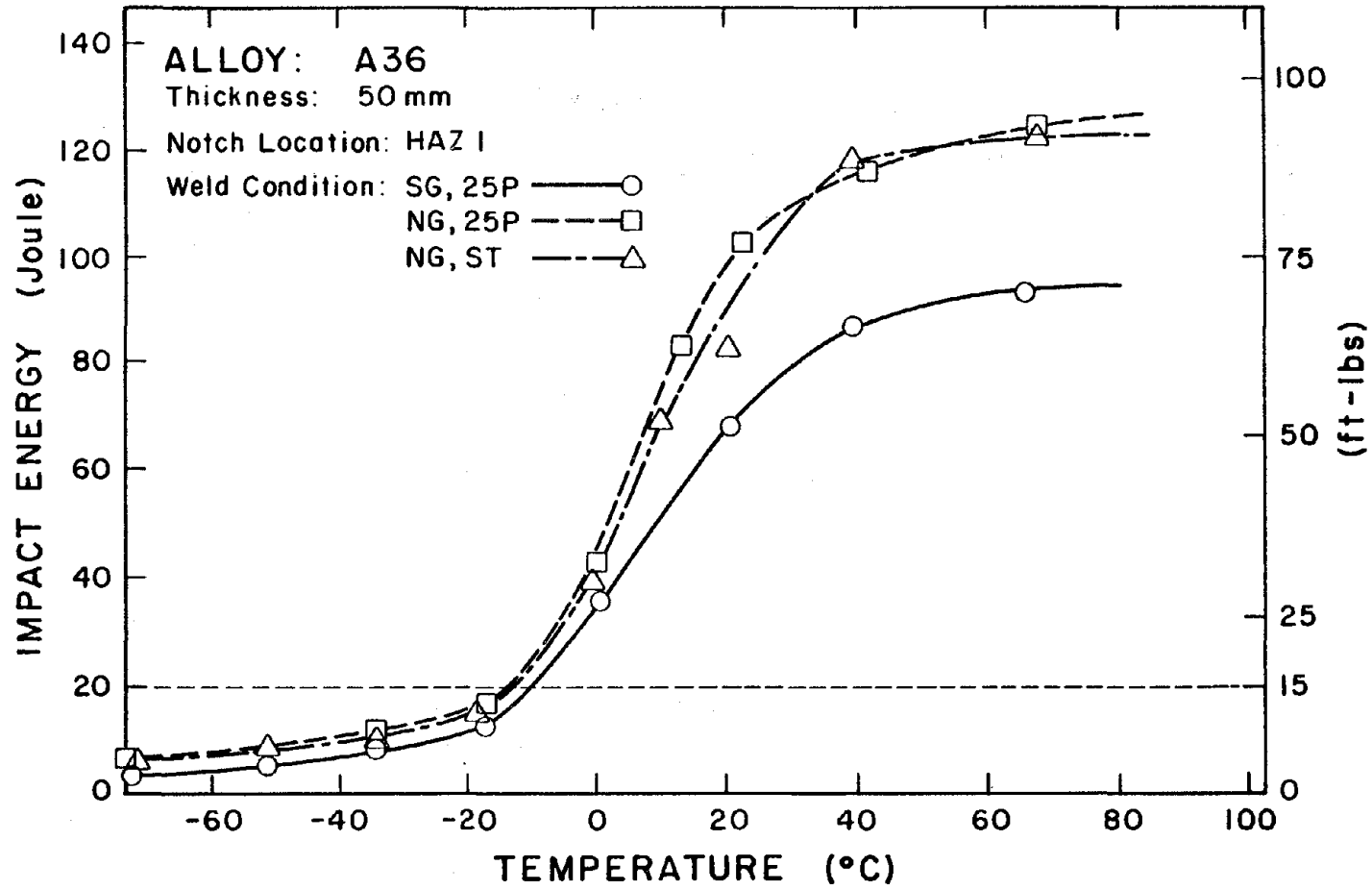


Figure 80. CVN transition curves for 50 mm A36, notch location: HAZ 1.

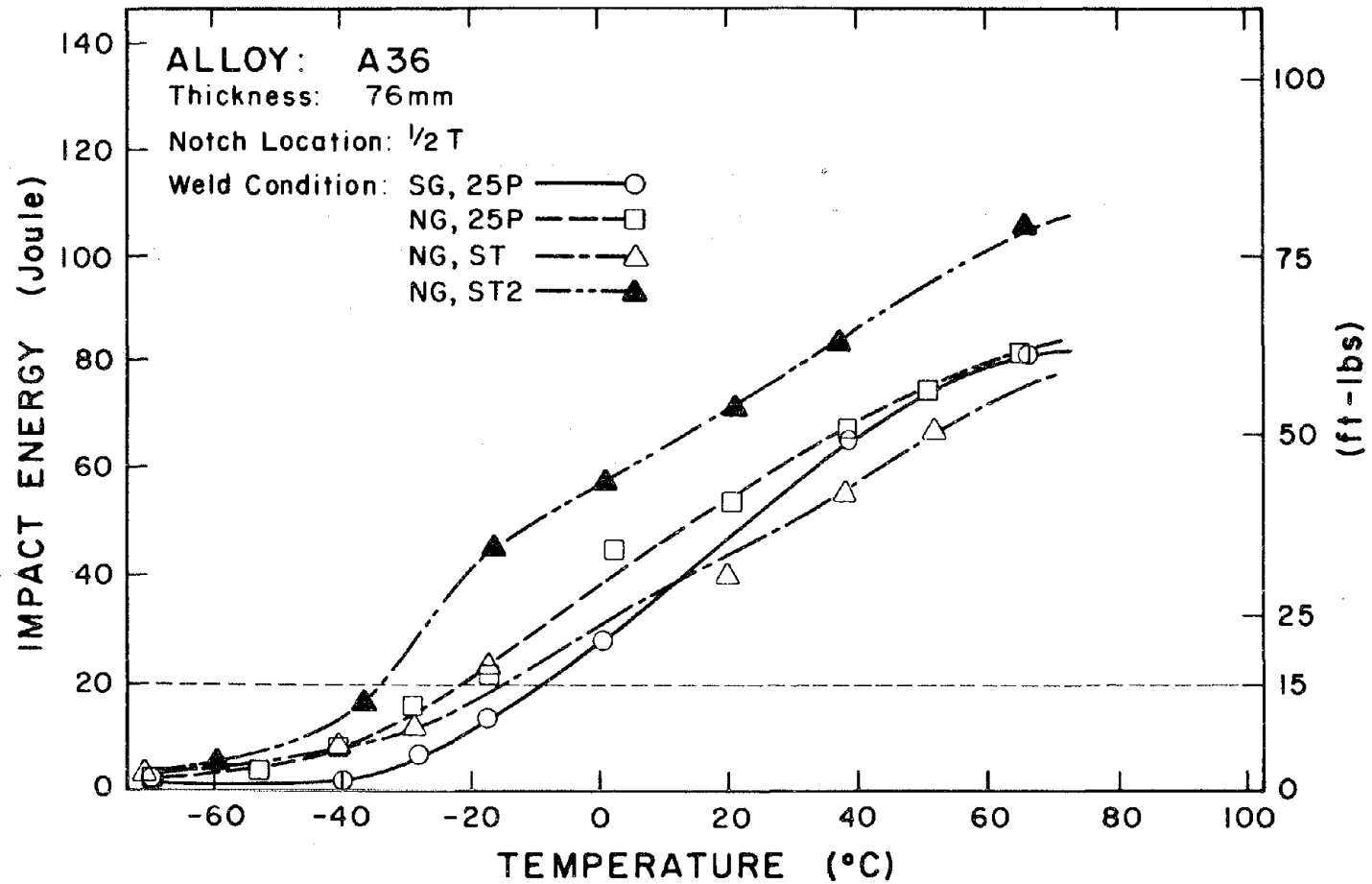


Figure 81. CVN transition curves for 76 mm A36, notch location: 1/2T.

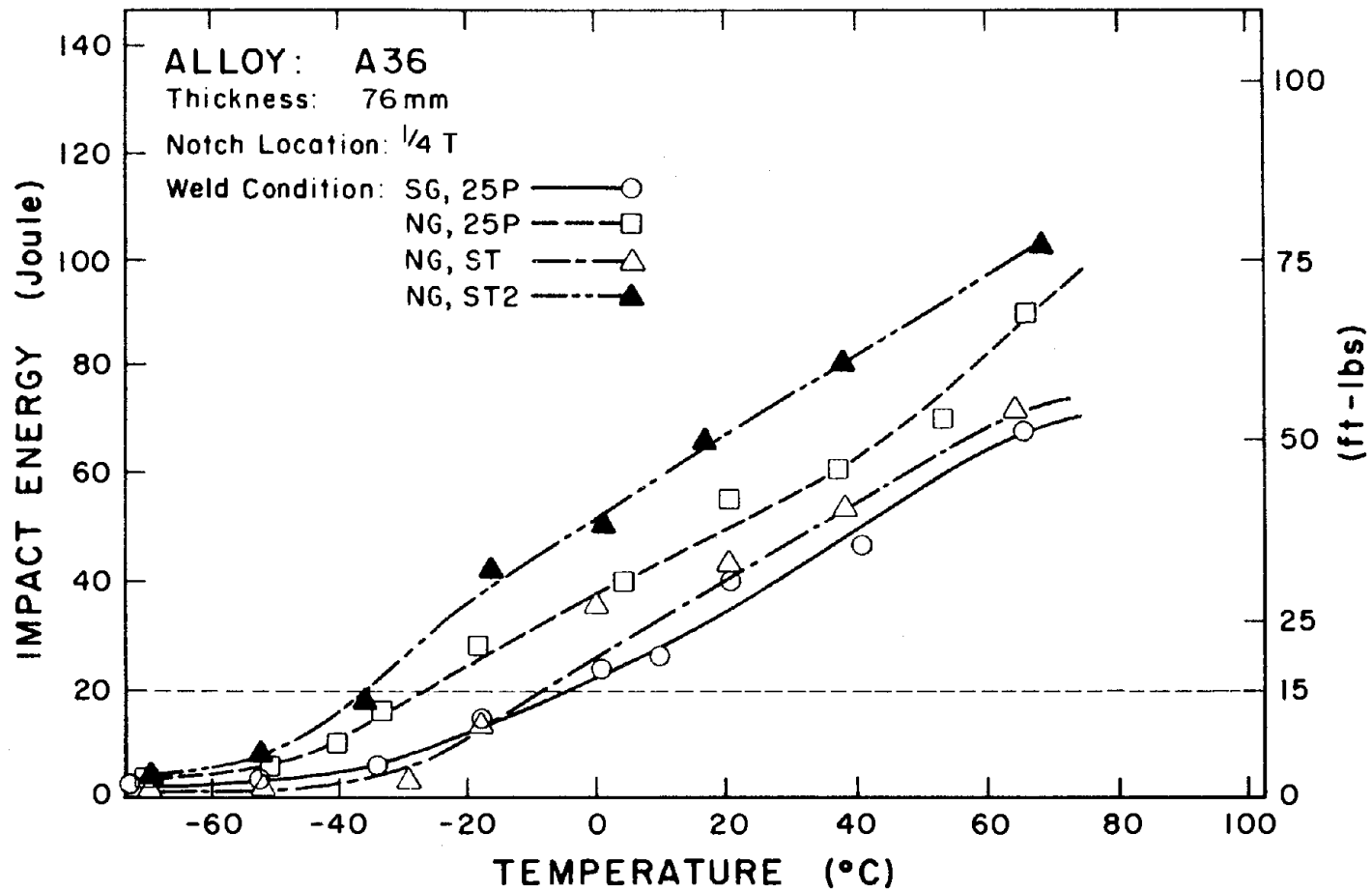


Figure 82. CVN transition curves for 76 mm A36, notch location: 1/4T.

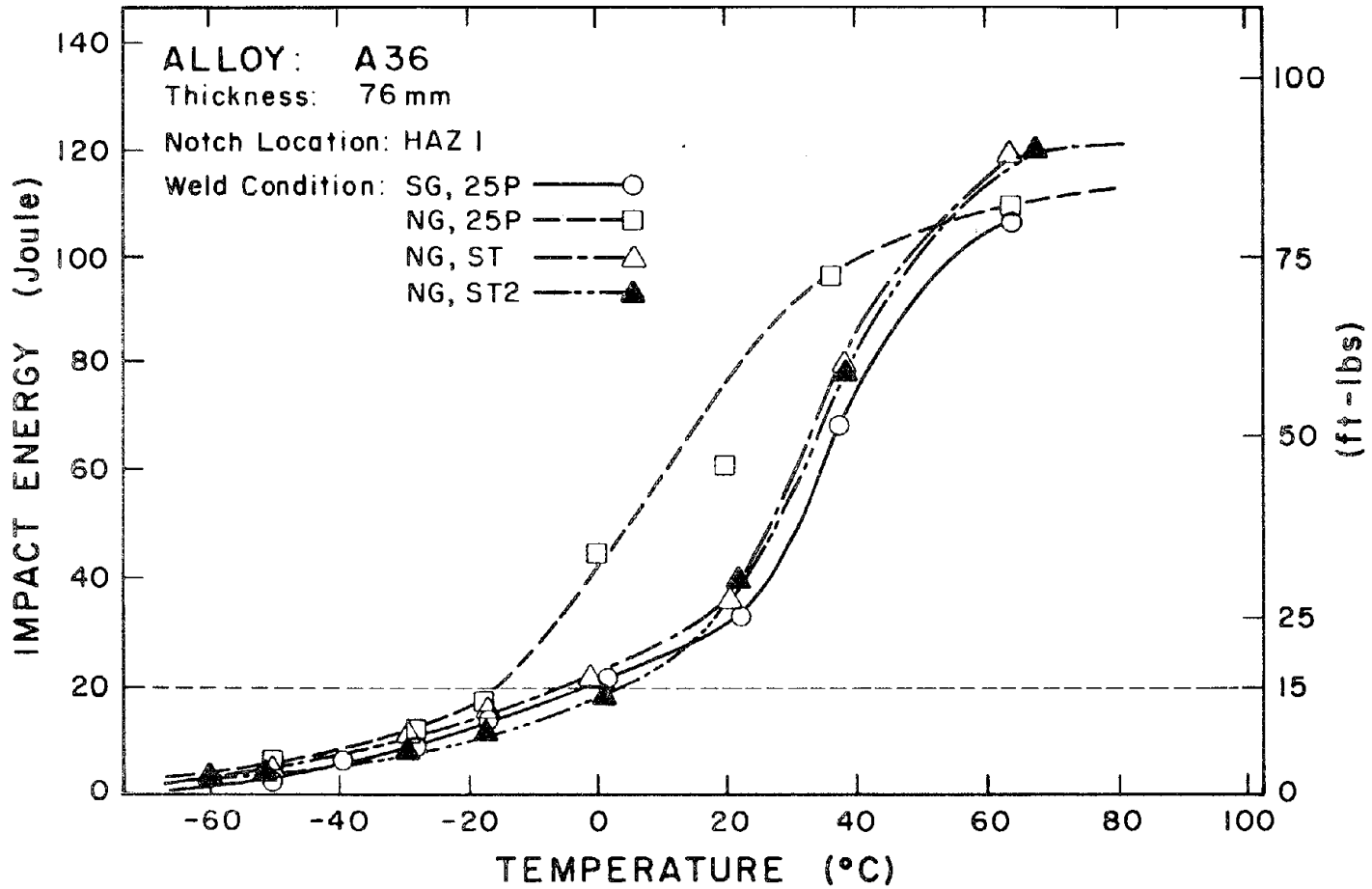


Figure 83. CVN transition curves for 76 mm A36, notch location: HAZ 1.

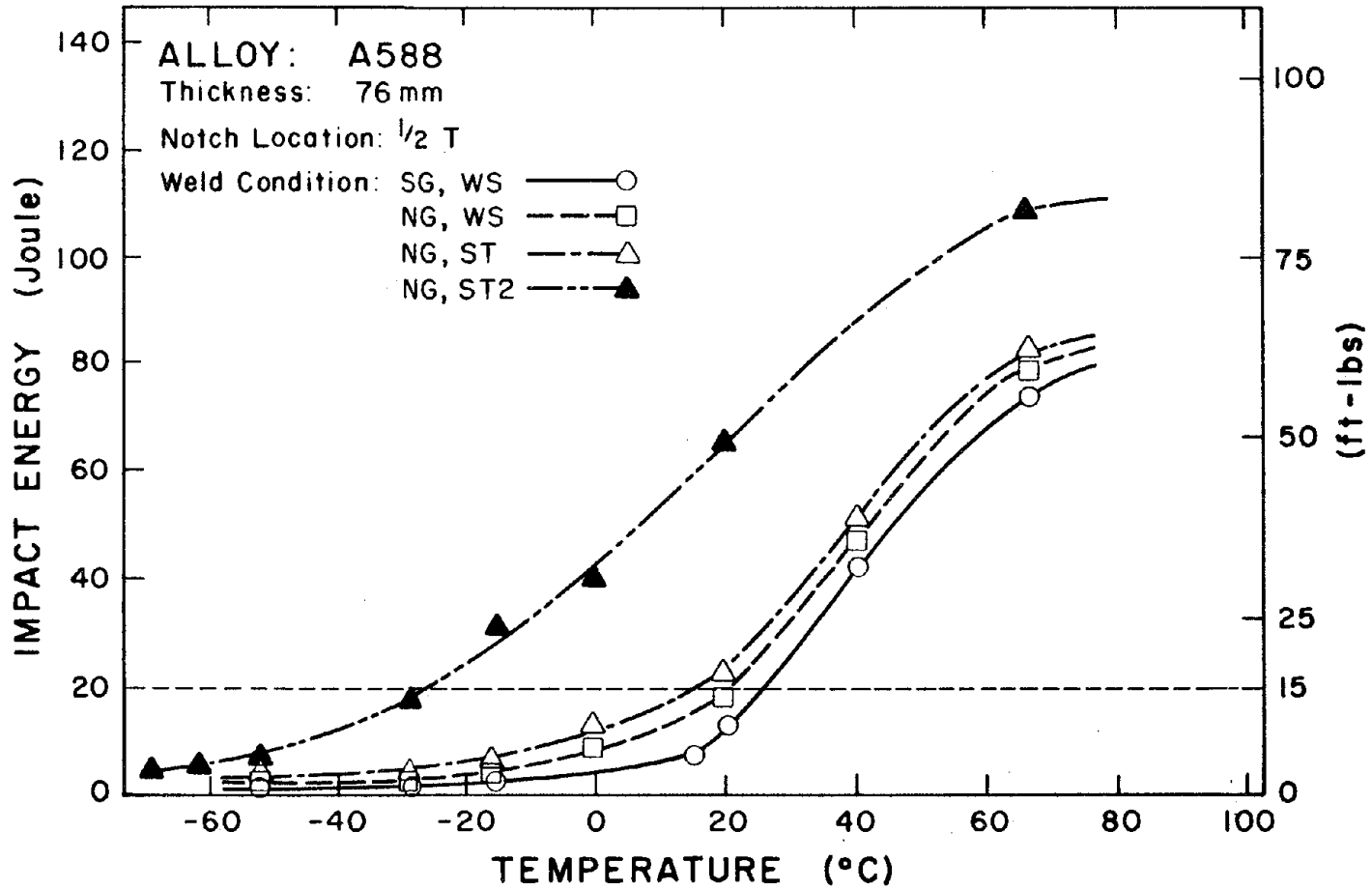


Figure 84. CVN transition curves for 76 mm A588, notch location: 1/2T.

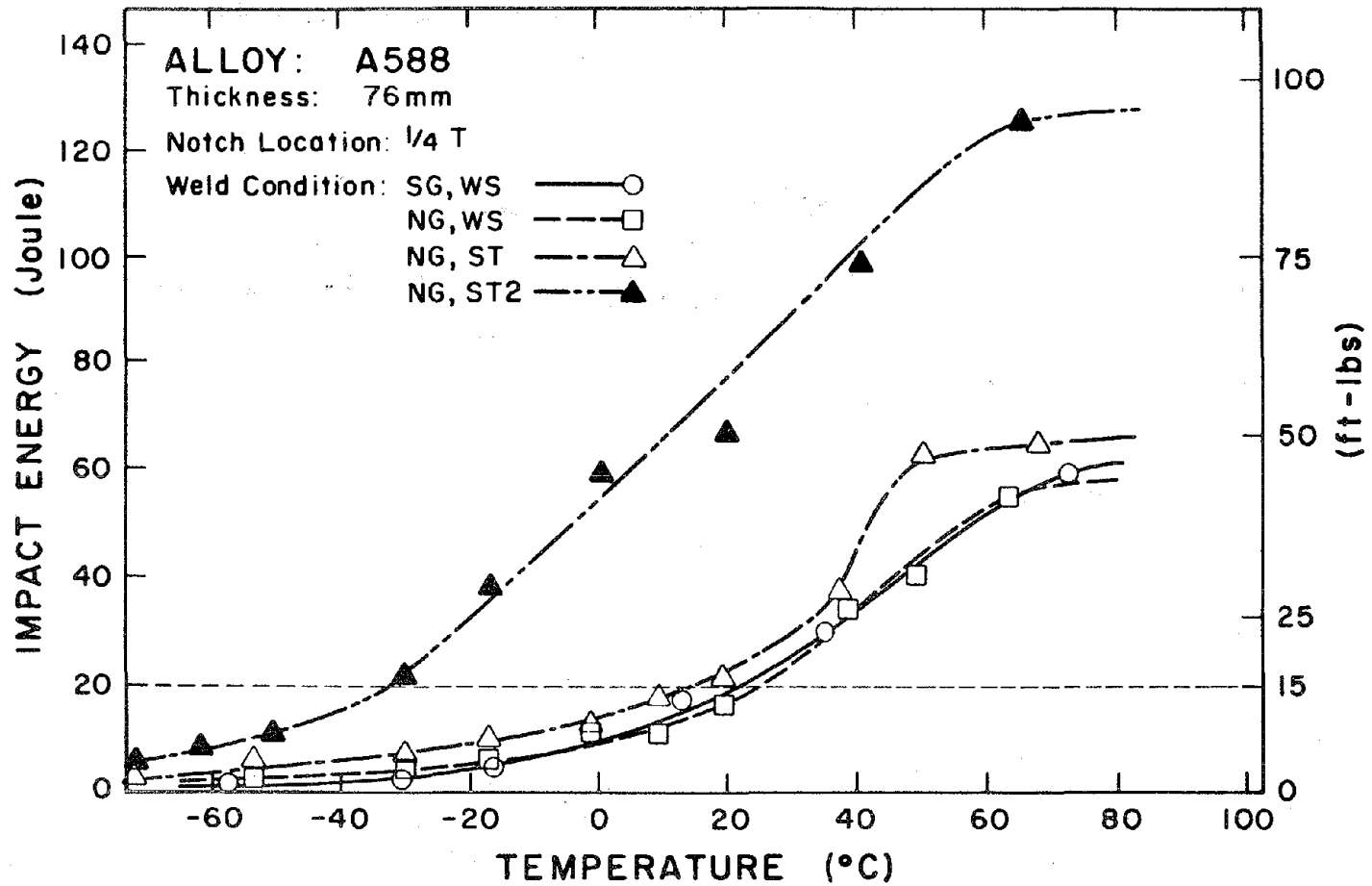


Figure 85. CVN transition curves for 76 mm A588, notch location: 1/4T.

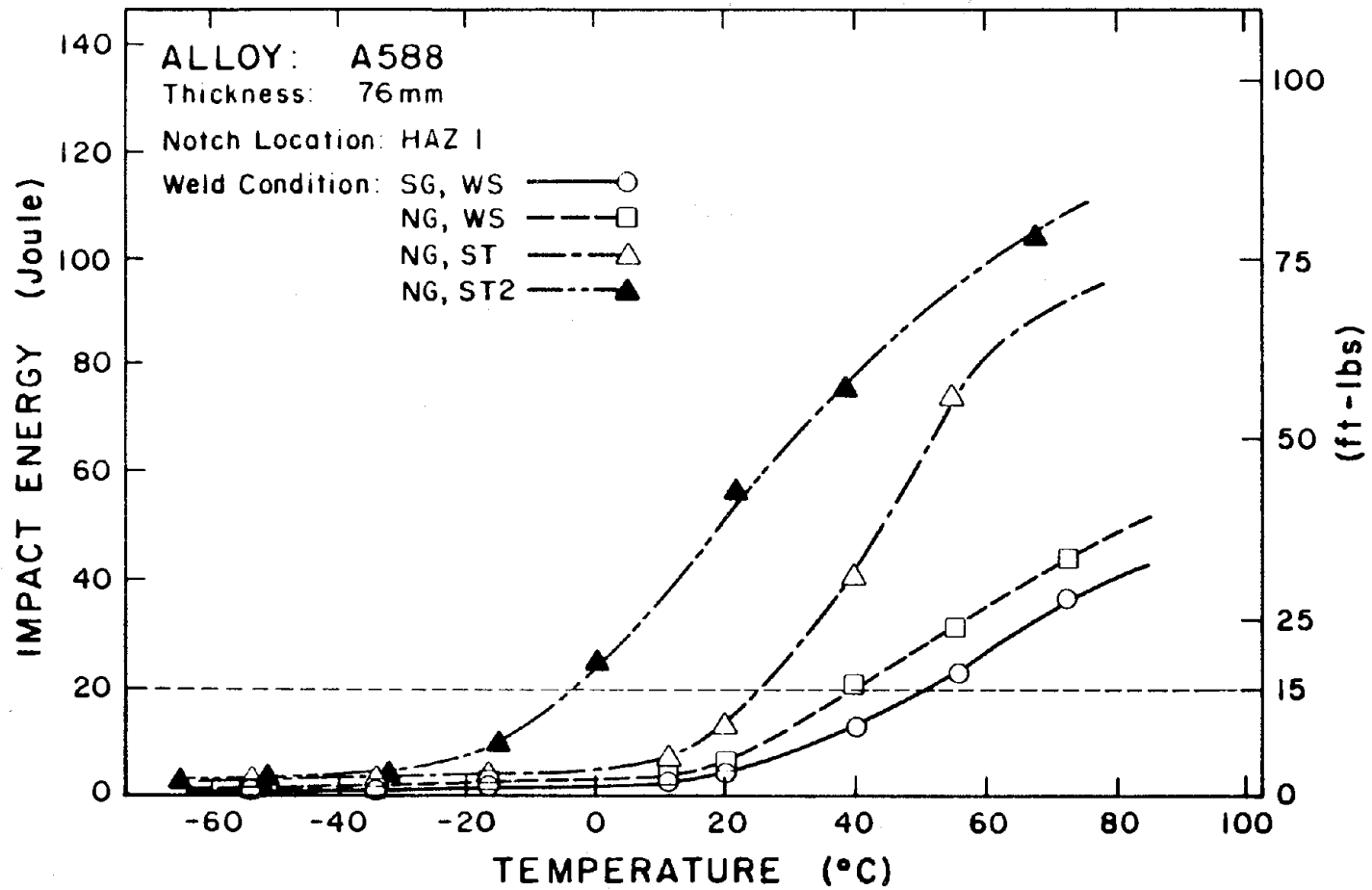


Figure 86. CVN transition curves for 76 mm A588, notch location: HAZ 1.

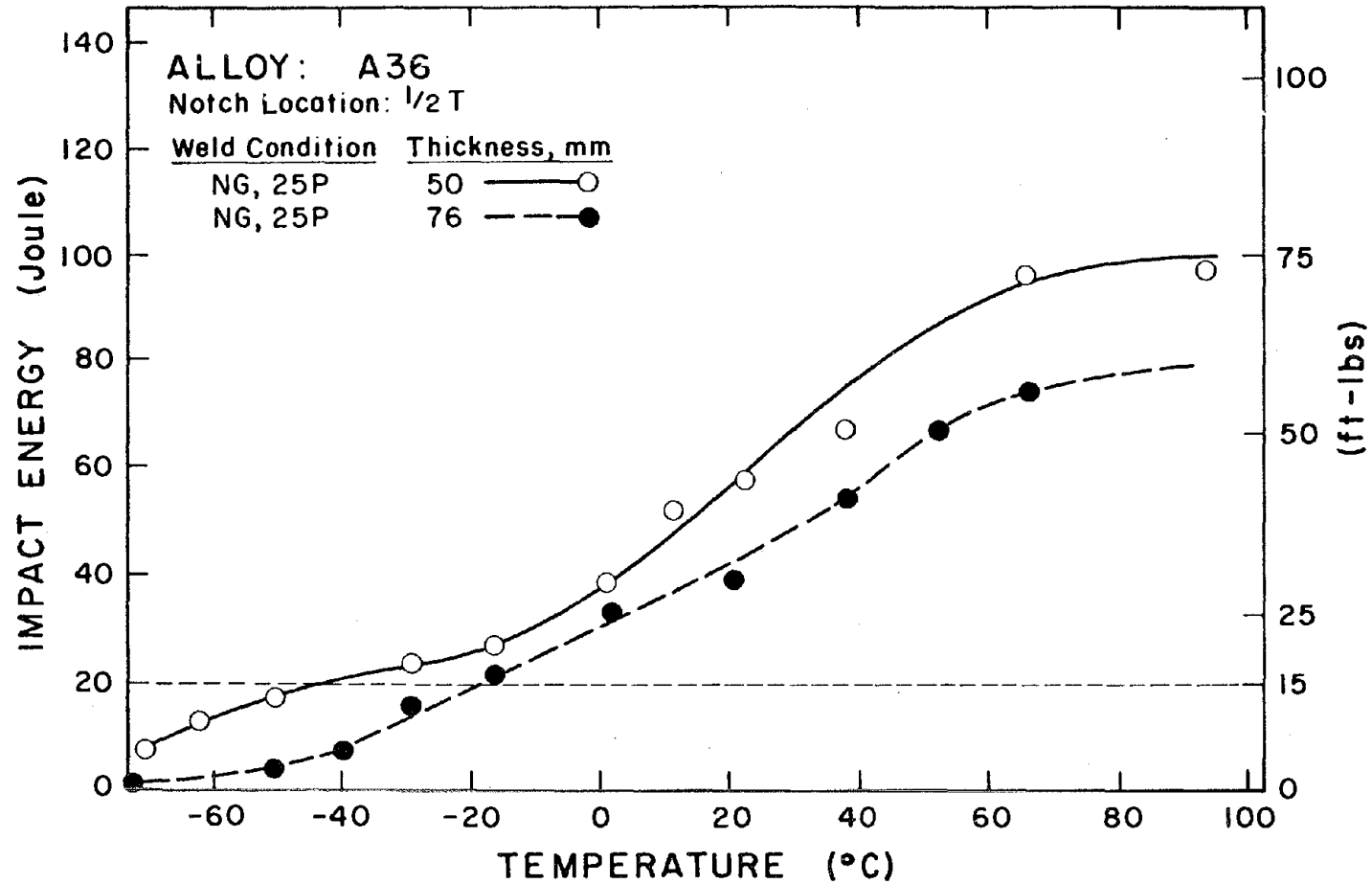


Figure 87. CVN transition curves for A36 at the $\frac{1}{2}T$ position, weld condition: NG 25P.

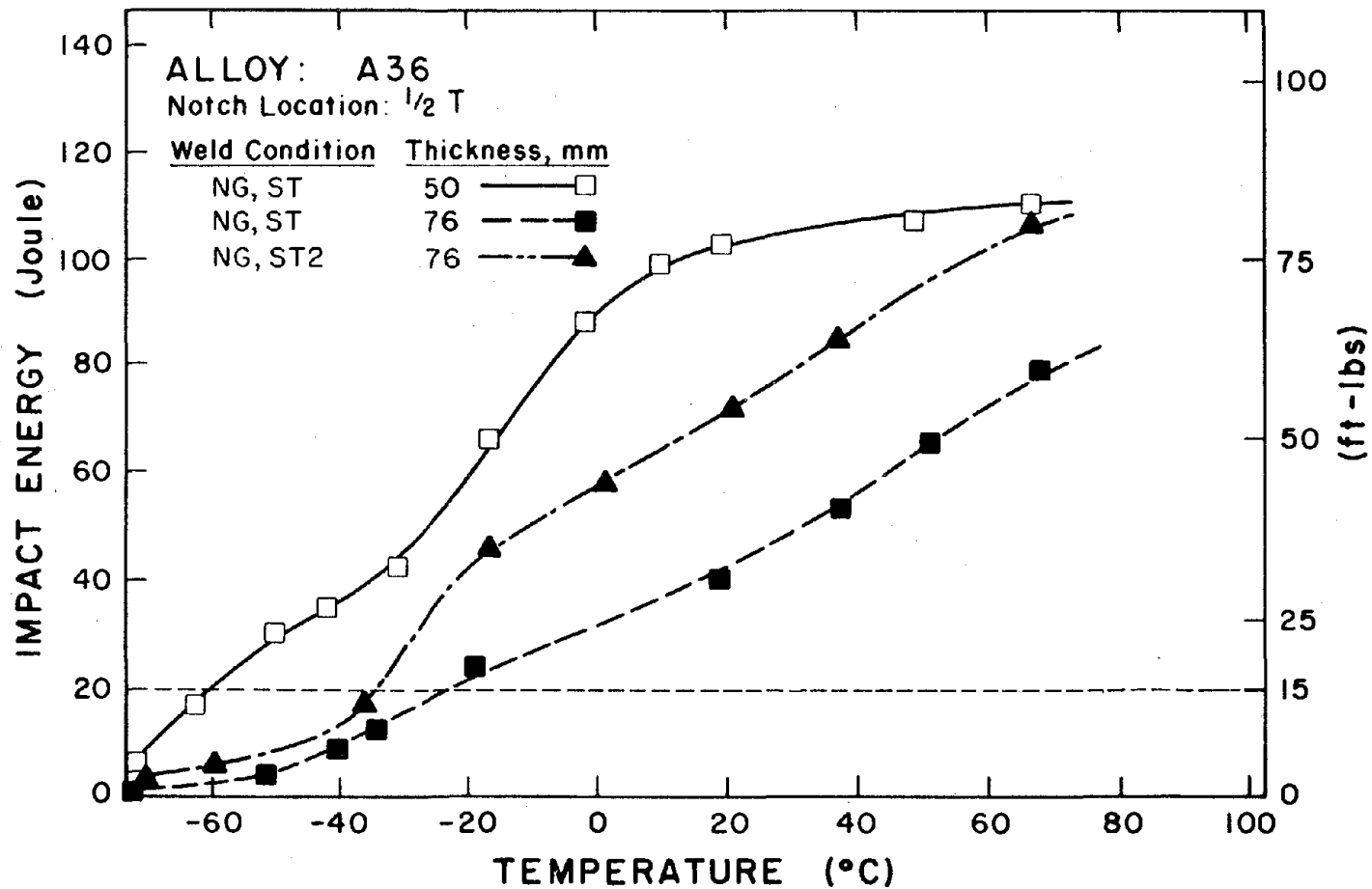


Figure 88. CVN transition curves for A36 at the $\frac{1}{2}$ T position, weld condition: NG, ST.

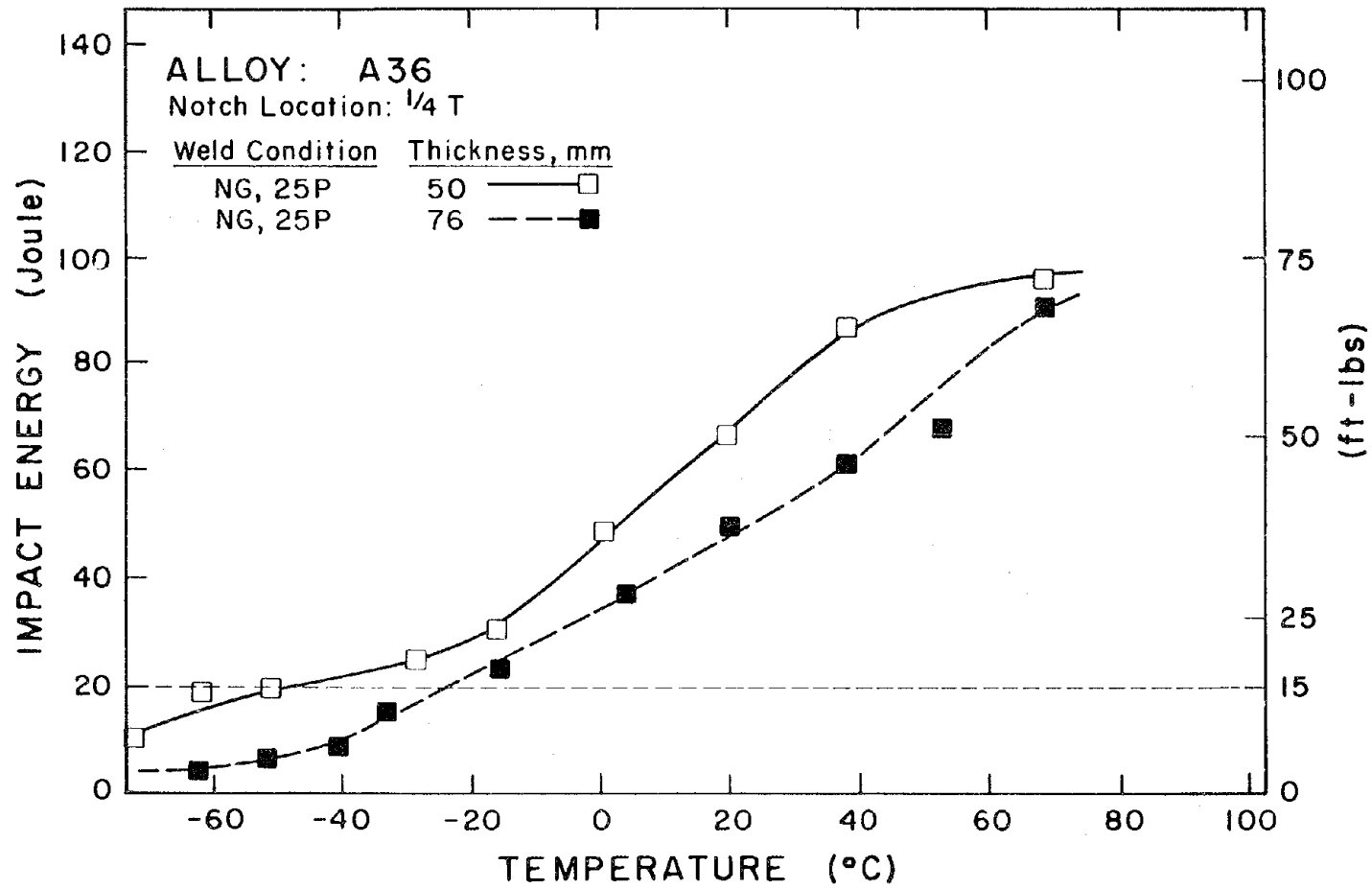


Figure 89. CVN transition curves for A36 at the $\frac{1}{4}$ T position.

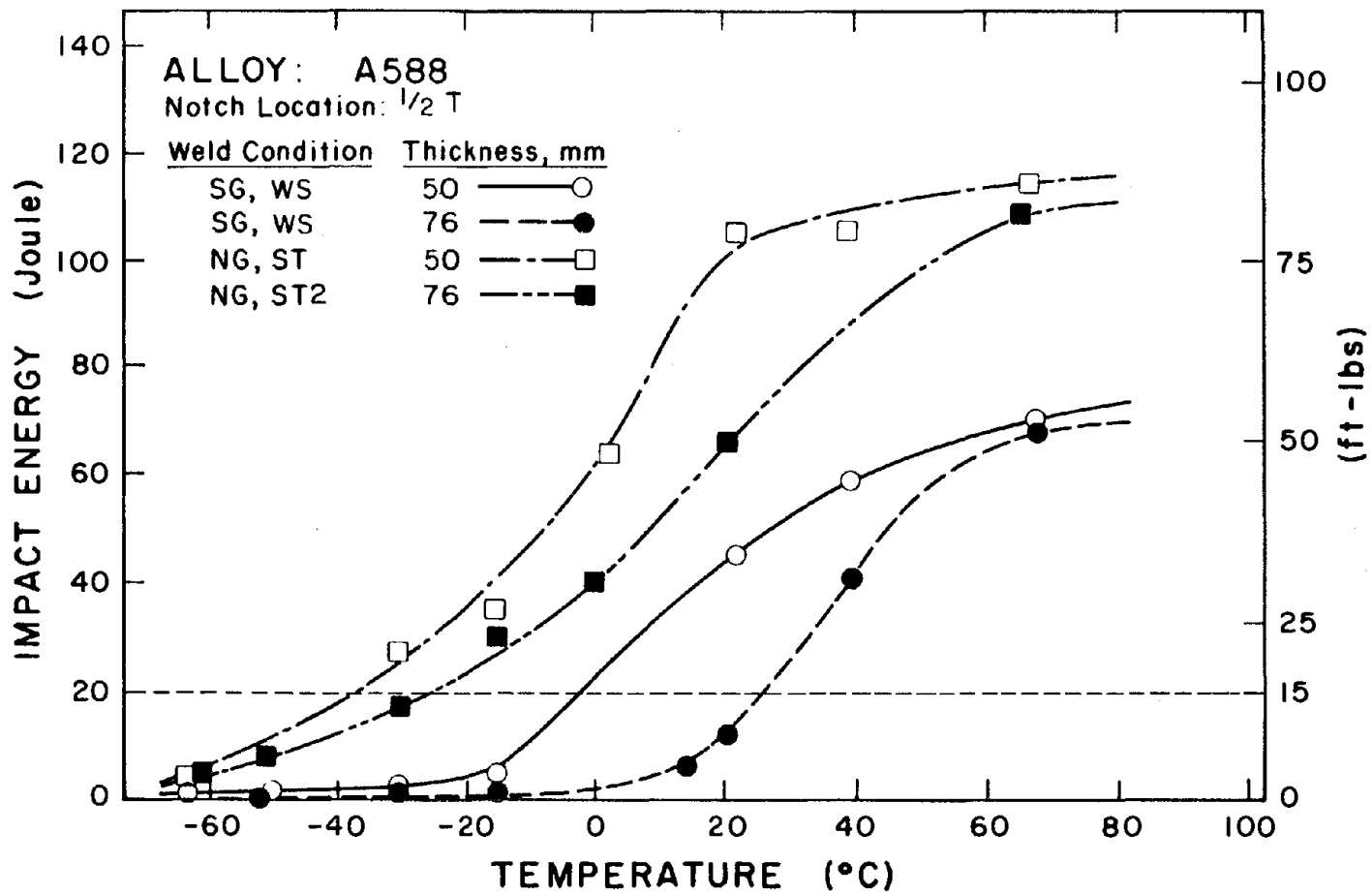


Figure 90. CVN transition curves for A588 at $\frac{1}{2}$ T position.

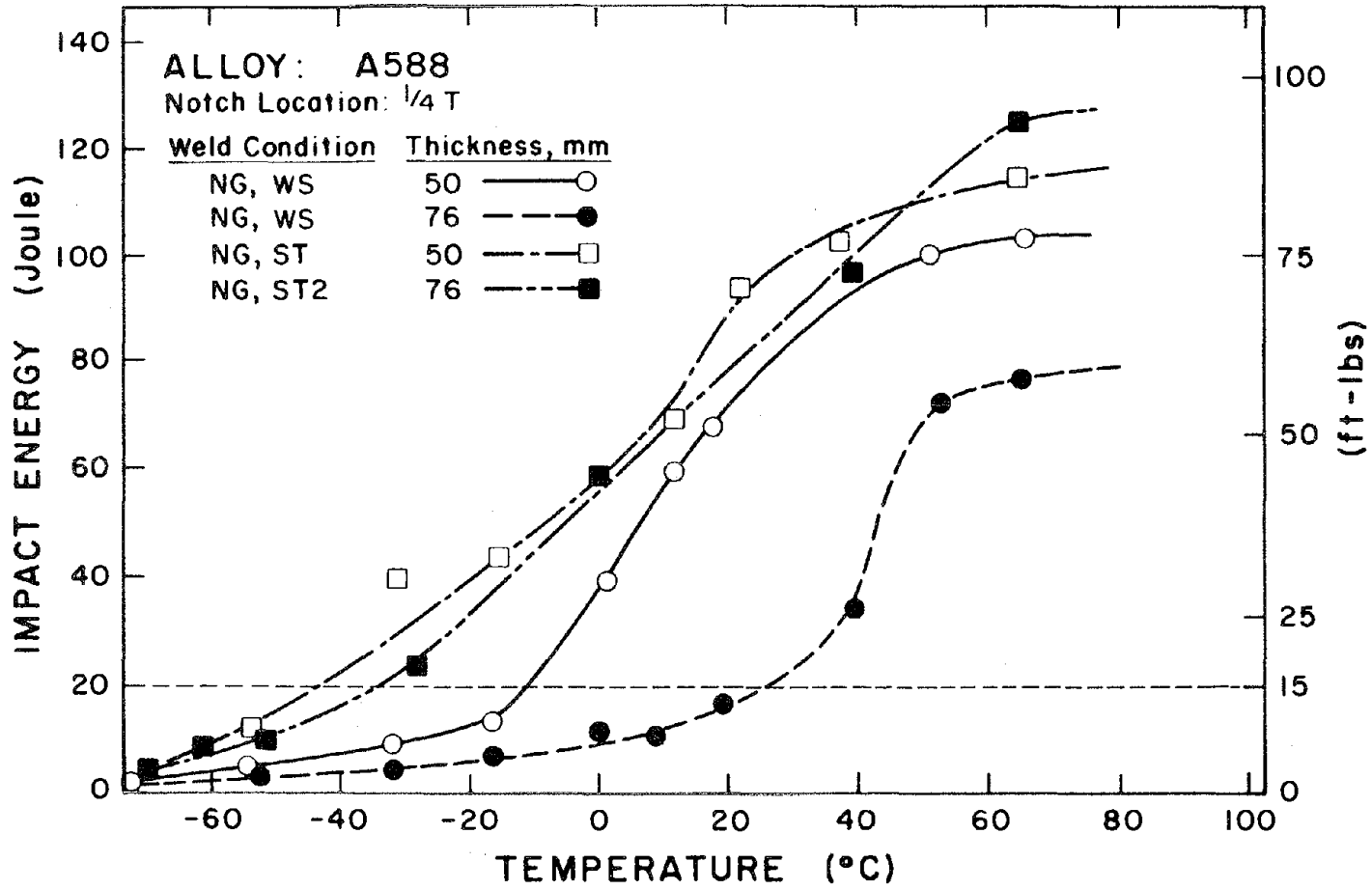


Figure 91. CVN transition curves for A588 at the $\frac{1}{4}$ T position.

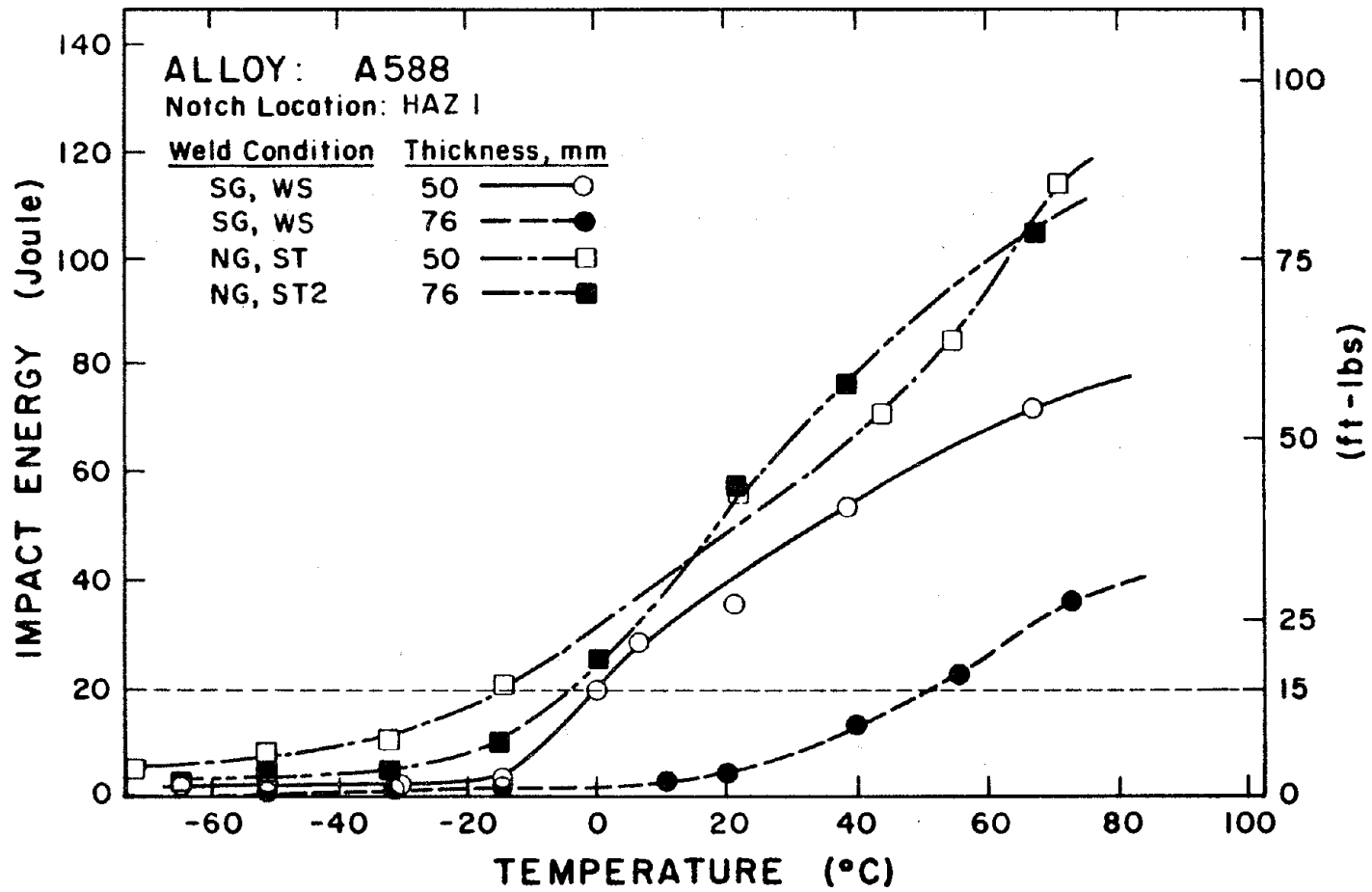


Figure 92. CVN transition curves for A588 in the heat affected zone.

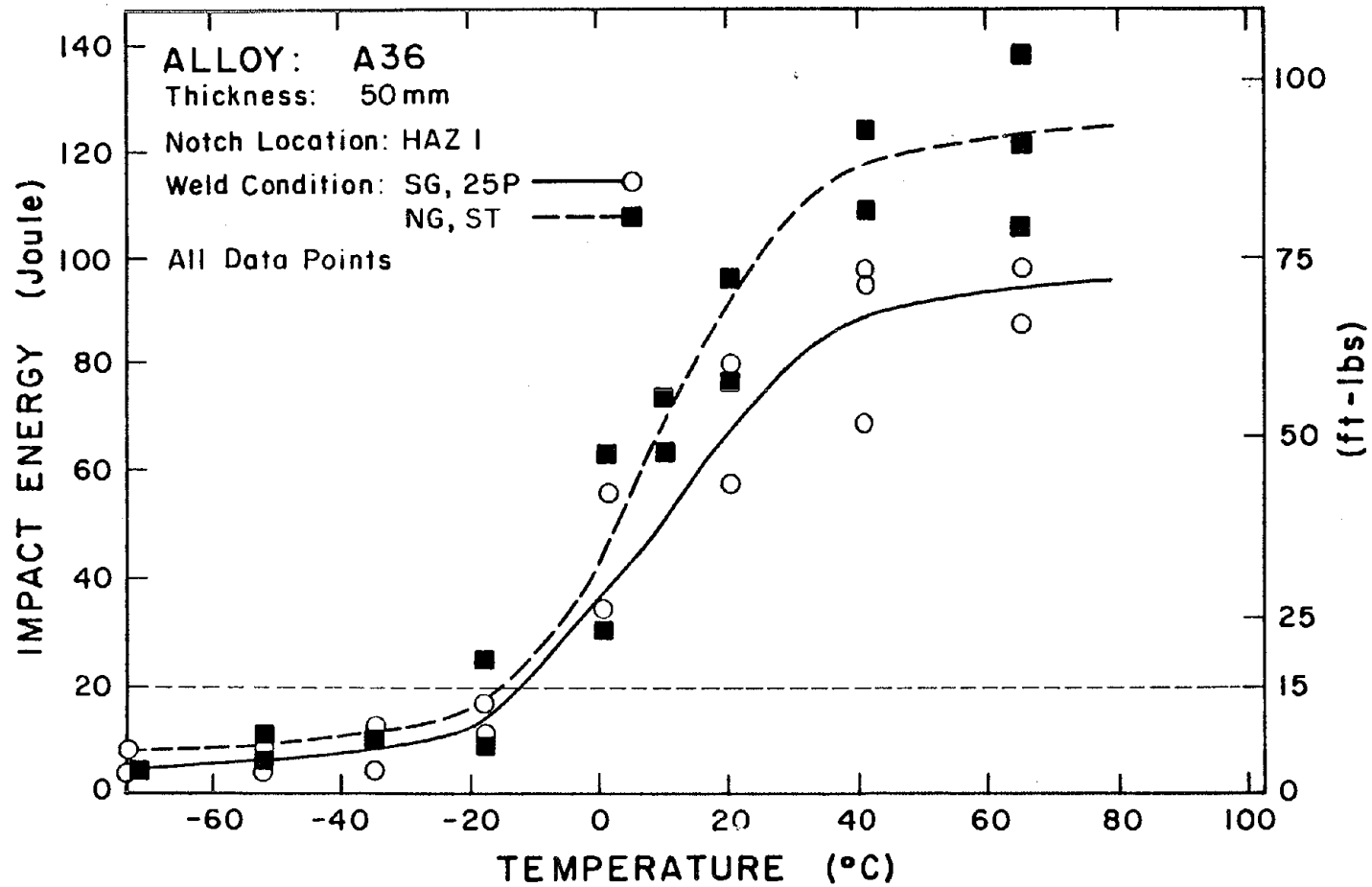


Figure 93. CVN transition curves for 50 mm A36, notch location: HAZ I.

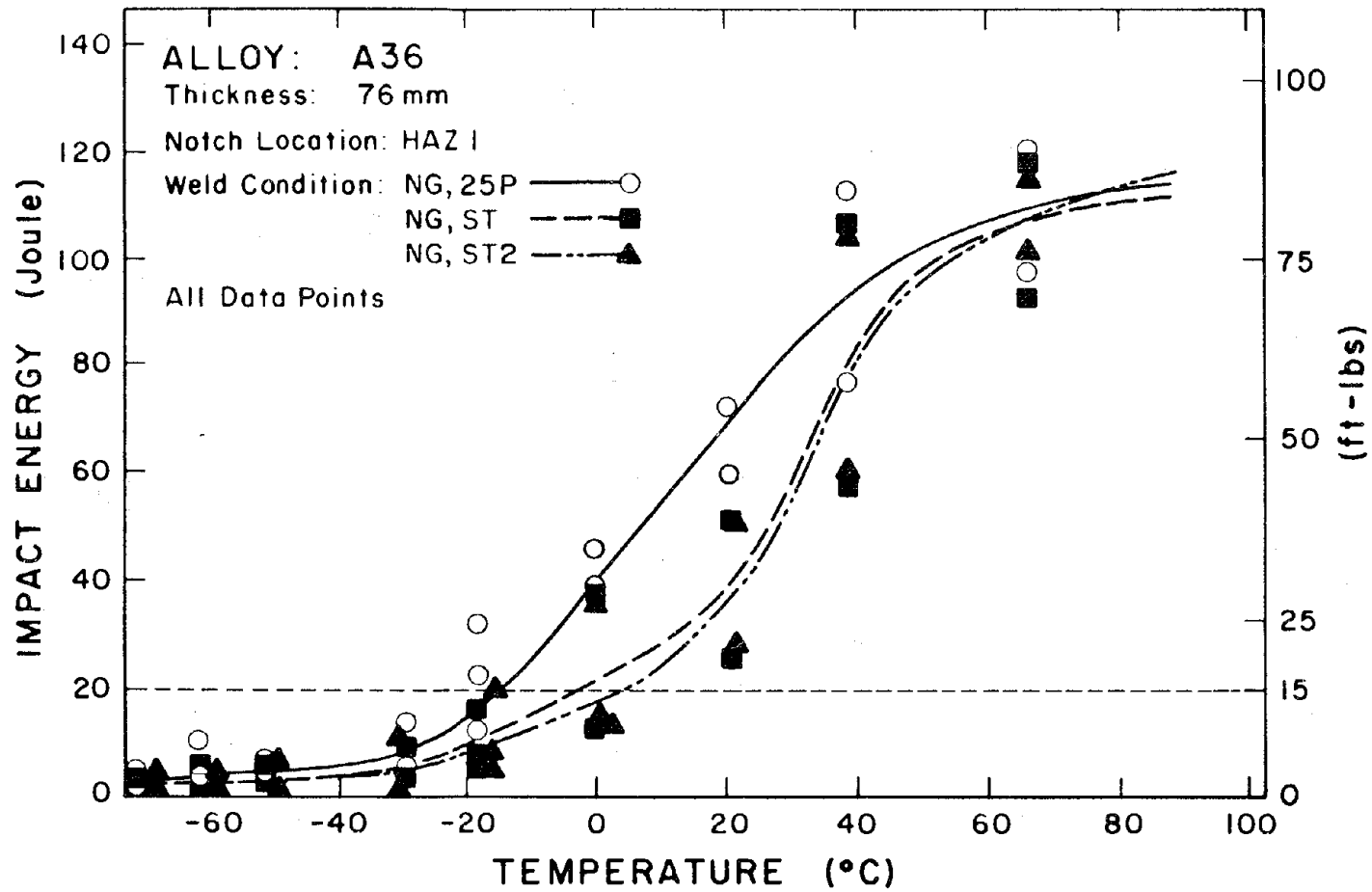


Figure 94. CVN transition curves for 76 mm A36,
notch location: HAZ 1.

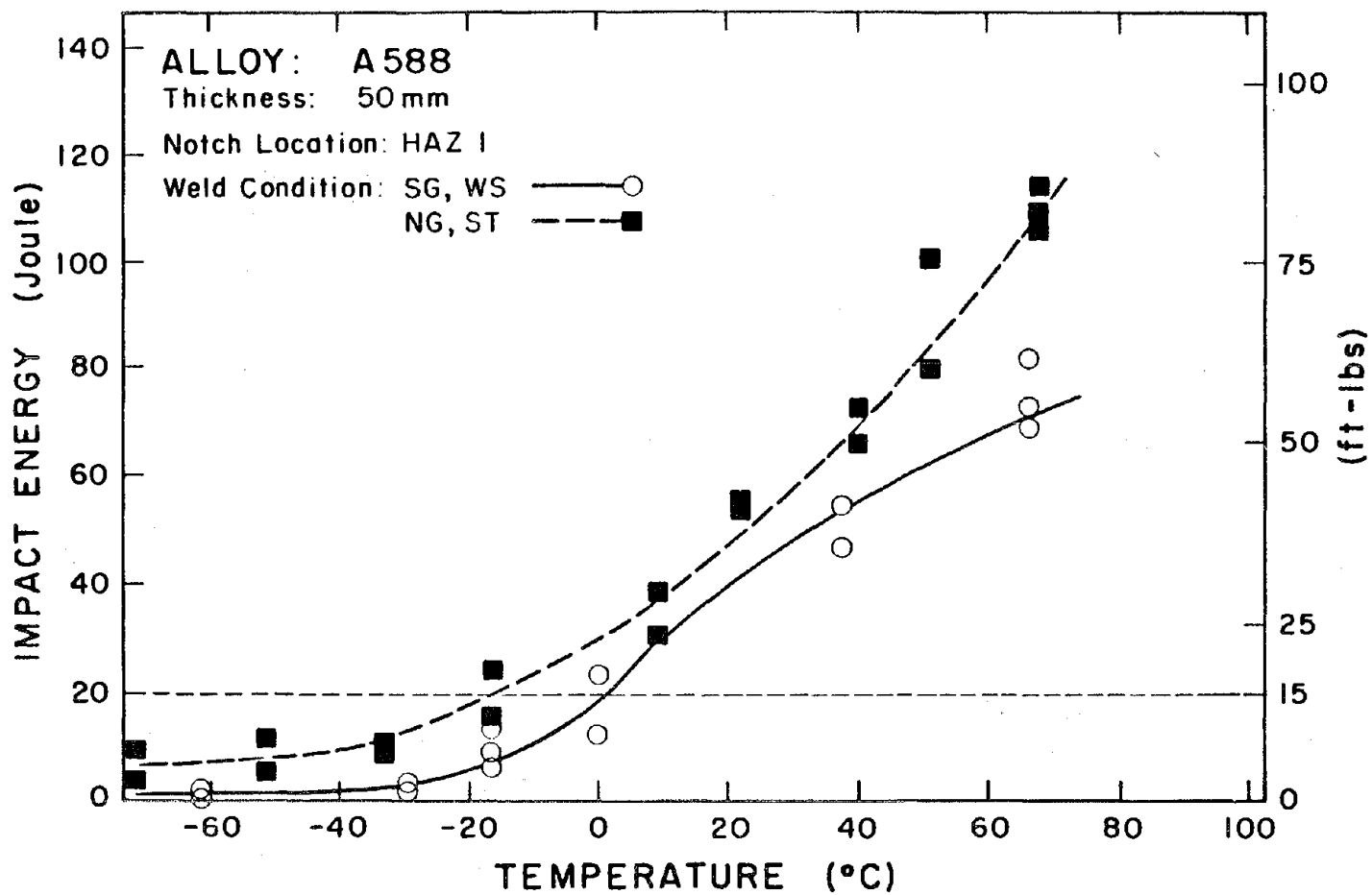


Figure 95. CVN transition curves for 50 mm A588, notch location: HAZ 1.

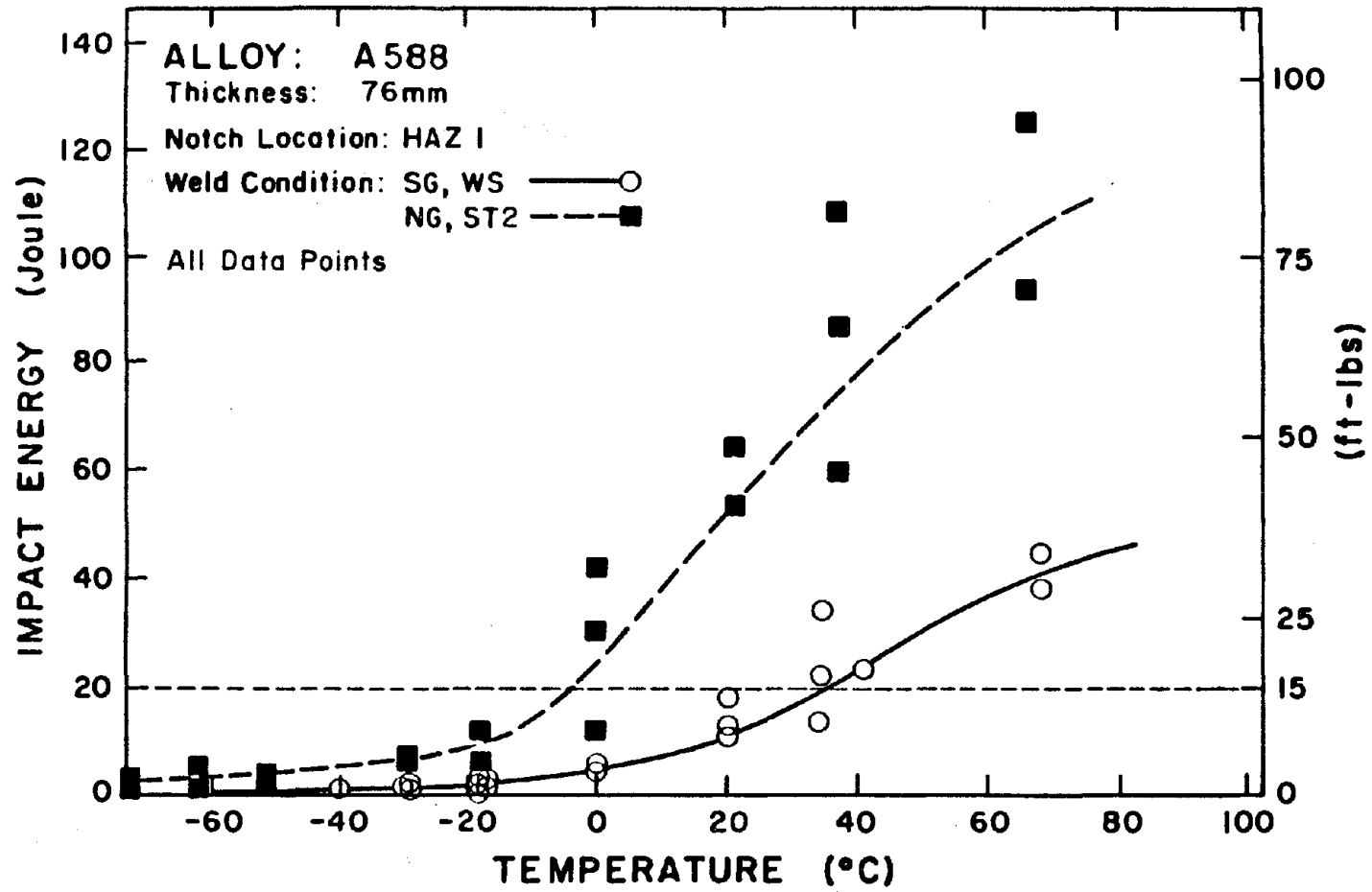


Figure 96. CVN transition curves for 76 mm A588,
 notch location: HAZ 1.

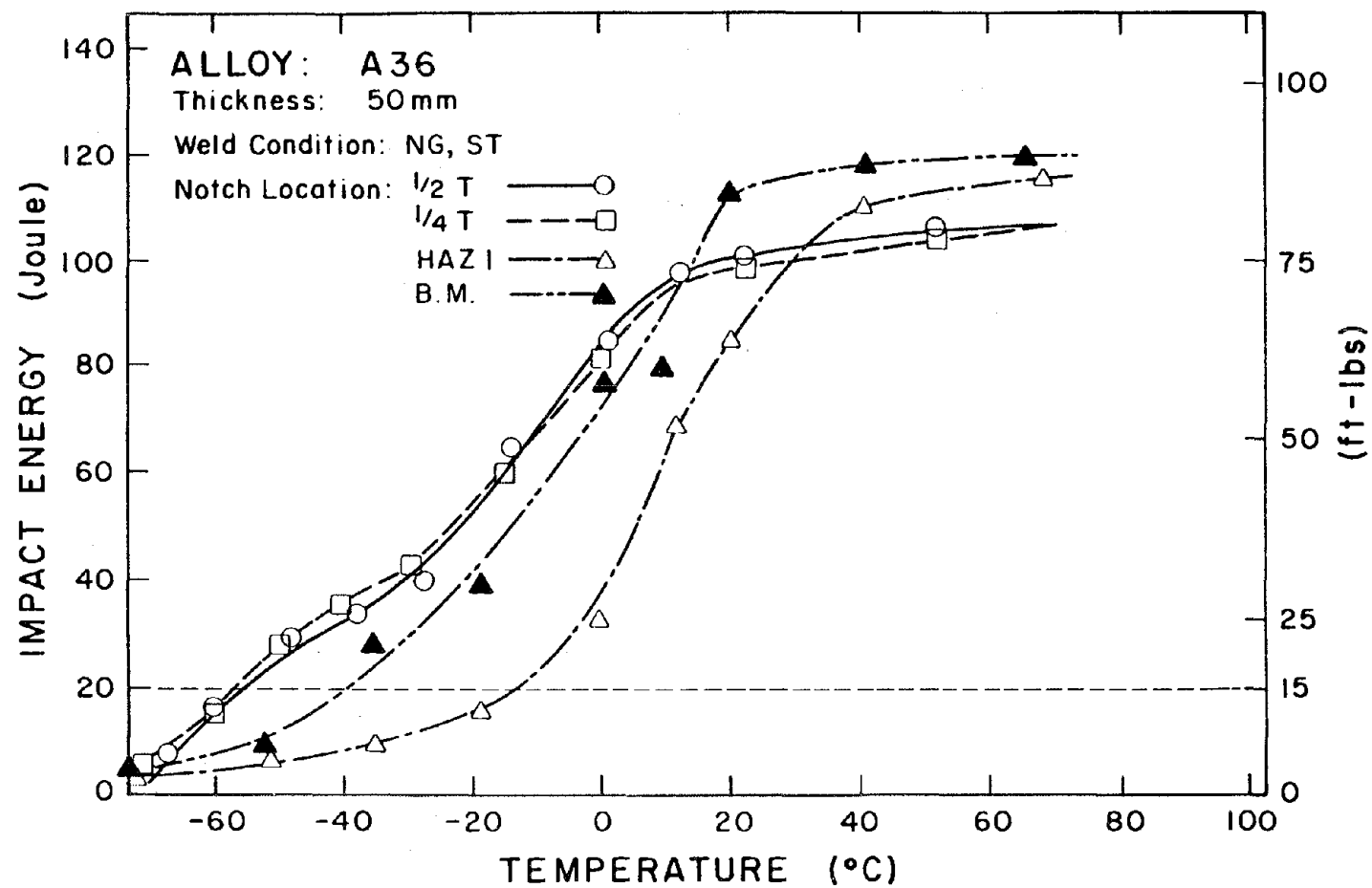


Figure 97. CVN transition curves for 50 mm A36, weld condition: NG, ST.

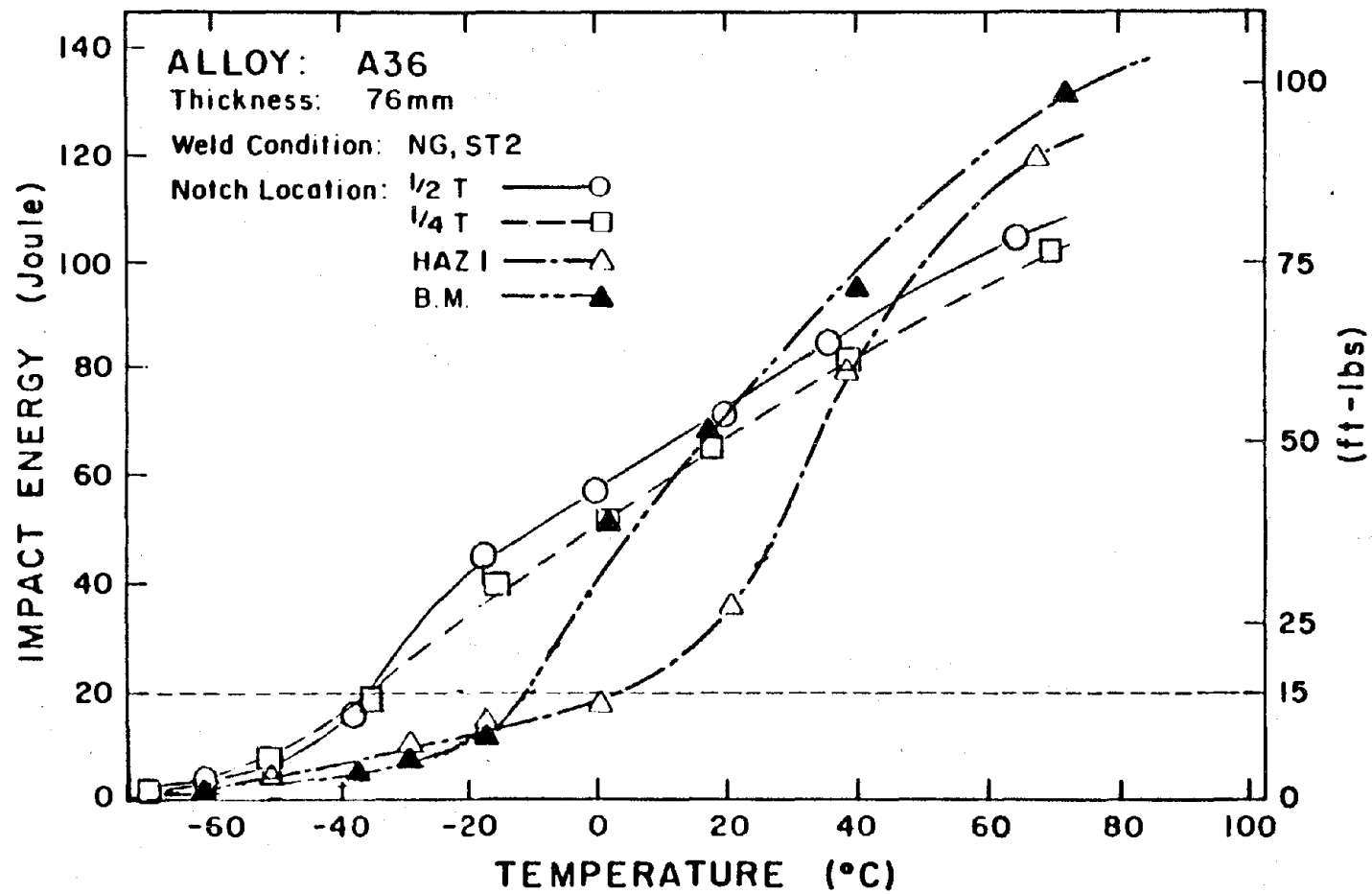


Figure 98. CVN transition curves for 76 mm A36, weld condition: NG, ST2.

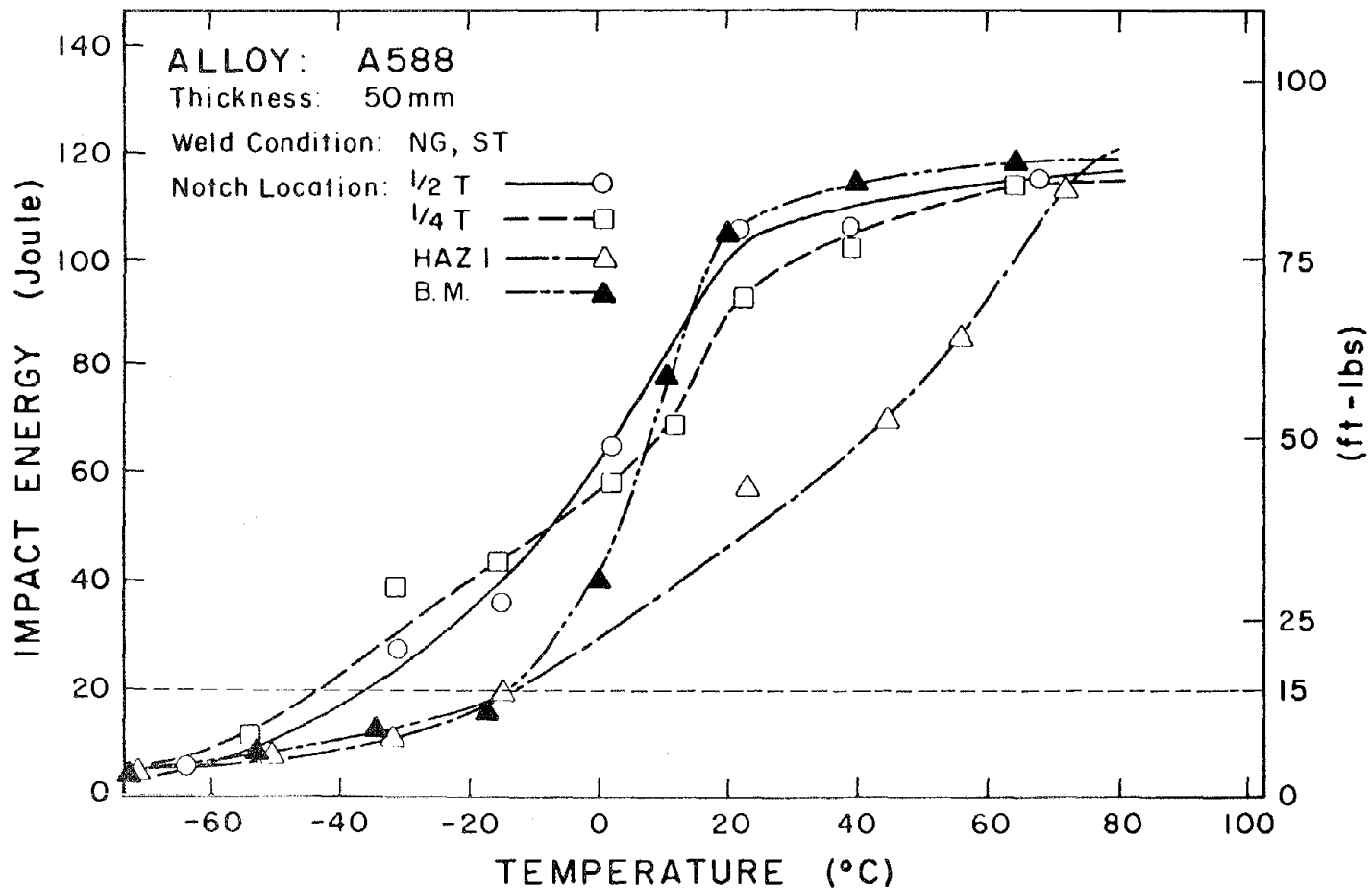


Figure 99. CVN transition curves for 50 mm A588,
weld condition: NG, ST.

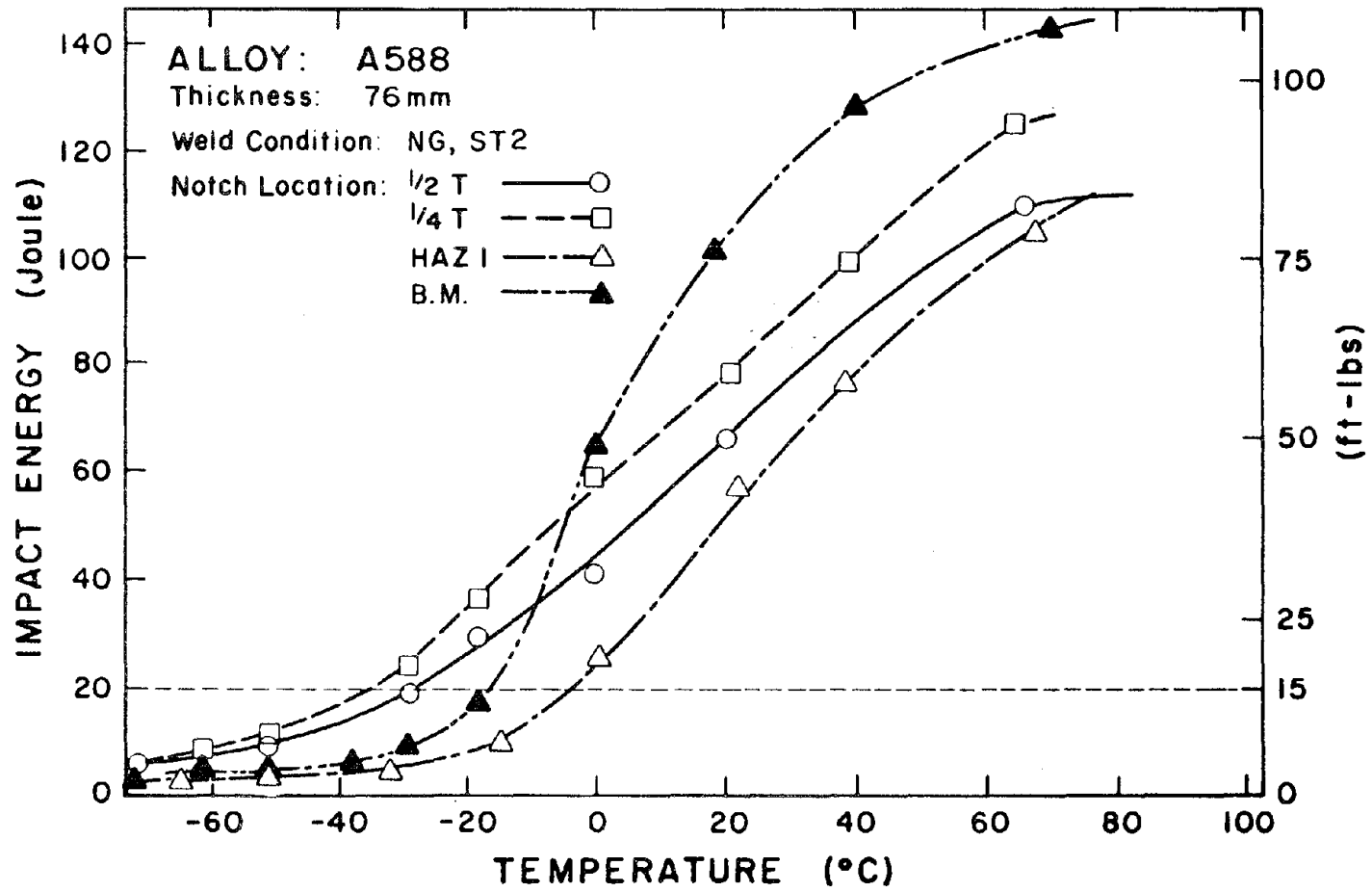


Figure 100. CVN transition curves for 76 mm A588, weld condition: NG, ST2.

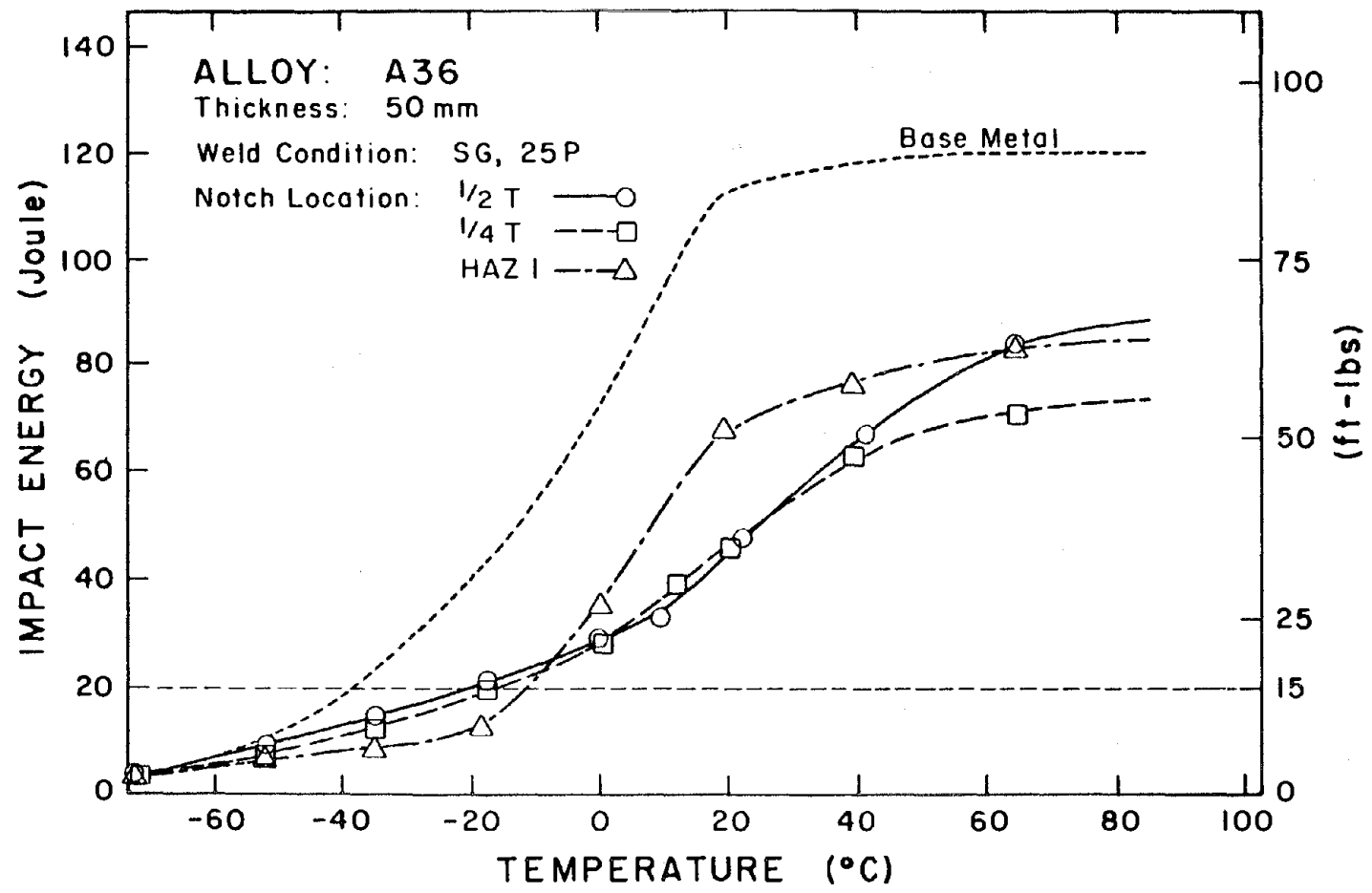


Figure 101. CVN transition curves for 50 mm A36, weld condition: SG, 25P.

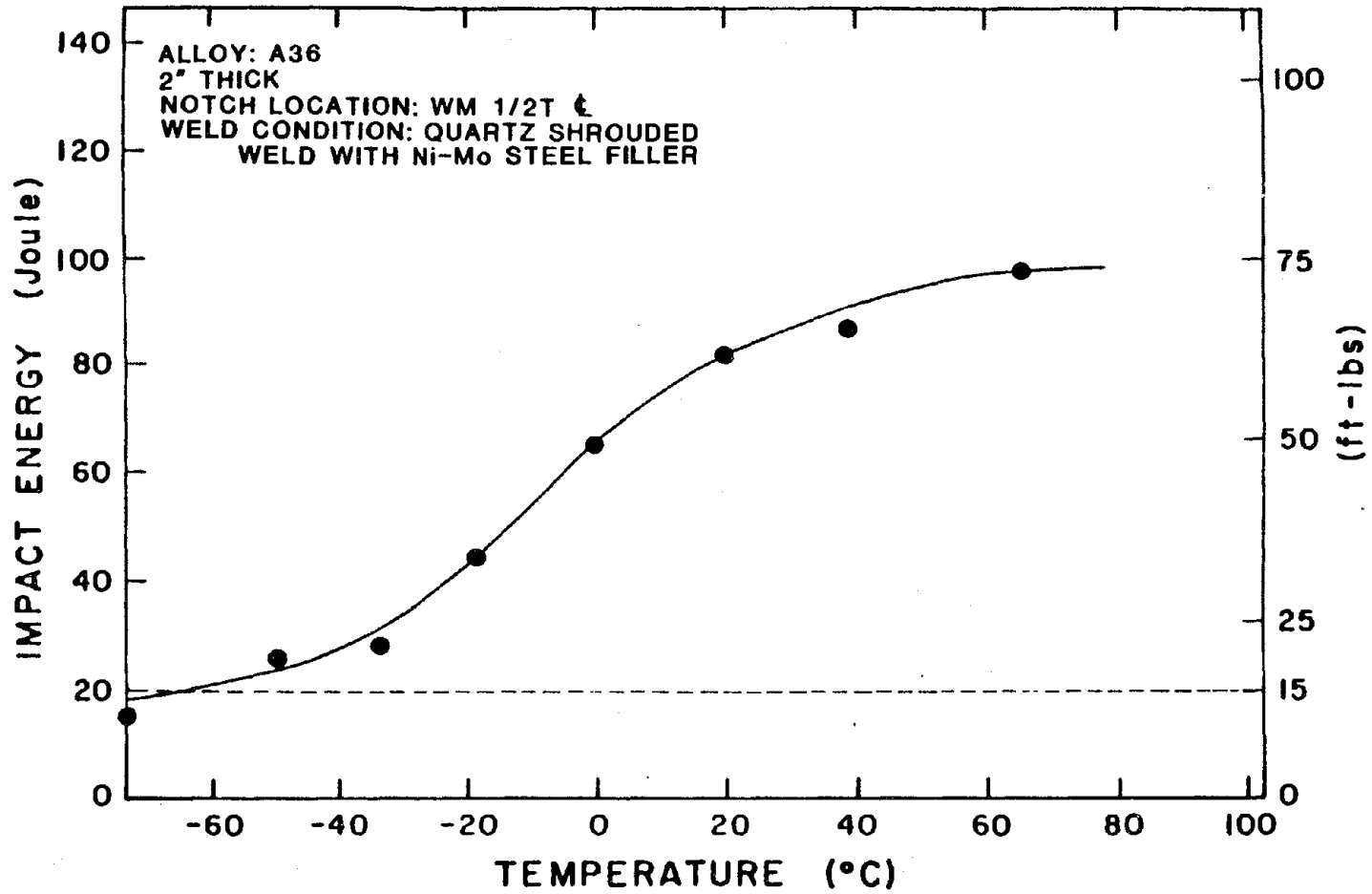


Figure 102. CVN transition curves for 50 mm A36.

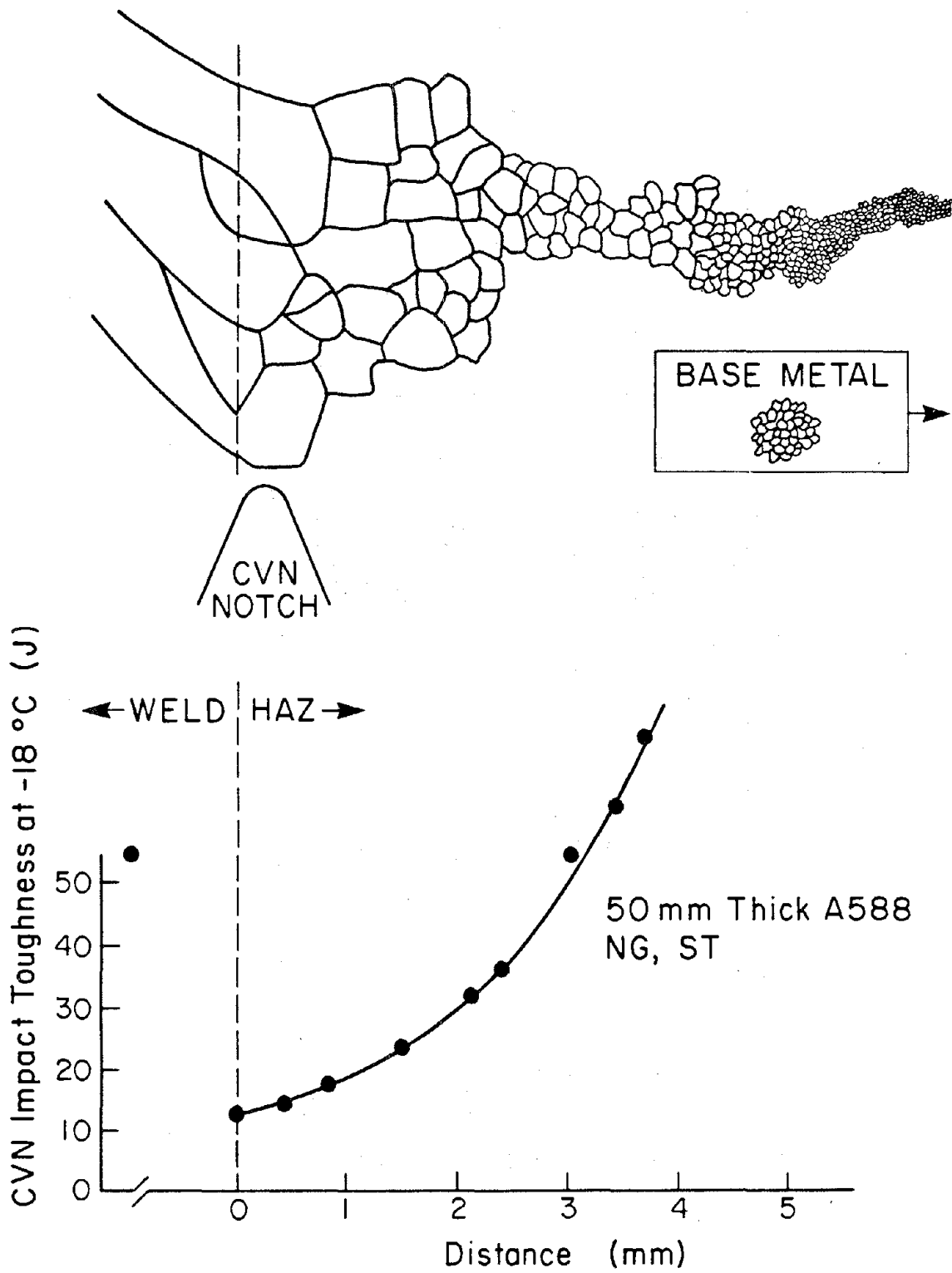


Figure 103. CVN toughness as a function of distance from the fusion line in 450 mm thick A588. (Schematic.)

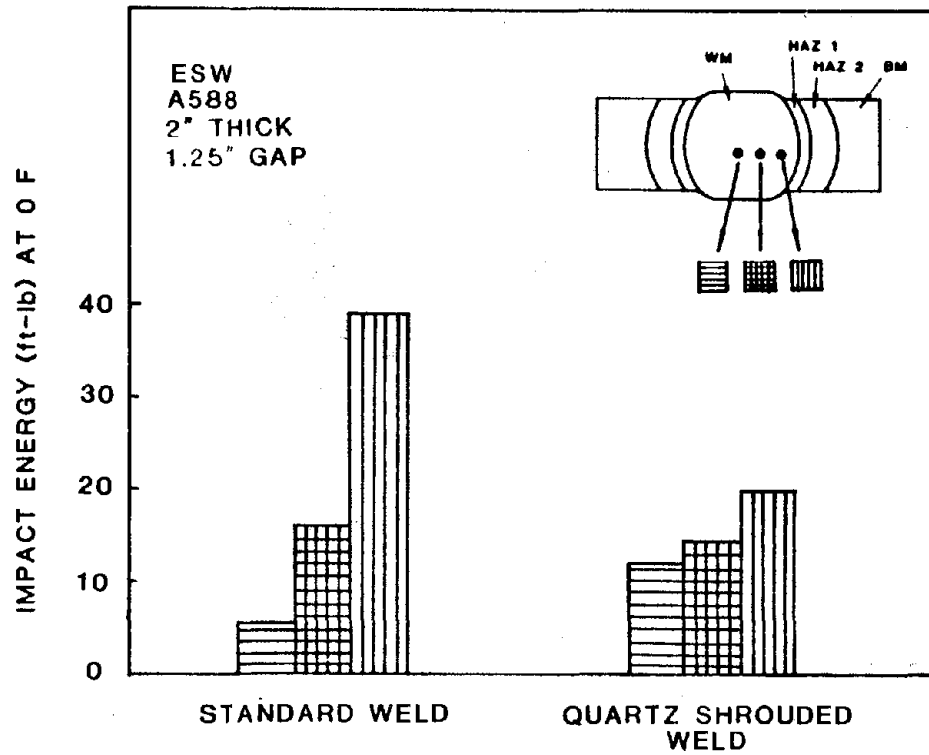


Figure 104. Impact energy summary for standard and quartz shrouded welds.
(Schematic.)

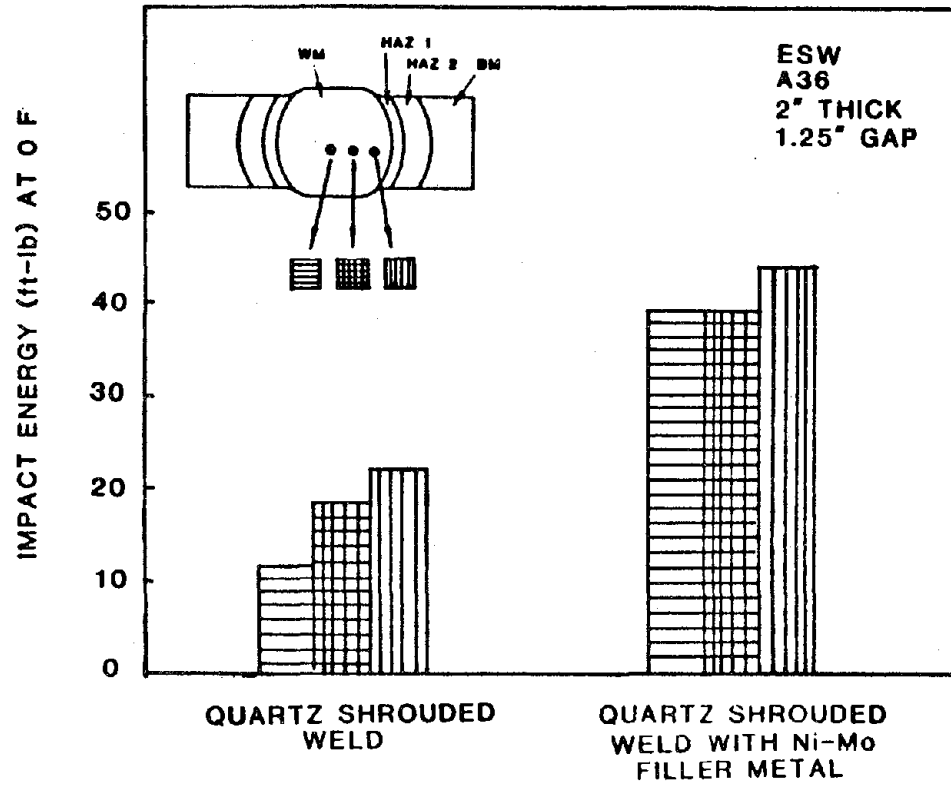


Figure 105. Impact energy summary for quartz grain refined plus the influence of alloy additions. (Schematic.)

Table 8. Weld metal and heat affected zone CVN impact toughness summary.

Alloy	Thickness (mm)	Weld Condition (gap, wire)	CVN Data (Average of 6 Tests)							
			WM $\frac{1}{2}$ T (-18°C)		WM $\frac{1}{2}$ T (-18°C)		HAZ1 (-18°C)		HAZ1 (+4°C)	
			Joule	Ft-lb	Joule	Ft-lb	Joule	Ft-lb	Joule	Ft-lb
A36	50	SG, 25P	22	16	20	15	13	10	40	30
		NG, 25P	27	20	32	24	16	12	46	34
		NG, ST	68	50	63	46	16	12	48	36
	76	SG, 25P	13	10	18	13	14	10	21	16
		NG, 25P	21	16	25	19	16	12	48	35
		NG, ST	27	20	17	13	11	8	24	18
A588	50	SG, WS	5	4	8	6	5	4	11	10
		NG, WS	15	11	14	10	11	8	18	13
		NG, ST	36	27	43	32	20	15	31	23
	76	SG, WS	4	3	5	4	3	2	4	3
		NG, WS	5	4	7	5	3	2	6	4
		NG, ST	8	6	8	6	4	3	7	5
		NG, ST2	31	23	40	30	10	8	25	18

Table 9. Test temperatures (°C) at which key levels of CVN toughness were obtained.

Alloy	Thickness	Weld Condition	(20 Joules) ¹ Notch Location			(27 Joules) ² Notch Location			(33 Joules) ³ Notch Location		
			¼T	½T	HAZ1	¼T	½T	HAZ1	¼T	½T	HAZ1
A36	50	SG, 25P	-18	-19	-10	- 4	- 3	- 6	5	6	- 2
		NG, 25P	-46	-32	-13	-23	-18	- 9	-14	- 6	- 4
		NG, ST	-57	-60	-13	-51	-51	-10	-44	-45	- 5
	76	SG, 25P	- 4	- 9	- 2	6	- 2	10	17	6	22
		NG, 25P	-27	-22	-16	-18	-13	-10	- 8	- 7	- 5
		NG, ST	- 9	-13	- 4	- 1	- 9	7	9	3	17
A588	50	SG, 25P	- 5	- 3	12	0	3	21	8	8	30
		NG, 25P	-10	- 9	3	- 5	- 3	11	2	6	21
		NG, ST	-44	-36	-13	-44	-30	- 3	-26	-23	7
	76	SG, 25P	26	26	50	33	34	59	38	35	69
		NG, 25P	22	20	40	31	26	48	38	31	56
		NG, ST	16	16	26	26	22	31	33	27	36
76	NG, ST2	-31	-26	-4	-24	-18	2	-20	-10	9	
	50	Quartz + Alloy	NT	-65	NT	NT	-43	NT	NT	-25	NT

Notes: 1. 15 ft-lb 2. 20 ft-lb 3. 25 ft-lb

- o Figure 98 summarizes the optimized 76-mm A36 data and shows that for the thicker material, the CVN HAZ properties are marginal
- o Figure 99 summarizes the optimized 50-mm A588 data and indicates that the properties are acceptable in all CVN locations
- o Figure 100 summarizes the optimized 76-mm A588 and, again, as for the 50-mm material, all CVN locations were acceptable, although HAZ1 data are marginal.
- o The quartz grain-refined weld that was also alloyed to control the grain substructure exhibited excellent impact toughness. However, persistent lack of fusion imperfections currently restricts this practice from going beyond the laboratory stage. Successful implementation of this technology still requires a significant flux/slag development effort, as well as joint geometry and weld parameter optimization.
- o The coarse HAZ, by virtue of the dramatically-increased weld metal properties, has become the limiting factor in ESW toughness. HAZ CVN data in this program was uniformly taken from between 1.0 and 1.5 mm from the fusion line at the midthickness location, unless otherwise noted. The proper location for the CVN notch location in the HAZ is not standardized and, as shown in figure 103, the location of the notch results in extreme variation in the impact toughness values. CVN data taken as a function of distance from the fusion line suggests that the lowest zone is within 1.5 mm of the fusion line and could be at the approximate fusion line itself. It is impossible from this data to define the exact minimum HAZ1 toughness level without further testing within 1 mm of the fusion line. It is clear, however, that without more specifically-defined HAZ1 notch location requirements, that HAZ1 impact properties are not conservative unless notch locations, with respect to the fusion line, are provided.

Finally, the results of the grain-refined welds are demonstrated in figures 104 and 105 where it is evident that the grain refinement without additional alloying increased the minimum toughness and reduced the variation across the weld zone while at the same time reducing the maximum level in the coarse columnar microstructural zone. The use of alloy additions, together with grain refining, however, increased the toughness of the weld while still maintaining a very uniform microstructure and impact toughness profile.

7. ASTM E399 Fracture Toughness Tests

The results obtained in this program are shown in tables 10 to 15. The tables include the ratio of the P_{\max} to P_Q , one measure of the test validity. Also, the fatigue crack front profile is listed as acceptable or not based on the ASTM E399 requirements. Based on the minimum thickness requirement:

$$B > 2.5 (K_q / \sigma_{ys})^{1/2} \quad (3)$$

where y_s is the yield strength, and K_q is defined in E399, neither of these alloys met the minimum thickness requirement for $B = 76$ mm, with the exception of A588 ESW using the standard wire and weld setup practice.

a. A36 Material

For A36, even at the lowest test temperature, invalid load displacement curves were obtained, and consistent K_q values of approximately $88,000 \text{ MPa}\cdot\text{m}^{1/2}$ were obtained. The weld metal toughness was not significantly affected by either the narrow gap or the alloy approaches used in this program, except perhaps at the lowest test temperature, where the higher strength alloyed material exhibited lower toughness, although only one test was carried out. In fact, the weld metal toughness was the same as the base metal properties for A36. Analysis of the HAZ is more difficult due to multiple microstructural zones. However, none of the HAZ data were exceptionally low in these tests and did not follow the CVN trend.

b. A588 Material

The higher strength A588 alloy did exhibit a valid-appearing load displacement curve at -18°C . For this alloy, unlike A36, the low heat input alloyed weld practice developed at OGC did result in significant improvement in the weld metal toughness equivalent to the base material. Also, this alloy appeared to exhibit strain rate sensitivity, whereas A36

Table 10. Full thickness ASTM E399 fracture toughness of 76-mm thick A36 and A588 base metal alloys.

Alloy	ID#	Test Temperature (°C)	Loading ¹ Rate	Load ² (KN)		Load Ratio P_{max}/P_Q	FCP ³	K_c^4 (MPa-m ^{1/2})	K_{max}^5 (MPa-m ^{1/2})
				P_Q	P_{max}				
A36	BM2	-18	S	238	291	1.22	A	92	112
	BM3	-34	S	258	305	1.18	A	92	109
	BM4	-7	I	245	276	1.13	A	89	101
	BM5	-7	S	229	305	1.33	A	86	114
	BM6	-18	I	258	287	1.11	A	93	103
	BM7	-46	S	236	298	1.26	A	83	105
	A588	BM1	-18	S	214	214	1.0	A	83
BM3		-18	S	223	223	1.0	A	81	81
BM4		-7	I	198	198	1.0	A	73	73
BM5		-18	I	185	185	1.0	A	67	67
BM6		-7	S	191	191	1.0	A	70	70

Notes:

1. (S) = ASTM E399 quasi-static loading; (I) = Intermediate loading rate, 2 seconds to failure
2. Defined in ASTM E399
3. Fatigue Crack Profile: A = Accepted by ASTM E399; R = Rejected by ASTM E399
4. Does not meet E399 test validity requirements for K_{Ic}
5. Critical stress intensity at maximum load

Table 11. Full thickness ASTM E399 fracture toughness of 76-mm thick A36 electroslag weld metal.

ID#	Weld Condition ¹	Test Temperature (°C)	Loading ² Rate	Load ³ (KN)		Load Ratio P_{max}/P_Q	FCP ⁴	K_c^5 (MPa-m ^{1/2})	K_{max}^6 (MPa-m ^{1/2})
				P_Q	P_{max}				
M151-1	SG, 25P	-18	S	229	383	1.67	A	87	145
M151-2	SG, 25P	-18	S	240	349	1.45	A	88	128
M151-3	SG, 25P	-34	S	238	380	1.60	A	86	137
M151-4	SG, 25P	-46	S	234	343	1.45	A	86	124
M155-1	NG, 25P	-18	S	265	369	1.40	A	99	138
M155-2	NG, 25P	-18	S	243	299	1.24	A	90	111
M155-3	NG, 25P	-34	S	218	223	1.02	A	85	87
M155-4	NG, 25P	- 7	I	231	274	1.18	A	89	105
M159-1	NG, ST2	-18	S	229	229	1.00	A	83	83
M159-2	NG, ST2	-18	S	236	236	1.00	A	85	85
M159-3	NG, ST2	-34	S	194	194	1.00	A	69	69
M159-4	NG, ST2	-18	S	240	254	1.06	A	92	97

Notes:

1. SG, 25P = conventional industry practice
 NG, 25P = OGC narrow gap reduced heat input practice
 NG, ST2 = OGC optimized low heat input/alloyed microstructure controlled practice
2. (S) = ASTM E399 quasi-static loading; (I) = Intermediate loading rate, 2 seconds to failure
3. Defined in ASTM E399
4. Fatigue Crack Profile: A = Accepted by ASTM E399; R = Rejected by ASTM E399
5. Does not meet E399 test validity requirements for K_{Ic}
6. Critical stress intensity at maximum load

Table 12. Full thickness ASTM E399 fracture toughness of 76-mm thick A36 electroslag weld coarse heat affected zone.

ID#	Weld Condition ¹	Test Temperature (°C)	Loading ² Rate	Load ³ (KN)		Load Ratio P_{max}/P_Q	FCP ⁴	K_c^5 (MPa-m ^{1/2})	K_{max}^6 (MPa-m ^{1/2})
				P_Q	P_{max}				
M163-1	SG, 25P	-18	S	234	238	1.02	A	88	89
M163-2	SG, 25P	-18	S	234	243	1.04	A	85	88
M163-3	SG, 25P	- 7	S	260	265	1.02	A	93	95
M163-4	SG, 25P	- 7	S	218	277	1.27	A	81	103
M156-1	NG, 25P	-18	S	260	263	1.01	A	88	89
M156-2	NG, 25P	-18	S	194	194	1.00	A	71	71
M156-3	NG, 25P	- 7	S	200	345	1.72	A	77	132
M156-4	NG, 25P	- 7	I	238	298	1.25	A	96	120
M160-1	NG, ST2	-18	S	238	251	1.06	A	98	103
M160-2	NG, ST2	-18	S	256	260	1.02	A	93	95
M160-3	NG, ST2	- 7	S	236	300	1.27	A	87	111
M160-4	NG, ST2	- 7	I	231	254	1.10	A	88	97

Notes:

1. SG, 25P = conventional industry practice
 NG, 25P = OGC narrow gap reduced heat input practice
 NG, ST2 = OGC optimized low heat input/alloyed microstructure controlled practice
2. (S) = ASTM E399 quasi-static loading; (I) = Intermediate loading rate, 2 seconds to failure
3. Defined in ASTM E399
4. Fatigue Crack Profile: A = Accepted by ASTM E399; R = Rejected by ASTM E399
5. Does not meet E399 test validity requirements for K_{Ic}
6. Critical stress intensity at maximum load

Table 13. Full thickness ASTM E399 fracture toughness of 76-mm thick A588 electroslag weld metal.

ID#	Weld Condition ¹	Test Temperature (°C)	Loading ² Rate	Load ³ (KN)		Load Ratio P_{max}/P_Q	FCP ⁴	K_c^5 (MPa-m ^{1/2})	K_{max}^6 (MPa-m ^{1/2})
				P_Q	P_{max}				
M150-1	SG, WS	-46	S	162	162	1.00	A	65	65
M150-2	SG, WS	-34	S	142	187	1.31	A	53	69
M150-3	SG, WS	-46	S	145	145	1.00	A	55	55
M150-4	SG, WS	- 7	I	136	187	1.38	A	49	68
M152-1	SG, WS	-18	S	162	171	1.05	A	60	63
M152-2	SG, WS	-18	S	129	169	1.31	A	50	66
M169-1	NG, WS	-18	S	145	145	1.00	A	56	56
M169-2	NG, WS	-18	S	145	145	1.00	A	55	55
M169-4	NG, WS	-18	S	142	174	1.22	A	56	69
M171-1	NG, ST2	-18	S	236	236	1.00	A	88	88
M171-2	NG, ST2	-18	S	236	236	1.00	A	85	85
M171-3	NG, ST2	-18	S	234	234	1.00	A	83	83
M171-4	NG, ST2	- 7	S	207	207	1.00	A	79	79

Notes:

1. SG, 25P = conventional industry practice
 NG, 25P = OGC narrow gap reduced heat input practice
 NG, ST2 = OGC optimized low heat input/alloyed microstructure controlled practice
2. (S) = ASTM E399 quasi-static loading; (I) = Intermediate loading rate, 2 seconds to failure
3. Defined in ASTM E399
4. Fatigue Crack Profile: A = Accepted by ASTM E399; R = Rejected by ASTM E399
5. Does not meet E399 test validity requirements for K_{Ic}
6. Critical stress intensity at maximum load

Table 14. Full thickness ASTM E399 fracture toughness of 76-mm thick A588 electroslag weld coarse heat affected zone.

ID#	Weld Condition ¹	Test Temperature (°C)	Loading ² Rate	Load ³ (KN)		Load Ratio P_{max}/P_Q	FCP ⁴	K_c^5 (MPa-m ^{1/2})	K_{max}^6 (MPa-m ^{1/2})
				P_Q	P_{max}				
M164-1	SG, WS	-18	S	149	166	1.11	A	61	68
M164-2	SG, WS	-18	S	154	158	1.03	A	60	61
M164-3	SG, WS	- 7	S	165	165	1.00	A	73	73
M164-4	SG, WS	- 7	I	147	146	1.01	A	63	63
M170-1	NG, WS	-18	I	167	205	1.23	R	68	81
M170-3	NG, WS	-18	S	174	174	1.00	A	74	74
M170-4	NG, WS	-18	S	231	367	1.59	A	90	141
M172-1	NG, ST2	-18	S	214	214	1.00	A	85	85
M172-2	NG, ST2	-18	S	260	260	1.00	A	93	93
M172-3	NG, ST2	- 7	S	165	191	1.16	A	65	75
M172-4	NG, ST2	- 7	I	231	231	1.00	A	90	90

Notes:

1. SG, 25P = conventional industry practice
 NG, 25P = OGC narrow gap reduced heat input practice
 NG, ST2 = OGC optimized low heat input/alloyed microstructure controlled practice
2. (S) = ASTM E399 quasi-static loading; (I) = Intermediate loading rate, 2 seconds to failure
3. Defined in ASTM E399
4. Fatigue Crack Profile: A = Accepted by ASTM E399; R = Rejected by ASTM E399
5. Does not meet E399 test validity requirements for K_{Ic}
6. Critical stress intensity at maximum load

Table 15. Full-scale category B I-beam fatigue tests of A588 at room temperature.

Beam #	ESW ID#	OGC Weld Procedure ¹	Total Fatigue Cycles	Stress Range (ksi)	Reason Test Terminated	Electroslag Weld Condition
1	IB- 1 IB- 2	SG, WS SG, WS	7,660,800	17.9	Tack weld HAZ cracked	No Crack No Crack
2	IB- 3 IB- 4	NG, WS NG, WS	1,970,800	18.7	Tack weld HAZ cracked	No Crack No Crack
3	IB- 5 IB- 6	SG, WS SG, WS	4,027,000	17.6	SAW flange weld cracked	No Crack No Crack
4	IB- 7 IB- 8	NG, WS NG, WS	3,374,700	17.7	>2,000,000 cycles	No Crack No Crack
5	IB- 9 IB-10	SG, WS SG, WS	4,116,700	17.3	SAW flange weld cracked	No Crack No Crack
6	IB-11 IB-12	NG, WS SG, WS	2,779,100	17.5	>2,000,000 cycles	No Crack No Crack

Notes: 1. SG, WS = standard recommended practice
 NG, WS = OGC narrow gap reduced heat input weld practice.

did not show any strain rate sensitivity within the range tested. For the standard weld practice, due to the low toughness, this alloy did meet the minimum thickness requirement.

The HAZ data suggests that the lower heat input improved the toughness. Again, since the zone is not straight, analysis is difficult. However, like the A36, the optimized practices resulted in the best data in the HAZ.

Overall, the full thickness tests indicated that the toughness was very consistent in the A36 alloy and that for either alloy the OGC-recommended practice can be expected to achieve the best toughness. The HAZ did not show very low toughness values consistent with the CVN data within three grains of the weld zone, although due to the mixed zones present in the full thickness sample, the fracture process may be controlled by the average toughness rather than by the very narrow low toughness zone sampled by the smaller CVN-type specimen. In summary, the full thickness toughness assessment did not show as sensitive a behavior as did the more localized CVN tests relative to the modifications that were studied at OGC, and CVN- K_{IC} correlation attempts would not predict full thickness trends. Plane strain fracture test data showed that both the weld metal and the HAZ can exhibit properties equivalent to the base material. However, the HAZ data tests a range of microstructures and not just a single microstructure, as can CVN. As for the CVN data, K_{IC} results support the use of lower heat input and alloy additions.

8. Full Scale I-Beam Fatigue Tests

This portion of the research program was designed to evaluate the electrosag weldment fatigue behavior of the OGC-modified weld practices versus standard or conventional consumable guide electrosag practice. A total of 12 electrosag welds were tested. Six represented standard practice with a conventional round guide tube, and six were made with the OGC narrow-gap wing-type guide tube and reduced heat input. All welds used

standard recommended weld wire chemistry. The fatigue tests failed to produce any cracks in any of the 12 electroslag welds. While 2 million cycles represented the required number for category B beams under the stress range tested, some beams were run to more than 7 million cycles with no cracks forming in the electroslag welds. For the first two I-beams, fatigue cracks developed in the HAZ of residual tack welds and propagated parallel to, but never into, the electroslag weld metal or HAZ. These tack welds were inadvertently placed on the outside of the run-in block rather than on the inside edge of the run-in block, where they are normally consumed during electroslag welding. While the reinforcements and run-out and run-in tabs were ground flush, a small portion of the tack weld remained, and in both weldments, failure originated from these locations. Significantly for one beam, cracks did not originate in these tack weld locations until approximately 7 million cycles; and in the other beam, cracks originated in the residual tack weld at approximately 2 million cycles, the required minimum number of cycles for category B weldments under these operating stress ranges. A summary of all fatigue tests is provided in table 15.

It should be noted that these welds were fabricated at OGC with standard practices that have been demonstrated not to contain imperfections by sectioning many welds made under identical conditions. These welds were also ultrasonically inspected. No imperfections of any type were detected, and it is believed that these welds are a test of the inherent electroslag weld fatigue behavior in the absence of any crack initiation sites, such as lack of fusion, slag entrapment or hot cracks. Additionally, the reinforcements were ground smooth and the corners of the flange lightly ground according to routine practice at Lehigh University. As such, these welds should be typical of electroslag welds made with good practices. No special "laboratory" techniques were used.

9. Weld Defect Formation and Detection

Through this and prior ESW programs, OGC has learned to control the occurrence and nature of a variety of weld-related imperfections. These include: 1) lack of fusion, 2) entrapped slag, 3) centerline hot cracking, 4) radial hot cracking, 5) ferrite vein cracking, and 6) wormhole porosity. Lack of fusion is caused predominantly by low voltage, off-center electrodes, improper grounding, and lack of proper wire straightening. Additionally, excessive or intermittent flux additions that chill the slag bath, or a weld interruption, such as a wire jam that causes a drop in slag temperature, may result in lack of fusion. Centerline hot cracking may be induced by either excess current resulting in a poor form factor (molten pool profile) or by addition of copper that is well known to induce hot cracking.

It is possible to produce radial-type hot cracking if the center weld zone microstructure is altered to create an equiaxed crack-resistant structure. This is produced by still higher welding current levels. Under these conditions and for solid filler wires, the resulting equiaxed structure is crack resistant and the highest crack potential location shifts from this zone to the columnar zone where cracking occurs along the prior austenite grain boundaries, which also coincide with the interdendritic solidification zones. Both types of cracking produce relatively large cracks, as shown in figure 43.

Ferrite vein cracking, as shown in figure 106, is largely produced by improper flux chemistry together with moist flux. Standard practice at OGC is to bake the flux until all weld setup is completed so that the flux is not removed from the oven until the weld is ready to be initiated. As the name implies, ferrite vein cracking forms along the ferrite films that nucleate along prior austenite grain boundaries. These cracks are very fine and are not visible by eye.

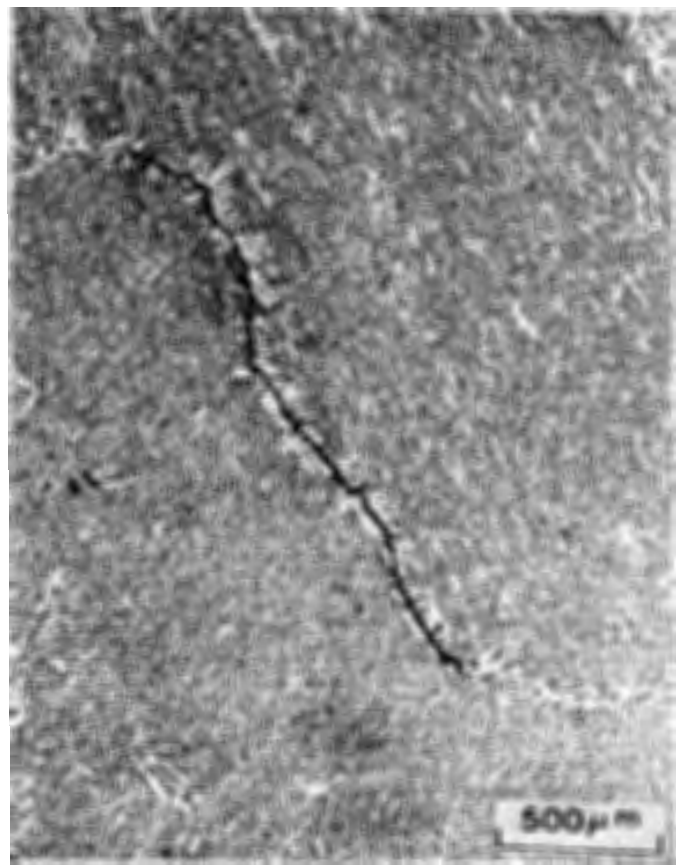


Figure 106. Typical ferrite vein cracking along prior austenite grain boundaries. (Microstructure.)

Entrapped slag inclusions are generally due to a change in welding conditions that result in an excess overhang of the base metal into the slag bath, or to a chilled slag by interrupting the voltage or making excessive slag additions to compensate for too shallow a slag bath. These conditions will generally, but not necessarily, also result in surface lack-of-fusion imperfections.

The imperfections produced in figure 107 and the accompanying weld conditions utilized in this program are summarized in table 16. These welds were subjected to routine ultrasonic and radiographic inspection by a commercial testing laboratory. This laboratory was not advised in advance of the nature of the electroslag weld practices nor imperfections that might be present. The results of both nondestructive tests are summarized in figures 108 to 111. A full copy of the NDE report is provided in appendix B. For the first test plate, identified as DF-1 by OGC and as plate #4 by the NDE firm, the radiographic inspection detected one of two hot crack zones in the test weldments, whereas the ultrasonic inspection also detected one of two hot cracking locations. Lack of fusion imperfections was generally noted for both situations. For the second test plate, identified as DF-2 by OGC, neither the ultrasonic nor the radiographic analysis detected the ferrite vein crackings as expected due to the very fine nature of these imperfections. Both tests detected hot cracking by copper additions, as well as lack of fusion imperfections, although the ultrasonic scans do not consistently detect lack of fusion nor slag entrapment. The third plate, identified as DF-3 by OGC, contained a variety of elemental inclusions as well as lack of fusion and hot cracks due to copper additions. In this case, the hot cracking with copper additions was not detected by radiographic analysis, but was detected by ultrasonic inspection. Both analyses detected the molybdenum-tungsten tungsten-carbide imperfections, although the indications of sizes were not accurate for the ultrasonic analyses. Finally, the fourth plate, which was a combination standard practice and quartz grain refinement practice and which contained lack of fusion along the length of the quartz in addition to elemental inclusions, was analyzed as the others for both radiographic and ultrasonic

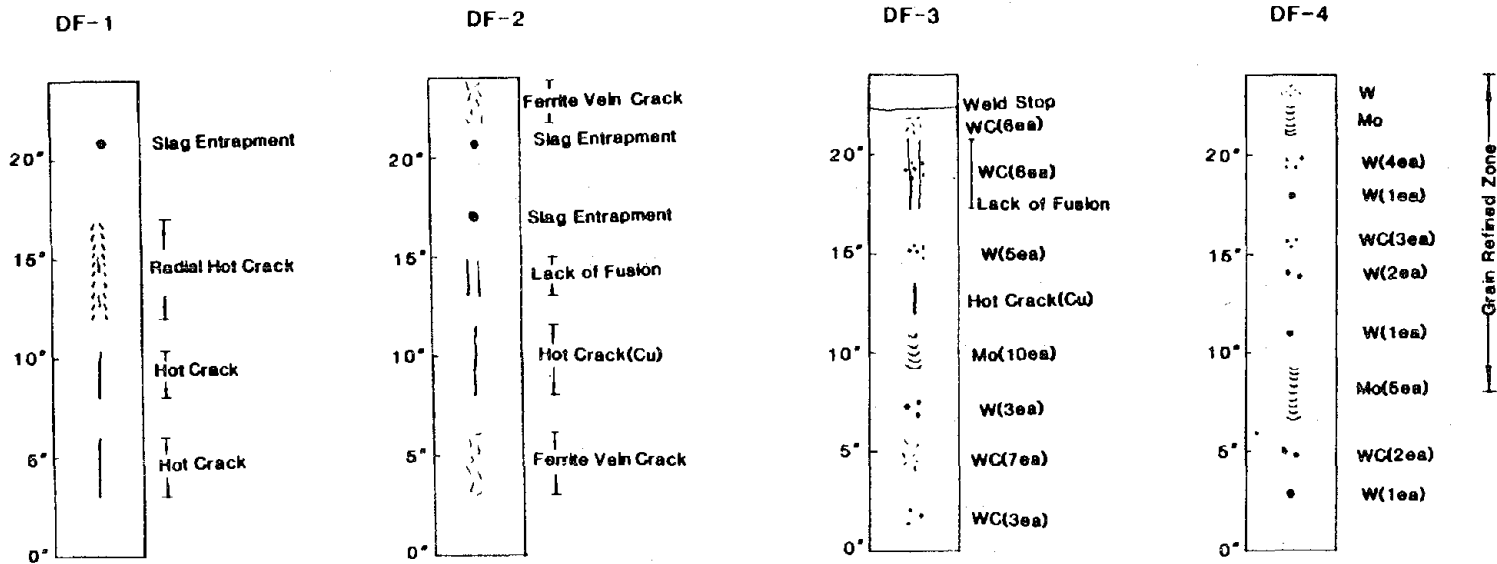


Figure 107. Schematic illustration of defects produced in OGC's defect-controlled electroslag welds. (Schematic.)

Table 16. Electroslag weld defect summary.

Weld ID	Alloy	Thickness (mm)	Defect Forming Weld Conditions	Induced Weld Imperfection	Ultrasonic ¹ Inspection	Radiographic ¹ Inspection
DF-1	A36	76	Excessive current (1200 A)	Centerline hot crack	Detected	Not Detected
			Excessive current (1300 A)	Radial hot crack	Not Detected	Detected
			Voltage drop/wire jam	Lack of fusion/entrapped slag	Detected	Detected
DF-2	A588	76	Wet flux	Ferrite vein crack	Not Detected	Not Detected
			Cu additions	Centerline hot crack	Detected	Detected
			Voltage drop	Lack of fusion--surface	Detected	Detected
			Wire jam	Entrapped slag	Not Detected	Detected
DF-3	A36	50	WC additions	WC inclusions	Detected	Detected
			W additions	W inclusions	Detected	Detected
			Mo additions	Mo inclusions	Detected	Detected
			Cu additions	Centerline hot crack	Detected	Not Detected
			WC + low voltage	WC inclusions & surface lacking fusion	Not Detected	Detected
DF-4	A36	50	W addition	W inclusions	Not Detected	Detected
			WC addition	WC inclusion	Detected	Detected
			Mo addition	Mo inclusions	Detected	Detected
			Mo + grain refine ²	Mo inclusions	Detected	Detected
			W + grain refine	W inclusions	Detected	Detected
			WC + grain refine	WC inclusions	Not Detected	Detected

Notes:

1. NDE test conditions defined in Appendix B
2. OGC Quartz grain refinement practice

DF-1 (PLATE 4)

174

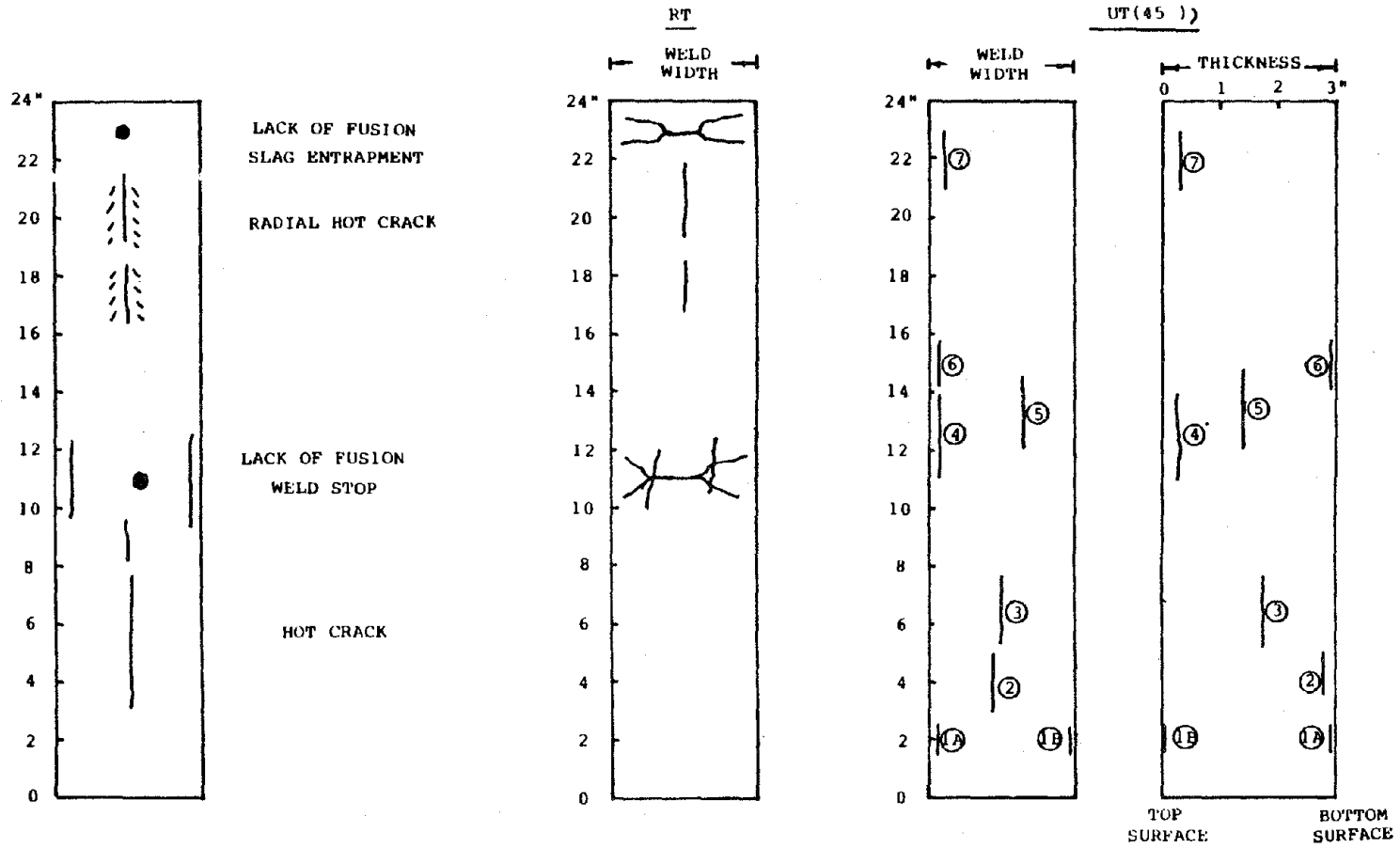


Figure 108. Ultrasonic and radiograph schematic results for controlled defect electroslag weld, plate 4.

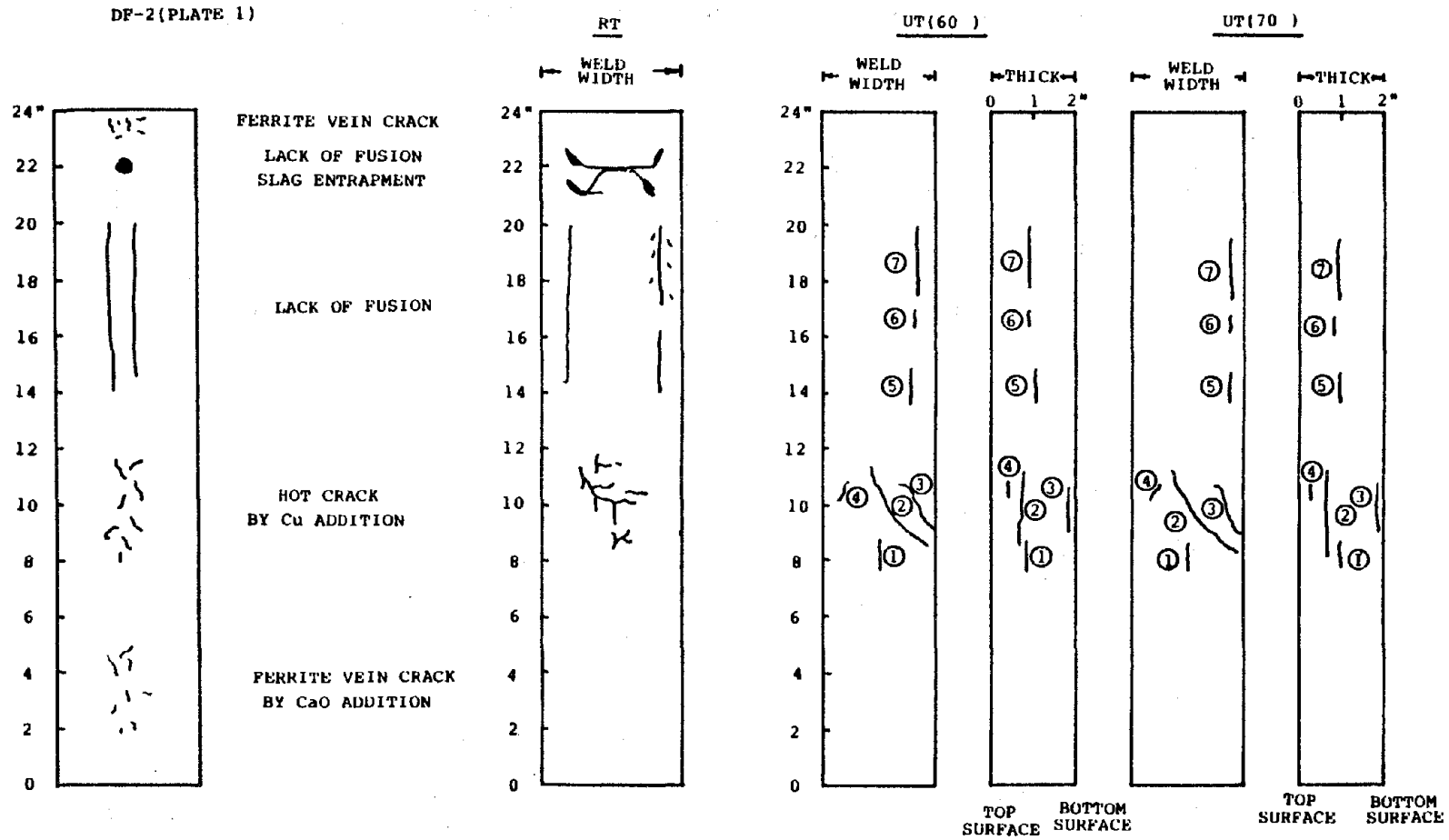


Figure 109. Ultrasonic and radiograph schematic results for controlled defect electroslag weld, plate 1.

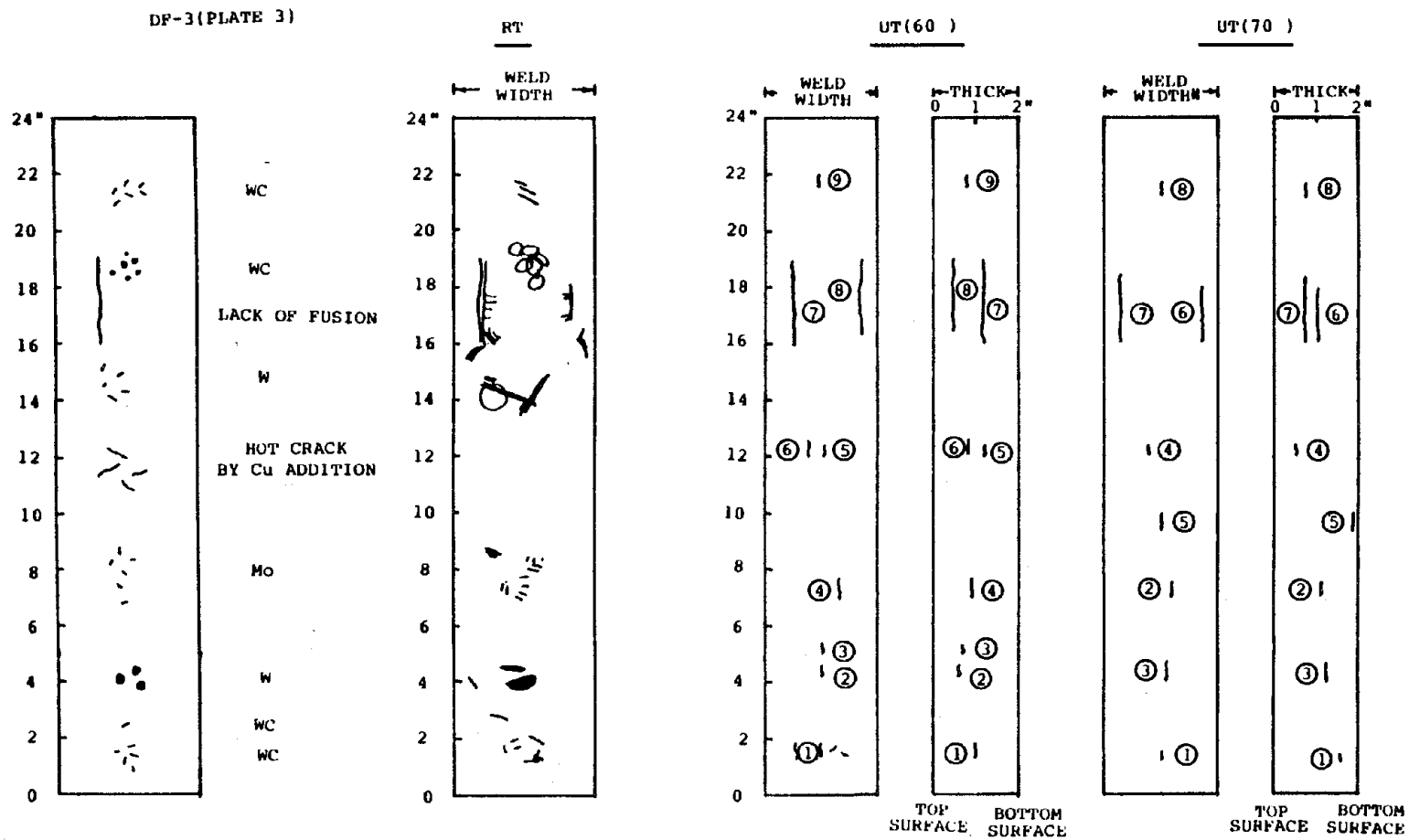


Figure 110. Ultrasonic and radiograph schematic results for controlled defect electroslag weld, plate 3.

DF-4 (PLATE 2)

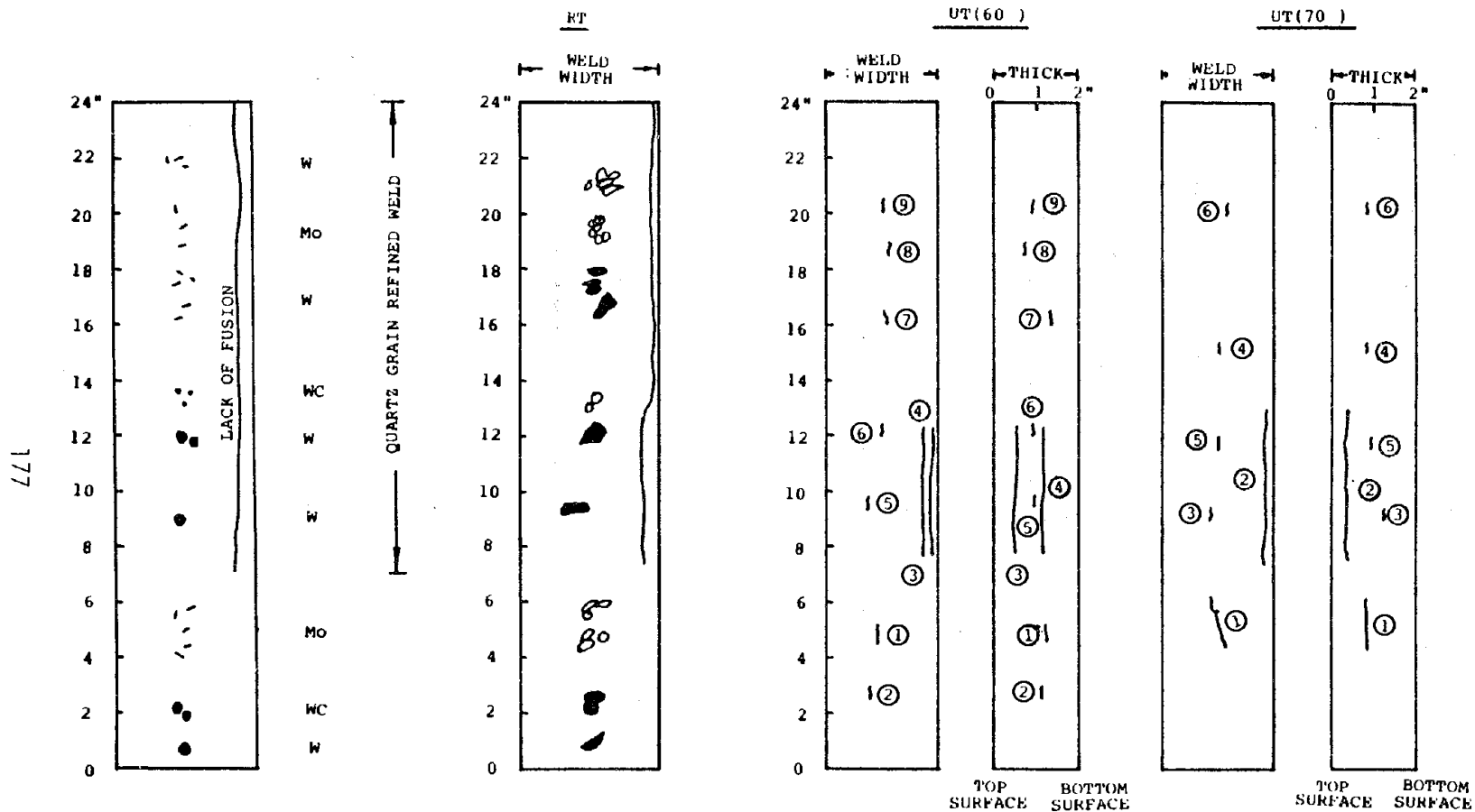


Figure 111. Ultrasonic and radiograph schematic results for controlled defect electroslag weld, plate 2.

analyses. The radiographic analysis for this plate detected all the inclusions and lack of fusion present in the plate, whereas the tungsten and tungsten-carbide additions were not clearly defined in the ultrasonic analyses.

Neither technique was able to detect ferrite vein cracking that is developed due to improper slag chemistry and flux handling techniques. Other imperfections, such as hot cracking, were inconsistently detected by either process. However, generally the combination of both practices was adequate in defining known imperfections, while either one, in individual cases, missed certain types. Additional tests appear to be required to properly assess capabilities and limitations of radiographic and ultrasonic techniques as applied to electroslog weldments. The four test plates with their characterized imperfections could be used in such an assessment. These plates are available for use by DOT for additional testing or by interested State highway departments.

10. Solidification Study

Five characteristic cases of grain structure were clearly observed in narrow-gap ESW of mild and low alloy steels, as shown in figure 59. In all cases, cellular dendrites grew epitaxially from the fusion boundaries towards the weld center and gradually transformed into columnar dendrites. This transition was defined as the occurrence of protrusions of noticeable secondary arms.

The growth of both cellular dendrites and columnar dendrites followed the direction opposite to the maximum thermal gradient vector (normal to the contour of the weld pool). In ESW, the direction of maximum thermal gradient changed gradually. A distinct feature of the dendritic structures was that, as different locations, they had different inclination angles, as shown in figure 112. It must be pointed out that dendrites always grew straight and did not bend. Thus, the adjustment of angular change due to

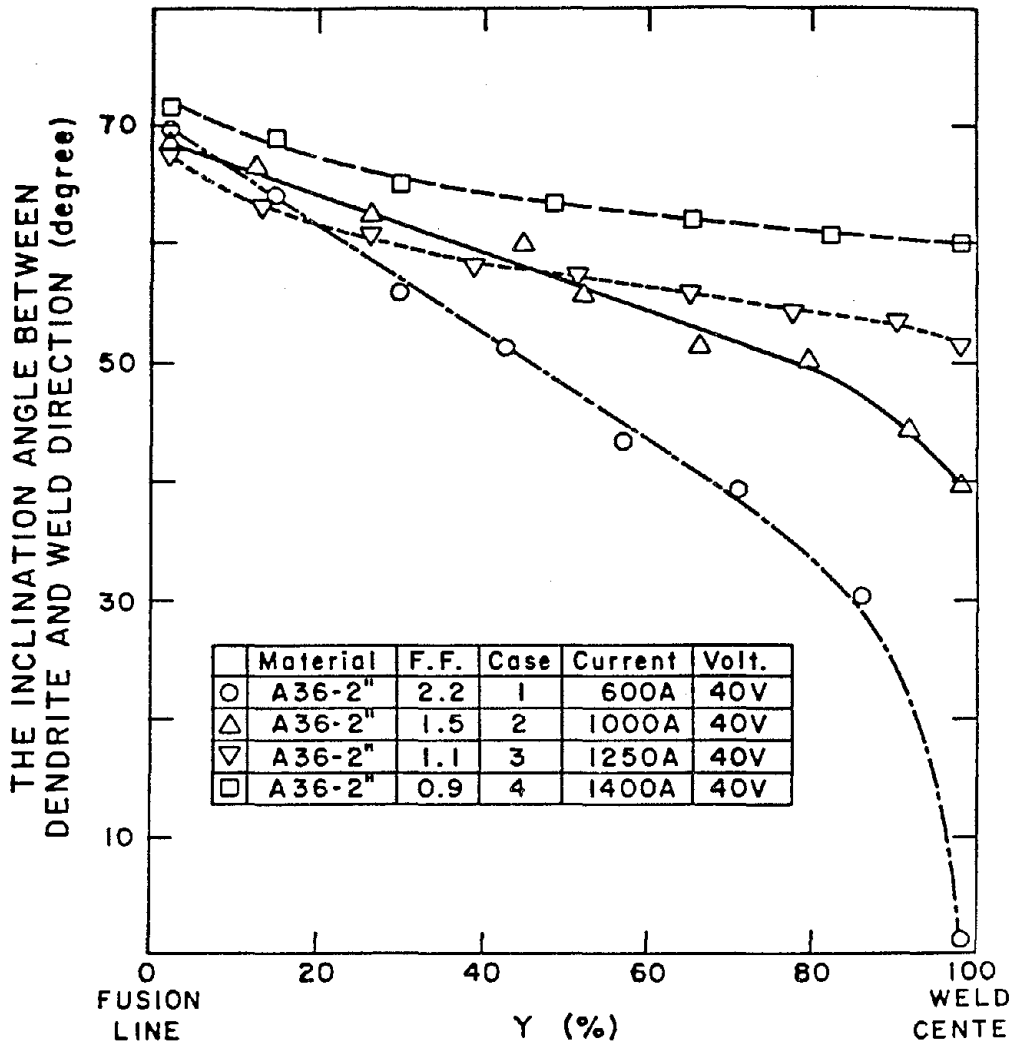


Figure 112. Variation of dendrite inclination angle for various weld cases. (Line Drawing).

the variation of the thermal gradient vector had to be accomplished by the dendrite renucleation events, as shown in figure 113.

As is well known, there is an inverse relationship between dendrite arm spacing (d) and local cooling rate (GR) in the form of:

$$d = A/(GR)^m \quad (4)$$

where A and m are material constants. The dendrite arm spacing accurately reflects the local cooling situation.

Measurement of primary dendrite spacing showed that: 1) the variation of welding speed did not have an obvious effect on dendrite arm spacing when heat input was held constant, as in the top section of figure 114, 2) the enhancement of heat input always increased dendrite arm spacing except near the fusion line, as in the bottom section of figure 114, and 3) during the transition from columnar dendrites to equiaxed dendrites, in cases 4 and 5, the dendrite arm spacing around the weld center always increased abruptly.

Weld parameters controlled the magnitude of the form factor. Two important parameters were the electrode feed rate, which changed the depth of the pool, and the weld voltage, which varied the penetration or width of the weld pool. High factor (> 2.0) resulted in a small percentage of coarse columnar grains. When the form factor dropped from 2 to 1.2 (case 2), the percentage of coarse columnar grains increased greatly. The relationship between form factor and the relative amount of coarse columnar grains is illustrated in figure 115.

Two kinds of solidification imperfections, the centerline cracking and the radial cracking, were observed depending upon the welding conditions as summarized in table 16.

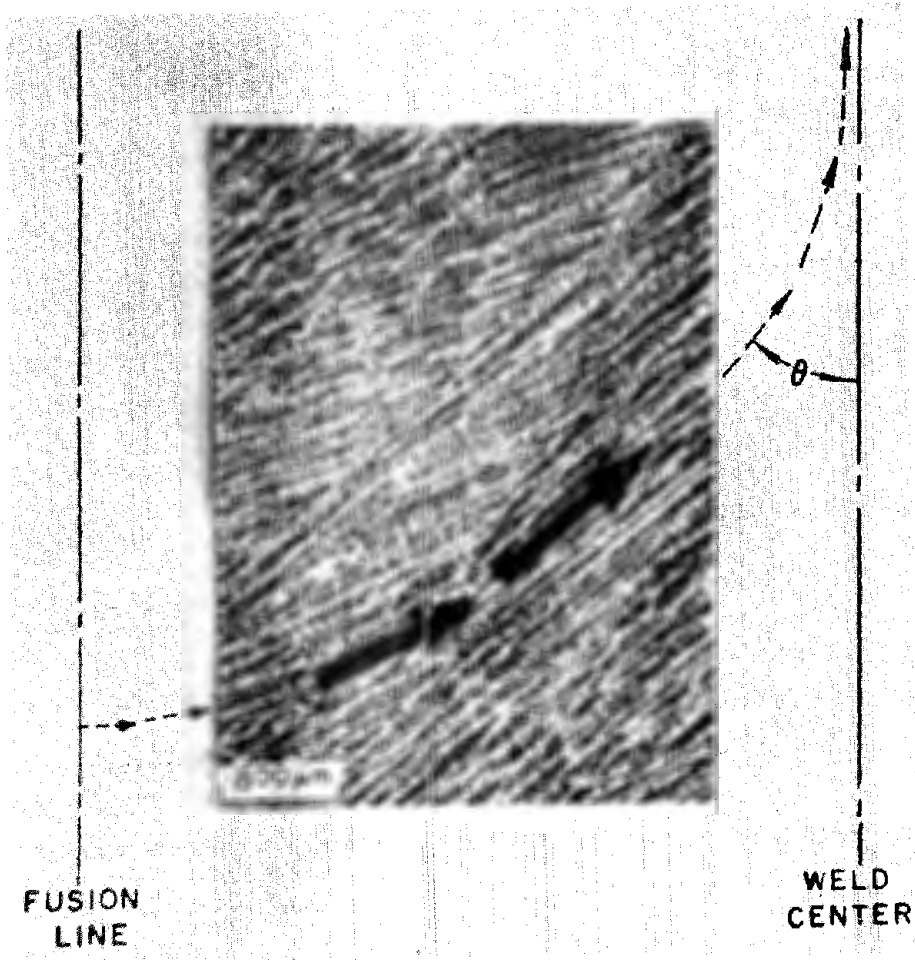


Figure 113. Renucleation events in primary solidification structure. (Micrograph.)



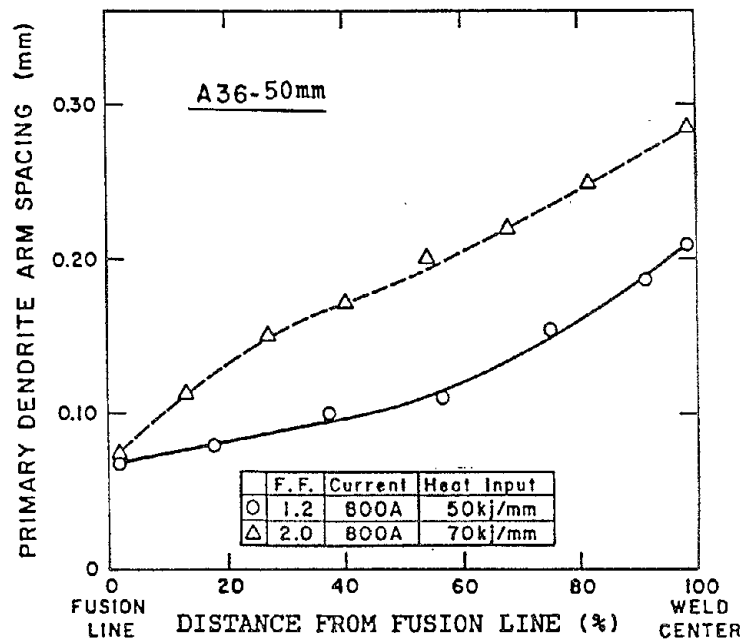
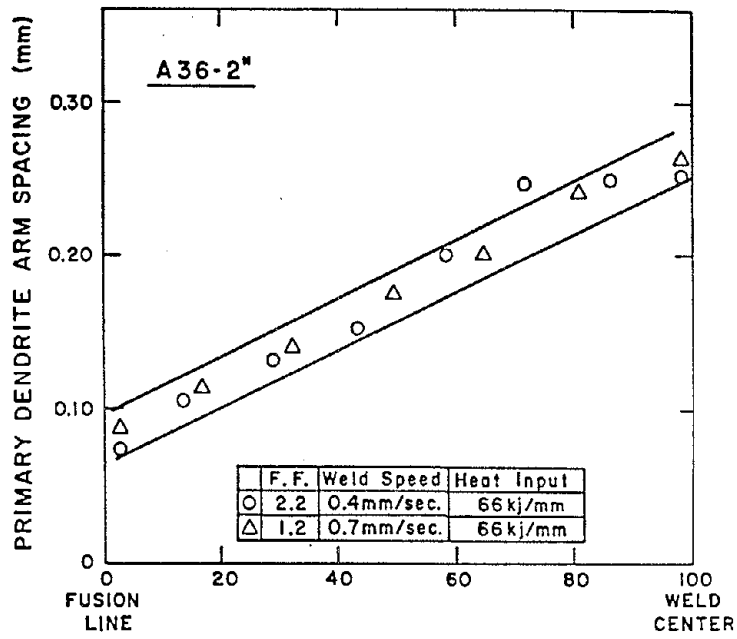


Figure 114. Primary dendrite arm spacing as a function of distance from the fusion line. (Line Drawing.)

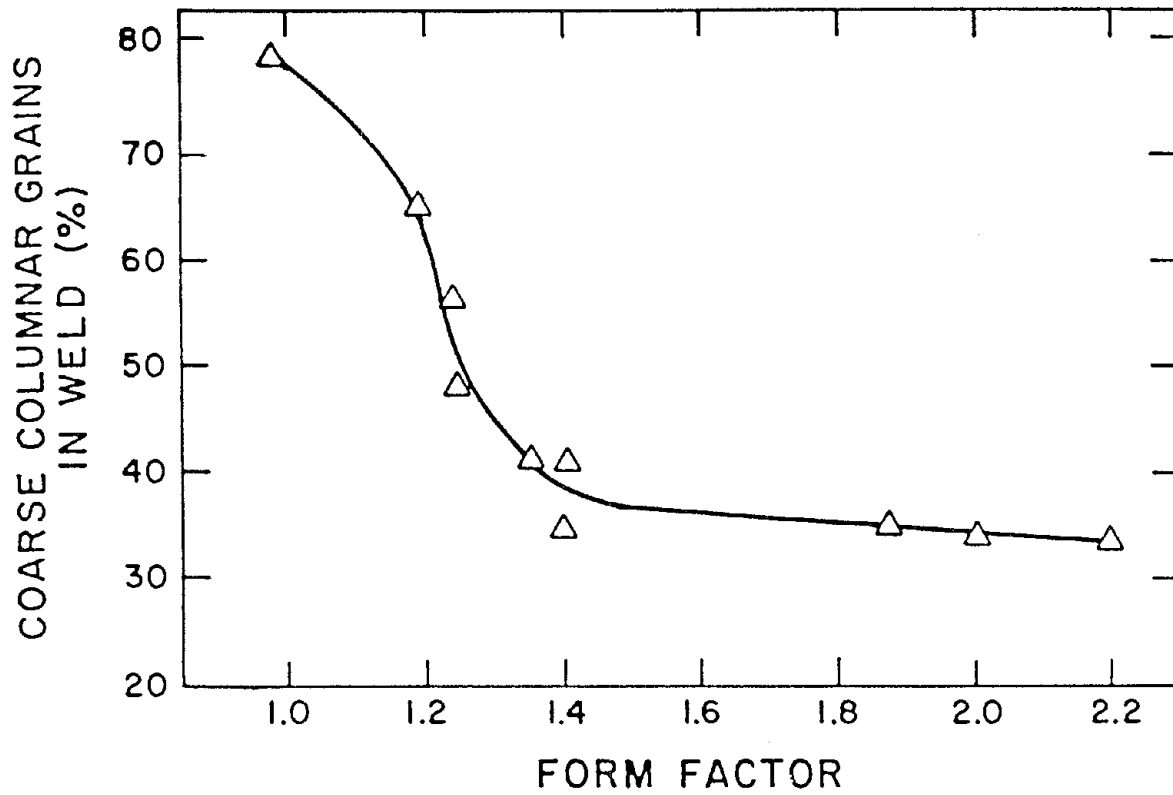


Figure 115. Correlation between form factor and amount of coarse columnar grains. (Line Drawing.)

The centerline hot cracking was caused by the formation of a plane of weakness at the weld center, where solidification fronts from two opposite sides of the weld impinged with an obtuse meeting angle due to high welding speeds. The radial hot cracking was strongly related to the final equiaxed growth near the center of the deep weld pool. Both kinds of hot cracking had a high probability of occurrence and caused a severe disparity of toughness distribution.

VI. DISCUSSION

1. Control of Weld Microstructure

The development of weld metal microstructure was dependent upon several factors: 1) weld cooling rate, 2) oxygen potential of the slag, 3) alloy content of the filler metal, 4) base metal dilution, and 5) the solidification process. Because of the low hardenabilities of both A36 and A588 and the extremely high heat input associated with conventional ESW, the microstructures of weld metal deposited with matching filler metal (25P for A36 and PS588 or WS for A588) contained mostly proeutectoid ferrite in the form of grain boundary ferrite, Widmanstätten and polygonal ferrite with only minimal acicular ferrite. Large quantities of acicular ferrite were required to generate satisfactory weld metal toughness. However, the cooling rates were so slow that the eutectoid transformation was limited to small islands of pearlite. The carbon equivalents (CE) of A36 and A588 (calculated by the method of Ito-Bessyo given in D1.1-86 Structural Welding Code) were 0.24 and 0.31, respectively. These values of CE simply indicated that if 76-mm thick plate of A588 and A36 were welded by conventional means, such as SAW or GMAW, the required preheating temperatures would be 38°C (100°F) and 18°C (65°F), respectively. Of course, a preheating temperature of only 0°C (32°F) is specified for ESW. As a result, the toughness of welds deposited by ESW of A36 and A588 steels was shown in this and other work to be inadequate for bridges.

A methodology was found to reduce the microstructural components that promoted the continuous brittle fracture paths provided by grain boundary ferrite, Widmanstätten ferrite and large polygonal ferrite regions while encouraging the transformation of acicular ferrite. Increasing weld cooling, adding minor alloying elements and optimizing the weld metal oxygen content were responsible for achieving weld metal microstructures containing more than 90 percent acicular ferrite, as shown in figure 54.

The weld cooling rate was increased substantially without introducing imperfections, such as lack of fusion, by using: 1) a narrow 19-mm gap, 2) high welding speed, 3) a wing guide for the 50-mm thick plate and a web guide for the 76-mm thick plate, and 4) a tubular powder-filled wire. It was important to weld with minimum heat input and a maximum weld characteristic in order to increase weld cooling rates and reduce the wasteful spread of heat into the HAZ and base metal. The heat input equation

$$H = EI/v \quad (2)$$

which is contained in the Adams cooling rate equation

$$R = \text{function of } (t/fH)^2 \quad (5)$$

and the weld characteristic equation

$$P = vd/4a \quad (6)$$

(where t , f , d and a are the plate thickness, heat transfer efficiency of the heat source, weld width, and thermal diffusivity, respectively) indicate that increasing the welding speed is key to increasing the weld cooling rate while increasing the welding efficiency. For example, the typical values of H and P for a standard gap electroslog weld were approximately 79 kJ/mm and 0.4, respectively. Comparing these values with the optimized welding parameters with a tubular powder-filled wire, the H and P quantities were 38 kJ/mm and 0.9. Clearly, the utilization of the high speed, narrow gap method reduced heat input and increased welding efficiency by factors of about 2 each.

The utilization of tubular filler metal and the wing/web guides were essential to reducing heat input. The resistance heating of the tubular filler metal provided an effective means of increasing weld travel speed while reducing heat input. Furthermore, the tubular filler metal was more resistant to hot cracking simply because the hollow filler could not

penetrate as deeply into the molten pool as could the comparable solid filler, thereby increasing the form factor substantially. Similarly, the wing and web guides increased the form factor substantially by reducing current density and distributing the heat input over the entire slag pool in comparison to a "single point source" guide tube used in standard 32-mm gap ESW.

As a result of these methods of increasing the cooling rate, the weld microstructure was substantially improved. The quantity of acicular ferrite increased dramatically while the amounts of grain boundary ferrite, Widmanstätten ferrite and polygonal ferrite correspondingly decreased.

Oxygen potential of the flux was an essential ingredient in the production of acicular ferrite in the weld, as shown in figure 63. An optimum of about 200 ppm oxygen was necessary to provide the maximum amount of acicular ferrite for a given set of ESW parameters. It is fortunate that the Hobart 201 running flux provided this optimum amount of oxygen in the weld to intragranularly nucleate acicular ferrite most efficiently. It is not likely that Mn, Ni, and Mo would promote acicular ferrite without the presence of oxygen, preferably the optimum 200 ppm.

The dilution of the weld metal by the base metal presented a practical problem for commercial utilization of the narrow gap ESW developed by OGC. Since the increased carbon content of the base metal could substantially reduce weld metal toughness, variations in dilution had to be considered. It is anticipated that, in commercial practice, care may not be taken to either properly adjust the (narrow) gap or adhere to the recommended welding parameters to ensure minimum acceptable toughness. Consequently, filler metal alloy development was essential to provide a tough weld metal microstructure regardless of the dilution variation in commercial welding practice.

Alloying with Mn, Ni and Mo provided an excellent means of achieving over 90 percent acicular ferrite in the weld metal. The alloying was

conveyed via a tubular filler metal instead of solid filler metal to take advantage of the low heat input characteristics of the tubular wire system. The combined presence of Ni and Mo, up to 1.5 percent Ni and 0.3 percent Mo, continuously decreased the volume fractions of both grain boundary ferrite and side plate ferrite while giving rise to a matrix which was predominantly fine acicular ferrite. By combining an alloy filler metal with optimized ESW procedures, a large margin of safety will exist to insure weld metal microstructures having substantial quantities of acicular ferrite despite an anticipated deviation from specified procedures in commercial practice.

The mechanism of the acicular ferrite transformation in as-deposited weld metal by ESW is poorly understood. Mn, Ni, Mo, and to some extent Cr were shown to promote the formation of acicular ferrite in weld metal; however, prior to this research, no quantitative correlation between alloy content, microstructure and toughness has been systematically studied. The transformation kinetics in weld metal are particularly difficult because both solidification effects on dendritic segregation and subsequent solid-state transformations must be accounted for.

The solidification mode of weld metal deposited on A36 and A588 steels using 25P, PS588 and WS filler metals was cellular dendritic near the weld edges and columnar dendritic near the weld center. A small amount of Cr, Ni and Mo added into the weld metal (which already contained over 1 percent Mn) produced a major change of solidification mode to equiaxed dendritic at the weld center. With a form factor value of about 1.2 to 1.4, a mild steel filler typically produced columnar dendrites at the weld center. But, a low Cr-Mo or Ni-Mo steel filler (AS521, AX90 or TW8544) brought about a substantial equiaxed dendritic region in the weld center. Some typical weld metal compositions are given in table 16. It is recognized [7] that the increase of solute content in the weld metal substantially influenced the transition of solidification mode from columnar dendritic to equiaxed dendritic growth. That was analogous to a decrease in the solidification parameter, G/R (where G is the local thermal gradient and R is the

growth rate). The central equiaxed dendrite zone induced by alloy additions showed superior resistance to hot cracking when the welding speed was increased. Simultaneously-nucleated equiaxed dendrites are believed to disperse remaining impurities to a comparatively large area other than a narrow centerline, thereby, reducing detrimental segregation.

In addition, due to the rightward displacement of maximum delta-ferrite composition in the Fe-Cr, Fe-Ni, and Fe-Mo phase diagrams compared with the Fe-C diagram, the primary dendrites in alloyed mild steel weld metal solidified as delta-ferrite, which had a higher impurity solubility and less interfacial segregation than austenite during primary solidification. Thus, Cr, Ni and Mo additions provided a relatively beneficial (crack resistant) solidification structure.

The role of alloying elements on the austenite transformation to acicular ferrite in the dendritically-segregated weld is complicated by the apparent need for non-metallic inclusions in the weld to nucleate acicular ferrite. Finely-dispersed inclusions inside austenite grains provide a large number of energetically-favorable sites for the nucleation of acicular ferrite, due to the strain energy caused by the difference in thermal contraction between inclusions and the austenite matrix.

Generally, in the absence of those additional alloying elements, grain boundaries are more favorable sites for ferrite nucleation than inclusions. In mild steel electroslog welds, the formation of grain-boundary ferrite raised the carbon content within the thin columnar austenite grains, thereby reducing the supersaturation and making intergranular nucleation even more difficult. As a result, less acicular ferrite formed in the thin columnar grain region. Only in the untransformed interior of coarse columnar austenite grains, where the enrichment of carbon played a less significant role, and with more undercooling, which made more inclusion sites become energetically favorable, could acicular ferrite form. Since Cr and Mo, both ferrite stabilizers, displaced the upper part of the austenite decomposition curve (C-curve) upward to the right and raised the ferritic

transformation temperature, the following process is proposed. Above a certain Cr-Mo content, the formation of acicular ferrite is less energetically favorable and there is a decreasing or even no chance for intersection between the cooling curve associated with ESW and the upper C-curve. Thus, the austenite matrix can bypass the upper C-curve and transform to a fully bainitic microstructure. On the contrary, the presence of Ni, an austenite stabilizer, shifts the whole C-curve downward to the right and causes the ferritic transformation temperature to decrease. Therefore, for relatively wide ranges of Ni content and transformation temperature, the cooling curve associated with ESW continuously intersects the ferritic transformation curve, resulting in a fine acicular ferrite-predominating microstructure throughout the weld metal. No doubt, excessive Ni will further delay the ferritic transformation and eventually produce bainite or even martensite. In this investigation, the beneficial role of Ni in promoting acicular ferrite has extended to at least 1.5 percent Ni (plus 0.3 percent Mo and 1.1 percent Mn). Of course, the comprehensive function of multi-alloy elements is often not a simple linear summation. In this investigation, the concurrent addition of Mo plus Cr exerted too much of a negative effect on ferritic transformation, but a small amount of Mo helped Ni to promote the formation of acicular ferrite.

2. Toughness Optimization through Microstructure Control

In all cases, there was a direct correlation between amount of acicular ferrite in the weld metal microstructure and the CVN impact toughness. In addition, the fineness of the acicular ferrite plates contributed to greater toughness and lower ductile-brittle transition because of the shorter cleavage crack paths. The development of the TW8544 tubular powder-filled wire containing 0.03 percent C, 1.20 percent Mn, 2.30 percent Ni and 0.45 percent Mo combined with the narrow gap process parameters to provide excellent weld metal toughness in both A36 and A588 steels in 50-mm and 76-mm thicknesses.

Excessively overmatched hardness in the weld metal due to alloying was not desired since maintaining high CVN toughness was the major concern. In comparison with the hardness of the base metals (figure 58), the Cr-Mo addition, due to its greater hardenability, raised the weld hardness far more than the Ni-Mo addition. Referring to a 20 Joule (15 ft-lb) minimum CVN impact energy at -18°C (0°F) and at the quarter-thickness/centerline location stipulated by AWS code D1.1, the experimental data very clearly demonstrated the main benefit to the impact toughness gained by Ni-Mo additions and the unsatisfactory behavior resulting from Cr-Mo additions (figure 58). On the basis of the foregoing, low toughness of the weld metal containing more than 1.1 percent Cr-0.4 percent Mo was attributed to the bainitic matrix which exhibited poor resistance to cleavage fracture, and that substantial improvement in the weld metal containing more than 0.9 percent Ni-0.2 percent Mo was brought about by the fine and interlaced acicular ferrite substructure which was advantageous in reducing the mean free path of cleavage fracture. For the mild steel electroslag weld metal, toughness at the half-thickness/centerline location was usually much worse than for the quarter-thickness/centerline. Ni-Mo additions significantly made both the hardness and toughness of the entire weld more uniform.

Obviously, keeping a certain Ni-Mo content was the key point to obtaining a satisfactory toughness level in the weld. A strictly maintained narrow joint gap became quite critical to obtain reduced base metal dilution and rapid welding speeds. Consequently, TW8544 tubular powder-filled wire (table 1) allowed higher welding speed, required less melting power and resulted in reduced penetration. Tubular filler metal effectively decreased the heat input (and base metal dilution) of welds and, thus, maintained higher percentages of alloying elements in the weld metal.

3. Toughness Assessment

It has been well established from the results of previous electroslag programs that the CVN properties found in conventionally-produced electroslag welds are widely variable and range from a low of only 3 to 4 joules

at -18°C in the weld center. HAZ values also vary widely. While previous programs developed a rationale for improving the processing parameters, such as guide tube design, voltage, and current conditions together with reduced gaps to improve the electroslag properties, they still failed to improve CVN values. This was identified as due to poor weld metal microstructure. Also, the optimized conditions were not fully identified. The initial optimization studies of this program were designed to minimize heat input and control both solidification and solid-state transformation macrostructures and microstructures. The resultant OGC optimized electroslag weld evaluations revealed improved CVN values.

a. Charpy V-Notch Impact Toughness

The results clearly show that dramatic improvements can be made in the weld metal impact toughness of electroslag welds by process control improvements combined with improved alloy content. In the 50-mm thick case, process improvements alone may be sufficient, but when used in conjunction with alloy additions, excellent weld metal properties can be expected. Proper alloy chemistry strongly depends on proper dilution and, hence, requires careful attention to weld setup practices and operating parameters. Lack of understanding the influences of each aspect can lead to poor properties. This may be minimized by increasing the alloy content above the minimum amount needed to insure proper microstructure formation. This, however, may result in excessive hardness levels. The purpose of the alloy study was to identify the minimum amount necessary to achieve adequate toughness with minimum increase in hardness.

The HAZ is large in electroslag welds, and there is no specification for the location for CVN tests. Since the microstructure varies radically in the HAZ, extreme variations in the reported toughness levels can be expected. Variations of nearly an order of magnitude were measured in this program just within the coarse HAZ. Analysis of one weld demonstrated that the CVN toughness decreased as the notch location approached the fusion line region, and that within about 1.5 mm of the apparent fusion line, the

toughness leveled off. Hence, for this program, the HAZ CVN data were taken from within 1.5 mm of the apparent weld metal fusion line. This was within three grains of the fusion line and should be representative of the lowest toughness region. Additional work is required to fully document the near fusion line region completely. For example, reduced heat input may raise the minimum toughness level or it may just compress the HAZ, or it may do both. Results of this program suggest that some improvement in the lowest levels can be expected. Due to the size of the full thickness K_{IC} specimens, additional material can be removed from the tested specimens to allow further analysis.

In general, the HAZ grain size itself does not provide a complete answer since very high levels of toughness are developed in the coarse-grained weld metal regions. Rather, the fundamental limitations and the methodology to control the toughness must lie in a more complex understanding of the grain substructure and, perhaps, grain boundary chemistry near the fusion line. Such a study would need to include the influence of base metal chemistry and initial processing conditions that might influence the subsequent electroslog-developed HAZ. While the microstructure/property relationships for the weld metal have been defined in this program, these relationships have not been defined for the HAZ and are apt to be more complex than the weld metal relationships.

b. K_{IC} Behavior

Analysis of the test data showed that only a few tests met all of the plane strain E399 test criteria. Specifically, the three-inch thickness was insufficient to meet the thickness criteria for all but a couple of tests. In some tests, the ratio of P_{max} to P_{min} was not met. Hence, the data is reported as K_C , the critical stress intensity. The full thickness fracture toughness tests did not show the sensitivity to microstructure and weld practice that the CVN tests did for these welds. This is not totally unexpected since it measured the toughness across all the microstructural zones at once and since only the weld center region exhibited

low CVN toughness. The data for alloy A36 showed no change in toughness for any of the weld changes, and was equivalent to the base alloy. For A588, the standard weld practice did not achieve a toughness equivalent to the base alloy, but by proper alloying and reduced heat input practice, the weld metal toughness was raised to that of the base metal. Also, the HAZ toughness was high for all cases, but again since the HAZ CVN data was very high in all of the coarse HAZ except for a thin region near the fusion line, it was not expected that the full thickness crack front would be confined to a microstructural zone just three grains wide. Hence, the full thickness toughness assessment demonstrated excellent toughness for these welds.

4. Fatigue Performance

One of the most surprising results of this program was the full-scale fatigue test data. Specifically, none of the electroslag welds developed a fatigue crack in any of the tests. For this program only, category B, i.e., weld reinforcement removed, welds were tested. Rather than conduct one or two tests for each condition as originally planned, additional tests were carried out on duplicate and triplicate beams so as to gain the most data for: 1) standard practice, and 2) reduced heat input. The results strongly suggest that without the presence of crack initiation sites, such as lack of fusion, the electroslag weld behavior is satisfactory. The results did reinforce that tack welds can result in fatigue cracks and that welded strongbacks should not be used. Hence, proper fixturing and careful attention to proper procedures is essential to insure sound welds. Also, these tests only evaluated sound electroslag welds. No repair procedures were evaluated in this program, and since fatigue cracks were not produced, no fatigue crack growth data is available.

In summary, the fatigue results demonstrated that sound category B electroslag welds have excellent fatigue behavior. Transition joints, other categories, and weld repairs were not evaluated and should be considered so as to broaden these conclusions.

5. Weld Metal Imperfection Formation/Detection

During the course of this investigation, specific practices that result in weld imperfections were defined, and sound electroslag weld practices should result in minimal weld metal imperfections formation. On the other hand, wire jams, improper flux addition practices and so on, will certainly result in imperfections formation. Probably, the most common imperfection is lack of fusion. This is almost always surface related and most easy to detect. Improper shoe design or alignment, flux additions or process control all result in lack of fusion. Other imperfections, such as ferrite vein cracking and hot cracking, should not be encountered with good welding practice.

Reliable inspection of electroslag welds as evidenced in this program are still questionable, since in some cases, for example, hot cracks were detected in parts of one weld and missed in another part of the same weld. Similarly, on some occasions, ultrasonic inspection (UT) detected a particular flaw type while radiographic testing (RT) inspection didn't, and on other occasions the reverse was true. The use of UT, RT and dye penetrant should result in minimum imperfections.

In no case was ferrite vein cracking detected. This is not surprising due to the extremely fine nature of these imperfections. Fortunately, this imperfection is readily controllable by good weld practices.

The inspection practices and analysis was done at a commercial laboratory site and no special directions were provided. The analysis was meant to represent an average NDE assessment.

VII. CONCLUSIONS

New methodologies have been developed to improve the microstructure, fracture toughness and fatigue characteristics of electrosag welds deposited on 50-mm and 76-mm thick A36 and A588 steel plate. This investigation led to the following primary conclusions:

- o The microstructures and CVN impact toughness values of electrosag welds are substantially improved by virtue of a narrow-gap, high welding speed and alloying introduced into the weld via a tubular powder-filled wire. Microstructures containing more than 90 percent acicular ferrite are achieved in the weld metal with corresponding toughness values substantially exceeding minimum required impact toughness levels.
- o OGC narrow-gap ESW procedure produces consistent and reliable welds with a minimum tendency for imperfections.
- o The HAZ CVN toughness of narrow gap welds decreases with decreasing distance from the fusion line. However, at a given distance from the fusion line, the HAZ toughness is substantially greater for low heat input narrow-gap welds using tubular filler metal than standard gap welds using solid fillers.
- o Specifically-designed testing requirements with respect to the HAZ notch location need to be defined before consistent data can be reported.
- o Full thickness plane strain fracture toughness testing, while generally not meeting the minimum thickness requirement for plane strain conditions, showed that both the weld metal and heat affected zone toughness, as measured by full thickness samples, showed excellent toughness.
- o Due to the non-uniform microstructures in the weld metal and heat affected zone of weldments, small size Charpy V-notch data vary with test location. On the other hand, full thickness fracture toughness type specimens measure the toughness throughout the weld or heat affected zone and also reflect greater levels of constraint due to the thickness. These fundamental differences preclude predicting the full thickness toughness behavior with small Charpy V-notch specimens, and suggest that CVN may not be the best method to evaluate electrosag toughness.
- o In fatigue testing of full-sized I-beams containing transverse-to-beam electrosag welds on the flange, both standard (normal gap) welds and

narrow-gap welds satisfy category B fatigue requirements within the stress range tested.

- o Standard nondestructive testing by either radiographic or ultrasonic methods is adequate to detect large slag inclusions in the weld metal. Long but "thin" imperfections, such as hot cracking, in electroslog welds were not detected reliably unless both radiographic and ultrasonic techniques were used for each weld under examination. Microscopic imperfections, such as ferrite vein cracks, are not reliably detected by any nondestructive method, but are easily controlled by sound practice.

VIII. RECOMMENDED PROCEDURE FOR ESW USING OPTIMIZED ALLOY FILLER METAL AND WELDING PARAMETERS

1. ESW Equipment

The equipment needed to perform narrow gap electroslag welding of 50-mm (2-in) and 76-mm (3-in) thick plates is commercially available except for the wing and the web guides, which must be constructed by the fabricator to the dimensions shown in figure 22. The consumable guide ESW equipment includes a power source, controls, wire feeder, wire straightener, flux feeder, guide assembly, welding cables, water-cooled retaining shoes, and strongbacks or clamps.

A DC-CV (direct current-constant voltage) power supply must be capable of delivering 1300 A at 100 percent duty cycle. Such power sources operate at 230 or 460 volts and 60 Hz input electric power. Continuous operation of the electroslag welding unit must be maintained until the entire joint is completed. Major defects will be produced if restarting is needed.

The controls may either be located on the front of the power supply or in a separate control box. There must be an ammeter and volt meter to measure, adjust and maintain the specified welding parameters. Typical controls should at least include: 1) an on-off switch, 2) a voltage control knob, 3) a wire feed speed knob, which also controls current, and 4) a button for advancing or reversing the wire feed.

The wire feeders used in ESW are similar to those utilized in submerged arc and gas metal arc welding. Because a constant-voltage power source is used for ESW, a constant-speed wire feeder is required. A single-wire feeding system is needed for wing guide, which requires a single filler wire drive. A dual-wire feeding system is required for the web guide, which uses two filler wire drives. If the dual wire feeders are no longer commercially available, each electrode wire can simply be driven by its own drive motor and feed rolls. Since tubular filler metal is

recommended, the drive rolls should have an oval configuration because they perform well with both solid and tubular filler wires.

A wire straightener is conventionally located above the welding head and is needed to remove the cast in the wire electrode. Removing this cast facilitates feeding the wire electrode through the guide and keeps it from curling toward the sides of the weld as it exits from the guide tube.

A continuous flux-feeding device is recommended to provide a constant slag depth between 1 and 1.5 in. These devices are commercially available.

The guide assembly used for this optimized ESW procedure is not standard equipment, but must be constructed by the fabricator. The dimensions for the 1/4 in thick wing and web guide assemblies are given in Figure 22. Because a narrow gap is used, the wing and web guides are mandatory to maintain adequate heat distribution in the weld pool.

Welding cables to maintain welding current levels up to 1300 amps at 100 percent duty cycle must be heavy duty. It is recommended that two parallel A.W.G. No. 4/0 cables be attached to the positive terminal of the power source and two parallel A.W.G. No. 4/0 cables be attached to the negative terminal of the power source for adequate current-carrying capacity.

Water-cooled retaining shoes in ESW are needed to not only keep the molten weld metal and slag pool in the joint cavity, but also to form the shape and size of the reinforcement. Each retaining shoe is made from copper and requires a water-circulating system which can consist of a connection to either a water tap or a water circulator capable of removing up to 30,000 BTU/hr (32 kJ/hr). A recirculator is preferred because it does not cause condensation on the shoes. When using tap water, the water should not be turned on until immediately before the welding starts because water may condense and run down to the bottom of the weld joint and cause welding imperfections.

A clamping system, or strongback, is used to hold the shoes in position and to maintain a 3/4 in (19 mm) gap during the ESW operation. Strongbacks are U-shaped bridges which are welded onto both sides of the joint for highest rigidity. Strongbacks are very convenient to use, but they are not recommended for welding critical applications where fatigue resistance and fracture toughness are required, as in fracture-critical members on bridges. If strongbacks are permitted, their location on the weld joint is important. The first strongback is placed at the top of the joint where it will clear the welding head. Twelve inch (300 mm) shoes require one strongback per shoe while the 18 in (450 mm) and 24 in (600 mm) shoes require two strongbacks per shoe.

2. Consumables

The consumables in the process include the filler metal, guide materials, and flux. The filler metal, Table 1, was developed at OGC to achieve high toughness weld metal, and is not commercially available at present. The AWS classification for this tubular filler wire would be EWTG. The wire has been fabricated in 3/32 in (2.4 mm) diameter by Stoodly Company upon request by OGC. Recommended steel to fabricate the wing or web guides in Figure 22 is AISI 1008 or 1010 steel. The flux must contain a neutral composition capable of producing weld metal having the desired Charpy impact toughness in the weld metal.

3. Operating Guidelines

The procedures for narrow-gap welding 2- and 3-in (50-mm and 76-mm) thick A36 and A588 plates are nearly similar to standard gap consumable guide ESW with some exceptions. Plates with square cut edges (plasma, oxyacetylene or saw cut) are fixtured in position with strongbacks or large clamps (if the structure is to be loaded in fatigue or is fracture critical) to permit a 3/4 inch (19 mm) gap between faying surfaces. Short run-off tabs are placed at the beginning and end of the plates to be joined because the first and last 2 in of electroslog weld metal may contain

defects. The appropriate guide design for either the 2 or 3 in thick plate selected from figure 22 is placed at the geometrical center of the gap between the two plates to be welded to assure uniform heat distribution in the slag pool. If the weld is longer than about 12 in, ceramic insulators should be used to brace the guide against the faying surfaces of the plates. The water-cooled shoes are placed around the joint to contain the molten slag and metal during subsequent ESW.

Welding parameters that are recommended to assure satisfactory weld metal toughness in A588 and A36 plate are given in table 17 specifically for 2- and 3-in thick square butt joints.

Welding parameters for 2- and 3-in thick welds were determined experimentally, but the current settings for thicknesses of 1.5, 2.5, and 3.5 in are only approximate, table 18.

During welding, the operator should watch the amp and volt meters to maintain the desired power settings. In addition, the operator must listen to the weld pool. Normal ESW is proceeding well when the weld is quiet (virtually inaudible). Loud, popping sounds with accompanying arcing flashes indicate an inadequately-low slag bath.

These recommendations point out the outstanding differences between conventional practice and the OGC-initiated changes. However, any additional information about ESW practice not specifically addressed above is provided by the Welding Handbook (Volume 2) and Hobart's Guide to ESW, No. EW-493.

Table 17. Welding parameters for 2- and 3-in square butt joints in A588 and A36 plates.

Parameter Type	Parameter Description
Filler Metal	AWS Classification EWTG 3/32 in diameter OGC alloy "TW8544" tubular wire
Initial Flux Addition	neutral composition 180 g for 2 in thick plate 270 g for 3 in thick plate during the first two minutes of operation
Current/Voltage	1100 A/35 V for 2 in thick plate 1300 A/35 V for 3 in thick plate
Guide Design	Wing (one filler wire) for 2 in thick plate Web (two filler wires) for 3 in thick plate
Automatic Flux Feeder	needed to automatically maintain a constant slag depth of 1 to 1.5 in (25 to 38 mm)
Grounding	each plate to be welded must be attached (grounded) to the negative terminal of the power source
Electrode/Guide Centering	precaution must be taken to assure that the web or wing guide is geometrically centered in the weld cavity
Initial Wire Stickout from Guidetube	the wire should extend 3/4 to 1 in beyond guidetube
Run-Off Tabs	at least 2" of run off (on to tabs)

Table 18. Welding parameters for 1.5- to 4-in square butt joints in A588 and A36 plates.

Parameter Type	Parameter Description
Filler Metal	AWS Classification EWTG 3/32 in diameter OGC alloy "TW8544" tubular wire
Initial Flux Addition	approximately 90 g per inch of thickness during the first two minutes of operation
Current/Voltage	1000 A/35 V for 1.5 in thick plate (wing guide) (not recommended for 1.5 in thick web guide) 1100 A/35 V for 2 in thick plate (wing and web) 1100 A/35 V for 2.5 in thick plate (wing guide) 1200 A/35 V for 2.5 in thick plate (web guide) (not recommended for 3 in thick wing guide) 1300 A/35 V for 3 in thick plate (web guide) (not recommended for 3.5 in thick wing guide) 1350 A/35 V for 3.5 in thick plate (web guide)
Guide Design	Wing (one filler wire) Web (two filler wires)
Initial Flux Addition	approximately 90 g per inch of thickness during the first two minutes of operation
Width of Guides	Designed for 2- and 3-in thick plates For both Wing and Web, the width should be adjusted to maintain a ratio of plate thickness/guide width of about 1.3 The distance between electrode wires should be maintained at the extremities of the guide

APPENDIX A: CVN IMPACT TEST DATA

Weld ID	Specimen ID	Current (A)	Voltage (V)	Zone	Temperature		CVN Toughness	
					°F	°C	ft-lb	Joules
50mm A36	7PR	--	--	BM	-100	-73	3	4
50mm A36	7PJ	--	--	BM	-100	-73	3	4
50mm A36	7PF	--	--	BM	- 60	-51	6	8
50mm A36	7PP	--	--	BM	- 60	-51	7	9
50mm A36	7PJ	--	--	BM	- 30	-34	21	28
50mm A36	7PE	--	--	BM	- 30	-34	23	31
50mm A36	7PS	--	--	BM	0	-18	32	43
50mm A36	7PO	--	--	BM	0	-18	31	42
50mm A36	7PG	--	--	BM	0	-18	30	41
50mm A36	7PN	--	--	BM	32	0	67	91
50mm A36	7PC	--	--	BM	32	0	48	65
50mm A36	7PQ	--	--	BM	50	10	60	81
50mm A36	7PH	--	--	BM	50	10	60	81
50mm A36	7PT	--	--	BM	68	20	86	117
50mm A36	7PL	--	--	BM	68	20	84	117
50mm A36	7PD	--	--	BM	104	40	90	122
50mm A36	7PB	--	--	BM	104	40	93	126
50mm A36	7PM	--	--	BM	104	40	81	110
50mm A36	7PK	--	--	BM	150	65	90	122
50mm A36	7PA	--	--	BM	150	65	85	115
76mm A36	36I	--	--	BM	- 80	-62	2.5	3
76mm A36	36F	--	--	BM	- 80	-62	3.5	5
76mm A36	36G	--	--	BM	- 20	-29	3.5	5
76mm A36	36D	--	--	BM	0	-18	4.5	6
76mm A36	36C	--	--	BM	0	-18	10	14
76mm A36	36N	--	--	BM	32	0	37	50
76mm A36	36P	--	--	BM	32	0	10	14
76mm A36	36N	--	--	BM	50	10	48	65
76mm A36	36K	--	--	BM	50	10	53	72
76mm A36	36E	--	--	BM	68	20	53	72
76mm A36	36J	--	--	BM	68	20	16	22
76mm A36	36L	--	--	BM	68	20	42	57
76mm A36	36H	--	--	BM	100	38	73	99
76mm A36	36O	--	--	BM	100	38	45	61
76mm A36	36A	--	--	BM	150	65	100	135
76mm A36	36B	--	--	BM	150	65	100	135

APPENDIX A: CVN IMPACT TEST DATA
(cont.)

Weld ID	Specimen ID	Current (A)	Voltage (V)	Zone	Temperature		CVN Toughness	
					°F	°C	ft-lb	Joules
76mm A588	88D	--	--	BM	- 80	-62	40	54
76mm A588	88C	--	--	BM	- 80	-62	2	3
76mm A588	88J	--	--	BM	- 80	-62	3.5	5
76mm A588	88I	--	--	BM	- 20	-29	1.5	2
76mm A588	88A	--	--	BM	0	-18	5	7
76mm A588	88L	--	--	BM	0	-18	9	12
76mm A588	88N	--	--	BM	32	0	59	80
76mm A588	88K	--	--	BM	32	0	37	50
76mm A588	88F	--	--	BM	50	10	70	95
76mm A588	88O	--	--	BM	50	10	80	108
76mm A588	88H	--	--	BM	68	20	68	92
76mm A588	88P	--	--	BM	68	20	56	76
76mm A588	88M	--	--	BM	100	38	89	120
76mm A588	88G	--	--	BM	100	38	92	125
76mm A588	88B	--	--	BM	150	65	120	163
76mm A588	88E	--	--	BM	150	65	114	154
50mm A588	7EH	--	--	BM	-100	-73	3	4
50mm A588	7EB	--	--	BM	-100	-73	4	5
50mm A588	7EE	--	--	BM	- 60	-51	8.5	12
50mm A588	7EN	--	--	BM	- 60	-51	6.5	9
50mm A588	7EL	--	--	BM	- 30	-34	5	7
50mm A588	7EI	--	--	BM	- 30	-34	10	14
50mm A588	7EP	--	--	BM	0	-18	8	11
50mm A588	7EG	--	--	BM	0	-18	15	20
50mm A588	7EK	--	--	BM	32	0	28	38
50mm A588	7EO	--	--	BM	32	0	31	42
50mm A588	7EJ	--	--	BM	50	10	47	64
50mm A588	7EF	--	--	BM	50	10	5	7
50mm A588	7EM	--	--	BM	68	20	35	47
50mm A588	7EC	--	--	BM	104	40	50	68
50mm A588	7EA	--	--	BM	150	65	56.5	77
50mm A588	7EQ	--	--	BM	150	65	48	65

APPENDIX A: CVN IMPACT TEST DATA
(cont.)

							Temperature		CVN Toughness	
							°F	°C	ft-lb	Joules
Weld ID	Specimen ID	Current (A)	Voltage (V)	Zone						
50mm A36 SG/25P	1DN	600	42	T/2	-100	-73	2.5	3		
50mm A36 SG/25P	1DA	600	42	T/2	-100	-73	3	4		
50mm A36 SG/25P	1DB	600	42	T/2	-60	-51	9	12		
50mm A36 SG/25P	1DS	600	42	T/2	-60	-51	5	7		
50mm A36 SG/25P	1DJ	600	42	T/2	-30	-34	20	27		
50mm A36 SG/25P	1DC	600	42	T/2	-30	-34	5	7		
50mm A36 SG/25P	1DT	600	42	T/2	0	-18	10	14		
50mm A36 SG/25P	1DL	600	42	T/2	0	-18	27	37		
50mm A36 SG/25P	1DP	600	42	T/2	0	-18	18	24		
50mm A36 SG/25P	1DB	600	42	T/2	0	-18	21	28		
50mm A36 SG/25P	1DQ	600	42	T/2	32	0	23	31		
50mm A36 SG/25P	1DG	600	42	T/2	32	0	24	33		
50mm A36 SG/25P	1DO	600	42	T/2	50	10	26	35		
50mm A36 SG/25P	1DH	600	42	T/2	50	10	25	34		
50mm A36 SG/25P	1DF	600	42	T/2	68	20	54	73		
50mm A36 SG/25P	1DK	600	42	T/2	68	20	30	41		
50mm A36 SG/25P	1DI	600	42	T/2	104	40	52	70		
50mm A36 SG/25P	1DR	600	42	T/2	104	40	28	38		
50mm A36 SG/25P	1DM	600	42	T/2	150	65	67	91		
50mm A36 SG/25P	1DE	600	42	T/2	150	65	65	88		
50mm A36 SG/25P	5DH	600	42	T/4	-60	-51	8	11		
50mm A36 SG/25P	5DN	600	42	T/4	-60	-51	5	7		
50mm A36 SG/25P	5DP	600	42	T/4	-30	-34	5	7		
50mm A36 SG/25P	5DF	600	42	T/4	-30	-34	4	5		
50mm A36 SG/25P	5DE	600	42	T/4	0	-18	19	26		
50mm A36 SG/25P	5DC	600	42	T/4	0	-18	8	11		
50mm A36 SG/25P	5DB	600	42	T/4	0	-18	14	19		
50mm A36 SG/25P	5DO	600	42	T/4	0	-18	16.5	22		
50mm A36 SG/25P	5DG	600	42	T/4	32	0	25	34		
50mm A36 SG/25P	5DM	600	42	T/4	32	0	22	30		
50mm A36 SG/25P	5DQ	600	42	T/4	50	10	26	35		
50mm A36 SG/25P	5DK	600	42	T/4	50	10	30	41		
50mm A36 SG/25P	5DR	600	42	T/4	68	20	33	45		
50mm A36 SG/25P	5DL	600	42	T/4	68	20	34	46		
50mm A36 SG/25P	5DJ	600	42	T/4	104	40	47	64		
50mm A36 SG/25P	5DI	600	42	T/4	104	40	28	40		
50mm A36 SG/25P	5DS	600	42	T/4	150	65	52	70		
50mm A36 SG/25P	5DT	600	42	T/4	150	65	55	75		

APPENDIX A: CVN IMPACT TEST DATA
(cont.)

Weld ID	Specimen ID	Current (A)	Voltage (V)	Zone	Temperature		CVN Toughness	
					°F	°C	ft-lb	Joules
50mm A36 SG/25P	2DQ	600	42	HAZ	-100	-73	3.5	5
50mm A36 SG/25P	2DD	600	42	HAZ	-100	-73	1.5	2
50mm A36 SG/25P	2DL	600	42	HAZ	-100	-73	3	4
50mm A36 SG/25P	2DJ	600	42	HAZ	-100	-73	4	5
50mm A36 SG/25P	2DG	600	42	HAZ	- 60	-51	8	11
50mm A36 SG/25P	2DB	600	42	HAZ	- 60	-51	5	7
50mm A36 SG/25P	2DO	600	42	HAZ	- 30	-34	9	12
50mm A36 SG/25P	2DF	600	42	HAZ	- 30	-34	5	7
50mm A36 SG/25P	2DP	600	42	HAZ	0	-18	23	31
50mm A36 SG/25P	2DK	600	42	HAZ	0	-18	9	12
50mm A36 SG/25P	2DU	600	42	HAZ	0	-18	26	35
50mm A36 SG/25P	2DN	600	42	HAZ	32	0	29	39
50mm A36 SG/25P	2DE	600	42	HAZ	32	0	45	61
50mm A36 SG/25P	2DA	600	42	HAZ	50	10	64	87
50mm A36 SG/25P	2DH	600	42	HAZ	50	10	35	48
50mm A36 SG/25P	2DS	600	42	HAZ	68	20	42	57
50mm A36 SG/25P	2DI	600	42	HAZ	68	20	60	81
50mm A36 SG/25P	2DJ	600	42	HAZ	104	40	52	70
50mm A36 SG/25P	2DR	600	42	HAZ	104	40	62	84
50mm A36 SG/25P	2DM	600	42	HAZ	180	82	61.5	83
50mm A36 NG/25P	3PC	1000	38	T/2	-100	-73	4	5
50mm A36 NG/25P	3PG	1000	38	T/2	-100	-73	5.5	7
50mm A36 NG/25P	3PD	1000	38	T/2	- 80	-62	11	15
50mm A36 NG/25P	3PF	1000	38	T/2	- 80	-62	6.5	9
50mm A36 NG/25P	3PB	1000	38	T/2	- 60	-51	7	19
50mm A36 NG/25P	3PJ	1000	38	T/2	- 60	-51	16	22
50mm A36 NG/25P	3PL	1000	38	T/2	- 20	-29	19	26
50mm A36 NG/25P	3PA	1000	38	T/2	- 20	-29	17	23
50mm A36 NG/25P	3PN	1000	38	T/2	- 20	-29	23	31
50mm A36 NG/25P	3PM	1000	38	T/2	0	-18	19	26
50mm A36 NG/25P	3PR	1000	38	T/2	0	-18	20	27
50mm A36 NG/25P	3PH	1000	38	T/2	0	-18	20	27
50mm A36 NG/25P	3PP	1000	38	T/2	32	0	29	39
50mm A36 NG/25P	3PA	1000	38	T/2	32	0	28	37
50mm A36 NG/25P	3PE	1000	38	T/2	100	38	50	68
50mm A36 NG/25P	3PH	1000	38	T/2	100	38	66	89
50mm A36 NG/25P	3PI	1000	38	T/2	100	38	48	65
50mm A36 NG/25P	3PK	1000	38	T/2	150	65	58	79
50mm A36 NG/25P	3PQ	1000	38	T/2	150	65	66	89

APPENDIX A: CVN IMPACT TEST DATA
(cont.)

Weld ID	Specimen ID	Current (A)	Voltage (V)	Zone	Temperature		CVN Toughness	
					°F	°C	ft-lb	Joules
50mm A36 NG/25P	6PH	1000	38	T/4	-100	-73	7	9
50mm A36 NG/25P	6PG	1000	38	T/4	- 80	-62	15	20
50mm A36 NG/25P	6PI	1000	38	T/4	- 60	-51	18	24
50mm A36 NG/25P	6PF	1000	38	T/4	- 60	-51	12	16
50mm A36 NG/25P	6PB	1000	38	T/4	- 20	-29	22	30
50mm A36 NG/25P	6PJ	1000	38	T/4	- 20	-29	14.5	20
50mm A36 NG/25P	6PC	1000	38	T/4	0	-18	29	39
50mm A36 NG/25P	6PD	1000	38	T/4	0	-18	21	28
50mm A36 NG/25P	6PK	1000	38	T/4	68	20	41	56
50mm A36 NG/25P	6PA	1000	38	T/4	100	38	42	60
50mm A36 NG/25P	6PE	1000	38	T/4	100	38	67	91
50mm A36 NG/25P	4PU	1000	38	HAZ	-100	-73	7	9
50mm A36 NG/25P	4PJ	1000	38	HAZ	-100	-73	3	4
50mm A36 NG/25P	4PQ	1000	38	HAZ	- 60	-51	12.5	17
50mm A36 NG/25P	4PK	1000	38	HAZ	- 60	-51	21	28
50mm A36 NG/25P	4PD	1000	38	HAZ	- 30	-34	8	11
50mm A36 NG/25P	4PG	1000	38	HAZ	- 30	-34	9	12
50mm A36 NG/25P	4PH	1000	38	HAZ	0	-18	35	47
50mm A36 NG/25P	4PB	1000	38	HAZ	0	-18	13	18
50mm A36 NG/25P	4PP	1000	38	HAZ	0	-18	46	62
50mm A36 NG/25P	4PB	1000	38	HAZ	0	-18	32	43
50mm A36 NG/25P	4PC	1000	38	HAZ	0	-18	14	19
50mm A36 NG/25P	4PS	1000	38	HAZ	0	-18	39	53
50mm A36 NG/25P	4PA	1000	38	HAZ	32	0	28	38
50mm A36 NG/25P	4PE	1000	38	HAZ	32	0	37	50
50mm A36 NG/25P	4PL	1000	38	HAZ	50	10	55	75
50mm A36 NG/25P	4PC	1000	38	HAZ	50	10	60	81
50mm A36 NG/25P	4PF	1000	38	HAZ	68	20	75	101
50mm A36 NG/25P	4PR	1000	38	HAZ	68	20	82	111
50mm A36 NG/25P	4PJ	1000	38	HAZ	104	40	61	83
50mm A36 NG/25P	4PO	1000	38	HAZ	104	40	90	122
50mm A36 NG/25P	4PI	1000	38	HAZ	104	40	75	102
50mm A36 NG/25P	4PN	1000	38	HAZ	150	65	97	131
50mm A36 NG/25P	4PN	1000	38	HAZ	150	65	91	123

APPENDIX A: CVN IMPACT TEST DATA
(cont.)

							Temperature		CVN Toughness	
							°F	°C	ft-lb	Joules
Weld ID	Specimen ID	Current (A)	Voltage (V)	Zone						
50mm A36 NG/ST	3RT	800	38	T/2	- 80	-62	4	5		
50mm A36 NG/ST	3RJ	800	38	T/2	- 80	-62	3	4		
50mm A36 NG/ST	3RG	800	38	T/2	- 60	-51	9	12		
50mm A36 NG/ST	3RC	800	38	T/2	- 60	-51	8.5	12		
50mm A36 NG/ST	3RE	800	38	T/2	- 20	-29	14.5	20		
50mm A36 NG/ST	3RF	800	38	T/2	0	-18	49	67		
50mm A36 NG/ST	3RD	800	38	T/2	32	0	65	88		
50mm A36 NG/ST	3RF	800	38	T/2	32	0	59	80		
50mm A36 NG/ST	3RE	800	38	T/2	68	20	59	80		
50mm A36 NG/ST	3RG	800	38	T/2	100	38	75	102		
50mm A36 NG/ST	3RC	800	38	T/2	150	65	79	107		
50mm A36 NG/ST	3RZ	800	38	T/2	150	65	85	115		
50mm A36 NG/ST	6RM	800	38	T/4	-100	-73	5.5	7		
50mm A36 NG/ST	6RN	800	38	T/4	-100	-73	5	7		
50mm A36 NG/ST	6RC	800	38	T/4	- 80	-62	8	11		
50mm A36 NG/ST	6RH	800	38	T/4	- 80	-62	11.5	16		
50mm A36 NG/ST	6RA	800	38	T/4	- 60	-51	18.5	25		
50mm A36 NG/ST	6RB	800	38	T/4	- 60	-51	22	30		
50mm A36 NG/ST	6RO	800	38	T/4	- 40	-40	27	37		
50mm A36 NG/ST	6RZ	800	38	T/4	- 40	-40	26	35		
50mm A36 NG/ST	6RD	800	38	T/4	- 20	-29	34	46		
50mm A36 NG/ST	6RE	800	38	T/4	- 20	-29	27	37		
50mm A36 NG/ST	6RF	800	38	T/4	0	-18	44	60		
50mm A36 NG/ST	6RG	800	38	T/4	0	-18	53	72		
50mm A36 NG/ST	6RQ	800	38	T/4	32	0	64	87		
50mm A36 NG/ST	6RP	800	38	T/4	32	0	69	93		
50mm A36 NG/ST	6RI	800	38	T/4	50	10	70	95		
50mm A36 NG/ST	6RJ	800	38	T/4	50	10	75	102		
50mm A36 NG/ST	6RH	800	38	T/4	68	20	74	100		
50mm A36 NG/ST	6RC	800	38	T/4	68	20	75	102		
50mm A36 NG/ST	6RK	800	38	T/4	104	40	80	108		
50mm A36 NG/ST	6RL	800	38	T/4	104	40	76	103		

APPENDIX A: CVN IMPACT TEST DATA
(cont.)

							Temperature		CVN Toughness	
							°F	°C	ft-lb	Joules
Weld ID	Specimen ID	Current (A)	Voltage (V)	Zone						
50mm A36 NG/ST	4RR	800	38	HAZ	-100	-73	3	4		
50mm A36 NG/ST	4RO	800	38	HAZ	-100	-73	4.5	6		
50mm A36 NG/ST	4RL	800	38	HAZ	-60	-51	7	9		
50mm A36 NG/ST	4RF	800	38	HAZ	-60	-51	5	7		
50mm A36 NG/ST	4RE	800	38	HAZ	-30	-34	22	30		
50mm A36 NG/ST	4RK	800	38	HAZ	-30	-34	9	12		
50mm A36 NG/ST	4RB	800	38	HAZ	0	-18	20	27		
50mm A36 NG/ST	4RT	800	38	HAZ	0	-18	13	18		
50mm A36 NG/ST	4RA	800	38	HAZ	0	-18	5	7		
50mm A36 NG/ST	4RC	800	38	HAZ	32	0	32	44		
50mm A36 NG/ST	4RQ	800	38	HAZ	32	0	23	31		
50mm A36 NG/ST	4RH	800	38	HAZ	50	10	49	66		
50mm A36 NG/ST	4RM	800	38	HAZ	50	10	56	76		
50mm A36 NG/ST	4RS	800	38	HAZ	68	20	58	79		
50mm A36 NG/ST	4RN	800	38	HAZ	68	20	73	99		
50mm A36 NG/ST	4RI	800	38	HAZ	104	40	84	114		
50mm A36 NG/ST	4RD	800	38	HAZ	150	65	81.3	110		
50mm A36 NG/ST	4RP	800	38	HAZ	150	65	91	123		
50mm A36 NG/ST	4YG	1000	35	HAZ	-100	-73	3.5	5		
50mm A36 NG/ST	4YG	1000	35	HAZ	-100	-73	3	5		
50mm A36 NG/ST	4YJ	1000	35	HAZ	-60	-51	4	5.4		
50mm A36 NG/ST	4YE	1000	35	HAZ	-60	-51	6.5	9		
50mm A36 NG/ST	4YO	1000	35	HAZ	-30	-34	9	12		
50mm A36 NG/ST	4YH	1000	35	HAZ	-30	-34	8	11		
50mm A36 NG/ST	4YB	1000	35	HAZ	0	-18	10	14		
50mm A36 NG/ST	4YK	1000	35	HAZ	0	-18	8	11		
50mm A36 NG/ST	4YC	1000	35	HAZ	0	-18	11	15		
50mm A36 NG/ST	4YR	1000	35	HAZ	0	-18	54	73		
50mm A36 NG/ST	4YM	1000	35	HAZ	32	0	49	66		
50mm A36 NG/ST	4YD	1000	35	HAZ	32	0	40	54		
50mm A36 NG/ST	4YC	1000	35	HAZ	50	10	45	61		
50mm A36 NG/ST	4YS	1000	35	HAZ	50	10	73	99		
50mm A36 NG/ST	4YF	1000	35	HAZ	68	20	67	91		
50mm A36 NG/ST	4YA	1000	35	HAZ	68	20	55	75		
50mm A36 NG/ST	4YN	1000	35	HAZ	104	40	85	115		
50mm A36 NG/ST	4YI	1000	35	HAZ	104	40	78	106		
50mm A36 NG/ST	4YL	1000	35	HAZ	150	65	104	141		
50mm A36 NG/ST	4YQ	1000	35	HAZ	150	65	93	126		

APPENDIX A: CVN IMPACT TEST DATA
(cont.)

Weld ID	Specimen ID	Current (A)	Voltage (V)	Zone	Temperature		CVN Toughness	
					°F	°C	ft-lb	Joules
76mm A36 SG/25P	1BE	850	38	T/2	-40	-40	2.3	3
76mm A36 SG/25P	1BD	850	38	T/2	-40	-40	19.2	26
76mm A36 SG/25P	1BG	850	38	T/2	-20	-29	6	8
76mm A36 SG/25P	1BF	850	38	T/2	-20	-29	4.6	6
76mm A36 SG/25P	1BA	850	38	T/2	0	-18	13	18
76mm A36 SG/25P	1BB	850	38	T/2	0	-18	13.1	18
76mm A36 SG/25P	1BC	850	38	T/2	0	-18	13.8	19
76mm A36 SG/25P	1BQ	850	38	T/2	32	0	28	38
76mm A36 SG/25P	1BP	850	38	T/2	32	0	20	27
76mm A36 SG/25P	1BR	850	38	T/2	50	10	37.5	51
76mm A36 SG/25P	1BS	850	38	T/2	50	10	42	57
76mm A36 SG/25P	1BH	850	38	T/2	68	20	47	64
76mm A36 SG/25P	1BI	850	38	T/2	68	20	44	60
76mm A36 SG/25P	1BN	850	38	T/2	100	38	42	60
76mm A36 SG/25P	1BO	850	38	T/2	100	38	60	81
76mm A36 SG/25P	1BM	850	38	T/2	150	65	75	102
76mm A36 SG/25P	1BC	850	38	T/2	150	65	79	107
76mm A36 SG/25P	1BJ	850	38	T/2	200	93	75	102
76mm A36 SG/25P	1BK	850	38	T/2	200	93	74	100
76mm A36 SG/25P	5NN	850	38	T/4	-100	-73	3.5	5
76mm A36 SG/25P	5NK	850	38	T/4	-100	-73	2	3
76mm A36 SG/25P	5NZ	850	38	T/4	-60	-51	6.5	9
76mm A36 SG/25P	5NS	850	38	T/4	-60	-51	2	3
76mm A36 SG/25P	5NB	850	38	T/4	-30	-34	3.5	5
76mm A36 SG/25P	5NQ	850	38	T/4	-30	-34	6	8
76mm A36 SG/25P	5NG	850	38	T/4	0	-18	5	7
76mm A36 SG/25P	5NJ	850	38	T/4	0	-18	5	7
76mm A36 SG/25P	5NE	850	38	T/4	0	-18	13	18
76mm A36 SG/25P	5NL	850	38	T/4	0	-18	20	27
76mm A36 SG/25P	5ND	850	38	T/4	32	0	18	24
76mm A36 SG/25P	5NR	850	38	T/4	32	0	20	27
76mm A36 SG/25P	5NT	850	38	T/4	50	10	20	27
76mm A36 SG/25P	5NP	850	38	T/4	50	10	22	30
76mm A36 SG/25P	5NF	850	38	T/4	68	20	36	49
76mm A36 SG/25P	5NL	850	38	T/4	104	40	29	39
76mm A36 SG/25P	5NO	850	38	T/4	104	40	39	53
76mm A36 SG/25P	5NN	850	38	T/4	150	65	49	66
76mm A36 SG/25P	5NA	850	38	T/4	150	65	55	75

APPENDIX A: CVN IMPACT TEST DATA
(cont.)

Weld ID	Specimen ID	Current (A)	Voltage (V)	Zone	Temperature		CVN Toughness	
					°F	°C	ft-lb	Joules
76mm A36 SG/25P	2BM	850	38	HAZ	-60	-51	4	5.4
76mm A36 SG/25P	2BL	850	38	HAZ	-60	-51	13.5	5
76mm A36 SG/25P	2BE	850	38	HAZ	-40	-40	4.8	7
76mm A36 SG/25P	2BD	850	38	HAZ	-40	-40	5.2	7
76mm A36 SG/25P	2BG	850	38	HAZ	-20	-29	6.3	9
76mm A36 SG/25P	2BF	850	38	HAZ	-20	-29	3.6	5
76mm A36 SG/25P	2BA	850	38	HAZ	0	-18	20.3	28
76mm A36 SG/25P	2BC	850	38	HAZ	0	-18	15.5	21
76mm A36 SG/25P	2BB	850	38	HAZ	0	-18	5	7
76mm A36 SG/25P	2BR	850	38	HAZ	32	0	12	16
76mm A36 SG/25P	2BS	850	38	HAZ	32	0	18	25
76mm A36 SG/25P	2BQ	850	38	HAZ	100	38	43	58
76mm A36 SG/25P	2BP	850	38	HAZ	100	38	48	65
76mm A36 SG/25P	2BN	850	38	HAZ	150	65	75	102
76mm A36 SG/25P	2BO	850	38	HAZ	150	65	78	106
76mm A36 NG/25P	3FT	1000	40	T/2	-100	-73	1.5	2
76mm A36 NG/25P	3FP	1000	40	T/2	-100	-73	1	1
76mm A36 NG/25P	3FN	1000	40	T/2	-70	-57	4.5	6
76mm A36 NG/25P	3FR	1000	40	T/2	-60	-51	2	3
76mm A36 NG/25P	3FO	1000	40	T/2	-60	-51	12	16
76mm A36 NG/25P	3FB	1000	40	T/2	-40	-40	6.5	9
76mm A36 NG/25P	3FE	1000	40	T/2	-30	-34	21	28
76mm A36 NG/25P	3FG	1000	40	T/2	-30	-34	16.5	22
76mm A36 NG/25P	3FF	1000	40	T/2	0	-18	23.5	32
76mm A36 NG/25P	3FJ	1000	40	T/2	0	-18	10	14
76mm A36 NG/25P	3FI	1000	40	T/2	0	-18	20	27
76mm A36 NG/25P	3FC	1000	40	T/2	40	4	37	50
76mm A36 NG/25P	3FK	1000	40	T/2	40	4	36	49
76mm A36 NG/25P	3FO	1000	40	T/2	68	20	30	41
76mm A36 NG/25P	3FM	1000	40	T/2	68	20	45	61
76mm A36 NG/25P	3FH	1000	40	T/2	100	38	45	61
76mm A36 NG/25P	3FA	1000	40	T/2	100	38	41	56
76mm A36 NG/25P	3FL	1000	40	T/2	125	51	48	65
76mm A36 NG/25P	3FS	1000	40	T/2	125	51	50	68
76mm A36 NG/25P	3FB	1000	40	T/2	150	65	55	75
76mm A36 NG/25P	3FU	1000	40	T/2	150	65	55	75

APPENDIX A: CVN IMPACT TEST DATA
(cont.)

Weld ID	Specimen ID	Current (A)	Voltage (V)	Zone	Temperature		CVN Toughness	
					°F	°C	ft-lb	Joules
76mm A36 NG/25P	6FA	1000	40	T/4	-100	-73	5	7
76mm A36 NG/25P	6FF	1000	40	T/4	-100	-73	1.5	2
76mm A36 NG/25P	6FT	1000	40	T/4	-70	-57	1.5	2
76mm A36 NG/25P	6FP	1000	40	T/4	-60	-51	5	7
76mm A36 NG/25P	6FK	1000	40	T/4	-60	-51	13.5	18
76mm A36 NG/25P	6FQ	1000	40	T/4	-40	-40	7	9
76mm A36 NG/25P	6FM	1000	40	T/4	-30	-34	15.1	20
76mm A36 NG/25P	6FI	1000	40	T/4	-30	-34	7	9
76mm A36 NG/25P	6FN	1000	40	T/4	0	-18	25	34
76mm A36 NG/25P	6FS	1000	40	T/4	0	-18	16	22
76mm A36 NG/25P	6FD	1000	40	T/4	40	4	32	44
76mm A36 NG/25P	6FE	1000	40	T/4	68	20	40	54
76mm A36 NG/25P	6FC	1000	40	T/4	68	20	49	66
76mm A36 NG/25P	6FL	1000	40	T/4	100	38	41	56
76mm A36 NG/25P	6FG	1000	40	T/4	100	38	42	57
76mm A36 NG/25P	6FO	1000	40	T/4	100	38	46	62
76mm A36 NG/25P	6FB	1000	40	T/4	125	51	51	69
76mm A36 NG/25P	6FR	1000	40	T/4	125	51	44	60
76mm A36 NG/25P	6FP	1000	40	T/4	150	65	77	104
76mm A36 NG/25P	6FH	1000	40	T/4	150	65	54	73
76mm A36 NG/25P	4FI	1000	40	HAZ	-100	-73	2	3
76mm A36 NG/25P	4FF	1000	40	HAZ	-80	-62	8	11
76mm A36 NG/25P	4FP	1000	40	HAZ	-80	-62	3	4
76mm A36 NG/25P	4FI	1000	40	HAZ	-60	-51	6	8
76mm A36 NG/25P	4FE	1000	40	HAZ	-60	-51	6	8
76mm A36 NG/25P	4FD	1000	40	HAZ	-60	-51	3.5	5
76mm A36 NG/25P	4FR	1000	40	HAZ	-60	-51	4.5	6
76mm A36 NG/25P	4FS	1000	40	HAZ	-20	-29	4	5
76mm A36 NG/25P	4FE	1000	40	HAZ	-20	-29	10	14
76mm A36 NG/25P	4FG	1000	40	HAZ	0	-18	20	27
76mm A36 NG/25P	4FN	1000	40	HAZ	0	-18	9	12
76mm A36 NG/25P	4FO	1000	40	HAZ	32	10	35.5	48
76mm A36 NG/25P	4FM	1000	40	HAZ	32	10	30.5	41
76mm A36 NG/25P	4FA	1000	40	HAZ	68	20	45	61
76mm A36 NG/25P	4FL	1000	40	HAZ	100	38	60	81
76mm A36 NG/25P	4FC	1000	40	HAZ	100	38	84	114
76mm A36 NG/25P	4FH	1000	40	HAZ	150	65	73	99
76mm A36 NG/25P	4FQ	1000	40	HAZ	150	65	91	123

APPENDIX A: CVN IMPACT TEST DATA
(cont.)

Weld ID	Specimen ID	Current (A)	Voltage (V)	Zone	Temperature		CVN Toughness	
					°F	°C	ft-lb	Joules
76mm A36 NG/ST	3JJ	1000	38	T/2	-100	-73	1.5	2
76mm A36 NG/ST	3JP	1000	38	T/2	-100	-73	1	1.3
76mm A36 NG/ST	3JC	1000	38	T/2	-60	-51	3	4
76mm A36 NG/ST	3JI	1000	38	T/2	-60	-51	3	4
76mm A36 NG/ST	3JA	1000	38	T/2	-40	-40	9.5	13
76mm A36 NG/ST	3JR	1000	38	T/2	-40	-40	4.5	6
76mm A36 NG/ST	3JM	1000	38	T/2	-40	-40	4.5	6
76mm A36 NG/ST	3JJ	1000	38	T/2	-30	-34	18	24
76mm A36 NG/ST	3JG	1000	38	T/2	-30	-34	2	3
76mm A36 NG/ST	3JT	1000	38	T/2	-30	-34	3.5	5
76mm A36 NG/ST	3JF	1000	38	T/2	0	-18	24	33
76mm A36 NG/ST	3JL	1000	38	T/2	0	-18	18	24
76mm A36 NG/ST	3JS	1000	38	T/2	34	1	7	9
76mm A36 NG/ST	3JH	1000	38	T/2	34	1	19	26
76mm A36 NG/ST	3JQ	1000	38	T/2	34	1	13.5	18
76mm A36 NG/ST	3JD	1000	38	T/2	68	20	23	31
76mm A36 NG/ST	3JM	1000	38	T/2	68	20	23	31
76mm A36 NG/ST	3JE	1000	38	T/2	100	38	41	36
76mm A36 NG/ST	3JN	1000	38	T/2	100	38	39	53
76mm A36 NG/ST	3JB	1000	38	T/2	125	51	49	66
76mm A36 NG/ST	3JK	1000	38	T/2	125	51	48	65
76mm A36 NG/ST	6JB	1000	38	T/4	-100	-73	3	4
76mm A36 NG/ST	6JC	1000	38	T/4	-100	-73	1.0	1.3
76mm A36 NG/ST	6JJ	1000	38	T/4	-60	-51	2	3
76mm A36 NG/ST	6JH	1000	38	T/4	-60	-51	2	3
76mm A36 NG/ST	6JP	1000	38	T/4	-30	-34	3	5
76mm A36 NG/ST	6JQ	1000	38	T/4	-30	-34	3.5	5
76mm A36 NG/ST	6JR	1000	38	T/4	0	-18	7.5	10
76mm A36 NG/ST	6JN	1000	38	T/4	0	-18	13	18
76mm A36 NG/ST	6JK	1000	38	T/4	34	1	24	33
76mm A36 NG/ST	6JL	1000	38	T/4	34	1	30	41
76mm A36 NG/ST	6JD	1000	38	T/4	68	20	30	41
76mm A36 NG/ST	6JA	1000	38	T/4	68	20	29	39
76mm A36 NG/ST	6JF	1000	38	T/4	68	20	39	53
76mm A36 NG/ST	6JE	1000	38	T/4	100	38	35	47
76mm A36 NG/ST	6JS	1000	38	T/4	100	38	43	58
76mm A36 NG/ST	6JM	1000	38	T/4	125	51	56	76
76mm A36 NG/ST	6JO	1000	38	T/4	125	51	54	73

APPENDIX A: CVN IMPACT TEST DATA
(cont.)

Weld ID	Specimen ID	Current (A)	Voltage (V)	Zone	Temperature		CVN Toughness	
					°F	°C	ft-lb	Joules
76mm A36 NG/ST	4JE	1000	38	HAZ	-60	-51	4	5
76mm A36 NG/ST	4JL	1000	38	HAZ	-60	-51	4.5	6
76mm A36 NG/ST	4JN	1000	38	HAZ	-20	-29	6.5	9
76mm A36 NG/ST	4JP	1000	38	HAZ	-20	-29	10	13
76mm A36 NG/ST	4JF	1000	38	HAZ	0	-18	14	19
76mm A36 NG/ST	4JS	1000	38	HAZ	0	-18	10	13
76mm A36 NG/ST	4JK	1000	38	HAZ	0	-18	32	43
76mm A36 NG/ST	4JA	1000	38	HAZ	32	0	18	24
76mm A36 NG/ST	4JT	1000	38	HAZ	32	0	12.5	17
76mm A36 NG/ST	4JH	1000	38	HAZ	68	20	30	41
76mm A36 NG/ST	4JC	1000	38	HAZ	68	20	22	30
76mm A36 NG/ST	4JV	1000	38	HAZ	100	38	85	115
76mm A36 NG/ST	4JI	1000	38	HAZ	100	38	38	51
76mm A36 NG/ST	4JJ	1000	38	HAZ	150	65	86	117
76mm A36 NG/ST	4JG	1000	38	HAZ	150	65	98	133
76mm A36 NG/ST2	3ZE	1300	35	T/2	-100	-73	3.5	5
76mm A36 NG/ST2	3ZQ	1300	35	T/2	-100	-73	4	5
76mm A36 NG/ST2	3ZN	1300	35	T/2	-60	-51	4	5
76mm A36 NG/ST2	3ZR	1300	35	T/2	-60	-51	5.5	7
76mm A36 NG/ST2	3ZL	1300	35	T/2	-30	-34	11	15
76mm A36 NG/ST2	3ZS	1300	35	T/2	-30	-34	4	5
76mm A36 NG/ST2	3ZJ	1300	35	T/2	0	-18	7	9
76mm A36 NG/ST2	3ZO	1300	35	T/2	0	-18	33	44
76mm A36 NG/ST2	3ZT	1300	35	T/2	0	-18	43	58
76mm A36 NG/ST2	3ZB	1300	35	T/2	0	-18	22	30
76mm A36 NG/ST2	3ZH	1300	35	T/2	32	0	32	43
76mm A36 NG/ST2	3ZI	1300	35	T/2	32	0	57	79
76mm A36 NG/ST2	3ZD	1300	35	T/2	50	10	29	39
76mm A36 NG/ST2	3ZF	1300	35	T/2	50	10	29	39
76mm A36 NG/ST2	3ZA	1300	35	T/2	68	20	55	75
76mm A36 NG/ST2	3ZM	1300	35	T/2	68	20	53	71
76mm A36 NG/ST2	3ZC	1300	35	T/2	104	40	53	71
76mm A36 NG/ST2	3ZP	1300	35	T/2	104	40	68	92
76mm A36 NG/ST2	3ZG	1300	35	T/2	150	65	81	110
76mm A36 NG/ST2	3ZK	1300	35	T/2	150	65	69	94

APPENDIX A: CVN IMPACT TEST DATA
(cont.)

Weld ID	Specimen ID	Current (A)	Voltage (V)	Zone	Temperature		CVN Toughness	
					°F	°C	ft-lb	Joules
76mm A36 NG/ST2	6ZT	1300	35	T/4	-100	-73	3	4
76mm A36 NG/ST2	6ZP	1300	35	T/4	-100	-73	2	3
76mm A36 NG/ST2	6ZO	1300	35	T/4	- 60	-51	3	4
76mm A36 NG/ST2	6ZA	1300	35	T/4	- 60	-51	3	4
76mm A36 NG/ST2	6ZE	1300	35	T/4	- 30	-34	14	19
76mm A36 NG/ST2	6ZL	1300	35	T/4	- 30	-34	5	7
76mm A36 NG/ST2	6ZH	1300	35	T/4	0	-18	32	43
76mm A36 NG/ST2	6ZF	1300	35	T/4	0	-18	38	51
76mm A36 NG/ST2	6ZJ	1300	35	T/4	0	-18	36	48
76mm A36 NG/ST2	6ZS	1300	35	T/4	32	0	45	61
76mm A36 NG/ST2	6ZM	1300	35	T/4	32	0	24	33
76mm A36 NG/ST2	6ZG	1300	35	T/4	50	10	38	51
76mm A36 NG/ST2	6ZN	1300	35	T/4	50	10	49	66
76mm A36 NG/ST2	6ZD	1300	35	T/4	68	20	51	69
76mm A36 NG/ST2	6ZS	1300	35	T/4	68	20	51	69
76mm A36 NG/ST2	6ZI	1300	35	T/4	104	40	62	84
76mm A36 NG/ST2	6ZQ	1300	35	T/4	104	40	24	33
76mm A36 NG/ST2	6ZC	1300	35	T/4	150	65	81	110
76mm A36 NG/ST2	6ZB	1300	35	T/4	150	65	72	98
76mm A36 NG/ST2	4ZK	1300	35	HAZ	-100	-73	3	4
76mm A36 NG/ST2	4ZH	1300	35	HAZ	-100	-73	3	4
76mm A36 NG/ST2	4ZS	1300	35	HAZ	- 60	-51	6	8
76mm A36 NG/ST2	4ZJ	1300	35	HAZ	- 60	-51	2.5	3
76mm A36 NG/ST2	4ZC	1300	35	HAZ	- 30	-34	8	11
76mm A36 NG/ST2	4ZG	1300	35	HAZ	- 30	-34	7	9
76mm A36 NG/ST2	4ZI	1300	35	HAZ	0	-18	20	27
76mm A36 NG/ST2	4ZA	1300	35	HAZ	0	-18	9	12
76mm A36 NG/ST2	4ZM	1300	35	HAZ	0	-18	13	18
76mm A36 NG/ST2	4ZF	1300	35	HAZ	0	-18	30	41
76mm A36 NG/ST2	4ZE	1300	35	HAZ	32	0	22	30
76mm A36 NG/ST2	4ZN	1300	35	HAZ	32	0	8	11
76mm A36 NG/ST2	4ZQ	1300	35	HAZ	50	10	47	64
76mm A36 NG/ST2	4ZL	1300	35	HAZ	50	10	66	89
76mm A36 NG/ST2	4ZP	1300	35	HAZ	68	20	38	52
76mm A36 NG/ST2	4ZO	1300	35	HAZ	68	20	21	29
76mm A36 NG/ST2	4ZI	1300	35	HAZ	104	40	52	71
76mm A36 NG/ST2	4ZR	1300	35	HAZ	104	40	66	90
76mm A36 NG/ST2	4ZB	1300	35	HAZ	150	65	74	100
76mm A36 NG/ST2	4ZT	1300	35	HAZ	150	65	104	141

APPENDIX A: CVN IMPACT TEST DATA
(cont.)

Weld ID	Specimen ID	Current (A)	Voltage (V)	Zone	Temperature		CVN Toughness	
					°F	°C	ft-lb	Joules
50mm A588 SG/WS	1EE	600	42	T/2	- 40	-40	2.7	4
50mm A588 SG/WS	1ED	600	42	T/2	- 40	-40	13.7	19
50mm A588 SG/WS	1EF	600	42	T/2	- 20	-29	17.7	24
50mm A588 SG/WS	1EG	600	42	T/2	- 20	-29	3.5	5
50mm A588 SG/WS	1EB	600	42	T/2	0	-18	9	12
50mm A588 SG/WS	1EC	600	42	T/2	0	-18	5	7
50mm A588 SG/WS	1EA	600	42	T/2	0	-18	7	9
50mm A588 SG/WS	1EQ	600	42	T/2	32	0	25	34
50mm A588 SG/WS	1ER	600	42	T/2	32	0	25	34
50mm A588 SG/WS	1ET	600	42	T/2	50	10	31	42
50mm A588 SG/WS	1ES	600	42	T/2	50	10	30	41
50mm A588 SG/WS	1EH	600	42	T/2	68	20	33.5	45
50mm A588 SG/WS	1EI	600	42	T/2	68	20	41	56
50mm A588 SG/WS	1EP	600	42	T/2	100	38	40	54
50mm A588 SG/WS	1ED	600	42	T/2	100	38	48.5	66
50mm A588 SG/WS	1EL	600	42	T/2	150	65	55	75
76mm A36 NG/ST2	1EN	600	42	T/2	150	65	50	68
50mm A588 SG/WS	5EQ	600	42	T/4	-100	-73	5	7
50mm A588 SG/WS	5EH	600	42	T/4	- 60	-51	4	5
50mm A588 SG/WS	5EI	600	42	T/4	- 60	-51	2.5	3
50mm A588 SG/WS	5ED	600	42	T/4	- 30	-34	20	27
50mm A588 SG/WS	5EA	600	42	T/4	- 30	-34	4	5
50mm A588 SG/WS	5EB	600	42	T/4	0	-18	6	8
50mm A588 SG/WS	5EP	600	42	T/4	0	-18	5	7
50mm A588 SG/WS	5EL	600	42	T/4	32	0	34	46
50mm A588 SG/WS	5EK	600	42	T/4	32	0	7	9
50mm A588 SG/WS	5EJ	600	42	T/4	50	10	25	34
50mm A588 SG/WS	5ER	600	42	T/4	50	10	27	37
50mm A588 SG/WS	5EN	600	42	T/4	68	20	41	56
50mm A588 SG/WS	5EG	600	42	T/4	68	20	30	41
50mm A588 SG/WS	5ET	600	42	T/4	104	40	40	54
50mm A588 SG/WS	5EC	600	42	T/4	104	40	47	64
50mm A588 SG/WS	5EF	600	42	T/4	150	65	60	81
50mm A588 SG/WS	5EE	600	42	T/4	150	65	55	75

APPENDIX A: CVN IMPACT TEST DATA
(cont.)

Weld ID	Specimen ID	Current (A)	Voltage (V)	Zone	Temperature		CVN Toughness	
					°F	°C	ft-lb	Joules
50mm A588 SG/WS	2EL	600	42	HAZ	- 60	-51	1	2
50mm A588 SG/WS	2EM	600	42	HAZ	- 60	-51	3	4
50mm A588 SG/WS	2EE	600	42	HAZ	- 40	-40	6	8
50mm A588 SG/WS	2ED	600	42	HAZ	- 40	-40	9	12
50mm A588 SG/WS	2EF	600	42	HAZ	- 20	-29	4	5
50mm A588 SG/WS	2EG	600	42	HAZ	- 20	-29	6.2	8
50mm A588 SG/WS	2EA	600	42	HAZ	0	-18	4	5
50mm A588 SG/WS	2EC	600	42	HAZ	0	-18	6.2	8
50mm A588 SG/WS	2EB	600	42	HAZ	0	-18	25.3	34
50mm A588 SG/WS	2ER	600	42	HAZ	32	0	10.5	14
50mm A588 SG/WS	2ES	600	42	HAZ	32	0	22	30
50mm A588 SG/WS	2EQ	600	42	HAZ	100	38	36	49
50mm A588 SG/WS	2EP	600	42	HAZ	100	38	20	27
50mm A588 SG/WS	2EN	600	42	HAZ	150	65	50	68
50mm A588 SG/WS	2EC	600	42	HAZ	150	65	56	76
50mm A588 SG/WS	2EK	600	42	HAZ	200	93	94	127
50mm A588 SG/WS	2EJ	600	42	HAZ	200	93	84.5	114
50mm A588 NG/WS	3QI	1000	38	T/2	-100	-73	5	7
50mm A588 NG/WS	3QE	1000	38	T/2	-100	-73	4	5
50mm A588 NG/WS	3QP	1000	38	T/2	- 60	-51	12	16
50mm A588 NG/WS	3QJ	1000	38	T/2	- 60	-51	8	11
50mm A588 NG/WS	3QF	1000	38	T/2	- 30	-34	10	14
50mm A588 NG/WS	3QA	1000	38	T/2	- 30	-34	9	12
50mm A588 NG/WS	3QD	1000	38	T/2	0	-18	9	12
50mm A588 NG/WS	3QM	1000	38	T/2	0	-18	10	14
50mm A588 NG/WS	3QQ	1000	38	T/2	0	-18	20	27
50mm A588 NG/WS	3QB	1000	38	T/2	0	-18	13	18
50mm A588 NG/WS	3QN	1000	38	T/2	32	0	18	24
50mm A588 NG/WS	3QC	1000	38	T/2	32	0	38	51
50mm A588 NG/WS	3QL	1000	38	T/2	50	10	54	73
50mm A588 NG/WS	3QH	1000	38	T/2	50	10	43	58
50mm A588 NG/WS	3QR	1000	38	T/2	68	20	70	95
50mm A588 NG/WS	3QS	1000	38	T/2	68	20	73	99
50mm A588 NG/WS	3QG	1000	38	T/2	104	40	57	99
50mm A588 NG/WS	3QS	1000	38	T/2	104	40	66	89
50mm A588 SG/WS	3QT	1000	38	T/2	150	65	77	104
50mm A588 SG/WS	3QK	1000	38	T/2	150	65	75	102

APPENDIX A: CVN IMPACT TEST DATA
(cont.)

Weld ID	Specimen ID	Current (A)	Voltage (V)	Zone	Temperature		CVN Toughness	
					°F	°C	ft-lb	Joules
50mm A588 NG/WS	6QJ	1000	38	T/4	-100	-73	1	1.4
50mm A588 NG/WS	6QL	1000	38	T/4	-60	-51	3	4
50mm A588 NG/WS	6QI	1000	38	T/4	-60	-51	3	4
50mm A588 NG/WS	6QE	1000	38	T/4	-30	-34	8	11
50mm A588 NG/WS	6QG	1000	38	T/4	-30	-34	7	9
50mm A588 NG/WS	6QN	1000	38	T/4	0	-18	18	24
50mm A588 NG/WS	6QP	1000	38	T/4	0	-18	8	11
50mm A588 NG/WS	6QF	1000	38	T/4	32	0	31	42
50mm A588 NG/WS	6QH	1000	38	T/4	50	10	45	61
50mm A588 NG/WS	6QM	1000	38	T/4	50	10	59	80
50mm A588 NG/WS	6QK	1000	38	T/4	68	20	46	62
50mm A588 NG/WS	6QA	1000	38	T/4	68	20	52	70
50mm A588 NG/WS	6QC	1000	38	T/4	125	51	76	103
50mm A588 NG/WS	6QB	1000	38	T/4	150	65	79	107
50mm A588 NG/WS	6QO	1000	38	T/4	150	65	76	103
50mm A588 NG/WS	4QN	1000	38	HAZ	-100	-73	4	5
50mm A588 NG/WS	4QQ	1000	38	HAZ	-60	-51	4	5
50mm A588 NG/WS	4QD	1000	38	HAZ	-60	-51	5.5	7
50mm A588 NG/WS	4QA	1000	38	HAZ	-30	-34	6	8
50mm A588 NG/WS	4QJ	1000	38	HAZ	-30	-34	5.5	7
50mm A588 NG/WS	4QP	1000	38	HAZ	0	-18	9	12
50mm A588 NG/WS	4QO	1000	38	HAZ	0	-18	11	15
50mm A588 NG/WS	4QG	1000	38	HAZ	32	0	15	20
50mm A588 NG/WS	4QE	1000	38	HAZ	50	10	19	26
50mm A588 NG/WS	4QS	1000	38	HAZ	50	10	15	20
50mm A588 NG/WS	4QH	1000	38	HAZ	68	20	29	39
50mm A588 NG/WS	4QK	1000	38	HAZ	68	20	26	35
50mm A588 NG/WS	4QF	1000	38	HAZ	100	38	31	42
50mm A588 NG/WS	4QI	1000	38	HAZ	100	38	30	40
50mm A588 NG/WS	4QC	1000	38	HAZ	125	51	55	75
50mm A588 NG/WS	4QT	1000	38	HAZ	125	51	60	81
50mm A588 NG/WS	4QM	1000	38	HAZ	150	65	72	98

APPENDIX A: CVN IMPACT TEST DATA
(cont.)

							Temperature		CVN Toughness	
							°F	°C	ft-lb	Joules
Weld ID	Specimen ID	Current (A)	Voltage (V)	Zone						
50mm A588 NG/ST	3SP	1000	38	T/2	-100	-73	9	12		
50mm A588 NG/ST	3SA	1000	38	T/2	-100	-73	6	8		
50mm A588 NG/ST	3SH	1000	38	T/2	-60	-51	6.6	9		
50mm A588 NG/ST	3SB	1000	38	T/2	-60	-51	6.7	9		
50mm A588 NG/ST	3SE	1000	38	T/2	-30	-34	22	30		
50mm A588 NG/ST	3SK	1000	38	T/2	-30	-34	21	28		
50mm A588 NG/ST	3SE	1000	38	T/2	0	-18	29	39		
50mm A588 NG/ST	3SD	1000	38	T/2	0	-18	34	46		
50mm A588 NG/ST	3SI	1000	38	T/2	32	0	49	66		
50mm A588 NG/ST	3SF	1000	38	T/2	50	10	50	68		
50mm A588 NG/ST	3SO	1000	38	T/2	50	10	77	104		
50mm A588 NG/ST	3SN	1000	38	T/2	68	20	77	104		
50mm A588 NG/ST	3SL	1000	38	T/2	100	38	82	111		
50mm A588 NG/ST	3SC	1000	38	T/2	100	38	72	98		
50mm A588 NG/ST	3SJ	1000	38	T/2	150	65	74	100		
50mm A588 NG/ST	3SM	1000	38	T/2	150	65	88	119		
50mm A588 NG/ST	6SL	800	38	T/4	-100	-73	4.5	6		
50mm A588 NG/ST	6SJ	800	38	T/4	-60	-51	8.2	11		
50mm A588 NG/ST	6SM	800	38	T/4	-60	-51	9.2	12		
50mm A588 NG/ST	6SP	800	38	T/4	-30	-34	35	47		
50mm A588 NG/ST	6SB	800	38	T/4	-30	-34	8	11		
50mm A588 NG/ST	6SE	800	38	T/4	0	-18	24.5	33		
50mm A588 NG/ST	6SO	800	38	T/4	0	-18	38	51		
50mm A588 NG/ST	6SI	800	38	T/4	32	0	44	65		
50mm A588 NG/ST	6SZ	800	38	T/4	32	0	37	50		
50mm A588 NG/ST	6SF	800	38	T/4	50	10	23	31		
50mm A588 NG/ST	6SG	800	38	T/4	50	10	25	34		
50mm A588 NG/ST	6SN	800	38	T/4	68	20	48	65		
50mm A588 NG/ST	6SK	800	38	T/4	68	20	45	61		
50mm A588 NG/ST	6SC	800	38	T/4	100	38	71	96		
50mm A588 NG/ST	6SH	800	38	T/4	150	65	90	122		
50mm A588 NG/ST	6SA	800	38	T/4	150	65	80	108		

APPENDIX A: CVN IMPACT TEST DATA
(cont.)

Weld ID	Specimen ID	Current (A)	Voltage (V)	Zone	Temperature		CVN Toughness	
					°F	°C	ft-lb	Joules
50mm A588 NG/ST	4SJ	800	38	HAZ	-100	-73	7	9
50mm A588 NG/ST	4SB	800	38	HAZ	-100	-73	3	4
50mm A588 NG/ST	4SP	800	38	HAZ	- 60	-51	9.5	13
50mm A588 NG/ST	4SE	800	38	HAZ	- 60	-51	4.5	6
50mm A588 NG/ST	4SC	800	38	HAZ	- 30	-34	7.2	10
50mm A588 NG/ST	4SA	800	38	HAZ	- 30	-34	8.5	12
50mm A588 NG/ST	4SF	800	38	HAZ	0	-18	12	16
50mm A588 NG/ST	4ST	800	38	HAZ	0	-18	18.5	25
50mm A588 NG/ST	4SL	800	38	HAZ	50	10	21	28
50mm A588 NG/ST	4SD	800	38	HAZ	50	10	23	31
50mm A588 NG/ST	4SR	800	38	HAZ	68	20	41	56
50mm A588 NG/ST	4SN	800	38	HAZ	100	38	56	76
50mm A588 NG/ST	4SS	800	38	HAZ	100	38	50	68
50mm A588 NG/ST	4SC	800	38	HAZ	125	51	57	77
50mm A588 NG/ST	4SO	800	38	HAZ	150	65	86	117
50mm A588 NG/ST	4SK	800	38	HAZ	150	65	82	111
76mm A588 SG/WS	1AD	850	38	T/2	- 40	-40	2.2	3
76mm A588 SG/WS	1AC	850	38	T/2	- 40	-40	2.2	3
76mm A588 SG/WS	1AE	850	38	T/2	- 20	-29	3.4	4.6
76mm A588 SG/WS	1AF	850	38	T/2	- 20	-29	3	4
76mm A588 SG/WS	1AA	850	38	T/2	0	-18	7	9
76mm A588 SG/WS	1AB	850	38	T/2	0	-18	4	5
76mm A588 SG/WS	1AO	850	38	T/2	32	0	7	9
76mm A588 SG/WS	1AP	850	38	T/2	32	0	8	11
76mm A588 SG/WS	1AQ	850	38	T/2	50	10	19	26
76mm A588 SG/WS	1AR	850	38	T/2	50	10	10	14
76mm A588 SG/WS	1AH	850	38	T/2	68	20	42.5	58
76mm A588 SG/WS	1AG	850	38	T/2	68	20	34.5	48
76mm A588 SG/WS	1AN	850	38	T/2	100	38	45	61
76mm A588 SG/WS	1AM	850	38	T/2	100	38	49	66
76mm A588 SG/WS	1AK	850	38	T/2	150	65	62	84
76mm A588 SG/WS	1AL	850	38	T/2	150	65	64	87
76mm A588 SG/WS	1AI	850	38	T/2	200	93	72	98

APPENDIX A: CVN IMPACT TEST DATA
(cont.)

							Temperature		CVN Toughness	
							°F	°C	ft-lb	Joules
Weld ID	Specimen ID	Current (A)	Voltage (V)	Zone						
76mm A588 SG/WS	5AE	850	38	T/4	- 65	-53	2	3		
76mm A588 SG/WS	5AM	850	38	T/4	- 65	-53	2	3		
76mm A588 SG/WS	5AL	850	38	T/4	- 20	-29	2	3		
76mm A588 SG/WS	5AC	850	38	T/4	0	-18	3	4		
76mm A588 SG/WS	5AD	850	38	T/4	0	-18	4	5		
76mm A588 SG/WS	5AG	850	38	T/4	50	10	14	19		
76mm A588 SG/WS	5AH	850	38	T/4	50	10	16.5	22		
76mm A588 SG/WS	5AB	850	38	T/4	68	20	21	28		
76mm A588 SG/WS	5AI	850	38	T/4	68	20	20	27		
76mm A588 SG/WS	5AA	850	38	T/4	104	40	63	85		
76mm A588 SG/WS	5AK	850	38	T/4	104	40	61	83		
76mm A588 SG/WS	5AF	850	38	T/4	160	68	71	96		
76mm A588 SG/WS	5AJ	850	38	T/4	160	68	68	92		
76mm A588 SG/WS	2AD	850	38	HAZ	- 40	-40	1.5	2		
76mm A588 SG/WS	2AC	850	38	HAZ	- 40	-40	1.5	2		
76mm A588 SG/WS	2AE	850	38	HAZ	- 20	-29	3.3	4		
76mm A588 SG/WS	2AF	850	38	HAZ	- 20	-29	3.6	4		
76mm A588 SG/WS	2AA	850	38	HAZ	0	-18	2	3		
76mm A588 SG/WS	2AB	850	38	HAZ	0	-18	2.7	4		
76mm A588 SG/WS	2AO	850	38	HAZ	32	0	4	5		
76mm A588 SG/WS	2AQ	850	38	HAZ	50	10	3	4		
76mm A588 SG/WS	2AR	850	38	HAZ	50	10	3	4		
76mm A588 SG/WS	2AH	850	38	HAZ	68	20	16	22		
76mm A588 SG/WS	2AG	850	38	HAZ	68	20	5	7		
76mm A588 SG/WS	2AN	850	38	HAZ	100	38	12	16		
76mm A588 SG/WS	2AT	850	38	HAZ	100	38	13	18		
76mm A588 SG/WS	2AL	850	38	HAZ	150	65	27	37		
76mm A588 SG/WS	2AI	850	38	HAZ	200	93	75	102		
76mm A588 SG/WS	2AJ	850	38	HAZ	200	93	41.5	56		

APPENDIX A: CVN IMPACT TEST DATA
(cont.)

							Temperature		CVN Toughness	
							°F	°C	ft-lb	Joules
Weld ID	Specimen ID	Current (A)	Voltage (V)	Zone						
76mm A588 NG/WS	3HL	1000	38	T/2	-100	-73	1	1.4		
76mm A588 NG/WS	3HI	1000	38	T/2	- 60	-51	1.5	2		
76mm A588 NG/WS	3HE	1000	38	T/2	- 60	-51	1.5	2		
76mm A588 NG/WS	3HG	1000	38	T/2	- 30	-34	2.2	3		
76mm A588 NG/WS	3HT	1000	38	T/2	- 30	-34	2	3		
76mm A588 NG/WS	3HK	1000	38	T/2	0	-18	3.5	5		
76mm A588 NG/WS	3HJ	1000	38	T/2	50	10	5	7		
76mm A588 NG/WS	3HH	1000	38	T/2	50	10	9	12		
76mm A588 NG/WS	3HA	1000	38	T/2	68	20	14	19		
76mm A588 NG/WS	3HB	1000	38	T/2	68	20	12.5	17		
76mm A588 NG/WS	3HD	1000	38	T/2	100	38	26	35		
76mm A588 NG/WS	3HM	1000	38	T/2	100	38	34	46		
76mm A588 NG/WS	3HP	1000	38	T/2	125	52	59	80		
76mm A588 NG/WS	3HC	1000	38	T/2	125	52	50	68		
76mm A588 NG/WS	3HO	1000	38	T/2	150	65	53	72		
76mm A588 NG/WS	3HN	1000	38	T/2	150	65	64	87		
76mm A588 NG/WS	6HP	1000	38	T/4	- 60	-51	1.5	2		
76mm A588 NG/WS	6HK	1000	38	T/4	- 60	-51	1.5	2		
76mm A588 NG/WS	6HI	1000	38	T/4	- 30	-34	2	3		
76mm A588 NG/WS	6HJ	1000	38	T/4	0	-18	5	7		
76mm A588 NG/WS	6HM	1000	38	T/4	0	-18	4	5		
76mm A588 NG/WS	6HL	1000	38	T/4	0	-18	3.5	5		
76mm A588 NG/WS	6HE	1000	38	T/4	50	10	7	9		
76mm A588 NG/WS	6HD	1000	38	T/4	50	10	9	12		
76mm A588 NG/WS	6HO	1000	38	T/4	68	20	17	23		
76mm A588 NG/WS	6HB	1000	38	T/4	68	20	9	12		
76mm A588 NG/WS	6HA	1000	38	T/4	100	38	42	57		
76mm A588 NG/WS	6HN	1000	38	T/4	100	38	15.5	21		
76mm A588 NG/WS	6HF	1000	38	T/4	125	52	34	46		
76mm A588 NG/WS	6HH	1000	38	T/4	125	52	29	39		
76mm A588 NG/WS	6HL	1000	38	T/4	150	65	42	57		
76mm A588 NG/WS	6HG	1000	38	T/4	150	65	40	54		

APPENDIX A: CVN IMPACT TEST DATA
(cont.)

Weld ID	Specimen ID	Current (A)	Voltage (V)	Zone	Temperature		CVN Toughness	
					°F	°C	ft-lb	Joules
76mm A588 NG/WS	4HI	1000	38	HAZ	- 60	-51	1.1	1.5
76mm A588 NG/WS	4HM	1000	38	HAZ	- 30	-34	1.5	2
76mm A588 NG/WS	4HP	1000	38	HAZ	- 30	-34	1	1
76mm A588 NG/WS	4HC	1000	38	HAZ	0	-18	2	3
76mm A588 NG/WS	4HG	1000	38	HAZ	0	-18	2	3
76mm A588 NG/WS	4HA	1000	38	HAZ	32	0	2	3
76mm A588 NG/WS	4HF	1000	38	HAZ	50	10	4	5
76mm A588 NG/WS	4HO	1000	38	HAZ	68	20	16.5	22
76mm A588 NG/WS	4HE	1000	38	HAZ	68	20	5.5	7
76mm A588 NG/WS	4HJ	1000	38	HAZ	68	20	4.5	6
76mm A588 NG/WS	4HL	1000	38	HAZ	100	38	15	21
76mm A588 NG/WS	4HN	1000	38	HAZ	125	52	18.5	25
76mm A588 NG/WS	4HH	1000	38	HAZ	125	52	27	36
76mm A588 NG/WS	4HD	1000	38	HAZ	150	65	38	45
76mm A588 NG/WS	3TS	1300	38	T/2	- 60	-51	2.5	3
76mm A588 NG/WS	3TC	1300	38	T/2	- 60	-51	2	3
76mm A588 NG/WS	3TM	1300	38	T/2	- 20	-29	3.5	5
76mm A588 NG/WS	3TJ	1300	38	T/2	- 20	-29	3	4
76mm A588 NG/WS	3TP	1300	38	T/2	0	-18	4.5	6
76mm A588 NG/WS	3TR	1300	38	T/2	0	-18	3.5	5
76mm A588 NG/WS	3TG	1300	38	T/2	32	0	7	9
76mm A588 NG/WS	3TD	1300	38	T/2	32	0	10.5	14
76mm A588 NG/WS	3TS	1300	38	T/2	68	20	14	19
76mm A588 NG/WS	3TH	1300	38	T/2	68	20	14	19
76mm A588 NG/WS	3TI	1300	38	T/2	100	38	40	54
76mm A588 NG/WS	3TA	1300	38	T/2	100	38	34	46
76mm A588 NG/WS	3TE	1300	38	T/2	125	52	37	50
76mm A588 NG/WS	3TR	1300	38	T/2	125	52	70	95
76mm A588 NG/WS	3TC	1300	38	T/2	150	65	58	79
76mm A588 NG/WS	3TL	1300	38	T/2	150	65	66	89

APPENDIX A: CVN IMPACT TEST DATA
(cont.)

Weld ID	Specimen ID	Current (A)	Voltage (V)	Zone	Temperature		CVN Toughness	
					°F	°C	ft-lb	Joules
76mm A588 NG/WS	6TD	1300	38	T/4	- 80	-62	4.5	6
76mm A588 NG/WS	6TC	1300	38	T/4	- 60	-51	3	4
76mm A588 NG/WS	6TP	1300	38	T/4	- 60	-51	2.5	3
76mm A588 NG/WS	6TR	1300	38	T/4	- 20	-29	4.5	6
76mm A588 NG/WS	6TN	1300	38	T/4	- 20	-29	3.5	5
76mm A588 NG/WS	6TM	1300	38	T/4	0	-18	4.5	6
76mm A588 NG/WS	6TJ	1300	38	T/4	0	-18	6.5	9
76mm A588 NG/WS	6TA	1300	38	T/4	32	0	5.5	7
76mm A588 NG/WS	6TP	1300	38	T/4	32	0	6.5	9
76mm A588 NG/WS	6TQ	1300	38	T/4	68	20	12.5	20
76mm A588 NG/WS	6TG	1300	38	T/4	68	20	15	20
76mm A588 NG/WS	6TL	1300	38	T/4	100	38	49	66
76mm A588 NG/WS	6TD	1300	38	T/4	100	38	22	30
76mm A588 NG/WS	6TF	1300	38	T/4	125	52	47	64
76mm A588 NG/WS	6TK	1300	38	T/4	125	52	69	93
76mm A588 NG/WS	6TI	1300	38	T/4	150	65	66	89
76mm A588 NG/WS	6TE	1300	38	T/4	150	65	57	77
76mm A588 NG/WS	4TQ	1300	38	HAZ	- 60	-51	1.5	2
76mm A588 NG/WS	4TF	1300	38	HAZ	- 20	-29	5	7
76mm A588 NG/WS	4TB	1300	38	HAZ	- 20	-29	2.5	3
76mm A588 NG/WS	4TS	1300	38	HAZ	0	-18	4.5	6
76mm A588 NG/WS	4TC	1300	38	HAZ	0	-18	5	7
76mm A588 NG/WS	4TI	1300	38	HAZ	32	0	3.5	5
76mm A588 NG/WS	4TF	1300	38	HAZ	32	0	3.5	5
76mm A588 NG/WS	4TD	1300	38	HAZ	68	20	12	16
76mm A588 NG/WS	4TG	1300	38	HAZ	68	20	16	22
76mm A588 NG/WS	4TT	1300	38	HAZ	100	38	19	26
76mm A588 NG/WS	4TH	1300	38	HAZ	100	38	50	68
76mm A588 NG/WS	4TE	1300	38	HAZ	125	52	44	60
76mm A588 NG/WS	4TB	1300	38	HAZ	125	52	10	14
76mm A588 NG/WS	4TC	1300	38	HAZ	150	65	84	114
76mm A588 NG/WS	4TK	1300	38	HAZ	150	65	53	72

APPENDIX A: CVN IMPACT TEST DATA
(cont.)

Weld ID	Specimen ID	Current (A)	Voltage (V)	Zone	Temperature		CVN Toughness	
					°F	°C	ft-lb	Joules
76mm A588 NG/ST	3LL	1000	38	T/2	-100	-73	1.5	2
76mm A588 NG/ST	3LQ	1000	38	T/2	-60	-51	2.5	3.4
76mm A588 NG/ST	3LS	1000	38	T/2	-60	-51	2	2.7
76mm A588 NG/ST	3LE	1000	38	T/2	-30	-34	4	5.4
76mm A588 NG/ST	3LR	1000	38	T/2	-30	-34	4	5.4
76mm A588 NG/ST	3LB	1000	38	T/2	0	-18	5	6.8
76mm A588 NG/ST	3LA	1000	38	T/2	0	-18	7	9.5
76mm A588 NG/ST	3LC	1000	38	T/2	32	0	14	19
76mm A588 NG/ST	3LK	1000	38	T/2	32	0	13	18
76mm A588 NG/ST	3LG	1000	38	T/2	50	10	15	20
76mm A588 NG/ST	3LP	1000	38	T/2	50	10	13	18
76mm A588 NG/ST	3LD	1000	38	T/2	68	20	14	19
76mm A588 NG/ST	3LI	1000	38	T/2	68	20	18	24.4
76mm A588 NG/ST	3LN	1000	38	T/2	100	38	31	42
76mm A588 NG/ST	3LO	1000	38	T/2	100	38	38	51.5
76mm A588 NG/ST	3LF	1000	38	T/2	150	65	34	46
76mm A588 NG/ST	3LH	1000	38	T/2	150	65	44	60
76mm A588 NG/ST	6LQ	1000	38	T/4	-60	-51	2.5	3.4
76mm A588 NG/ST	6LP	1000	38	T/4	-60	-51	2	2.7
76mm A588 NG/ST	6LL	1000	38	T/4	-30	-34	3.5	4.7
76mm A588 NG/ST	6LK	1000	38	T/4	-30	-34	4	5.4
76mm A588 NG/ST	6LR	1000	38	T/4	-30	-34	4	5.4
76mm A588 NG/ST	6LS	1000	38	T/4	0	-18	7	9.5
76mm A588 NG/ST	6LT	1000	38	T/4	0	-18	5	6.8
76mm A588 NG/ST	6LC	1000	38	T/4	32	0	8	10.8
76mm A588 NG/ST	6LE	1000	38	T/4	32	0	7	9.5
76mm A588 NG/ST	6LB	1000	38	T/4	50	10	17	23.1
76mm A588 NG/ST	6LJ	1000	38	T/4	50	10	10	13.6
76mm A588 NG/ST	6LD	1000	38	T/4	68	20	14	19
76mm A588 NG/ST	6LG	1000	38	T/4	68	20	15	20
76mm A588 NG/ST	6LN	1000	38	T/4	100	38	29	39.3
76mm A588 NG/ST	6LM	1000	38	T/4	100	38	26	36
76mm A588 NG/ST	6LA	1000	38	T/4	125	52	50	67.8
76mm A588 NG/ST	6LH	1000	38	T/4	125	52	44	60
76mm A588 NG/ST	6LI	1000	38	T/4	150	65	44	60
76mm A588 NG/ST	6LF	1000	38	T/4	150	65	43	58.5

APPENDIX A: CVN IMPACT TEST DATA
(cont.)

Weld ID	Specimen ID	Current (A)	Voltage (V)	Zone	Temperature		CVN Toughness	
					°F	°C	ft-lb	Joules
76mm A588 NG/ST	4LH	1000	38	HAZ	- 60	-51	1	1.4
76mm A588 NG/ST	4LK	1000	38	HAZ	- 60	-51	1.2	1.6
76mm A588 NG/ST	4LF	1000	38	HAZ	- 30	-34	2	2.7
76mm A588 NG/ST	4LJ	1000	38	HAZ	0	-18	3	4.1
76mm A588 NG/ST	4LA	1000	38	HAZ	0	-18	2	2.7
76mm A588 NG/ST	4LN	1000	38	HAZ	50	10	5.5	7.4
76mm A588 NG/ST	4LO	1000	38	HAZ	50	10	4	5.4
76mm A588 NG/ST	4LC	1000	38	HAZ	68	20	10	13.6
76mm A588 NG/ST	4LP	1000	38	HAZ	68	20	9	12.2
76mm A588 NG/ST	4LG	1000	38	HAZ	100	38	15	20
76mm A588 NG/ST	4LL	1000	38	HAZ	100	38	45	61
76mm A588 NG/ST	4LD	1000	38	HAZ	125	52	67	90.9
76mm A588 NG/ST	4LQ	1000	38	HAZ	125	52	55	74.6
76mm A588 NG/ST	4LB	1000	38	HAZ	150	65	61	82.7
76mm A588 NG/ST	4LM	1000	38	HAZ	150	65	65	88
76mm A588 NG/ST2	3VS	1300	35	T/2	-100	-73	4.5	6.1
76mm A588 NG/ST2	3VD	1300	35	T/2	-100	-73	4	5.4
76mm A588 NG/ST2	3VI	1300	35	T/2	- 80	-62	5	6.8
76mm A588 NG/ST2	3VH	1300	35	T/2	- 80	-62	5	6.8
76mm A588 NG/ST2	3VT	1300	35	T/2	- 60	-52	5.5	7.5
76mm A588 NG/ST2	3VR	1300	35	T/2	- 20	-29	13	17.7
76mm A588 NG/ST2	3VE	1300	35	T/2	- 20	-29	16	21.7
76mm A588 NG/ST2	3VA	1300	35	T/2	0	-18	26	35.3
76mm A588 NG/ST2	3VC	1300	35	T/2	0	-18	26	35
76mm A588 NG/ST2	3VN	1300	35	T/2	32	0	30	40
76mm A588 NG/ST2	3VP	1300	35	T/2	32	0	27	36.6
76mm A588 NG/ST2	3VS	1300	35	T/2	68	20	50	67.8
76mm A588 NG/ST2	3VO	1300	35	T/2	68	20	50	67.8
76mm A588 NG/ST2	3VG	1300	35	T/2	68	20	50	67.8
76mm A588 NG/ST2	3VM	1300	35	T/2	150	65	85	115
76mm A588 NG/ST2	3VJ	1300	35	T/2	150	65	79	107

APPENDIX A: CVN IMPACT TEST DATA
(cont.)

Weld ID	Specimen ID	Current (A)	Voltage (V)	Zone	Temperature		CVN Toughness	
					°F	°C	ft-lb	Joules
76mm A588 NG/ST2	6VH	1300	35	T/4	-100	-73	3.5	4.7
76mm A588 NG/ST2	6VI	1300	35	T/4	-100	-73	3.5	4.7
76mm A588 NG/ST2	6VT	1300	35	T/4	- 80	-62	7.5	10.2
76mm A588 NG/ST2	6VF	1300	35	T/4	- 80	-62	6	8.2
76mm A588 NG/ST2	6VQ	1300	35	T/4	- 60	-51	6.5	8.8
76mm A588 NG/ST2	6VO	1300	35	T/4	- 60	-51	10	13.6
76mm A588 NG/ST2	6VP	1300	35	T/4	- 20	-29	17	23.1
76mm A588 NG/ST2	6VN	1300	35	T/4	- 20	-29	22	29.8
76mm A588 NG/ST2	6VE	1300	35	T/4	0	-18	33	45
76mm A588 NG/ST2	6VK	1300	35	T/4	0	-18	27	36.6
76mm A588 NG/ST2	6VD	1300	35	T/4	32	0	42	57
76mm A588 NG/ST2	6VJ	1300	35	T/4	32	0	44	60
76mm A588 NG/ST2	6VB	1300	35	T/4	68	20	48	65
76mm A588 NG/ST2	6VG	1300	35	T/4	68	20	50	68
76mm A588 NG/ST2	6VA	1300	35	T/4	100	38	78	105
76mm A588 NG/ST2	6VC	1300	35	T/4	100	38	70	95
76mm A588 NG/ST2	6VL	1300	35	T/4	150	65	90	122
76mm A588 NG/ST2	6VS	1300	35	T/4	150	65	97	131
76mm A588 NG/ST2	4VC	1300	35	HAZ	-100	-73	2	3
76mm A588 NG/ST2	4VK	1300	35	HAZ	- 80	-62	4	5.4
76mm A588 NG/ST2	4VQ	1300	35	HAZ	- 60	-51	2.5	3.4
76mm A588 NG/ST2	4VI	1300	35	HAZ	- 60	-51	3	4
76mm A588 NG/ST2	4VA	1300	35	HAZ	- 20	-29	5	6.8
76mm A588 NG/ST2	4VM	1300	35	HAZ	- 20	-29	5	6.8
76mm A588 NG/ST2	4VH	1300	35	HAZ	0	-18	8	11.5
76mm A588 NG/ST2	4VF	1300	35	HAZ	0	-18	5	6.8
76mm A588 NG/ST2	4VG	1300	35	HAZ	32	0	9	12
76mm A588 NG/ST2	4VR	1300	35	HAZ	32	0	34	46
76mm A588 NG/ST2	4VB	1300	35	HAZ	32	0	34	46
76mm A588 NG/ST2	4VE	1300	35	HAZ	68	20	49	67
76mm A588 NG/ST2	4VS	1300	35	HAZ	68	20	39	53
76mm A588 NG/ST2	4VO	1300	35	HAZ	100	38	43	58
76mm A588 NG/ST2	4VP	1300	35	HAZ	100	38	83	113
76mm A588 NG/ST2	4VQ	1300	35	HAZ	100	38	64	87
76mm A588 NG/ST2	4VV	1300	35	HAZ	150	65	93	126
76mm A588 NG/ST2	4VJ	1300	35	HAZ	150	65	69	94

APPENDIX B: Full Copy of NDE Report



PITTSBURGH TESTING LABORATORY
ESTABLISHED 1881

PITTSBURGH, PA. 15220
AREA CODE 412 • TELEPHONE 922-4000

AS A MUTUAL PROTECTION TO CLIENTS, THE PUBLIC AND OURSELVES, ALL REPORTS ARE SUBMITTED AS THE CONFIDENTIAL PROPERTY OF CLIENTS, AND AUTHORIZATION FOR PUBLICATION OF STATEMENTS, CONCLUSIONS OR EXTRACTS FROM OR REGARDING OUR REPORTS IS RESERVED PENDING OUR WRITTEN APPROVAL.

FORM 1434A R80

ORDER NO.: POR-9169
LAB NO.: 001430
CLIENT NO.: P.O. 43326
REPORT NO.: 02
REPORT DATE: 10-19-85

REPORT OF
ULTRASONIC EXAMINATION OF WELDS

CLIENT OREGON GRADUATE CENTER 19600 S.W. Von Neuman Drive Beaverton, Oregon 97005	PROJECT Electroslag Welds With Known Defects	
	LOCATION Pittsburgh Testing Laboratory, Portland Oregon	
REPORT TO Mr. Bob Turpin	DRAWING NO.	ULTRASONIC UNIT SERIAL NO. <u>131D-351</u>

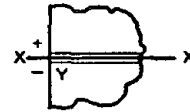
WELD LOCATION AND IDENTIFICATION SKETCH
(RECORD LENGTH, THICKNESS, AND X-Y MARKERS)

TEST METHOD STANDARD AWS D1.1-84/ASME Sec. IX
ACCEPTANCE STANDARD Section 9.25.3/Section IX

SEE ADDITIONAL DRAWING FOR WELD MAPPING

Scanned for Laminations

24" Length 1" Width Approximately
Numerous Reflectors by Indication 1, 2, 3



X-Y MARKERS

* Use Leg I, II, or III.

DATE	WELD IDENTIFICATION	ACCEPTABLE	REJECTABLE	Indication number	Transducer angle	From Face	Leg *	DECIBELS				DISCONTINUITY				
								Indication level	Reference level	Attenuation factor	Indication rating	Length	Angular distance (sound path)	Depth from "A" surface	Distance	
															a	b
October 08, 1985	Plate 1			1	70°	A	1	79	77	0	+2	1.25"	1.22"	.45"	7"	0
				2	70°	A	1	80	77	1	+2	1"	1.60"	.54"	9.0"	.125"
				3	70°	A	1	78	77	1	0	1.5"	1.39"	.47"	8.75-9.5"	.5-.5"
				4	70°	A	1	86	77	6	+3	.75"	3.94"	1.35"	10.25"	.5-.5"
				5	70°	A	1	79	77	3	-1	3"	2.37"	.81"	13.25"	.5"
				6	70°	A	1	82	77	3	+2	4"	2.51"	.85"	15-3/4"	.5"

TECHNICIAN: Frederick J. Neimann Level: II

Interpreter: Frederick J. Neimann Level: II

Reviewer: _____ Date: _____

Page 01 of 11 nancy

PITTSBURGH TESTING LABORATORY

Donald R. Scott
Donald R. Scott, Level III



PITTSBURGH TESTING LABORATORY

ESTABLISHED 1881

PITTSBURGH, PA. 15220
 AREA CODE 412 • TELEPHONE 922-4000

AS A MUTUAL PROTECTION TO CLIENTS, THE PUBLIC AND OURSELVES, ALL REPORTS ARE SUBMITTED AS THE CONFIDENTIAL PROPERTY OF CLIENTS, AND AUTHORIZATION FOR PUBLICATION OF STATEMENTS, CONCLUSIONS OR EXTRACTS FROM OR REGARDING OUR REPORTS IS RESERVED PENDING OUR WRITTEN APPROVAL.

FORM 1434A R80

ORDER NO.: POR-9169
 LAB NO.: 001430
 CLIENT NO.: P.O. 43326
 REPORT NO.: 02
 REPORT DATE: 10-19-85

REPORT OF ULTRASONIC EXAMINATION OF WELDS

CLIENT OREGON GRADUATE CENTER 19600 S.W. Von Neuman Drive Beaverton, Oregon 97005	PROJECT Electroslag Welds With Known Defects	
	LOCATION Pittsburgh Testing Laboratory, Portland Oregon	
REPORT TO Mr. Bob Turpin	DRAWING NO.	ULTRASONIC UNIT SERIAL NO. 131D-351

WELD LOCATION AND IDENTIFICATION SKETCH
 (RECORD LENGTH, THICKNESS, AND X-Y MARKERS)

(Scanned For Lamination)

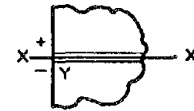
SEE ADDITIONAL DRAWING FOR WELD MAPPING

No Rejectable or Interfacing Laminations
 Noted-Either Side of Weld

Plate #1 24" Length 1" width approximate

60° Scan at 103 dB

TEST METHOD STANDARD AWS D1.1-84/ASME Sec. IX
ACCEPTANCE STANDARD Section 9.25.3/Section IX



X-Y MARKERS

* Use Leg I, II, or III.

DATE	WELD IDENTIFICATION	ACCEPTABLE	REJECTABLE	Indication number	Transducer angle	From Face	Leg *	DECIBELS				DISCONTINUITY					
								Indication level	Reference level	Attenuation factor	Indication rating	Length	Angular distance (sound path)	Depth from "A" surface	Distance		
															From X	From Y	
a	b	c	d														
October 08, 1985	Plate #1																
	Indication No. 1			1	60°	A	1	82	73	2	+7	1.0"	1.89"	.90"	7.75"	0	
	2			2	60°	A	1	78	73	1	+4	2.75"	1.50"	.75"	8.5"	-.5-	.75
	3			3	60°	A	1	81	73	6	+2	1.80"	3.70"	1.85"	9"	-.5-	
	4			4	60°	A	2	93	73	12	+8	.625"	7.27"	.37"	10.25"	-.5-	
	5			5	60°	A	1	77	73	2	+2	1"	1.93"	.96"	13.75"	-.375"	
	6			6	60°	A	1	79	73	1	+5	.5"	1.72"	.85"	16-.125"	.375"	
	7			7	60°	A	1	80	73	1	2.625"	1.86"	.92"	17.125"	.5"		

TECHNICIAN: Frederick J. Neimann Level: II
 Interpreter: Frederick J. Neimann Level: II
 Reviewer _____ Date _____
 Page 02 of 11 nancy

PITTSBURGH TESTING LABORATORY
Donald R. Scott
 Donald R. Scott, Level III

PLATE NO: 1

60° 73 Reference Level

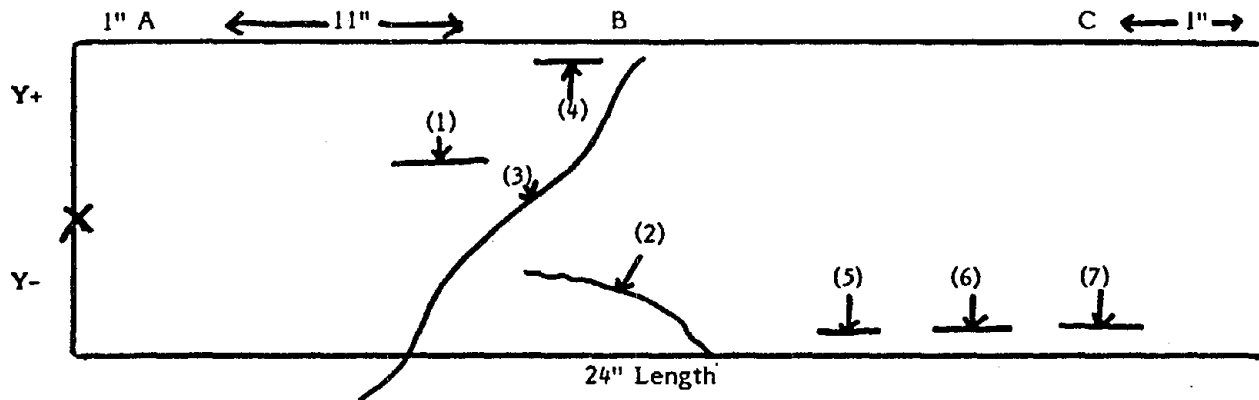
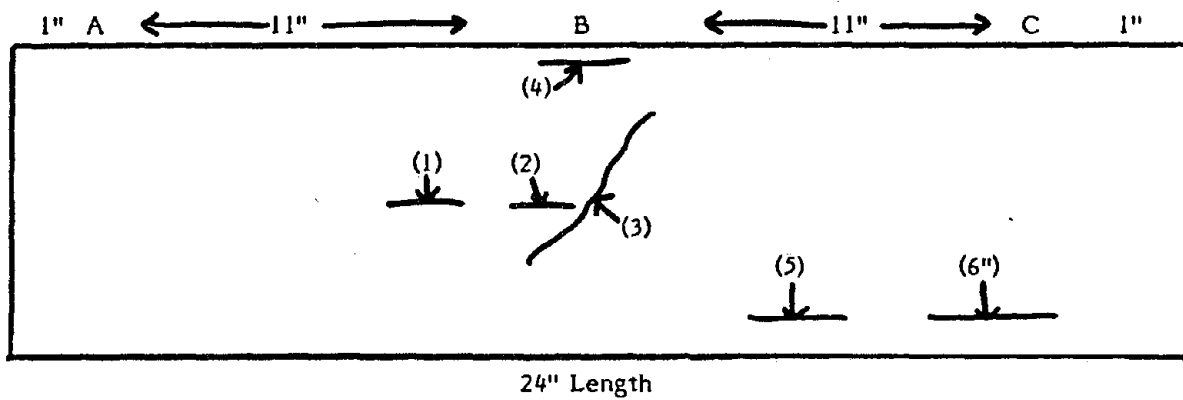


PLATE NO: 1

70° 73 Reference Level



1. Hot crack by an addition
2. " "
3. " "
4. " "
5. Lack of Fusion
6. " "
7. " "



PITTSBURGH TESTING LABORATORY

ESTABLISHED 1881

PITTSBURGH, PA. 15220
AREA CODE 412 · TELEPHONE 922-4000

AS A MUTUAL PROTECTION TO CLIENTS, THE PUBLIC AND OURSELVES, ALL REPORTS ARE SUBMITTED AS THE CONFIDENTIAL PROPERTY OF CLIENTS, AND AUTHORIZATION FOR PUBLICATION OF STATEMENTS, CONCLUSIONS OR EXTRACTS FROM OR REGARDING OUR REPORTS IS RESERVED PENDING OUR WRITTEN APPROVAL

FORM 1434A R80

ORDER NO.: POR-9169
LAB NO.: 001430
CLIENT NO.: P.O. 43326
REPORT NO.: 02
REPORT DATE: 10-19-85

REPORT OF ULTRASONIC EXAMINATION OF WELDS

CLIENT OREGON GRADUATE CENTER 19600 S.W. Von Neuman Drive Beaverton, Oregon 97005	PROJECT Electroslag Welds With Known Defects	
	LOCATION Pittsburgh Testing Laboratory, Portland Oregon	
REPORT TO Mr. Bob Turpin	DRAWING NO.	ULTRASONIC UNIT SERIAL NO. <u>131D-351</u>

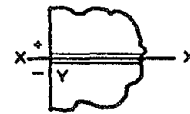
WELD LOCATION AND IDENTIFICATION SKETCH
(RECORD LENGTH, THICKNESS, AND X-Y MARKERS)

PLATE NO: 02

SEE ADDITIONAL DRAWING FOR WELD MAPPING

No Laminations Noted

TEST METHOD STANDARD AWS D1.1-84/ASME Sec. IX
ACCEPTANCE STANDARD Section 9.25.3/Section IX



X-Y MARKERS

* Use Leg I, II, or III.

DATE	WELD IDENTIFICATION	ACCEPTABLE	REJECTABLE	Indication number	Transducer angle	From Face	Leg °	DECIBELS				DISCONTINUITY				
								Indication level	Reference level	Attenuation factor	Indication rating	Length	Angular distance (sound path)	Depth from "A" surface	Distance	
															From X	From Y
a	b	c	d													
October 08, 1985	Plate No. 2			1	60°	A	1	87	73	5	+9	.375"	3.54"	1.20"	4.5"	-.25"
				2	60°	A	1	93	73	4	+13	.25"	3.17"	1.08"	2.5"	+.5"
				3	60°	A	1	83	73	1	+9	4.5"	1.52"	.52"	7-3/4"	-.5"
				4	60°	A	1	86	73	4	+9	4.5"	3.06"	1.05"	7-3/4"	-.75"
				5	60°	A	1	88	73	4	+11	.5"	2.91"	1.00"	9.25"	+.5"
				6	60°	A	1	79	73	3	+3	.375"	2.73"	.93"	12"	0
				7	60°	A	1	97	73	5	+19	.5"	3.54"	1.2"	16"	+.5"
				8	60°	A	1	95	73	2	+20	.5"	1.89"	.64"	18.5"	-.5"
				9	60°	A	1	95	73	5	+17	.5"	2.8"	.97"	20.5"	0

TECHNICIAN: Frederick J. Neimann Level: II
 Interpreter: Frederick J. Neimann Level: II
 Reviewer: _____ Date: _____
 Page 04 of 12 nancy

PITTSBURGH TESTING LABORATORY
Donald R. Scott
 Donald R. Scott, Level III



PITTSBURGH TESTING LABORATORY

ESTABLISHED 1881

PITTSBURGH, PA. 15220
 AREA CODE 412 • TELEPHONE 922-4000

AS A MUTUAL PROTECTION TO CLIENTS, THE PUBLIC AND OURSELVES, ALL REPORTS ARE SUBMITTED AS THE CONFIDENTIAL PROPERTY OF CLIENTS, AND AUTHORIZATION FOR PUBLICATION OF STATEMENTS, CONCLUSIONS OR EXTRACTS FROM OR REGARDING OUR REPORTS IS RESERVED PENDING OUR WRITTEN APPROVAL.

FORM 1434A R80

ORDER NO.: POR-9169
 LAB NO.: 001430
 CLIENT NO.: P.O. 43326
 REPORT NO.: 02
 REPORT DATE: 10-19-85

REPORT OF ULTRASONIC EXAMINATION OF WELDS

CLIENT OREGON GRADUATE CENTER 19600 S.W. Von Neuman Drive Beaverton, Oregon 97005	PROJECT Electroslag Welds With Known Defects	
	LOCATION Pittsburgh Testing Laboratory, Portland Oregon	
REPORT TO Mr. Bob Turpin	DRAWING NO.	ULTRASONIC UNIT SERIAL NO. <u>131D-351</u>

WELD LOCATION AND IDENTIFICATION SKETCH
 (RECORD LENGTH, THICKNESS, AND X-Y MARKERS)

TEST METHOD STANDARD
AWS D1.1-84/ASME Sec. IX

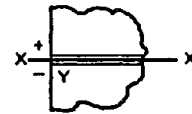
ACCEPTANCE STANDARD
 Section 9.25.3/Section IX

SEE ADDITIONAL DRAWING FOR WELD MAPPING

Plate No. 2

No Laminations Noted

Weld Width 1.25" to 1.5"



X-Y MARKERS

* Use Leg I, II, or III.

DATE	WELD IDENTIFICATION	ACCEPTABLE	REJECTABLE	Indication number	Transducer angle	From Face	Leg *	DECIBELS				Length	Angular distance (sound path)	Depth from "A" surface	DISCONTINUITY	
								Indication level	Reference level	Attenuation factor	Indication rating				Distance	
															From X	From Y
October 08, 1985	Plate No. 2			1	70°	A	1	97	77	2	+18	7.25	2.27"	.77"	4.25"	0-.25"
				2	70°	A	1	85	77	0	+8	5.75"	1.26"	.43"	7.25"	-.75"
				3	70°A		1	96	77	5	+14	.5"	3.51"	1.2"	9"	-.125"
				4	70°	A	1	98	77	3	+18	.5"	2.5"	.84"	15"	0
				5	70°	A	1	98	77	3	+18	.5"	2.61"	.89"	11.5"	0
				6	70°	A	1	100	77	2	+13	.5"	2.36"	.80"	20.5"	-.125"

TECHNICIAN: Frederick J. Neimann Level: II
 Interpreter: Frederick J. Neimann Level: II
 Reviewer: _____ Date: _____
 Page 05 of 11 nancy

PITTSBURGH TESTING LABORATORY
Donald R. Scott
 Donald R. Scott, Level III

PLATE NO: 2

70°

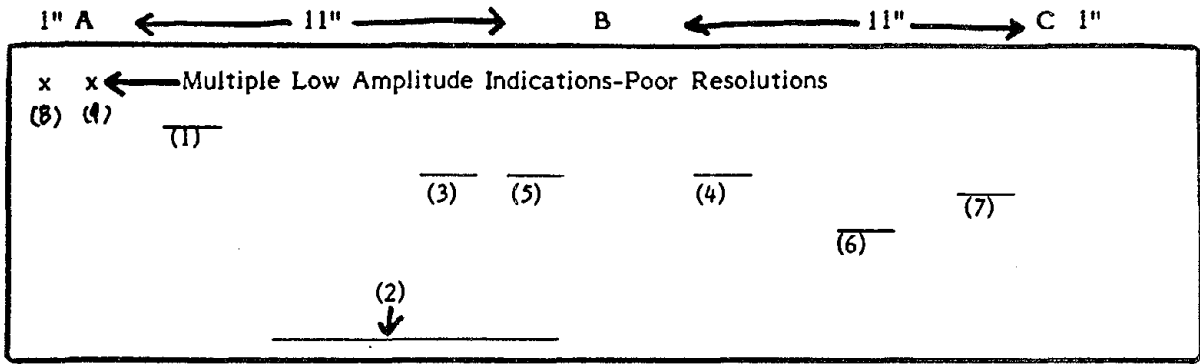
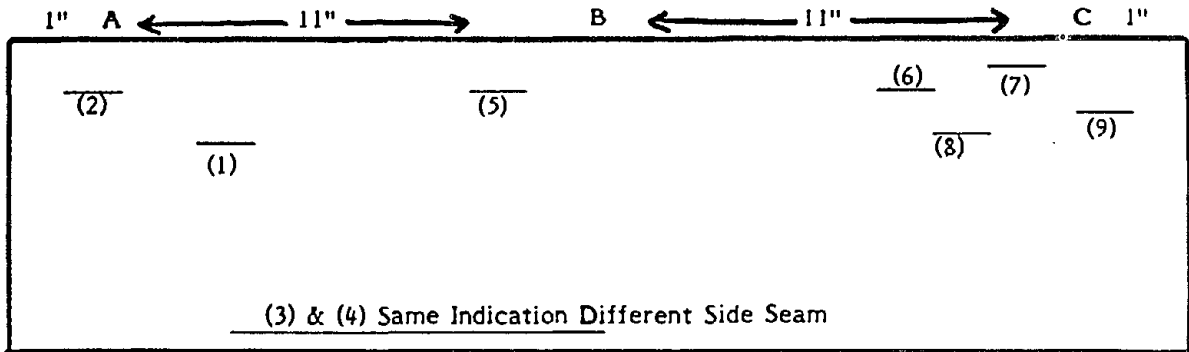


PLATE NO: 2

60°



70°

1. No
2. Lack of Fusion
3. W
4. WC
5. W
6. No

60°

1. No
2. WC
3. } Lack of Fusion
4. }
5. W
6. W
7. W
8. No
9. No



PITTSBURGH TESTING LABORATORY

ESTABLISHED 1881

PITTSBURGH, PA. 15220

AREA CODE 412 • TELEPHONE 922-4000

AS A MUTUAL PROTECTION TO CLIENTS, THE PUBLIC AND OURSELVES, ALL REPORTS ARE SUBMITTED AS THE CONFIDENTIAL PROPERTY OF CLIENTS, AND AUTHORIZATION FOR PUBLICATION OF STATEMENTS, CONCLUSIONS OR EXTRACTS FROM OR REGARDING OUR REPORTS IS RESERVED PENDING OUR WRITTEN APPROVAL.

FORM 1434A R80.

ORDER NO.: POR-9169

LAB NO.: 001430

CLIENT NO.: P.O. 43326

REPORT NO.: 02

REPORT DATE: 10-19-85

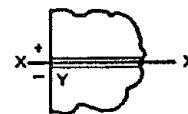
REPORT OF ULTRASONIC EXAMINATION OF WELDS

CLIENT OREGON GRADUATE CENTER 19600 S.W. Von Neuman Drive Beaverton, Oregon 97005	PROJECT Electroslag Welds With Known Defects	
	LOCATION Pittsburgh Testing Laboratory, Portland Oregon	
REPORT TO Mr. Bob Turpin	DRAWING NO.	ULTRASONIC UNIT SERIAL NO. <u>131D-351</u>

WELD LOCATION AND IDENTIFICATION SKETCH
(RECORD LENGTH, THICKNESS, AND X-Y MARKERS)

TEST METHOD STANDARD AWS D1.1-84/ASME Sec. IX
ACCEPTANCE STANDARD Section 9.25.3/Section IX

SEE ADDITIONAL DRAWING FOR WELD MAPPING



X-Y MARKERS

Weld Width 1.5" Approximately

* Use Leg I, II, or III.

DATE	WELD IDENTIFICATION	ACCEPTABLE	REJECTABLE	Indication number	Transducer angle	From Face	Leg *	DECIBELS				DISCONTINUITY				
								Indication level	Reference level	Attenuation factor	Indication rating	Length	Angular distance (round path)	Depth from "A" surface	Distance	
															From X	From Y
October 08, 1985	Plate 3			1	60	A	1	97	73	4	+20	Various	2.93"	1.0"	1.5"	-25"
				2	60	A	1	95	73	2	+20	.125"	1.89"	.64"	4.25"	0
	3 Variations Various Depths			3	60°	A	1	94	73	2	+19	.125"	1.95"	.67"	5"	0
				4	60°	A	1	87	73	2	+12	.625"	2.21"	.75"	7"	-5"
				5	60°	A	1	98	73	5	+20	.25"	3.6"	1.2"	12"	+125"
				6	60°	A	1	97	73	2	+21	.375"	2.44"	.83"	12"	-5"
				7	60°	A	1	80	73	4	+3	3"	3.34"	1.14"	16"	+5"
				8	60°	A	1	80	73	1	+6	2.75"	1.67"	.56"	16.25"	-5"
				9	60°	A	1	90	73	3	+14	.25"	2.42"	.82"	21.75"	-125"

TECHNICIAN: Frederick J. Neimann Level: II
 Interpreter: Frederick J. Neimann Level: II
 Reviewer: _____ Date: _____
 Page 07 of 11 nancy

PITTSBURGH TESTING LABORATORY

 Donald R. Scott, Level III



PITTSBURGH TESTING LABORATORY

ESTABLISHED 1881

PITTSBURGH, PA. 15220

AREA CODE 412 • TELEPHONE 922-4000

AS A MUTUAL PROTECTION TO CLIENTS, THE PUBLIC AND OURSELVES, ALL REPORTS ARE SUBMITTED AS THE CONFIDENTIAL PROPERTY OF CLIENTS, AND AUTHORIZATION FOR PUBLICATION OF STATEMENTS, CONCLUSIONS OR EXTRACTS FROM OR REGARDING OUR REPORTS IS RESERVED PENDING OUR WRITTEN APPROVAL

FORM 1434A R80

ORDER NO.: POR-9169

LAB NO.: 001430

CLIENT NO.: P.O. 43326

REPORT NO.: 02

REPORT DATE: 10-19-85

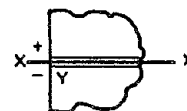
REPORT OF ULTRASONIC EXAMINATION OF WELDS

CLIENT OREGON GRADUATE CENTER 19600 S.W. Von Neuman Drive Beaverton, Oregon 97005	PROJECT Electroslag Welds With Known Defects	
	LOCATION Pittsburgh Testing Laboratory, Portland Oregon	
REPORT TO Mr. Bob Turpin	DRAWING NO.	ULTRASONIC UNIT SERIAL NO. <u>131D-351</u>

WELD LOCATION AND IDENTIFICATION SKETCH
(RECORD LENGTH, THICKNESS, AND X-Y MARKERS)

TEST METHOD STANDARD AWS D1.1-84/ASME Sec. IX
ACCEPTANCE STANDARD Section 9.25.3/Section IX

SEE ADDITIONAL DRAWING FOR WELD MAPPING



X-Y MARKERS

* Use Leg I, II, or III.

DATE	WELD IDENTIFICATION	ACCEPTABLE	REJECTABLE	Indication number	Transducer angle	From Face	Leg °	DECIBELS				DISCONTINUITY				
								Indication level	Reference level	Attenuation factor	Indication rating	Length	Angular distance (sound path)	Depth from "A" surface	Distance	
															a	b
October 08, 1985	Plate No: 3			1	70°	A	1	96	77	6	+13	.375"	4.38"	1.5"	1.25"	0
				2	70°	A	1	98	77	5	+16	.625"	3.48"	1.19"	7"	-.5"
				3	70°	A	1	96	77	5	+14	.75"	3.72"	1.27"	4"	-.125"
				4	70°	A	1	91	77	1	+13	.250"	1.71"	.58"	12"	+.5"
				5	70°	A	1	109	77	9	+23	.5"	5.44"	1.85"	9.5"	0
				6	70°	A	1	93	77	4	+12	2"	2.97"	1.01"	16"	+.5"
				7	70°	A	1	95	77	2	+16	2.25"	2.1"	.72"	16"	-.5"
				8	70°	A	1	90	77	1	+12	.25"	1.79"	.61"	21.25"	0

TECHNICIAN: Frederick J. Neimann Level: II

Interpreter: Frederick J. Neimann Level: II

Reviewer _____ Date _____

Page 08 of 11 nancy

PITTSBURGH TESTING LABORATORY

Donald R. Scott

Donald R. Scott, Level III

PLATE NO: 3

60°

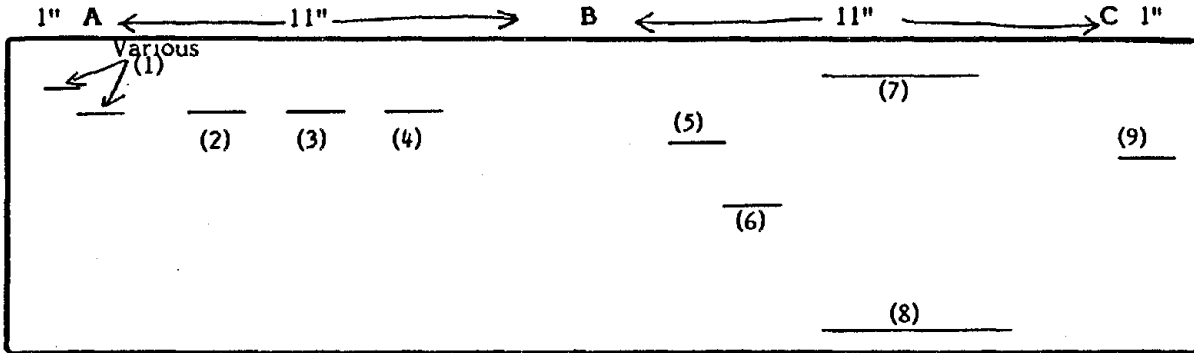
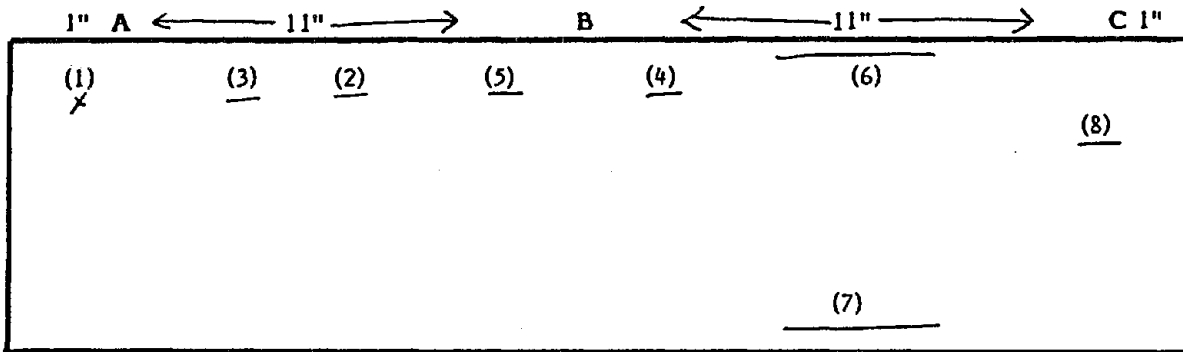


PLATE NO: 3

70°



60°

1. WC
2. W
3. W
4. Mo
5. HC
6. "
- 7 } Lack of Fusion
- 8 } + WC
- 9 WC

70°

1. WC
2. MD
3. W
4. HC
5. Mo
6. } Lack of Fusion
7. } + WC
- 8 WC



PITTSBURGH TESTING LABORATORY

ESTABLISHED 1861

PITTSBURGH, PA. 15220
 AREA CODE 412 • TELEPHONE 922-4000

AS A MUTUAL PROTECTION TO CLIENTS, THE PUBLIC AND OURSELVES, ALL REPORTS ARE SUBMITTED AS THE CONFIDENTIAL PROPERTY OF CLIENTS, AND AUTHORIZATION FOR PUBLICATION OF STATEMENTS, CONCLUSIONS OR EXTRACTS FROM OR REGARDING OUR REPORTS IS RESERVED PENDING OUR WRITTEN APPROVAL.

FORM 1434A R80

ORDER NO.: POR-9169
 LAB NO.: 001430
 CLIENT NO.: P.O. 43326
 REPORT NO.: 02
 REPORT DATE: 10-19-85

REPORT OF ULTRASONIC EXAMINATION OF WELDS

CLIENT OREGON GRADUATE CENTER 19600 S.W. Von Neuman Drive Beaverton, Oregon 97005	PROJECT Electroslag Welds With Known Defects	
	LOCATION Pittsburgh Testing Laboratory, Portland Oregon	
REPORT TO Mr. Bob Turpin	DRAWING NO.	ULTRASONIC UNIT SERIAL NO. <u>131D-351</u>

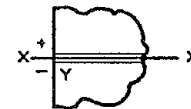
WELD LOCATION AND IDENTIFICATION SKETCH
 (RECORD LENGTH, THICKNESS, AND X-Y MARKERS)

3" Material Thickness

SEE ADDITIONAL DRAWING FOR WELD MAPPING

5/8" X 3/4" 2.25 Krautkramer KA-216
 Weld Width 1.25"

TEST METHOD STANDARD AWS D1.1-84/ASME Sec. IX
ACCEPTANCE STANDARD Section 9.25.3/Section IX



X-Y MARKERS

* Use Leg I, II, or III.

DATE	WELD IDENTIFICATION	ACCEPTABLE	REJECTABLE	Indication number	Transducer angle	From Face	Leg °	DECIBELS				DISCONTINUITY				
								Indication level	Reference level	Attenuation factor	Indication rating	Length	Angular distance (sound path)	Depth from "A" surface	Distance	
															a	b
October 08, 1985	Plate 4	<input checked="" type="checkbox"/>		1A	45°	A	1	66	48	6	+12	1.2"	4.19"	2.85"	1.5"	+5"
				1B	45°	A	23	74	48	15	+11	1.2"	8.56"	Surface	1.5"	-5"
				2	45°	A	2	62	48	7	+7	2"	4.56"	2.75"	3"	.125"
				3	45°	A	1	61	48	3	+10	2.75"	2.44"	1.72"	.5" (3)	0
				4	45°	A	2	65	48	14	+3	3"	8.05"	.32"	11.125"	+5"
				5	45°	A	1	63	48	2	+13	2.5"	2.02"	1.43"	12"	-.125"
				6	45°	A	1	71	48	6	+17	1.75"	4.1"	2.91"	1.4" (4)	+5"
				7	45°	A	1	84	48	14	+22	2"	8.13"	.29"	21"	+5"
				8												

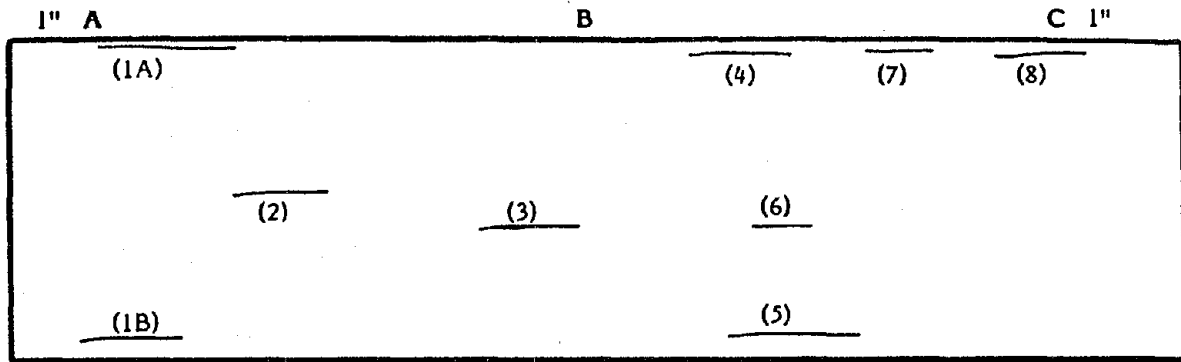
TECHNICIAN: Frederick J. Neimann Level: II
 Interpreter: Frederick J. Neimann Level: II
 Reviewer _____ Date _____
 Page 10 of 11 nancy

PITTSBURGH TESTING LABORATORY

 Donald R. Scott, Level III

PLATE NO: 4

45° Only



- 1A Geometrical Indication
- 1B " "
- 2 " "
- 3 Hot crack
- 4 Geometrical Indication
- 5 Hot crack
- 6 Geometrical Indication
- 7 Lack of Fusion
- 8 slag entrapment

REFERENCES

- (1) J. Skirinar, Metals Technical Conference, International Institute of Welding, Sydney, Australia, 1976.
- (2) A. L. Liby and D. L. Olson, Quarterly of the Colorado School of Mines, 1 (1974), p. 41.
- (3) K. E. Dorschu, J. E. Norcross, and C. C. Gage, Welding Journal, 52, No. 11 (1973), p. 710.
- (4) A. W. Pense, J. D. Wood, and J. W. Fisher, Welding Journal, 60, No. 12 (1981), p. 33.
- (5) J. D. Culp, Electroslag Weldments: Performance and Needed Research (Lansing, MI: Michigan Department of State Highways and Transportation, 1977).
- (6) B. E. Paton, Electroslag Welding, second edition (New York: AWS, 1962).
- (7) W. P. Benter, Acceptance Criteria for Electroslag Weldments in Bridges, Report 201, (National Corp. Hwy. Res. Program, National Res. Council, 1979).
- (8) A. T. D'Annessa, Welding Journal, 45, No. 12 (1966), p. 569-s.
- (9) R. D. Thomas, Welding Journal, 39, No. 2 (1960), p. 111.
- (10) M. Solar and H. Biloni, Welding Journal, 56, No. 9 (1977), p. 274-s.
- (11) H. B. Cary, Portaslag Welding (Troy, OH: Hobart Brothers Tech. Center, 1970).
- (12) R. H. Frost, G. R. Edwards, and M. D. Rheinlander, Welding Journal, 60, No. 1 (1981), p. 1-s.
- (13) M. G. Kozulin, A. P. Syatishev, and V. V. Emel'yanov, Welding Prod., 12 (1969), p. 18.
- (14) J. E. Jones, D. L. Olson, and G. P. Martins, Welding Journal, 59, No. 9, (1980), p. 245-s.
- (15) M. V. Nolan and R. L. Apps, Welding and Met. Fab., (November 1969), p. 464.
- (16) M. V. Nolan, Founding, Welding, Production Eng. Journal, (April 1970), p. 14.
- (17) H. C. Campbell, (Welding Research Council Bulletin, No. 154, 1970).

- (18) N. Isamoto, J. Nose, Y. Naganawa, Y. Tsunawaki, and Y. Makino, Trans. of Japan Welding Res. Inst., 6, No. 1 (1977), p. 23.
- (19) N. E. Andersen, Svetsaren, 1, (1973), p. 9.
- (20) A. H. Dilawari, T. W. Eagar, and J. Szekely, Welding J., 57, No. 1 (1978), p. 24-s.
- (21) T. DebRoy, J. Szekely, and T. W. Eagar, Heat Generation Patterns and Temperature Profiles in ESW, (Cambridge, MA: Massachusetts Inst. of Tech., 1980).
- (22) T. Narahari and B. A. Graville, Welding and Met. Fab., (June 1976), p. 350.
- (23) K. Watanabe, I. Sejima, S. Kokura, G. Taki, and H. Miyake, Advanced Welding Technology, (Tokyo, Japan: Japan Welding Society, 1975), p. 519.
- (24) E. E. Banks and J. Ritchie, Australian Welding Journal, (Jan./Feb. 1975), p. 7.
- (25) T. Kunihiro and H. Nakajima, Proceedings of "Significance of Defects in Welded Structures", (Tokyo, Japan: Univ. of Tokyo Press, October 1973), p. 105.
- (26) P. H. Hutton, R. F. Klein and E. B. Schverk, Proceedings of "Third Acoustic Emission Symposium", Tokyo, Japan, September 1976.
- (27) J. R. Mitchell, C. H. McGogney, and J. Culp, (San Juan Capistrano, CA: Dunegan/Endevco Tech. Report DE 79-13, 1980), p. 124.
- (28) G. I. Evstratov, Welding Prod., 6, (1979), p. 43.
- (29) B. M. Patchett, "Vertical Welding Efficiently with the Consumable Guide Electroslag Process", Tech. Paper AD74-407, Soc. of Manufacturing, (1974).
- (30) V. Vaidya, W. Coulter, and B. A. Graville, Welding and Met. Fab., (June 1976), p. 345.
- (31) A. Ujiie, S. Sata, S. Sakai, and A. Hamanaka, Advanced Welding Technology, Japan Welding Soc., Tokyo, Japan, (1975), p. 543.
- (32) Y. Ito, M. Ideda, N. Yamauchi, and J. Furuichi, Advanced Welding Technology, Japan Welding Soc., Tokyo, Japan, (1975), p. 513.
- (33) B. M. Patchett, F. W. Collins, and D. Timpson, Cranfield Inst. of Tech., Memo No. 72, (June 1972)

- (34) A. Haslam, R. L. Apps, and B. M. Patchett, "Advances in Welding Process", 3rd International Conference, Harrogate, 1974, p. 47.
- (35) R. B. Turpin, M.S. Thesis, Oregon Graduate Center, Beaverton, OR, 1981.
- (36) I. I. Sushchuk-Slyusarenko, Aut. Welding, 2 (1974), p. 49.
- (37) G. R. Edwards and R. H. Frost, Report No. DOE/ET/12313-T1, (Golden, CO: Colorado School of Mines, 1980), p. 138.
- (38) K. R. Venkataramaiah, M.S. Thesis, University of Toronto, 1967.
- (39) Yu V. Sharapov, Welding Prod., 7 (1967), p. 38.
- (40) E. M. Kuzmak and M. S. Skuditskii, Welding Prod., 22, No. 6 (1975), p. 39.
- (41) F. Eichhorn and P. Hirsch, DVS-Berichte, 31 (1974), p. 37.
- (42) F. Eichhorn, P. Hirsch, W. G. Burchard, and F. S. Chen, Schweissen Und Schneiden, 28, No. 6 (1976), p. 210.
- (43) A. N. Khakimov, et al., Welding Prod., 1 (1974), p. 39.
- (44) S. A. Smirnov and L. A. Efimenko, Aut. Welding, 9 (1973), p. 45.
- (45) R. G. Garlick and J. F. Wallace, American Foundrymen's Soc. Trans., 67 (1959), p. 366.
- (46) A. H. Freedman and J. F. Wallace, Foundry, 85 (1957), p. 578.
- (47) M. D. Coward, J. of Iron and Steel Inst., (August 1973), p. 586.
- (48) I. P. Trochun and V. P. Chernysh, Welding Prod., 11 (1965), p. 6.
- (49) P. G. Schmidt, Steel in the USSR, 4 (1977), p. 216.
- (50) "Magnetic Stirring of Aluminum Weld Metals", Current Awareness Bulletin, (1979).
- (51) G. V. Sutyurin, Russian Metallurgy, 4 (1974), p. 84.
- (52) H. S. Marr, Iron and Steel International, (February 1979), p. 29.
- (53) D. C. Brown, F. A. Crossley, J. F. Rudy, and H. Schwartzbart, Welding Journal, 41, No. 6 (1962), p. 241-s.
- (54) J. Campbell, International Metal Review, 2 (1981), p. 71.

- (55) R. L. Apps and E. Smith, in Proc. Weldability of Heightened and High Strength Metals, (Zagreb, Yugoslavia: Assoc. of Yugoslav Welding Soc., 1974), p. 163.
- (56) I. Sijima, H. Kita, T. Rokutani, and T. Wada, Advanced Welding Tech., Japan Welding Society, Tokyo, Japan, (1975), p. 537.
- (57) L. A. DeVedia and B. M. Patchett, Welding and Met. Fab., (July-August 1977), p. 1977.
- (58) B. M. Patchett, F. W. Collins and R. L. Apps, In Conf. on Welding Low Temperature Containment Plant, (Cambridge, London, England: The Welding Institute, 1973), p. 117.
- (59) R. E. Dolby, In Proc. Mechanic and Physics of Fracture, (Cambridge, England: Metals Society, 1975), p. 95.
- (60) Y. Kawaguchi, Y. Yamaguchi, G. Ohtani and S. Watanabe, The Sumitomo Search, No. 20, (November 1978).
- (61) B. I. Medovar, L. V. Chekotilo, and S. I. German, Welding Prod., 9 (1965), p. 58.
- (62) E. Pikna, Zvaranie, 26, No. 4 (1977), p. 105.
- (63) H. Suzuki, et al., U.S. Patent 3,352,993 (February 7, 1966).
- (64) "Consumable Nozzle Type ESW Process Using Flux Cored Wire", (Japan: Nippon Steel Corporation), p. 105.
- (65) L. Muncner, Proceedings N.Y. Amer. Soc. Mech. Eng., Part II: Materials, Fabrication and Inspection, II-82, (1973), p. 1121.
- (66) S. S. Tuliani, K. S. Probert and A. H. Briscoe, In Proc. Welding and Fab. in the Nuclear Ind., (London, England: British Nuclear Energy Society, 1979), p. 327.
- (67) M. G. Dawes, Welding International Research and Development, 4 (1971), p. 1.
- (68) D. N. Shakleton, Progress Report E/59/75, (Cambridge, England: The Welding Institute, 1975).
- (69) D. N. Shakleton, Report 73/1978/PE, (Cambridge, England: The Welding Institute, 1978).
- (70) C. E. Jackson, Welding Research Council Bulletin No. 190, (December 1973).
- (71) E. Mryka, Aut. Welding, 1 (1974), p. 23.

- (72) A. W. Pense, J. B. de S. Ramos, and R. D. Stout, Welding Journal, 55, No. 1, p. 1-s.
- (73) K. Matsumoto and K. Takai, "Tetsu-tor Hagane", J. of the Iron and Steel Inst. of Japan, 64, No. 7 (1978), p. 141.
- (74) V. A. Soroka, Aut. Welding, 10 (1979), p. 30.

~~B16~~
11